9th Hull Performance & Insight Conference

HullPIC'24

Edited by Volker Bertram

Sponsored by

www.jotun.com

tutech.de

albis-mp.com

www.ascenzmarorka.com

www.coach-solutions.dk

www.danelec.com

www.deepsea.ai

www.enamor.pl

www.hasytec.com

www.hempel.com

www.hoppe-marine.com

www.idealship.de

www.napa.fi

www.numeca.de

theoceanly.com

www.ppg.com

toqua.ai

Veinland.net

https://vesops.dk/

www.vpsolutions.dk

Media Partners

https://hansa-online.de/

https://home.rina.org.uk/

Index

Third-Power Law – Friend or Foe?

Volker Bertram, DNV, Hamburg/Germany, volker.bertram@dnv.com
Richard Marioth, Idealship, Itzehoe/Germany, rm@idealship.de

Abstract

This paper discusses the background and limitations of the third-power law, a.k.a. admiralty formula. The formula derives from generic considerations for power and resistance as functions of speed. It assumes constant resistance coefficients and propeller efficiency. These assumptions can only be used for small deviations from a given point on a baseline. Abusing the simple "law" may lead to wrong conclusions.

1. The Admiralty Formula

The maritime industry likes simple, largely empirical methods which allow quick estimates even if only a few global parameters are known. A prime example is the 'Admiralty formula':

$$P_B = \frac{\Delta^{2/3} \cdot V^3}{C} \tag{1}$$

P_B is the (brake) power, Δ the displacement (mass), V the speed through water, and C is a constant. The formula may give good estimates if the baseline is "close enough (in geometrical properties and speed [])", *Bertram (2012)*. A simplified version omits the mass term, implicitly assuming a given ship at constant draft and trim, and then puts power as proportional to the third power of speed ('Third-power law'):

$$P \sim V^3 \tag{2}$$

The term 'law' may lead to a wrongful perception that the Admiralty formula expresses some fundamental physical relation that is always true. This is not the case and has often been stated, e.g. *Völker (1974), Kristensen (2010), Bertram (2012), Berthelsen and Nielsen (2022)*. Hans Otto Kristensen found for containerships exponents between 2.5 and 7, where the low values appear for lower speeds, and the high values for (now unrealistically) high speeds [personal communication]. *Berthelsen and Nielsen (2022)* found for tankers exponents significantly lower than 3, the lower the speed, the lower the exponent.

However, such is the lure of simple formulas that basic assumptions and resulting limitations are often forgotten or ignored. The Admiralty formula derives its name from the British Admiralty, which in its heydays (say, 200 years ago in the days of Horatio Nelson) was the leading authority on maritime knowledge. Those were simpler days in many ways. For example, ships did not have propellers yet.

2. Effective power and delivered power

The following subchapters will explain cursorily the theoretical background of the Admiralty formula. For more background, see e.g. chapter 3.1. of *Bertram (2012).*

2.1. It looks reasonably fine for effective power

The general definition 'power = force · speed' yields the effective power:

$$P_E = R_T \cdot V \tag{3}$$

R_T is the total calm-water resistance of the ship excluding resistance of appendages of the propeller and its periphery. The effective power P_E is the power we would have to use to tow the ship without a propulsive system. It makes most sense for a resistance test in a model basin, where the ship model without a propeller is moved by a carriage through the water, Fig.1.

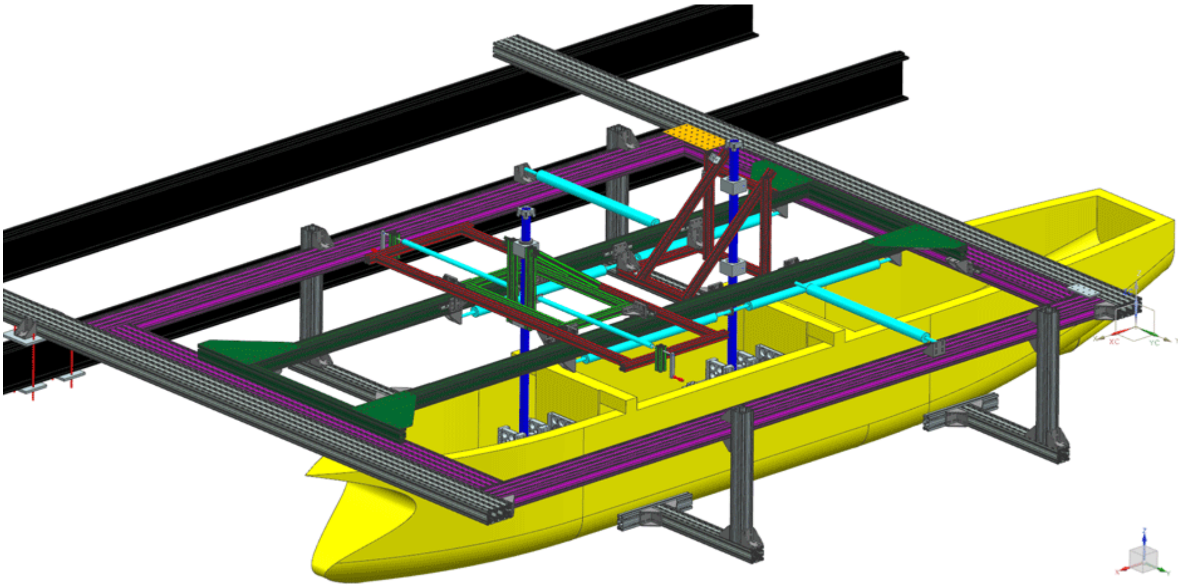

Fig.1: Set-up for resistance test in model basin, source: HSVA

The calm-water resistance in Eq.(3) in turn is generally expressed as:

$$R_T = c_T \cdot \frac{\rho}{2} \cdot V^2 \cdot S \qquad (4)$$

Eq.(4) expresses then the resistance in the classical way, using a nondimensional resistance coefficient c_T, speed squared, a reference area (typically using the zero-speed wetted surface of the hull), and the water density ρ to get the dimension of a force. If c_T were constant over speed, then combining Eqs.(3) and (4) would yield a third-power law. Of course, it is not. That would be too simple. But maybe we can assume it in reasonably good approximation?

Naval architects typically decompose the calm-water resistance into four components, *Bertram (2012)*:

- Friction resistance – induced by shear forces between hull and water
- Wave resistance – induced by wave making also in an ideal fluid without viscosity or friction
- Air resistance – induced by the part above the water
- Viscous pressure resistance – “the rest”, accounting for flow separation, interaction between the other resistance parts, changing wetted surface at forward speed, etc.

The friction resistance coefficient is generally computed using the so-called ITTC’57 formula:

$$c_F = \frac{0.075}{(log_{10}R_n - 2)^2} \qquad (5)$$

R_n is the Reynolds number (non-dimensional speed). The ITTC’57 formula is not a constant, but the resulting curve is rather horizontal, Fig.2; we may accept c_F then as nearly constant.

For medium speeds, the wave resistance coefficient is complex with local minima and maxima, definitely not constant, Fig.3. However, for lower speeds, the wave resistance goes rapidly to zero.

The viscous pressure resistance is again a complex function of speed, but generally much smaller than the friction resistance. The air resistance is generally quite small.

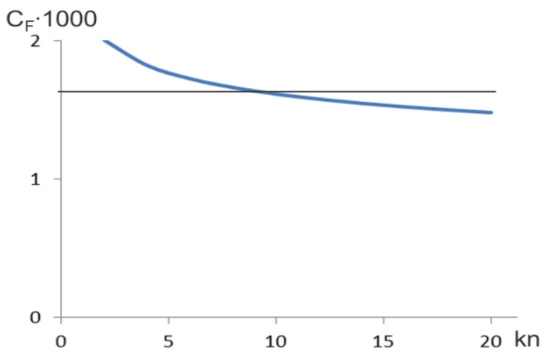

Fig.2: Friction resistance coefficient over speed

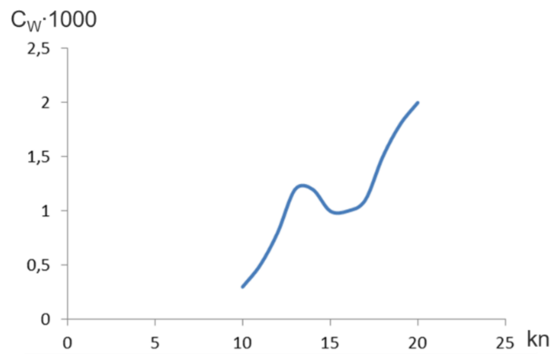

Fig.3: Wave resistance coefficient over speed

Frictional resistance in design conditions is between 50% (offshore supply vessel) and 80% (very large crude carrier) of the total calm-water resistance in sea trial conditions. Fouling increases the percentage, so do lower speeds. Generally, we can assume that frictional resistance dominates most of the time in operational profiles of ocean-going vessels.

2.2. Added resistance due to wind and waves

So far, we have discussed only the resistance contributions for calm-water conditions. In real operation, there are further resistance contributions, notably due to wind and waves.

Wind resistance corrections generally assume the wind resistance coefficient as independent of speed (and also typically that wind resistance coefficient is not dependent on draft respectively air draft, which is questionable, *Bertram (2017)*, but at least ISO 19030 has a crude correction for the windage area. While large-scale flow separation makes a third-power law in principle questionable for wind resistance, we have no better suggestion.

Wind waves and swell induce added resistance to ships. The popular Kreitner formula suggests no speed dependence of added resistance in waves, *Bertram (2016)*. This is definitely wrong, but the relation between added resistance and ship speed is complex, and also not just quadratic on speed.

In performance monitoring, wind, wind wave and swell added resistance components are estimated by more or less simplified correction formulas, assumed to scale as calm-water resistance for their contribution on power and fuel consumption, and the measured power is then corrected ("normalized"). If the calm-water resistance is small, e.g. at low ship speed, the resulting errors from added resistance corrections can be significant.

2.3. The propeller screws it up

Unlike in the days when the Admiralty formula was formulated, normal ships now have propellers and we are not really interested in an effective power P_E, but rather in the brake power P_B at the engine which drives our fuel consumption. The two are connected through various efficiencies:

$$P_E = \eta_H \cdot \eta_0 \cdot \eta_R \cdot \eta_S \cdot P_B \qquad (6)$$

These four efficiencies denote:

- η_H – The 'hull efficiency' depends on the thrust deduction factor t and wake fraction w, which in turn depend on speed, draft, hull geometry etc. η_H can be less or greater than 1. It is thus not really an efficiency, which by definition cannot be greater than 100%. Most performance monitoring approaches conveniently consider it to be constant, taken from one condition in model tests or some obscure design formula. Oops, but compared to the other errors this is of secondary importance.

- η_0 – The 'open-water efficiency' of a propeller is a highly nonlinear function of speed, Fig.4. Typically the design point is slightly to the left of the maximum, and propeller efficiency decreases towards lower speeds, say from 70% to 50%. This is the main factor why for slow-steaming power depends rather on speed squared than on speed to the third power.

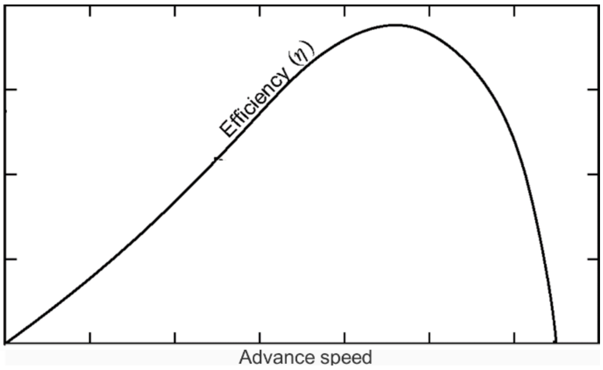

Fig.4: (Open-water) propeller efficiency curve

- η_R – Theoretically, the 'relative rotative efficiency' accounts for the differences between the open-water test and the inhomogeneous three-dimensional propeller inflow encountered in propulsion conditions. In reality, the propeller efficiency behind the ship cannot be measured and all hydrodynamic effects not included in the hull efficiency, are included in η_R. η_R again is not truly an efficiency. Typical values for single-screw ships range from 1.02 to 1.06. As variations are small, it will not affect the third-power law assumption much.
- η_S – The 'shaft efficiency' accounts for the transmission losses through shaft and – if applicable – gear boxes. It is close to 1 and we can ignore any speed dependence for our purposes.

The key contribution to a change in the third-power law comes thus through the open-water propeller efficiency which introduces a different exponent dependent on ship speed.

3. Limitations of applicability

3.1. Where it works

To slightly modify a quote from Lord of the Rings: One does not simply approximate a speed-power curve over a larger speed range. But one can use such simple approximation for <u>small</u> variations in speed or displacement. ISO 19030 allows using the Admiralty formula for variations up to 5% from a given baseline. The problem is that for most ships, the baselines do not extend far enough to lower speeds and are not spaced close enough over draft; thus many data points would be lost if following the strict 5% margins. The temptation to ignore the standard is understandable – and a trap.

The formula may also be used for very qualitative considerations, e.g. for trying the basic EEDI philosophy of IMO. The EEDI is computed following (a simplified formula):

$$\text{EEDI} = \frac{\textbf{Power} \cdot \text{SFOC} \cdot \text{CO}_2 \text{ factor}}{\text{Cargo capacity} \cdot \textbf{speed}} \qquad (6)$$

Assuming the third-power law, we then get EEDI to be proportional to speed squared. IMO wants ships to go slower, implicitly rewarding slower ship design speeds resulting in installed engines with lower power (and lower fuel consumption respectively lower emissions to air).

3.2. Where it is abused

Most naval architectural estimation formulas are intended for contract/design conditions. *Berthelsen and Nielsen (2022)* analyzed the exponents of 85 tanker vessels. Fig.5 shows the results of this study with an added cubical curve (red) that crosses the model test at 14 kn. The curves deviate significantly below 12 kn, i.e. for these low speeds assuming the third-power law leads to large errors.

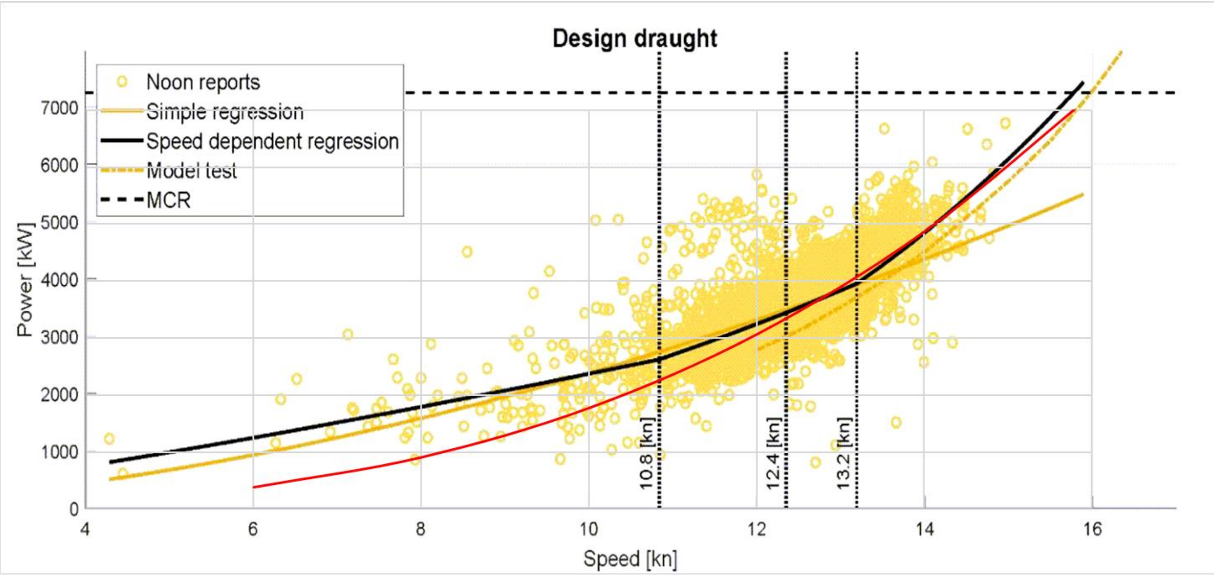

Fig.5: Draught and speed dependent regression model from *Berthelsen and Nielsen (2022)* study with an added cubical speed vs. power curve in red.

Interpolating between far-spaced baselines (e.g. ballast and design conditions) and extrapolating to much lower speeds, as frequently done to avoid creating dense hydrodynamic knowledge bases by either CFD (Computational Fluid Dynamics) or machine learning, leads to high errors. *Krapp and Bertram (2016)* report 10% difference on average between simple third-power application vs. detailed CFD analyses for a containership. Trying to bridge large variations using simple formulas does not work in ship hydrodynamics. There are too many factors and non-linearities in the physics involved. Fig.6 shows as an example of the massive wave breaking at intermediate draft for a containership, where the resulting resistance is almost the same as for design draft, albeit with a very different mix in the resistance components.

Fig.6: Breaking waves at partial draft introduce strong linearities

4. Conclusion

All models are wrong, but some are useful. The simple Admiralty formula (or third-power law) is decidedly wrong, but still useful when

- order of magnitude suffices
- only calm-water conditions are considered
- friction resistance dominates
- used for small variations of speed or displacement (< 5%)

It may be misleading in other cases.

Acknowledgement

We thank Hans Otto Kristensen (HOK Marineconsult) for his off-the-record discussions on speed-power curves and unpublished analyses. He did pioneer work in our field more than a decade ago.

References

BERTHELSEN, F.H.; NIELSEN, U.D. (2022), *Assessment of Ships' Speed-Power Relationship at Lower Sailing Speeds*, 7th HullPIC Conf., Tullamore, pp.4-15, http://data.hullpic.info/HullPIC2022_Tullamore.pdf

BERTRAM, V. (2012), *Practical Ship Hydrodynamics*, Butterworth & Heinemann, Oxford

BERTRAM, V. (2016), *Added Power in Waves – Time to Stop Lying (to Ourselves)*, 1st HullPIC Conf., Pavone, pp.5-13, http://data.hullpic.info/HullPIC2016.pdf

BERTRAM, V. (2017), *Some Heretic Thoughts on ISO 19030*, 2nd HullPIC Conf., Ulrichshusen, pp.3-11, data.hullpic.info/hullpic2017_ulrichshusen.pdf

KRAPP, A.; BERTRAM, V. (2016), *Hull Performance Analysis – Aspects of Speed-Power Reference Curves*, 1st HullPIC Conf., Pavone, pp.41-48, http://data.hullpic.info/HullPIC2016.pdf

KRISTENSEN, H.O. (2010), *Notes on dependency between propulsive power and speed of ships*, Danish Technical University, unpublished paper (received in personal communication)

VÖLKER, H. (1974), *Entwerfen von Schiffen [Ship Design]*, Handbuch der Werften XII, Hansa-Verlag

Simulation-based Digital Twins for Ship Performance Monitoring

Sven Albert, Numeca Ingenieurbüro, Altdorf/Germany, sven.albert@numeca.de
Thomas Hildebrandt, Numeca Ingenieurbüro, Altdorf/Germany, thomas.hildebrandt@numeca.de
Volker Bertram, DNV, Hamburg/Germany, volker.bertram@dnv.com

Abstract

This paper introduces the state of the art in flow simulations with relevance to hull performance monitoring: resistance & propulsion simulations, seakeeping, rudder forces and wind forces. The paper describes general approaches, applications where we have confidence in CFD simulations and those where current applications reach their limits.

1. Introduction to numerical fluid dynamics

Numerical ship hydrodynamics denotes techniques to solve equations describing the physics of flows, *Bertram (2012)*. The most important techniques for us are:

- Potential-flow computations – Potential-flow codes do not model viscosity (and associated effects like the boundary layer). They also do not model breaking waves. On the other hand, they are fast and relatively easy to handle.
- CFD (Computational Fluid Dynamics) – Codes (usually based on the Reynolds Averaged Navier Stokes Equations = RANSE) model viscosity directly in the field equations and are able to capture breaking waves. All major commercial codes and the open-source alternative OpenFOAM are verified in terms of numerical implementation, and their application is validated for many marine applications.

More recently, such simulations have been denoted as hydrodynamic "Digital Twins", where potential-flow simulations are low-fidelity twins and CFD simulations high-fidelity twins. Digital Twins may be created based on first principles (white box models) or machine learning (black box models), but mostly combine direct physical insight with empirical tuning or fitting. We will discuss here mainly the classical first-principle digital-twin approach, before discussing the next generation of Digital Twins employing machine learning.

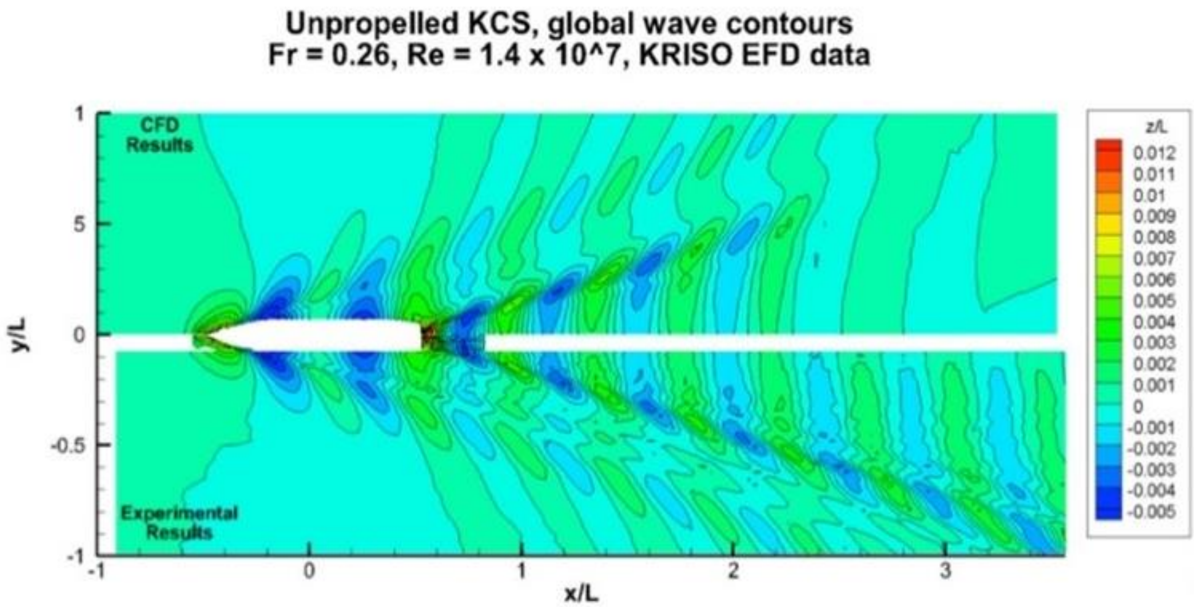

Fig.1: Example of more accessible CFD: CADENCE OnCloud for Fine/Marine

Over the past two decades, CFD has become more accessible (or "democratic") to the wider maritime community, due to various developments:

- Software has become more user-friendly, with streamlined, largely automated processes for geometry description, grid generation, computational model set-up, and post-processing. Modelling expertise may in narrow applications (such a speed-power curves for conventional ships) be incorporated in macros, i.e. automatic routines, allowing essentially "anybody" to run the application, *Hochkirch and Hahn (2017), Gatin et al. (2019).*
- Computing power has become more accessible, even for small and medium enterprises, through more flexible business schemes where both CFD software licenses and computing power in the cloud can be rented "by the hour", Fig.1, *Hildebrandt and Reyer (2015)*.

2. Applications

2.1. Resistance & propulsion

For performance monitoring, we are primarily interested in expressing ideal (= for smooth ships) power as function of draft, trim, and speed, in "baseline curves". Important points in this respect are:

- Wave making and wave breaking
  For design condition, wave making is generally minimized (using usually low-fidelity Digital Twins and/or model tests). For performance monitoring, we also need to look at off-design conditions, where breaking waves are important, Fig.2, *Krapp and Bertram (2016)*. Thus high-fidelity Digital Twins should be employed ("free-surface RANSE" simulations in the jargon of CFD experts).

Fig.2: Off-design draft and speed leads often to massive wave-breaking

- Model scale or full scale
  Model tests violate some similarity laws, *Bertram (2012)*: Wave-breaking and boundary layers are different from the full-scale ship, *Hochkirch and Mallol (2013).* Thus, CFD computations should be performed at full scale ("numerical sea trials"). Unfortunately, many CFD simulations in practice are performed at model-scale conditions, as customers like to use model tests to check the CFD simulations. With growing understanding of CFD, we should see a change in this practice and a move towards full-scale simulations.

- Geometry simplifications
  Hull details such as welds are not captured by CFD models for power prediction. Variations in welds can account for significantly higher resistance. For a tanker, *Ciortan and Bertram*

(2014) give 2% for poor welds. Such welds also generate higher turbulence intensity than generally assumed in CFD computations, Fig.3. *Sfiris et al. (2023)* describe a weld fairing coating solution for welds, investigated by CFD.

Microscopic or even changes in the order of mm are not captured geometrically in CFD models. While the roughness of surfaces can be varied in CFD computations, e.g. *Östman et al. (2017,2019)*, *Vargas and Shan (2017)*, *Vargas et al. (2019)*, *Zhang et al. (2021)*, there is no consensus among CFD experts how reliable such parameter studies are. However, the qualitative changes appear plausible. Our theoretical knowledge on roughness and boundary layers stems from ideal laboratory conditions, mostly for flat plates. Sea water with many impurities flowing over ship hulls with roughness levels in the mm order of magnitudes (with welds and fouling) may behave differently. Research into proving such differences is still in its infancy. In a notable example, *Kaminaris et al. (2023)* used CFD and 3D printed artificial barnacles on plates in experiments.

Krapp et al. (2016) report 5.6% variations in measured power in sea trials for seven sister vessels. It is anybody's guess how much of these variations are due to differences in the as-built hulls and how much due to variations in the measuring process. However, unless detailed scans of the as-built hull are used to generate the CFD model, such variations will always have to be expected. CFD predictions (like model tests) can never be more accurate than these variations. For performance monitoring, a pragmatic approach is calibrating computations against sea trials. The difference between as-designed and as-built in geometry, as well as assorted simplification in the Digital Twin (e.g. the transition from laminar to turbulent flow) are then largely compensated.

Often the propeller is not geometrically modelled, Fig.4; instead the main effects of the propeller are included via so-called body-forces. These are externally specified forces to mimic thrust and swirl of the propeller. For performance monitoring purposes, this modelling approach is fine.

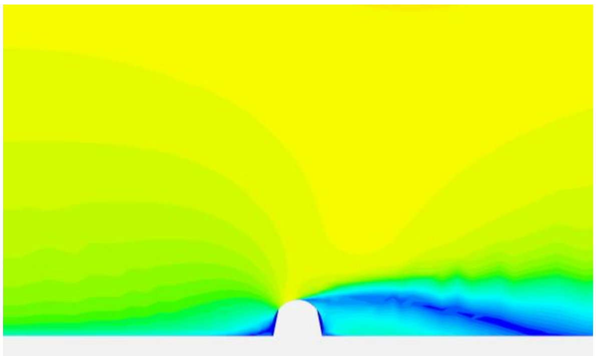

Fig.3: Welds increase frictional resistance, but are generally not captured in CFD models.

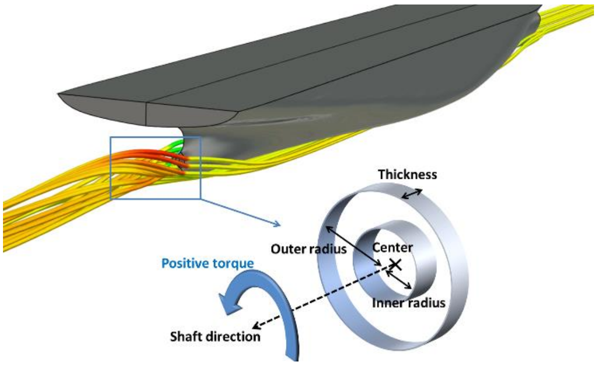

Fig.4: Body-force propeller model in RANSE simulations

- Flow simplifications
  Model tests assume laminar-turbulent flow transition at a given distance from the leading edge. As this distance does not scale properly, model tests enforce the transition by turbulence stimulators (sand strips or studs). In CFD, generally fully turbulent flow is assumed from the very beginning, although some researchers have used "numerical sand strips". We believe that the standard approach with fully turbulent flow from the beginning may reflect the conditions for the real ship in even moderate sea states better than the model tests.

  The propeller behind the ship dominates the flow and makes discussions over the turbulence model rather academic for performance monitoring.

Take-home messages:

- Properly performed CFD simulations are by now at least as accurate as model tests for full-scale predictions.
- Neither model tests nor CFD can account for as-built variations in sister vessels, but calibrating to sea trials can largely compensate for this.
- For parameter variations (such as trim, draft and speed for a given hull), CFD is superior due to parallel processing and easier automation of analyses. (CFD simulations for trim optimization tools should be reused for performance monitoring. If properly planned, this reuse of hydrodynamic information can lead to much better economics.)
- CFD may support better hull maintenance strategies, such as deciding where to clean better or where to use more expensive coatings.

2.2. Seakeeping and manoeuvring

There is a multitude of computational methods for seakeeping with assorted strengths and shortcomings, *Bertram (2012,2016)*. Primarily, performance monitoring needs added power estimates in small to moderate seaways. Here, linear analyses based on potential-flow theory are recommended as best overall approach. These analyses are relatively fast, allowing the investigation of many parameters (wavelength, wave direction, ship speed, draft, etc.). More complicated CFD methods capture also breaking waves and assorted nonlinearities, resulting in very good agreement for motions, Fig.6, e.g. *Lagemann (2019)*. However, these codes require high computational effort and do not necessarily give better results for added resistance in waves, due to a combination of grid-resolution issues and problems with subtracting the calm-water resistance, *Bertram (2016)*. For long waves, CFD approaches may also be used to compute added resistance and power in waves, e.g. *Gatin and Boxall (2021)* for added resistance in swell to resolve a party-charter claim on ship performance. However, in most cases, there is little sense in going to the required expense of CFD simulations to create a knowledge base for added power in waves (think at least 30000-60000 € if you want to cover the variations of parameters needed), as long as we use crude estimates for the seaway.

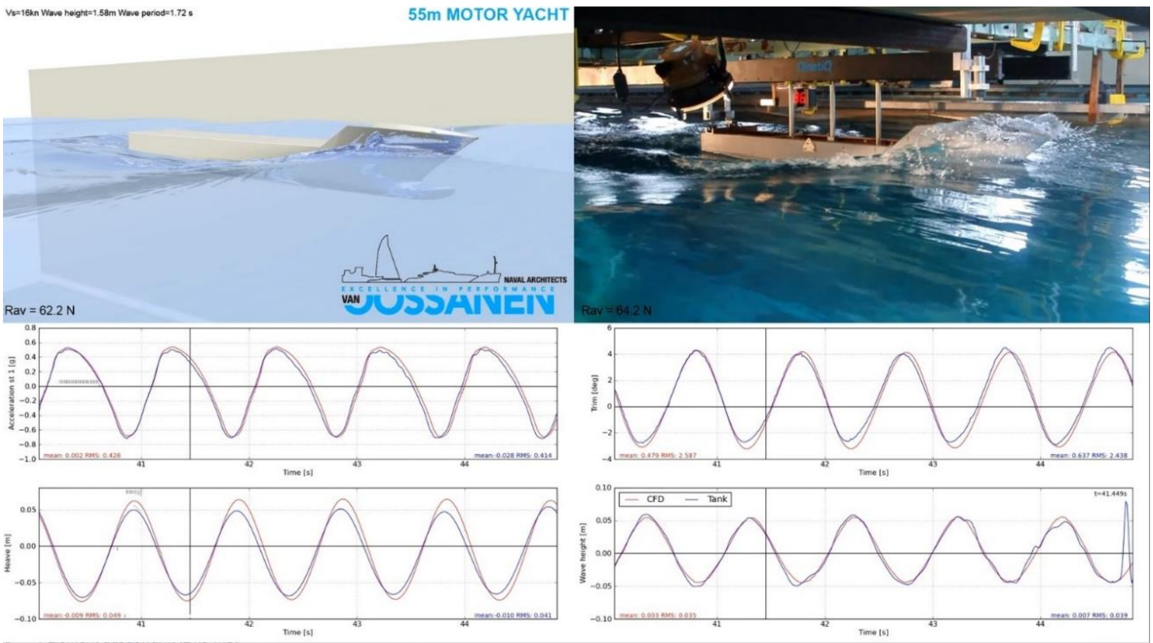

Fig.6: High-fidelity CFD simulation (left) and model texts (right) for yacht in head waves

Rudder forces for rudders at small-to-moderate angles can be computed by semi-empirical methods, *Söding (1998), Bertram (2012)*. CFD simulations are unnecessary overkill for performance monitoring. In normal ship operation at higher speeds, rudder angles are small.

2.3. Aerodynamics

Although wind tunnel tests are still widely used, CFD has evolved as an alternative comparable in accuracy, level of detail, time requirements and cost, Fig.7. CFD could be combined with machine learning approaches to create fast and accurate models for wind forces, ideally for individual ships, but possibly also for classes of ships such a representative ship types. The validity of the semi-empirical formulas used in ISO 19030 should be investigated by CFD, e.g. the assumption that the non-dimensional wind force coefficients remain (virtually) constant with draft variations for a ship, *Bertram (2017)*. CFD might also be used to determine local flow variation at the location of wind anemometer, *Moat et al. (2005)*, to compensate for local flow distortion due to the deckhouse and the other equipment. Alas, a lot could be done, and little is actually done in using CFD for better air resistance models.

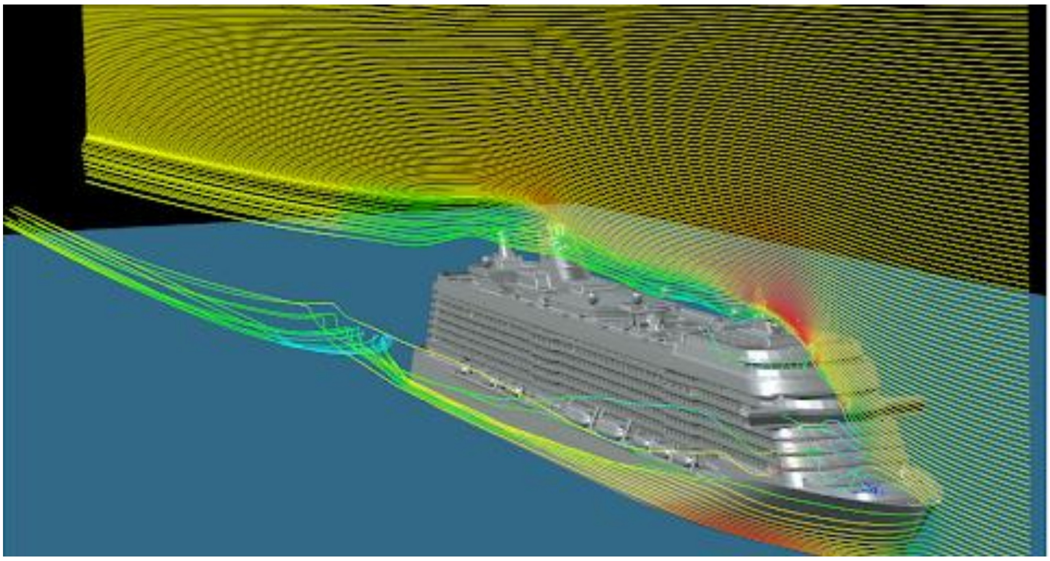

Fig.7: CFD simulations for wind forces and local flow investigations, source: Meyer Turku and FINE™/Marine (Numeca)

3. Next-generation Digital Twins

Meta-models derived using machine learning on CFD simulations for series of variations on a base hull geometry can yield reasonably accurate predictions virtually instantaneously. For (Wageningen B-series) propellers, this has been convincingly demonstrated by Numeca, Fig.8, with response times reduced from 2-3 hours to 20 s, *Van den Boogard et al. (2022)*. Similarly, *Ahmed et al. (2023)* demonstrated the use of meta-models for power predictions for a family of planing hulls. In general, CFD simulations for parametric model variations can be used to train machine learning to predict both global quantities (such as forces) and local quantities (such as pressure distributions).

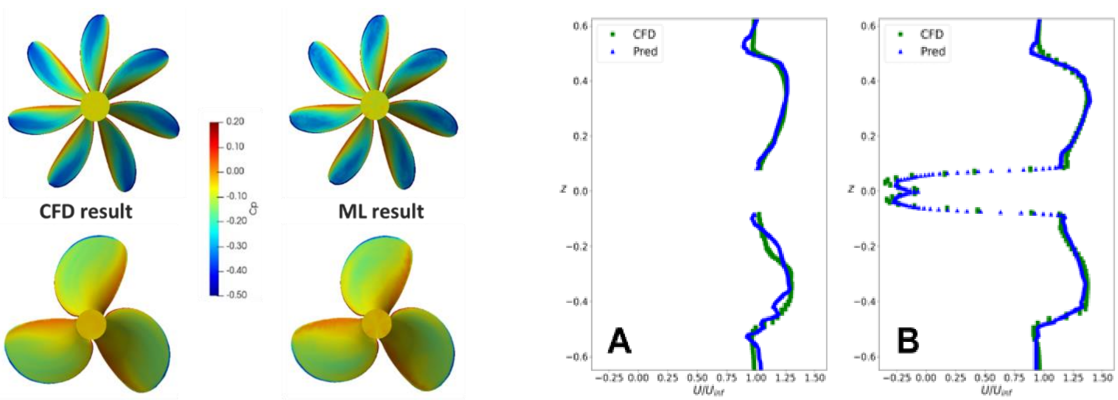

Fig.8: CFD prediction and meta-model based on machine learning (ML)

4. Conclusions

CFD has matured to be a viable and sometimes superior alternative to model tests. Specific applications with relevance to performance monitoring are:

- Numerical sea trials, steady speed of ship in initially calm water with working propeller at full-scale conditions. Such simulations give reliable hydrodynamic knowledge bases for the calm-water performance of ships. They should be based on RANSE simulations (CFD) and may be performed now at reasonable cost in the cloud.
- Seakeeping simulations are less important as we filter generally for moderate and higher seaways. Simulations only make sense if seaways are identified with greater accuracy. Similarly, simple semi-empirical approaches suffice for manoeuvring and rudder forces.
- CFD could be used more to derive better models for aerodynamics in performance monitoring.
- Meta-modelling (applying machine learning techniques such as Artificial Neural Nets) may be used based on CFD results to derive fast and accurate Digital Twins.

References

AHMED, O.; HARRIES, S.; LOHSE, J.; SALECKER, S.E. (2023), *Parametric Modeling, CFD Simulations, DoE and Machine Learning for the Design of a Planing Boat*, 22nd COMPIT Conf., Drübeck, pp.176-192, http://data.hiper-conf.info/compit2023_drubeck.pdf

BERTRAM, V. (2012), *Practical Ship Hydrodynamics*, Butterworth & Heinemann, Oxford

BERTRAM, V. (2016), *Added Power in Waves – Time to Stop Lying (to Ourselves)*, 1st HullPIC Conf., Pavone, pp.5-13, http://data.hullpic.info/HullPIC2016.pdf

BERTRAM, V. (2017), *Some heretic thoughts on ISO 19030*, 2nd HullÜIC Conf., Ulrichshusen, pp.5-11, http://data.hullpic.info/hullpic2017_ulrichshusen.pdf

CIORTAN, C.; BERTRAM, V. (2014), *RANSE simulations for the effect of welds on ship resistance*, 17th Numerical Towing Tank Symp. (NuTTS), Marstrand, https://www.uni-due.de/imperia/md/content/ist/nutts_17_2014_marstrand.pdf

GATIN, I.; BOXALL, D. (2021), *Calculating speed loss due to swell using CFD*, 6th HullPIC Conf., Pontignano, pp.63-71, http://data.hullpic.info/HullPIC2021_Pontignano.pdf

GATIN, I.; VUKCEVIC, V.; JASAK, H. (2019), *Fully Automated CFD Analysis for Full-Scale Ship Hydrodynamics*, 4th HullPIC Conf., Gubbio, pp.153-161, http://data.hullpic.info/HullPIC2019_gubbio.pdf

HILDEBRANDT, T.; REYER, M. (2015), *Business and technical adaptivity in marine CFD simulations - Bridging the gap*, 14th COMPIT Conf., Ulrichshusen, pp.394-406, http://data.hiper-conf.info/compit2015_ulrichshusen.pdf

HOCHKIRCH, K.; HAHN, C. (2017), *Cloud-based numerical towing tanks – Anytime, anywhere and for anybody*, 11th HIPER Symp., Zevenwacht, pp.66-69, http://data.hiper-conf.info/Hiper2017_Zevenwacht.pdf

HOCHKIRCH, K.; MALLOL, B. (2013), *On the importance of full-scale CFD simulations for ships*, 12th COMPIT Conf., Cortona, pp.85-95, http://data.hiper-conf.info/compit2013_cortona.pdf

KAMINARIS, I.K.; BALARAS, E.; SCHULTZ, M.P.; HOLM, E.R. (2023), *Hydrodynamics of Biofouling: Blending Hull Inspections to High-Fidelity Computations and Experiments*, 4th PortPIC

Conf., Pontignano, pp.16-25, http://data.hullpic.info/HullPIC2023_Pontignano.pdf

KRAPP, A.; BERTRAM, V. (2016), *Hull performance analysis – Aspects of speed-power reference curves*, 1st HullPIC Conf., Pavone, pp.41-48, http://data.hullpic.info/HullPIC2016.pdf

LAGEMANN, B. (2019), *Efficient seakeeping performance predictions with CFD*, PhD thesis, KTH Stockholm, https://www.diva-portal.org/smash/get/diva2:1359848/FULLTEXT01.pdf

MOAT, B.I.; YELLAND, M.J.; MOLLAND, A.F.; PASCAL, R.W. (2005), *The effect of ship shape and anemometer location on wind speed measurements obtained from ships*, 4th Int. Conf. Marine Computational Fluid Dynamics, Southampton pp.133-139

ÖSTMAN, A.; KOUSHAN, K.; SAVIO, L. (2017), *Numerical and experimental investigation of roughness due to different type of coating*, 2nd HullPIC Conf., Ulrichshusen, pp.227-235, http://data.hullpic.info/hullpic2017_ulrichshusen.pdf

ÖSTMAN, A.; KOUSHAN, K.; SAVIO, L. (2019), *Study on Additional Ship Resistance due to Roughness using CFD*, 4th HullPIC, Gubbio, pp.153-161, http://data.hullpic.info/HullPIC2019_gubbio.pdf

SFIRIS, P.; DEMIREL, Y.K.; FARKAS, A.; SOFIA PAGONI, S. (2023), *A Case Study: Combined Effect of a Silicone-Based Low Friction Coating and a Weld Seam Fairing Solution*, 15th HIPER Conf, Bernried, pp.273-284, http://data.hiper-conf.info/Hiper2023_Bernried.pdf

SÖDING, H. (1998), *Limits of potential flow theory in rudder flow predictions*, 22nd Symp. Naval Hydrodyn., Washington

VAN DEN BOOGARD, M.; ALESSI, G.; MALLOL, B., WUNSCH, D.; CLERO, N.; AMADORI, D.; HIRSCH, C.; ZAMPIERI, L.; HILDEBRANDT, T. (2022), *Accelerating marine propeller development in early design stages using machine learning*, 21st COMPIT Conf., Pontignano, pp.24-32

VARGAS, A.; SHAN, H. (2017), *Modeling of ship resistance as a function of biofouling type, coverage, and spatial variation*, 2nd HullPIC Conf., Ulrichshusen, pp.264-281, http://data.hullpic.info/hullpic2017_ulrichshusen.pdf

VARGAS, A.; SHAN, H.; HOLM, E. (2019), *Using CFD to Predict Ship Resistance due to Biofouling and Plan Hull Maintenance*, 4th HullPIC Conf., Gubbio, pp.242-253, http://data.hullpic.info/HullPIC2019_gubbio.pdf

ZHANG, Y.W.; YEGINBAYEVA, I.; BRINK, A. (2021), *Modelling and Simulation of the Effect of Antifouling Coating on Ship Resistance*, 6th HullPIC Conf., Pontignano, pp.41-48, http://data.hullpic.info/HullPIC2021_Pontignano.pdf

Deep Dive into Trim Optimisation: Physical Phenomena Behind the Fuel Savings

Inno Gatin, Cloud Towing Tank, Zagreb, Croatia, inno.gatin@cloudtowingtank.com
Robert Keser, Cloud Towing Tank, Zagreb, Croatia, robert.keser@cloudtowingtank.com
Vuko Vukčević, Cloud Towing Tank, Zagreb, Croatia, vuko@cloudtowingtank.com

Abstract

This paper is an attempt to analyse in detail how changing the trim of the vessel changes fuel consumption. We are going to use a few examples of speed and draught combinations to reveal how changing trim changes different aspects of resistance and propulsion characteristics. The goal is to separate the changes in different resistance components: such as viscous and pressure, as well as different propulsion characteristics (wake fraction, thrust deduction factor), to better understand how trim optimisation works. The subject of this study is a container vessel, ship type that so far benefits from trim optimisation the most.

1. Introduction

Apart from being very colourful, CFD has another benefit: it allows us to dissect hull resistance and propulsion into its constituents, in a way that is difficult or impossible to do with experimental measurements. Let us use this feature to get a better understanding of how changing the trim saves fuel. First, we can look at how two main resistance components change with trim. Since they originate from different sources, pressure and friction resistance are calculated separately in CFD computations: the former by integrating pressure along the surface of the hull, and the latter by integrating viscous stress forces. In the experiment the two combine to compress the dynamometer together, and ratios can only be recovered by using some clever physics based on (well founded) assumptions.

Reichel et al. (2014) give an overview of influential factors on fuel saving by changing the trim. Their findings are based on experience from model test experiments and give a useful insight into the individual components of trim optimisation savings. Similar overview is done here, however with attention to trends of different parameters with changing trim.

2. Resistance and propulsion factors

Here is a quick overview of the factors that we will be analysing in this paper. The most important factor is resistance. As mentioned earlier, using CFD, resistance force can be separated into pressure and friction resistance:

$$\boldsymbol{R_T = R_P + R_F}, \tag{1}$$

with R_T standing for total resistance, R_P is pressure resistance, R_F is friction resistance. Resistance is calculated in towed condition, i.e. without the effect of the propeller. In CFD and in the experiments, this is performed by towing the model, which is not equipped with a propeller, and measuring its resistance force. To calculate fuel savings, self-propelled condition needs to be considered as well. Here, the model is equipped with the propeller, whose action changes the hydrodynamic force acting on the hull, typically increasing it. The thrust T of the propeller needs to be equal in magnitude to this force. The difference between thrust and towed resistance is expressed through the thrust deduction factor:

$$\boldsymbol{t = \frac{T - R_T}{T}}. \tag{2}$$

The thrust deduction factor changes with trim, and thus influences the thrust required to propell the vessel. Changing the trim changes the submerged shape of the hull, which influences the flow around it. By the time the flow reaches the propeller at the stern, it has changed in different ways for different trims. This changes the average inflow speed of the propeller, which is important since it determines the power that the propeller delivers to the flow, called thrust power:

$$\boldsymbol{P_T = T \cdot V_a}, \tag{3}$$

V_a denotes average inflow speed to the propeller. Lower thrust power means lower fuel consumption, which is achieved by lowering V_a. V_a is typically expressed relative to ship speed by defining the wake fraction:

$$\boldsymbol{w = \frac{V_s - V_a}{V_s}}, \tag{4}$$

V_s denotes ship speed. The main goal of ship propulsion is to propel the vessel with a certain speed. Theoretically the power that is required to do that is calculated as:

$$\boldsymbol{P_E = V_s \cdot R_T}, \tag{5}$$

This effective power is overcome with thrust power. The ratio between the two is the hull efficiency:

$$\boldsymbol{\eta_H = \frac{P_E}{P_T}}, \tag{6}$$

which, after a bit of algebraic fiddling, can be written as:

$$\boldsymbol{\eta_H} = \frac{1 - t}{1 - w}. \tag{7}$$

There are still a few pieces missing to get to fuel consumption: to achieve a thrust, the propeller needs to be rotated about its axis. This rotation requires power, the propeller delivered power, and can be calculated as the moment required to rotate the propeller at certain RPM. The ratio between delivered power P_D and thrust power P_T is determined by propeller efficiency, which is determined by conducting open water tests. The propeller has slightly different efficiency when working in open water, and when working behind the vessel. Thus, total propeller efficiency is calculated as a product of open water efficiency η_O and relative rotative efficiency η_R. In CFD trim optimisation studies, the propeller is modelled using the actuator disc model which does not consider the relative rotative efficiency. It is assumed to be equal to 1 in this study for all conditions. This is justified by the fact that η_R ranges from 0.98 and 1.02 in most cases, and according to *Reichel et al. (2014)* varies up to 2% with changing trim. With that assumption, we can write:

$$\boldsymbol{P_D = \frac{P_T}{\eta_O}}. \tag{8}$$

Delivered power P_D is proportional to fuel consumption, hence it serves a good proxy for observing fuel savings. Open water efficiency of the propeller depends on the RPM and inflow velocity V_a, where the RPM is in turn influenced by thrust. Hence, this factor also depends on trim.

To summarize, the following factors will be analysed in this paper, since they depend on trim and influence fuel consumption:

1. R_T, total resistance,
2. R_P, pressure resistance,
3. R_F, friction resistance,
4. t, thrust deduction factor,
5. w, wake fraction factor,
6. η_O, propeller open water efficiency.

3. Container ship trim optimisation

The subject of this analysis is a container vessel, with design speed of around 24 kn and design draught of 12 m. Select number of draught/speed combinations are analysed here in detail. In this paper, trim is expressed in the usual way: in meters, where it represents the difference between the stern and forward draught. Thus, positive trim corresponds to a deeper stern draught and therefore a bow up inclination.

Fig.1 shows the trends of different factors for the first analysed condition: 7 m draught, 10 kn speed. This is a shallow draught for this vessel, as well as a low speed. The graphs are expressed in % change of the factor, with the mean value of the factor taken as referent. Obviously, pressure resistance dominates, with relative changes of 20%, where increasing the trim reduces resistance. However, since the speed is quite low, pressure resistance makes up a relatively small portion of the total resistance. Hence, the change in total resistance and power (~11.5% variation) is much less dramatic. Change in friction resistance is modest, however in the same direction as the change of pressure resistance. Propeller efficiency is also increasing with increasing trim, while hull efficiency is reducing. Wake fraction reduces with trim, which is favourable, but the trust deduction factor increases (albeit oscillatory), together producing a downward trend of the hull efficiency. Finally, if we compare the relative change in resistance and power, we observe that ignoring changes in propulsion factors would overestimate savings at 4 m trim.

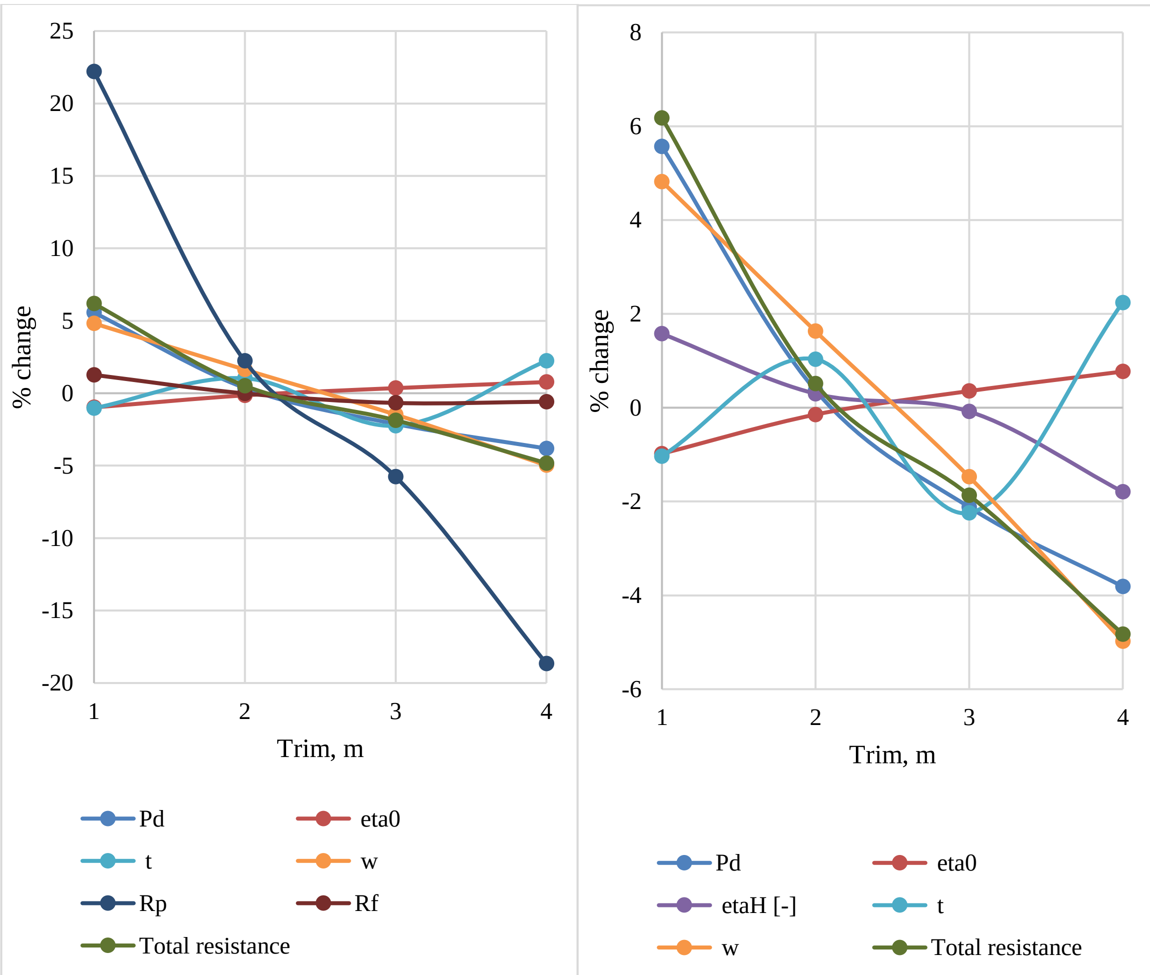

Fig.1: Draught = 7 m, Speed = 10 kn. Trends of different factors with varying trim. Right graph excludes pressure and friction resistance for better legibility of other factors.

Why is the pressure resistance changing by so much? Fig.2 shows the pressure distribution along the hull for trims of 1 and 4 m. At 4 m trim, the bulbous bow is mostly above the waterline, creating a smaller bow wave. This is likely to be the key reason why pressure resistance reduces by increasing trim. Since this condition is far from the design point of this vessel, the bulbous bow is a disadvantage, and reducing its effect reduces resistance.

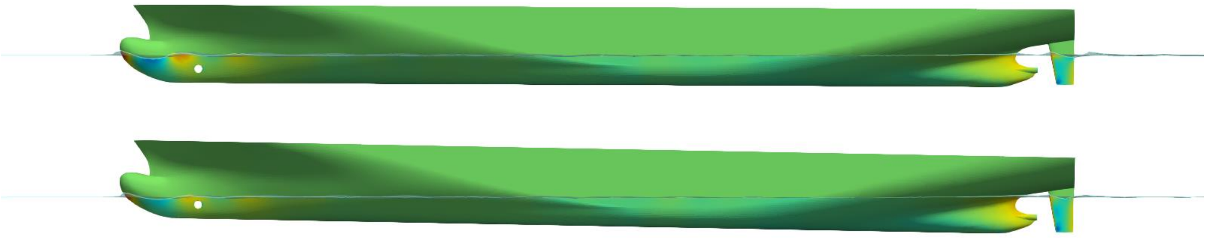

Fig.2: Pressure distribution: Draught = 7 m, Speed = 10 knots. Trim: 1 m (top) and 4 m (bottom).

Let us skip ahead to the next operational point. We will now consider three different speeds for draught of 10 m, which is closer to the design draught. Considered speeds are 10, 15 and 20 kn, where the last one approaches the design speed.

Fig.3 shows the factor trends for 10 kn at 10 m draught. Again, the largest variation is exhibited by pressure resistance, but it is not dominating in the same way as for the previous condition. Interestingly, there is a local maximum for power and resistance between 0 and 1 m trims. Wake fraction again shows a reduction with increasing trim, which is expected since the propeller disc is more exposed to the oncoming flow. Significant variation is found for wake, around 18% from minimum to maximum value. This time the thrust deduction factor shows an oscillatory and modest variation. The resulting hull efficiency mostly follows the downward trend of the wake fraction change with increasing trim. Unlike in the previous case, resistance and hull efficiency have opposite trends, hance their effect is superimposed.

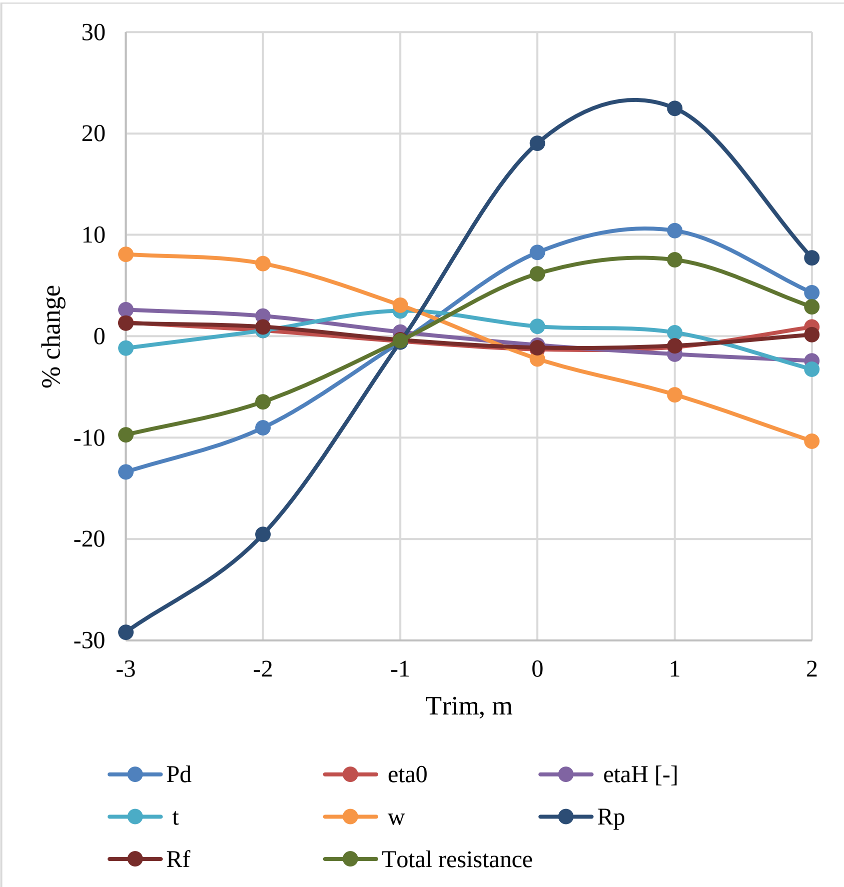

Fig.3: Draught = 10 m, Speed = 10 kn. Trends of different factors with varying trim.

Factor trends for 15 kn at 10 m draught are shown in Fig.4. Trends of propulsion factors resemble those at 10 kn, with the wake fraction falling with increasing trim with a variation of 24%. Hull efficiency again shows a small variation with a negative trend. Unlike at 10 kn, the pressure resistance shows a steep increase for positive trims. For negative trims it shows a less steep trend in the favourable direction. The result is a massive 40% variation in delivered power, because pressure resistance makes a larger portion of total resistance. Since pressure resistance is the dominating factor again, we expect to see differences in the ship-generated wave system. Indeed, Fig.5 shows that there is a large difference between pressure distribution around the bow, due to a significantly larger bow wave being generated at trim of 2 m. At this trim, the bulbous bow is approaching the free surface and there is a breaking wave crest developing, dissipating a lot of energy. Evidently the wave field generated by the bulbous bow does not interfere with the bow wave system in a favourable way. Hence, submerging the bulb deeper reduces its effect. We can conclude that this is because the speed of 15 kn is still far away from the design speed of the vessel, and that the bulb is doing more harm than good at this speed.

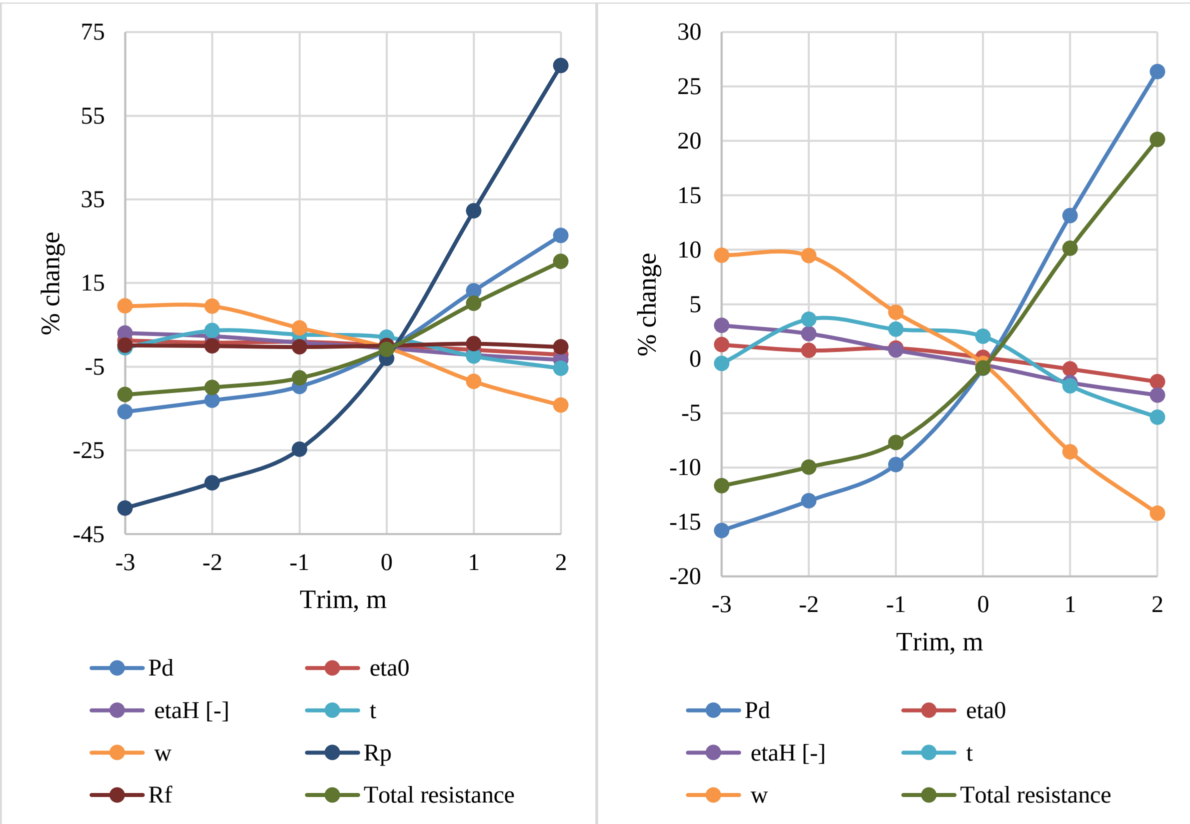

Fig.4: Draught = 10 m, Speed = 15 kn. Trends of different factors with varying trim. Right graph excludes pressure and friction resistance for better legibility of other factors.

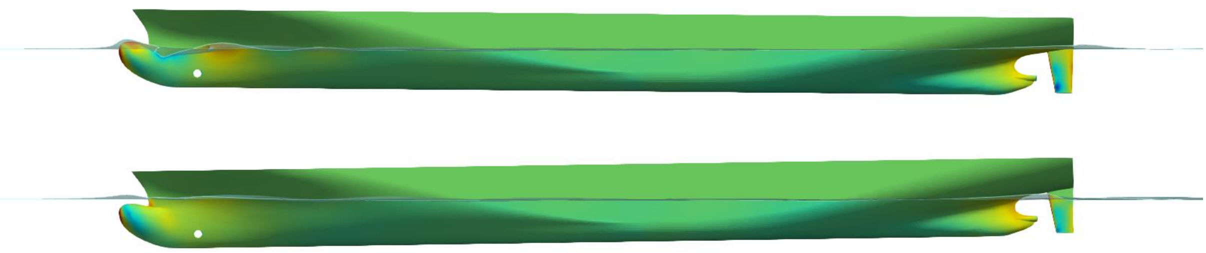

Fig.5: Pressure distribution: Draught = 10 m, Speed = 15 kn. Trim: 2 m (top) and -3 m (bottom).

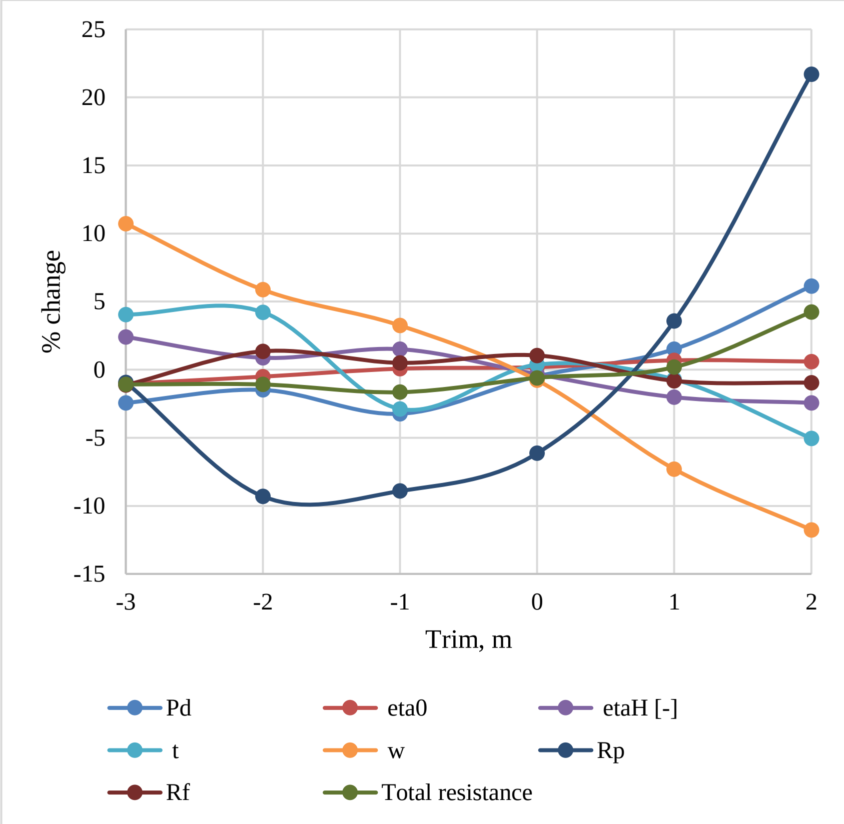

Fig.6: Draught = 10 m, Speed = 20 kn. Trends of different factors with varying trim.

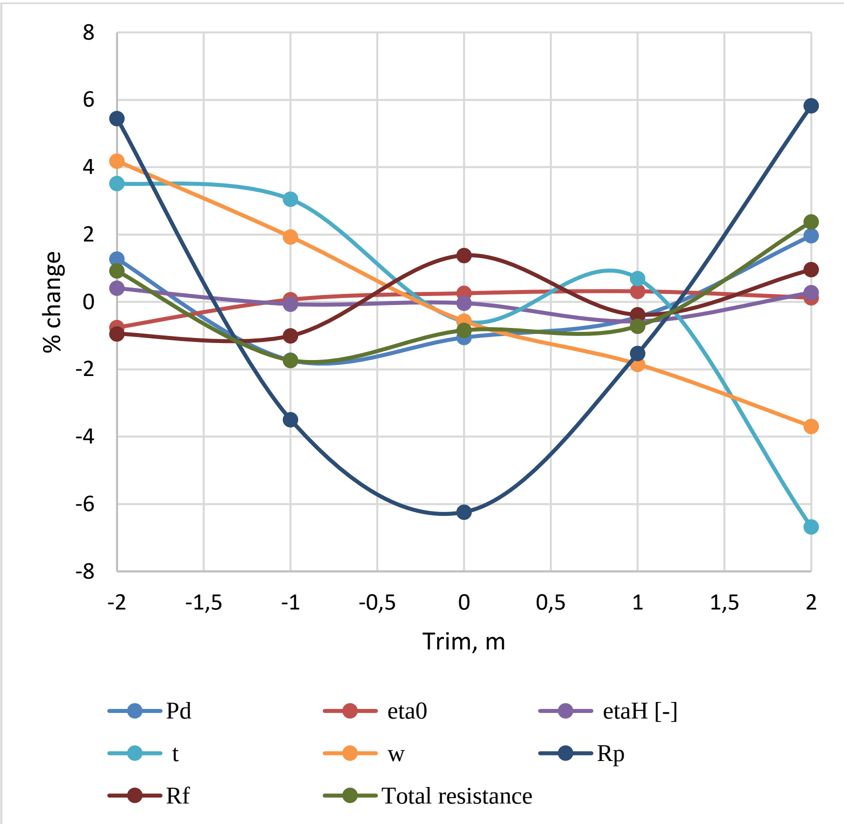

Fig.7: Draught = 12 m, Speed = 20 kn. Trends of different factors with varying trim.

Moving further, Fig.6 shows factor variations for speed of 20 kn at 10 m draught. Pressure resistance has a significantly lower variation than at 15 kn of only 30%. Power changes by only 8%, much less than at 15 kn. Add to this the fact that at even keel the vessel is close to performing optimally, and we can conclude that this is closer to the design operational point of the vessel compared to previous cases. Wake again shows a pronounced negative trend, while hull efficiency falls with higher trims. Like the previous case, trimming the bow up increases pressure resistance, again due to the bulb coming closer to the free surface. However, this is not nearly as dramatic as at 15 kn. It is likely that the interference is more favourable at 20 kn since bulb and bow wave system wavelengths have increased.

Approaching the design condition for this vessel, Fig.7 shows the trends for draught 12 m and speed 20 kn. Looking at the graph, it is apparent that the naval architects optimised the hull shape very well for minimising wave making resistance at even keel. Here, pressure resistance is minimal at even keel, while only small oscillations of other factors exist. Increasing or reducing the trim increases power, however the changes are relatively small. Possible savings in terms of fuel consumption are significantly smaller here than at shallower draughts and slower speeds.

4. Conclusion

From observing the trim optimisation data for a container ship, the following can be concluded:

1. Pressure resistance varies the most with changing the trim, due to the large variations in wave-making resistance,
2. Variations in friction resistance are modest,
3. Variations in resistance and consequently power, are larger at lower draughts and lower speeds, further away from the operational design point of the vessel,
4. Propulsion factors contribute to power trends with changing trim, even if the influence is significantly smaller than that of pressure resistance,
5. Variation of propulsion factors does not depend as much on the proximity of the ship's design point,
6. Variations in wake and thrust deduction factor can be significant (25%!), however they tend to compensate to yield a rather small variation in hull efficiency, and consequently in power.

References

REICHEL, M.; MINCHEV, A.; LARSEN, N.L. (2014), *Trim Optimisation - Theory and Practice*. Int. J. Marine Navigation and Safety of Sea Transportation 8(3), pp.387–392

Fleet Monitoring's Impact on Maritime Sustainability

Matteo Barsotti, Oceanly, Genova, Italy, matteo.barsotti@theoceanly.com
Ingela Mandl, Oceanly, Bergen, Norway, ingela.mandl@theoceanly.com

Abstract

The paper investigates the transformative impact of advanced fleet performance monitoring on the maritime industry, focusing on enhancing operational efficiency, ensuring environmental compliance, and improving safety. It evaluates the role of sensor technologies and data analytics in optimizing maritime operations, outlines the environmental advantages of such optimizations, and provide some (clever) ideas on how to use a Fleet Monitoring system for the Maritime sustainability. Moreover, the paper addresses implementation challenges, advocating for innovation and industry-wide collaboration to navigate these hurdles successfully.

1. Introduction

In an era marked by rapid technological advancements and a pressing need for sustainable practices, the maritime industry is experiencing a paradigm shift towards more integrated and intelligent operations, advanced fleet performance monitoring systems stand at the forefront of this shift, leveraging sensor technologies and sophisticated data analytics to usher in a new era of maritime efficiency, environmental stewardship, and safety. Through an analysis of current capabilities and a forward-looking perspective on potential technological evolutions, the study aims to evaluate the operational improvements afforded by these technologies, explores their role in facilitating compliance with increasingly stringent environmental regulations, and anticipates the challenges and opportunities that lie ahead. By doing so, the paper seeks to contribute to the ongoing discourse on maritime innovation, offering insights and recommendations for stakeholders navigating the complexities of modern seafaring.

2. Technological Advancements in Fleet Performance Monitoring

The maritime industry's commitment to innovation has led to significant advancements in fleet performance monitoring technologies. These advancements are pivotal in optimizing operational efficiency, enhancing safety, and ensuring environmental sustainability. The integration of advanced sensor technologies has transformed traditional maritime operations into data-driven decision-making processes.

2.1. Sensor Technologies in Maritime Operations

Sensor technologies have become the cornerstone of modern fleet performance monitoring systems. These sensors, deployed extensively across vessels, collect real-time data on various parameters including engine performance, fuel consumption, cargo load, and navigational efficiency. The data collected offers a granular view of a vessel's operational status, enabling precise monitoring and optimization strategies.

- **Engine Performance Sensors**: Engine performance sensors monitor the mechanical and thermal efficiency of a vessel's engine, providing data on fuel consumption, power output, and engine wear. This information is crucial for predictive maintenance and operational optimization.
- **Fuel Consumption Sensors**: These sensors track the amount of fuel consumed during voyages, allowing for the analysis of fuel efficiency and the identification of strategies to reduce fuel consumption, thereby lowering operational costs and emissions.
- **Cargo and Stability Sensors**: Cargo and stability sensors measure the weight and distribution of cargo, ensuring optimal balance and stability of the vessel. This is essential for safe and

efficient voyages, especially in adverse weather conditions. For some ships, Trim optimization can be extremely beneficial.

- **Navigational Efficiency Sensors**: Navigational sensors, including GPS and AIS, provide real-time data on a vessel's location, speed, and course. This data is used for route optimization, avoiding congested or hazardous areas, and ensuring timely arrivals.

3. Operational Efficiency through Data Analysis

In the maritime industry, the leap towards digitalization, powered by advanced data analytics, has significantly enhanced operational efficiency. The interpretation and application of data collected through sensor technologies lead to optimized maritime operations, emphasizing fuel efficiency, predictive maintenance, and route optimization.

3.1 Fuel Efficiency and Environmental Sustainability

The quest for fuel efficiency is at the heart of maritime operational improvements, given its direct impact on operational costs and environmental sustainability. Advanced data analytics enable ship operators to analyze fuel consumption patterns in real-time, facilitating adjustments that lead to significant fuel savings and emission reductions. Techniques such as weather routing, speed optimization and trim optimization supported by data analytics, have proven effective in enhancing fuel efficiency.

- **Weather Routing**: Utilizing predictive analytics to assess weather conditions and sea states, enabling the selection of routes that minimize fuel consumption while ensuring safety. This approach not only conserves fuel but also reduces greenhouse gas emissions, contributing to environmental sustainability.
- **Speed Optimization**: Data analytics allow for the dynamic adjustment of vessel speed to optimize fuel efficiency. By analyzing data on sea conditions, vessel load, and fuel consumption, operators can determine the most fuel-efficient speed for different segments of a voyage.
- **Trim Optimization**: the constant monitoring of the trim comparing to the optimal one lead to the least power and therefore to the lease consumption.

3.2. Predictive Maintenance

Predictive maintenance represents a significant advancement in maritime operations, enabled by data analytics. By analysing data from various sensors, operators can predict potential failures before they occur, scheduling maintenance activities proactively and avoiding unplanned downtime.

- **Vibration Analysis**: Sensors monitoring engine and machinery vibrations can detect anomalies that precede failures, allowing for timely maintenance interventions.
- **Oil Analysis**: Analysing data on oil properties can provide insights into the health of engines and machinery, predicting when maintenance is required to prevent wear or damage.
- **Alerting system**: having an advanced Alerting system can lead to create very detailed and effective Alert that can help in identifying potential failure before they occur.

Predictive maintenance, underpinned by sophisticated data analysis, not only enhances operational efficiency but also extends the lifespan of maritime assets.

4. Environmental Impact and Regulatory Compliance

In the context of growing environmental concerns and stringent regulatory standards, the maritime industry has increasingly focused on minimizing its environmental footprint while adhering to compliance mandates. Fleet performance monitoring systems play a pivotal role in achieving these objectives, leveraging advanced technologies to ensure operational practices are both efficient and environmentally sustainable.

4.1. Reduction of Environmental Footprint

Advanced fleet performance monitoring systems enable the maritime industry to significantly reduce its environmental impact. By providing real-time data on fuel consumption, emissions, and engine efficiency, these systems facilitate informed decision-making that leads to more sustainable practices.

- **Emissions Monitoring**: Real-time tracking of emissions, such as CO2, NOx, and SOx, helps ensure vessels operate within environmental compliance limits and adopt cleaner practices. The calculation and constant monitoring of these emissions helps in identifying potential issue and potential environmental noncompliance.
- **Fuel Optimization**: Data analytics driven by fleet performance monitoring allows for the optimization of fuel use, substantially reducing greenhouse gas emissions. Strategies include optimizing voyage routes and speeds based on weather conditions and sea states, thus enhancing fuel efficiency.

4.2. Compliance with Global and Regional Environmental Regulations

Fleet performance monitoring systems are not only tools for operational optimization but also mechanisms for ensuring regulatory compliance. With the maritime industry subject to a complex framework of global and regional environmental regulations, these systems provide the necessary data and analytics to navigate compliance challenges effectively.

- **Global Compliance**: The International Maritime Organization (IMO) sets global standards for emissions, waste management, and marine conservation. Fleet performance monitoring systems help operators stay abreast of these requirements, ensuring global compliance through detailed emissions reporting and fuel consumption logs.
- **Regional Regulations**: In addition to global standards, maritime operations must also navigate regional regulations, such as Emission Control Areas (ECAs) and specific national laws like Biofouling Management and Ballast Water treatment. Real-time monitoring and data analysis enable vessels to adjust operations as needed to comply with these varied requirements.
- **Data Collection and ETS**: Of course, we cannot avoid mentioning the Data collection regulation and ETS. Real-time monitoring but most importantly data reliability checks help in identify any issue in regards of the Emission that can cause several amounts of money of penalty.

5. Challenges and Considerations in Implementing Advanced Monitoring Systems

The adoption of advanced fleet performance monitoring systems, while offering significant benefits, also introduces a range of challenges and considerations that must be navigated by the maritime industry. The primary obstacles in the implementation of these technologies and proposes strategies to address them, ensuring successful integration and maximization of benefits.

5.1 Technological Integration and Compatibility

One of the foremost challenges lies in integrating new technologies with existing maritime infrastructure. The heterogeneity of systems across different vessels and fleets can complicate the deployment of unified monitoring solutions.

- **Interoperability Issues**: Ensuring new monitoring systems can communicate and function seamlessly with older technologies onboard is crucial for comprehensive data analysis and operational efficiency.

- **Upgrade Costs**: The financial investment required to upgrade existing systems or retrofit older vessels with new technologies can be significant, potentially hindering widespread adoption. In general, there is the need to invest time and money to get money back.

5.2. Cybersecurity and Data Privacy

As maritime operations become increasingly reliant on digital technologies, the risks associated with cybersecurity breaches and data privacy violations grow. Protecting sensitive operational data against cyber threats is paramount.

- **Cybersecurity Measures**: Implementing robust cybersecurity protocols and systems to safeguard against unauthorized access and cyberattacks is essential.
- **Data Privacy Regulations**: Compliance with international data protection regulations ensures the confidentiality and integrity of collected data.

5.3. Skilled Workforce and Training

The effective utilization of advanced fleet performance monitoring systems requires a workforce proficient in digital technologies. Bridging the skills gap and ensuring personnel are adequately trained poses a significant challenge.

- **Workforce Development**: Initiatives to educate and train maritime personnel in the use of advanced monitoring technologies are critical for their successful implementation.
- **Continuous Learning**: Establishing programs for ongoing training and professional development ensures the workforce remains adept at leveraging new technologies as they emerge.

6. Monitoring towards Efficiency Some Ideas

The implementation of advanced fleet performance monitoring technologies across the maritime industry has yielded significant operational, environmental, and safety benefits. These are some ideas that highlight the successful applications of these technologies and underline, again, why it is vital nowadays to have a Fleet Monitoring system.

6.1 Idea 1: Optimizing Fuel Efficiency through Hull/propeller degradation over time

Monitoring the Hull and Propeller degradation over time using continuous monitoring of Power and Consumption for propulsion is crucial to compare an actual value to a target; such KPI over time can be monitored to detect basically two aspects:

1. The degradation over time can help in identifying which is the degradation limit that we would like to set. I.e. the degradation is now 10% above the expected and the ship will have to wait 1 year and half before next drydock. The operator can monitor the degradation over time and receive an alert if such degradation is around 15%, so it can proceed with an inspection.
2. The effectiveness of an intervention: sometimes, due to the environmental condition or due to not the very best provider or simply just because the Hull or the propeller where too dirty or old the intervention was not effective.

6.2. Idea 2: Enhancing Safety with Predictive Analytics

The system analysed historical data and real-time inputs to predict potential safety incidents before they occurred; using also intelligent Alerting system can led to a potential significant reduction in safety incidents over two years. The proactive approach to safety management significantly reduced downtime and insurance costs. Employing predictive analytics to anticipate and mitigate safety risks can lead to a safer operational environment and reduce the financial impact of incidents.

6.3. Idea 3: Achieving Environmental Compliance through Emissions Monitoring

Facing stringent environmental regulations deploying an emissions monitoring and optimization system across its fleet. The system tracked emissions in real-time, ensuring compliance with global and regional standards. The regulatory requirements are successfully met all, avoiding potential fines and operational restrictions. The system can also identify areas where emissions could be further reduced, supporting the company's sustainability goals. Real-time emissions monitoring systems are essential for ensuring regulatory compliance and identifying opportunities to exceed environmental performance targets.

6.4. Idea 4: Many ships but just one system

Having various age, type and size ships can lead the operators to have multiple system to monitor all the ships. However, having only one platform to monitor all the ships having the same KPI is beneficial and time (and cost) saving.

6.5. Idea 5: Biofouling Management

A system that can collect the position, speed and idling of the ship, but also collect the Inspection, Cleaning, drydock is the perfect tool for Biofouling management. By mapping the riskiest area of the world for fouling and monitoring the speed and time spent idling it is quite simple create alert and analytics to monitor and detect any possible situation that can lead to fouling. This is an example of smart monitoring and preventing excessive consumption nevertheless any issue with regulation.

6.6. Idea 6: Hotel load monitoring and optimization

In the Cruise sector, the Hotel Load monitoring and optimization is a key for enhancing the efficiency of their ships. By mapping all the consumers, it is then possible to see trends, to filter by cruise, weather, season and then identify the area to optimize.

7. Policy Implications and Industry Standards

The evolution of fleet performance monitoring technologies not only transforms maritime operations but also influences the regulatory landscape and industry standards. Regulatory bodies are always trying to standardize but sometimes they fail, or they take long time to create something. It is quite important that every party is represented in this discussion to not privilege any stakeholder of this industry.

7.1. IMO and Classification society

IMO and Classification society already contribute (for better or for worse) into create standard but also helps in complying with such regulation with all verification process. In the latest year Emission has been the focus but there are many areas where it is needed a standardization, for example AMS data ownership and protocol that are very different and very customized. This is, of course, not the fault of the Automation vendors but the problem is that there is not a high-level decision on the property of the data but only some interpretations and there is not a standard communication protocol for the output buy a real jungle of output's languages custom NMEA, Modbus, OPC and analog. This lack of Standardization has only the effect to slow-down all the process and then limit the goal to be achieved (and drive data collection provider very crazy)

7.2. Regional law

From 2017 with MRV we have seen in recent years the continuous creation of new and sometimes quite different regulation from regional entity. Here is the best example of non-standardization because with IMO DCS, EU MRV and UK MRV that coexist that basically have the same aim but with different rules. ETS also enters the game, and it has new rules (different from EU MRV), and more regulation will come. Not only pollutant data collection is affected by this phenomenon, also Ballast water treatment, Biofouling Management, Scrubber and most recently Shapoli.

8. Conclusion

The maritime industry stands at the threshold of a transformative era, propelled by the integration of advanced fleet performance monitoring technologies. Only Emission seems now to have convinced that good data are needed to not waste too much money (thanks to ETS, but let's not forget FUEL EU MARITIME, defined by one customer "the bomb" for the shipping companies)

The journey towards digital transformation is not without its challenges. Technological integration, cybersecurity, data privacy, and the development of a skilled workforce emerge as critical hurdles that must be navigated with strategic foresight. Moreover, the evolving regulatory landscape and the imperative for harmonized industry standards underscore the necessity for collaborative efforts among maritime stakeholders, regulatory bodies, and classification societies.

Looking ahead, the maritime industry must remain agile, embracing continuous innovation and adaptation to leverage the full spectrum of benefits offered by fleet performance monitoring technologies and this is the real challenge because as it is known the maritime industry is the very last that apply technology.

The active participation of maritime operators in policy advocacy and standard development is crucial for aligning regulatory frameworks with technological advancements, ensuring that the industry moves forward cohesively and sustainably.

In conclusion, the future of maritime operations is undeniably digital. The successful integration of advanced monitoring systems promises not only to optimize operational practices but also to redefine the industry's environmental footprint and safety protocols. As the maritime sector sails into this new digital horizon, it does so with the potential to achieve unprecedented levels of efficiency and sustainability, marking a new chapter in the age-old narrative of seafaring.

As the industry continues to evolve, it is the collective responsibility of all maritime actors to steer towards a future where technology and tradition sail in unison towards safer, cleaner, and more efficient horizons.

References

BARSOTTI, M. (2021), *Road to digitalization, not so simple*, 13th HIPER Conf., Tullamore, http://data.hiper-conf.info/Hiper2021_Tullamore.pdf

Assessing Marine Coating Performance on Full-Scale Ship using an Experimental Channel-Flow Setup

Zakari Midjiyawa, Irma Yeginbayeva, Angelika Brink, Jotun, Sandefjord/Norway,
Zakari.midjiyawa@jotun.com

Abstract

This study provides valuable insights into hydrodynamic performance and fuel efficiency of different coating types and roughness in a steady-state simulation of a container ship. The simulation process involves the use of computational fluid dynamics (CFD) software, which can model the flow around the ship's hull without head of oblique incoming wave effects. Initially, the experimental channel flow tests were used to measure the frictional drag of different marine coatings and application finishes. The relationship between the coating roughness and frictional drag was quantified using empirical correlations, which relate the frictional characteristics of coatings to combination of roughness parameters. As a result, a roughness function is derived and used as input to CFD simulation to improve the accuracy and reliability of the simulation results. The CFD software incorporates the effects of different coating types and roughness on the hull and provides a range of performance parameters, including viscous, pressure and total resistance under steady-state condition as a baseline study. By comparing the performance parameters of ships with different coating types and roughness, the simulation can identify the optimal combination of coating type and roughness that provides the best hydrodynamic performance and fuel efficiency.

1. Introduction

The combination of channel flow facilities and CFD simulations provides an effective approach for investigating roughness effects on hydrodynamic performance. The roughness allowance in the ITTC (International Towing Tank Conference) is a simplified approach based on empirical formulae that may fail to account for the effects of current coatings with low variable roughness values, *ITTC (1978)*. The results from the channel flow facility, along with CFD simulations, provide a more comprehensive and flexible tool for studying and isolating the impacts of coating roughness on flow behaviour. Our experimental approach, combined with CFD simulations, addresses the limitations of older roughness allowance models, allowing authors to obtain more accurate roughness functions and gain a better understanding of the flow behaviours of modern coatings under in-service surface conditions, as was performed in previous research studies, *Yeginbayeva (2017), Schultz et al. (2015), Murphy et al. (2018)*. This information could be extremely useful in optimizing the coating application areas and performance of various marine vessels.

Here are some key points that emphasize the benefits of channel flow facility and CFD simulations for studying roughness effects of hull coatings:

- Isolation of Roughness Effects: channel flows allow researchers to isolate the influence of roughness without the confounding effects of external factors present in the testing vessel since it has a well-defined boundary condition, *Monty (2005)*. By conducting controlled experiments with different coating types and roughness values systematically and under high Reynolds number regimes (Re_m≈215000), researchers can quantify the specific impact of roughness on flow patterns, drag, and boundary layer characteristics, *Schultz et al. (2000), Schultz and Flack (2013)*. In contrast, the ITTC Performance Prediction Model is primarily based on empirical formulations derived from towing tank experiments *Demirel et al. (2015), Kiosidou et al. (2017)*, and its applicability might be limited to specific vessel shapes and conditions. It can be challenging to precisely isolate the roughness effects in towing tanks, especially when other factors like scale effects, model shape, and boundary conditions come into play. In addition, corrections to adapt to different vessel types or operating conditions are required. The towing tank method may not allow as much customization as CFD simulations in terms of complex geometries and flow conditions.

- Generating Roughness Functions: Channel flow experiments can provide valuable data to establish roughness functions for different coating types. These functions describe the relationship between the roughness height and the resultant skin frictional drag or velocity profile alterations, *Ligrani and Moffat (1968)*, *Shapiro (2004)*. These very coating specific functions can then be incorporated into CFD simulations, allowing the simulation of real-world conditions with varying roughness.
- Improved Accuracy: The combination of channel flow experiments and CFD simulations offers a more accurate and reliable method to predict the impact of a specific coating on the vessels drag. By incorporating real roughness data into CFD models, researchers can achieve more accurate predictions of velocity profiles and boundary layer development.
- Application to Modern Coatings: with advancements in coating technologies and improved application techniques, the roughness characteristics of modern coatings may differ significantly from traditional surfaces. Traditionally, a standard value of k_s=150 μm has been inputted in the roughness allowance equation, ΔC_F. Here k_s indicates the roughness of hull surface and the roughness allowance ΔC_F per definition describes the effect of the roughness of the hull on the resistance, *ITTC (1978)*. Channel flow facility and CFD simulations provide a flexible platform to investigate and account for these new coating types' effects on hydrodynamic performance (that could be a drag increase or reduction) more accurately.

The primary aim of this paper is to evaluate the performance of selected hull coatings under the steady-state numerical simulations of full-scale vessels using experimental channel-flow data as input. Our research seeks to provide valuable insights into the performance of different coatings, applied both in ideal laboratory conditions and simulated worst case dry-dock scenarios. By comprehensively evaluating the coatings' hydrodynamic behaviour in these controlled and roughened settings, the study aims to offer a holistic understanding of their impact on hydrodynamic resistance. By conducting this baseline study, the study can pave the way for future research to explore more complex scenarios that involve dynamic changes in flow like waves and propeller and biofouling effects. To accomplish the aim of this study, the following objectives are outlined:

- Measuring the pressure-drop in channel flows with different marine coatings under varying flow velocities;
- Utilizing the pressure drop data to calculate roughness functions as input for Computational Fluid Dynamics (CFD) simulations, enabling the assessment of coating effectiveness in mitigating resistance in the steady-state numerical simulations;
- Compare the performance of novel coating formulations with conventional coatings to identify potential improvements and areas for further research.

While channel flows may have certain limitations regarding representing large-scale flow structures, their use in conjunction with CFD simulations and roughness functions can significantly enhance the understanding of coating performance and its impact on full-scale vessels. This combined approach offers a powerful toolset for researchers to investigate and optimize coating designs and configurations for improved hydrodynamic performance.

2. Methods

2.1. Test samples

By applying coatings in the controlled laboratory environment, the study aimed at ensuring precise and consistent application methods for different coating types which encompass a diverse range of properties that promise enhanced hydrodynamics and improved resistance to fouling. However, it is acknowledged that complex environments and dynamic conditions are encountered by real-world marine vessels during dry-docking and operations. Therefore, to bridge the gap between controlled laboratory experiments and practical applications a roughness was deliberately introduced to some of the test coatings. In the Table I, the various coatings used in our research are classified based on surface type: coatings denoted with an 'R' signify 'Rough' surfaces simulating the roughness encountered during dry-docking conditions, while coatings denoted with an 'S' represent 'Smooth' surfaces applied in a controlled laboratory environment. Table I also includes smooth (PMMA) and rough reference (Course silicon grit) surfaces to facilitate the classification of coating results in terms of their hydrodynamic performances.

Table I. Surface types and corresponding surface characteristics

Coating type	Surface condition	Description	2D roughness profiles
Smooth reference	Nominally smooth surface used as a reference surface to evaluate the effectiveness of different coatings in reducing or increasing hydrodynamic drag	Poly (methyl methacrylate) (PMMA) which is commonly known as acrylic or plexiglass	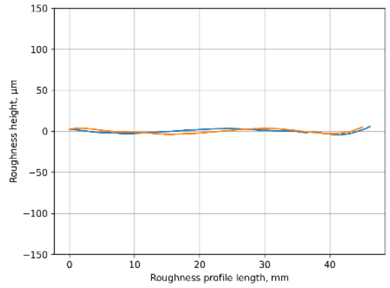
Course silicon grit	Rough reference	F80 silicon carbide particles with average grain size of 150-212 µm	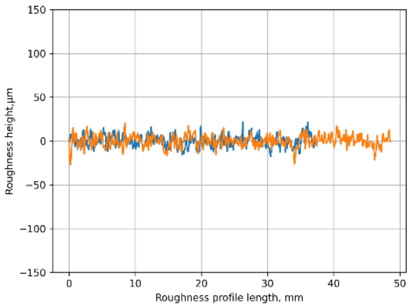
Sea-Quantum X200-S	Applied in controlled laboratory conditions	A high-performing self-polishing coating with resistance-mitigating properties	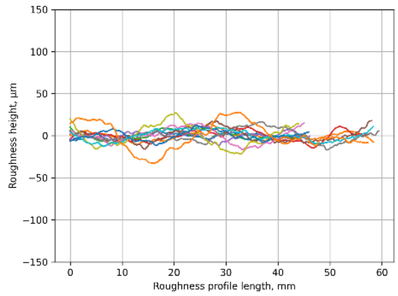
Sea-Quantum X200 -R	Rough surface deliberately roughened to simulate dry-docking conditions	A high-performing self-polishing coating with resistance-mitigating properties	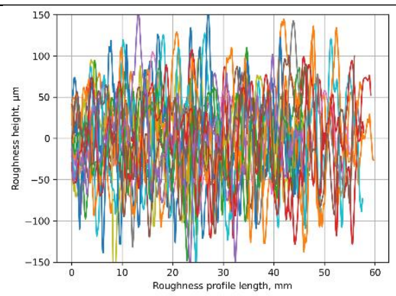

SeaQuest Endura-S	Applied in controlled laboratory conditions	A state-of-the-art biocide-infused silicone-based coating	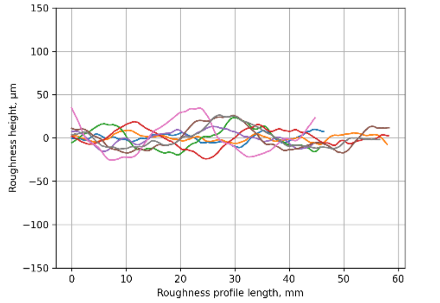
SeaQuest Endura -R	Rough surface deliberately roughened to simulate dry-docking conditions	A state-of-the-art biocide-infused silicone-based coating	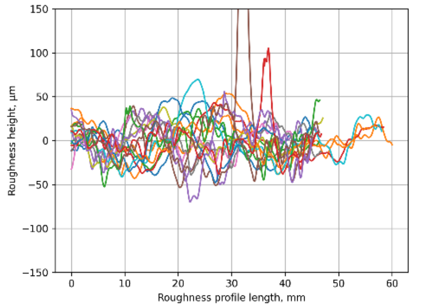
New Product	Applied in controlled laboratory conditions	A hybrid coating with a smooth, silk-like finish	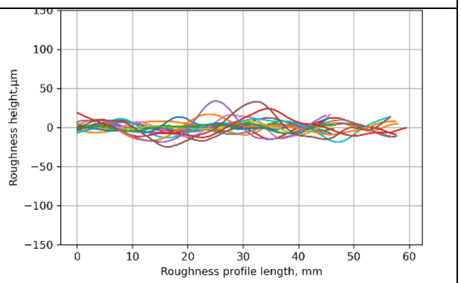

2.2. Experimental study and roughness function calculations

The surfaces presented in Table I were subjected to drag testing in our experimental channel-flow setup, allowing us to observe their behaviour under realistic hydrodynamic conditions. The technical details of the flowcell device installed at Jotun and the experimental setup can be found in *Yeginbayeva et al. (2022)*. By employing the pressure drop methodology, which involves measuring the pressure drop across the surface in the channel flow within wide range of velocities, the effects of coatings on skin friction under different flow velocities is captured. The pressure drop over a channel surface can be related to the skin friction of the surface.

The roughness function derived from the wide range roughness parameters offers a more refined representation of the coating's roughness effects. It captures the nuanced relationship between surface characteristics and skin friction across different flow velocities:

$$(\Delta U^{+})_{rough} = \left(\sqrt{\frac{2}{C_f}}\right)_{smooth} - \left(\sqrt{\frac{2}{C_f}}\right)_{rough} - 19.7\left[\left(\sqrt{\frac{C_f}{2}}\right)_{smooth} - \left(\sqrt{\frac{C_f}{2}}\right)_{rough}\right] \tag{1}$$

Where ΔU^{+} is a dimensionless velocity decrement, C_f-skin frictional coefficient. ΔU^{+} is typically used to describe turbulent boundary layer flows over rough surfaces. It is a measure of how the velocity near the wall differs from what it would be in a smooth (no roughness) boundary layer. k^{+} is another dimensionless parameter used to characterize the effects of surface roughness. It represents the roughness

Reynolds number and provides information about the size and distribution of roughness elements on the surface. $k^+$is calculated as the height of the roughness elements or k (typically normalized by the boundary layer thickness, δ) divided by the viscous length scale ($\frac{\nu}{u^*}$), where ν is the kinematic viscosity of a fluid and u^* is the friction velocity or $k^+ = \frac{ku^*}{\nu}$. In the ITTC method, the coating roughness is based on a single velocity and a single roughness parameter, such as *Rt50* (the highest peak to lowest valley roughness sampled over 50 mm of evaluation length). This approach can be limiting and may not fully capture the coating finish. The roughness function approach allows for the consideration of various roughness parameters beyond just *Rt50*. It can encompass a broader set of roughness characteristics, such as height distributions, shape factors, and spatial arrangements, depending on the complexity of the coating surface. This flexibility enables a more realistic representation of the coating's impact on skin friction, making the roughness function a more adaptable and robust tool for numerical simulations. The foundation of our roughness investigation lies in the meticulous collection and analysis of roughness data. To achieve this, an optical surface profilometry was used scanning each coating sample to obtain a comprehensive representation of its surface as can be seen in Table I. As a result, we have derived an encompassing mathematical function that serves as a robust representation of the coatings roughness length scale:

$$k = 1.9 \times \left(\frac{R_t}{S_m}\right) \times R_t \times e^{R_{sk}} \times e^{R_{ku}} \tag{2}$$

k denotes the roughness length scale, capturing the characteristic dimensions of the roughness features.
R_t signifies the peak-to-valley roughness.
S_m corresponds to the spatial roughness parameter, representing the average spacing between surface features. Smoother surfaces inherently exhibit more widely spaces features, leading to a larger S_m, while rougher surfaces tend to have smaller S_m values.
R_{sk} represents skewness, capturing the asymmetry in the height distribution of the surface
R_{ku} stands for kurtosis, reflecting the sharpness of the profile peaks.

The use of these parameters in the roughness length scale serves a vital purpose. Importantly, the inclusion of the spatial roughness parameter, S_m, R_{sk} and R_{ku}, in the equation accounts for the distinctive arrangement of roughness features on the surface. The ratio $\frac{R_t}{S_m}$ captures the relative amplitude of surface variations to their distance, allowing us to discern finer details in the surface profile. The exponential terms $e^{R_{sk}}$ and $e^{R_{ku}}$ enhance the function's sensitivity to asymmetry and sharpness of the surface profile, respectively.

2.3. CFD simulations

The numerical simulations are performed using *foam-extend* version 5.1 coupled with the commercial extension Naval Hydro Pack developed by WIKKI, http://wikki.co.uk/. The commercial extension has been validated for steady resistance, sea keeping, manoeuvring and free sailing simulations with and without propulsion using Overset meshing techniques. The interface capturing methods includes both VOF and LevelSet. Turbulence in Naval Hydro Pack is modelled using the ordinary k – ωSST as well as the corrected k – ωSST. The use of the ordinary k – ωSST leads to unusually high turbulence viscosity at the interface, *Larsen and Fuhrman (2018)*.

The VOF method, which is widely used in numerical hydrodynamics for interface capturing, offers the advantages of simple implementation and computational efficiency. In addition, it is well suited for large scale phase separation. However, it can lead to interface smearing or numerical ventilation, *Gray-Stephens (2019)*. This, sometimes, can lead to inaccurate estimation of wetted surface and ship viscous resistance. In this study, the LevelSet technique is used despite the additional computation effort.

2.4. Surface characteristics and numerical implementation

The different surfaces described and quantified in section 2.1 are summarized in Fig.1 and Fig.2. Fig.1 presents the flat plate skin frictional coefficients corresponding to the different surfaces designed at Jotun. The curves presented in Fig.1 serve as fundamental insights into the interplay between surfaces and fluid dynamics, crucial for enhancing hydrodynamic efficiency and optimizing drag reduction strategies: the SeaQuantum-S maintains the drag levels exactly as the smooth reference even under turbulent flow conditions or higher Reynolds numbers. Conversely, the SeaQuantum-R, deliberately roughened to simulate dry-docking conditions, exhibit an abrupt increase as the flow starts, attesting to the dominance of roughness induced turbulence at all flow velocities which ranges from 1m/s to 11 m/s. When comparing the SeaQuantum-R to the rough reference represented by a course silicon grit, this suggests a noteworthy similarity in terms of roughness characteristics and the resulting skin frictional behaviour. Roughness and drag performance vary when silicon coating or SeaQuest Endura-R are treated with a comparable kind of roughness, such as those found in SeaQuantum-R. This results in a significant reduction of roughness parameters, approximately two times lower, and a considerable decrease (38-45% over a tested Reynolds numbers) in skin friction characteristics for coatings with a biocide infused silicon-based coating. This difference in performance can be attributed to several factors, including the specific properties of the coatings, and how these properties interact with the fluid flow. It implies that even if two coatings have similar underlying roughness, other factors in their composition or structure can significantly affect their frictional behaviour.

The curve for New-product throughout all range of Reynolds numbers remains below the smooth reference curve reflecting its ability to maintain low resistance. This performance unveils the products' finely tuned silk-like surface texture to delay the onset of turbulent flow, to minimize drag and increase its hydrodynamic efficiency.

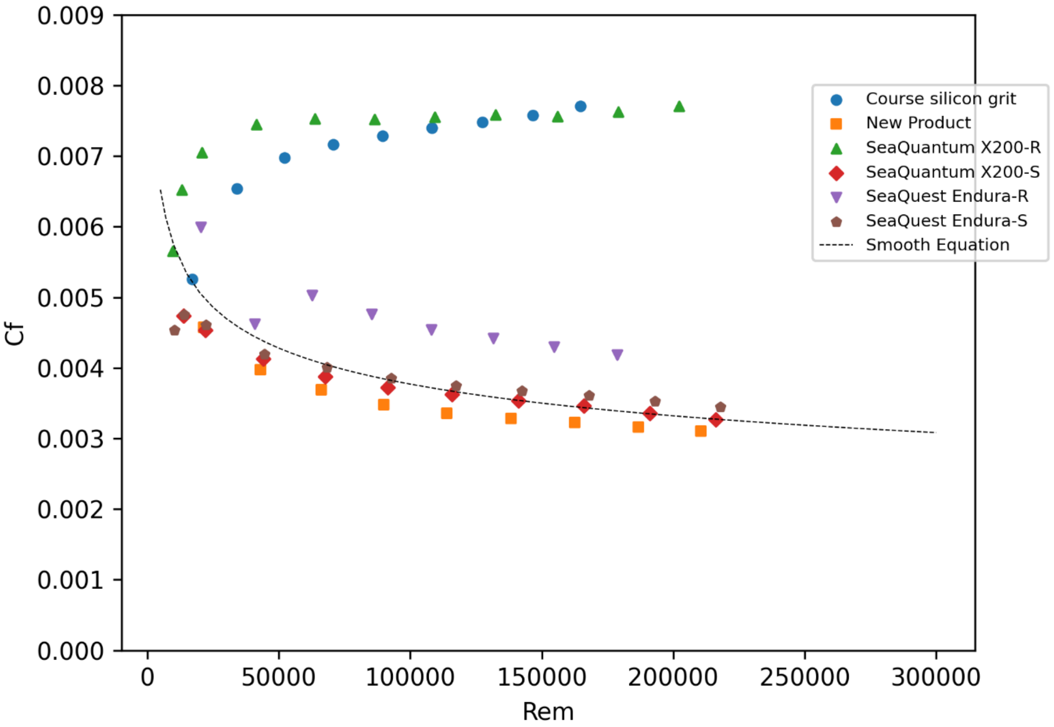

Fig.1: Skin frictional coefficients of tested surfaces as a function of Reynolds number

Fig.2 shows the velocity decrement function caused by the frictional drag of the different rough surfaces. Referred also as roughness function, $\Delta U^+ = f(k^+)$, it helps researchers understand the relationship between surface characteristics (such as texture, irregularities, or roughness height) and the resulting frictional drag. In Fig.2, k or the roughness length scale is derived from various roughness parameters as shown in Eq.(2). The roughness curves for SeaQuantum-R and Course silicon grit are steeper on the upward slope, this means that as the parameter (e.g., Reynolds number) increases, the effect of surface roughness on the skin frictional drag increases rapidly. While others have a monotonic roughness function with a more straightforward relationship.

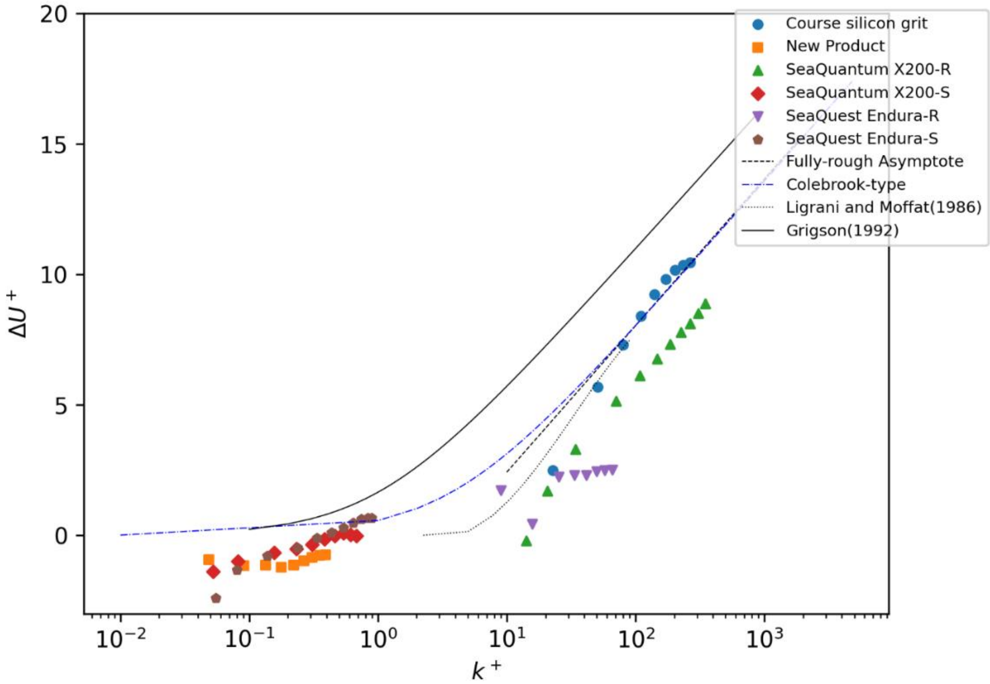

Fig.2: Relationship between roughness function, ΔU^+, of the surfaces and roughness Reynolds number k^+, based on roughness length scale shown in Eq.(2)

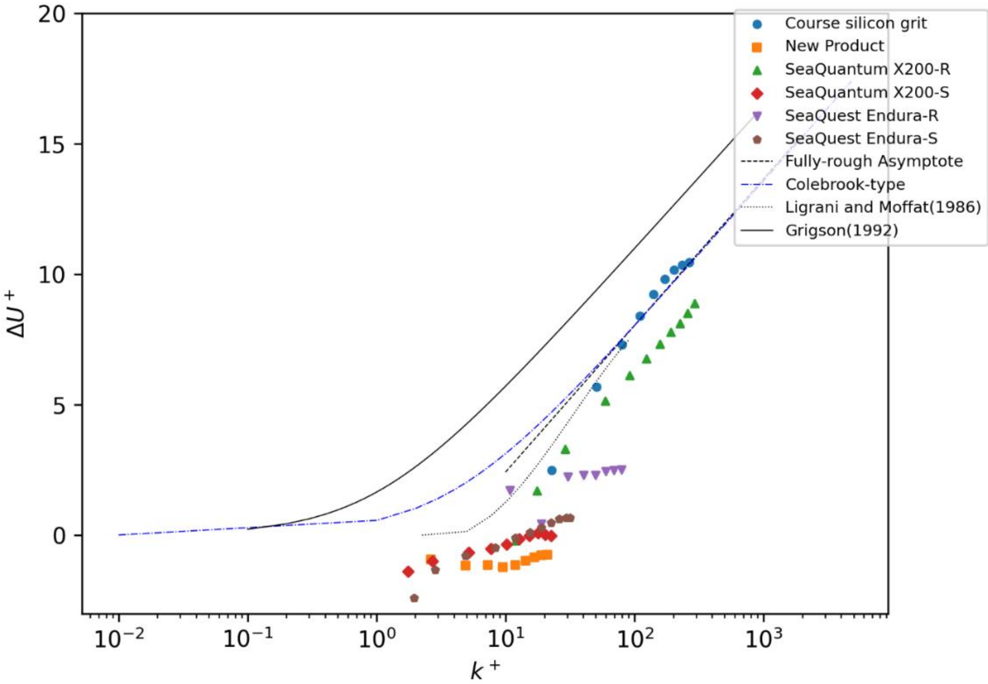

Fig.3: Relationship between roughness function, ΔU^+, of the surfaces and the roughness Reynolds number, k^+, based on roughness length scale, $k = 1.9xR_t$

The relationship between $\Delta U^+$and $k^+$was established by fitting an equation to experimental data points in Fig.2. This fitting was applied to all data sets except for the one associated with coarse silicon grit. Given that coarse silicon grit serves primarily as a reference and is rarely encountered in practical applications, fitting a model or function to the data points of this surface type is not typically necessary or relevant. The roughness function, as originally described in *Clauser (1956)*, has been implemented in OpenFOAM. The wall function formulation used for flows over rough solid wall was modified by introducing the coefficients obtained through regression analysis based on the experimental work to represent the various coated surfaces employed in this study.

Fig.3 shows the relationship between $\Delta U^{+} = f(k^{+})$, when k is based on R_t parameter only obtained from laser profilometer measurements. As opposed to Fig.2, Fig.3 demonstrates an increasing gap between coatings with similar, smooth roughness profiles (see Table I) such as SeaQuantum X200-S, SeaQuest Endura-S and New Product. However, when multiple parameters are considered, Fig.2, these coatings collapse onto a single line of Colebrook-type monotonic curve. This observation suggests that the choice of roughness parameter used to define the roughness length scale can have a significant impact on the behaviour of an experimental data. When R_t parameter is used in isolation, it might not fully capture all the nuances of the surface, resulting in a wider spread of data since surfaces with similar R_t values may have different textures. A "different texture" in this context means variation in the arrangement, density and spacing of the roughness elements on a surface.

3. Geometry and numerical set-up

The ship used in this study is the KRISO (Korea Research Institute of Ships & Ocean) Container Ship (KCS), Fig.4, Table II, https://simman2014.dk/ship-data/moeri-container-ship/geometry-and-conditions-moeri-container-ship/. The simulation is performed in full scale for a ship with LBP ≈ 230 m. The KCS ship, together with the KVLCC2 (Korean Very Large Crude Carrier), are some of the ships widely used for benchmarking studies in theoretical and experimental hydrodynamics which motivates the use of the KCS in this study.

Fig.4: KRISO Container Ship

Table II: KCS characteristics

Length between the perpendiculars (LBP)	230.0 m
Length of waterline (LWL)	232.5 m
Beam at waterline (BWL)	32.2 m
Depth (D)	19.0 m
Design draft (T)	10.8 m
Displacement (Δ)	52,030 m^3
Block coefficient (CB)	0.6505
Ship wetted area with rudder (S)	9539 m^2
Longitudinal centre of gravity (LCG) from the aft peak	111.603 m
Vertical centre of gravity (KG) from keel	7.28 m
Moment of inertia (Kxx/B)	0.40
Moment of inertia (Kyy/LBP, Kzz/LBP)	0.25

The computational domain is illustrated in Fig.5, and the surface resolution in Fig.6. The domain extends one and half ship length from the ship forward to the inlet boundary. This ensures that the inlet is not affected by ship generated waves in the steady resistance simulations. Two ship lengths from the aft to the outflow and one ship length from the port and starboard sides to the side boundaries of the computational domain. The choice of these domain extension guarantees the development of wake flows from the aft, non-reflection, and non-diffraction of waves at the computational boundaries.

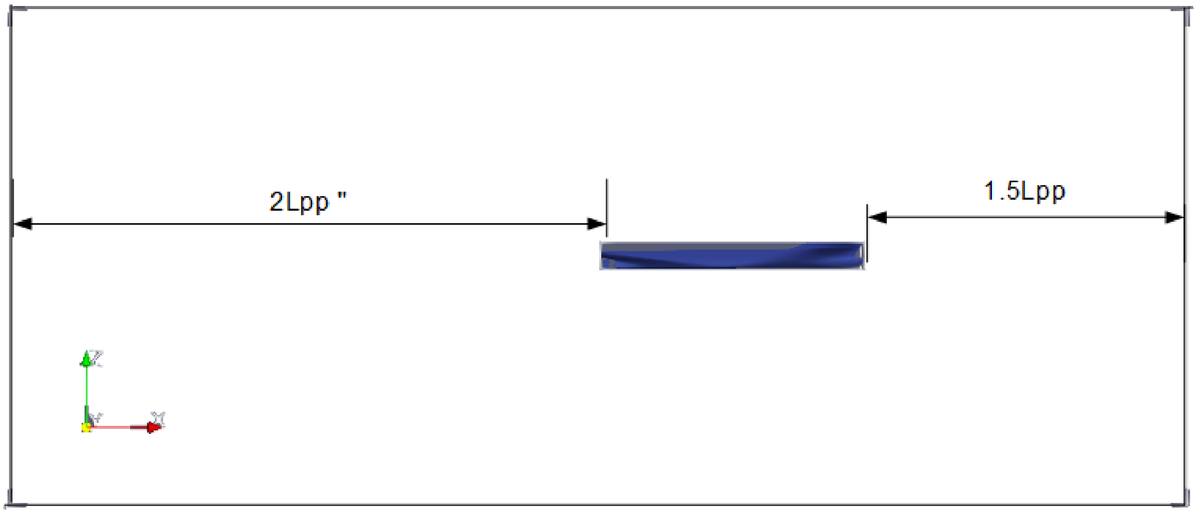

Fig.5: Computational domain

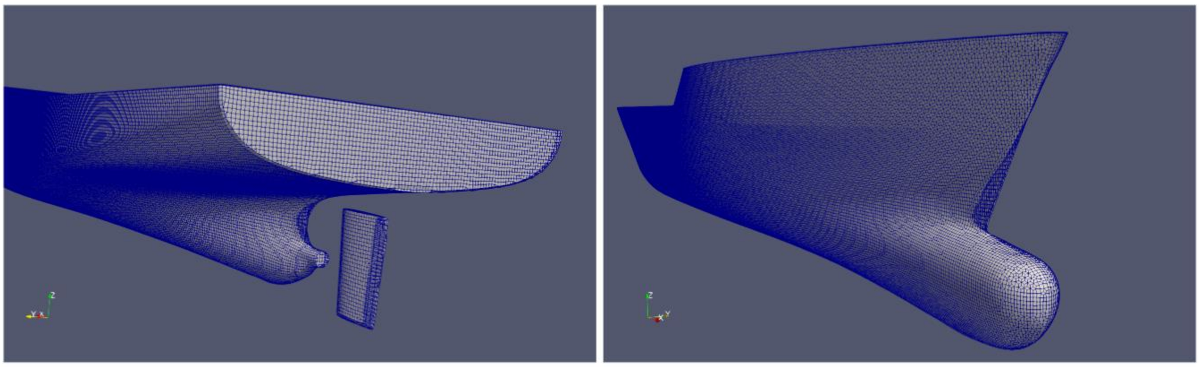

(a) Hull surface grid viewed from aft. (b) Hull surface grid viewed from forward.

Fig.6: Hull surface mesh resolution

4. Results

4.1. Wetted area and pressure distribution

The wetted area and pressure distribution for the smooth surface is shown in Fig.7. The result shows the interface with clear distinction between water and air. The numerical ventilation sometimes observed in methods involving VOF interface capturing is not observed in this study. As the ship sails through a calm sea, in the steady resistance set-up, ship generated waves can be observed via wetted surface profile as seen from the results. The corresponding dynamic pressure are also given in the same figure. The bulbous bow records the maximum local pressure as expected.

The ship generated Kelvin waves are shown in Fig.8. The results are shown for the New Product, SeaQuest Endura-S, and SeaQuantum X200 (R and S). The maximum waves elevation is ~3.3 m for all the cases. However, there is a slight discrepancy between the maximum elevation at the wake for SeaQuantum X200-R. This suggest that further studies involving waves should be performed to understand the impact of surface coatings on the flow profiles and well as ship motions which might have a considerable impact on the resistance and corresponding carbon footprint.

The corresponding turbulent kinetic energy (TKE) is also shown in Fig.9. Even though the general highest TKE is obtained at the interface due to the ship generated waves, it can also be seen that the SeaQuantum X200-R, which corresponds to the roughest surface, has the highest TKE at the surface. This suggest that coating method of application has a considerable influence on the turbulence generation at the surface and, consequently, increase in viscous resistance. This agrees with the result obtained in *Demirel et al. (2017)*, whereby some relationship is observed between increase in TKE and resistance when the surface is characterised by considerable fouling.

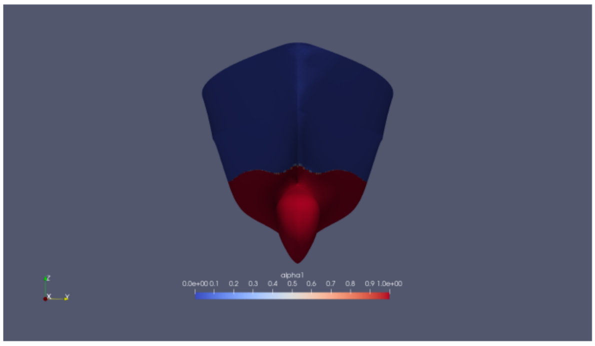

(a) Free surface representation on the ship hull viewed from forward.

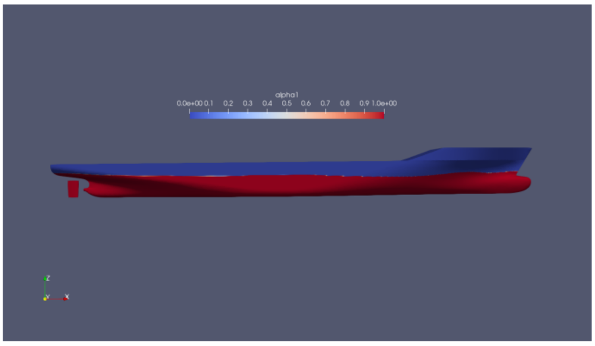

(b) Free surface representation on the ship hull viewed from starboard.

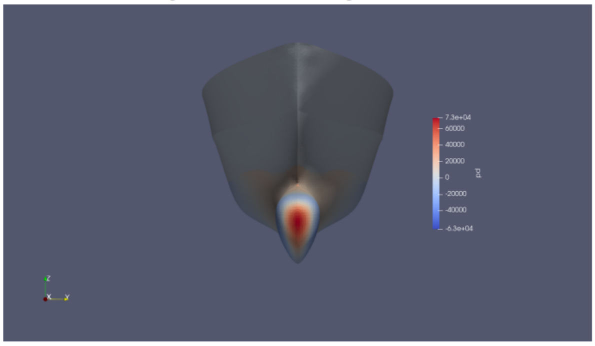

(c) Dynamic pressure distribution viewed from forward.

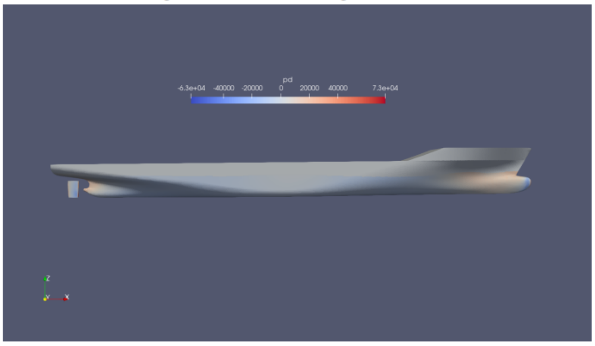

(d) Dynamic pressure distribution viewed from starboard.

Fig.7: Estimated free surface elevation and dynamic pressure distribution for reference smooth case

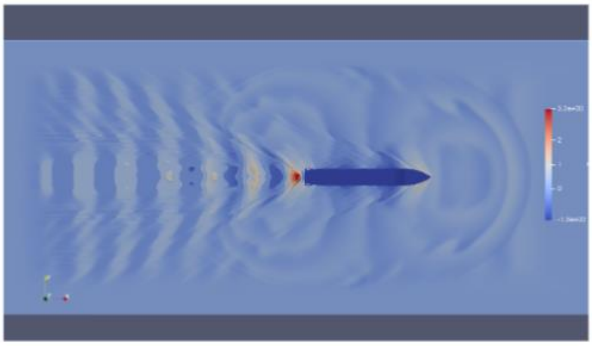

(a) New Product

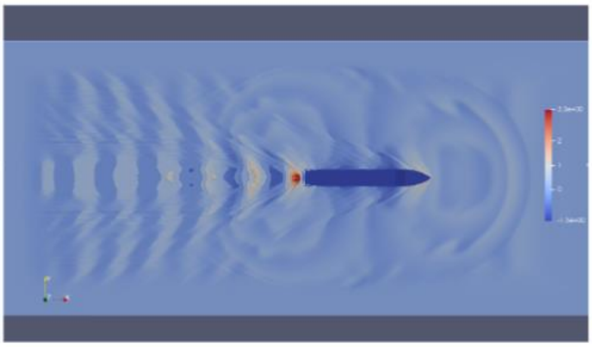

(b) SeaQuest Endura-S

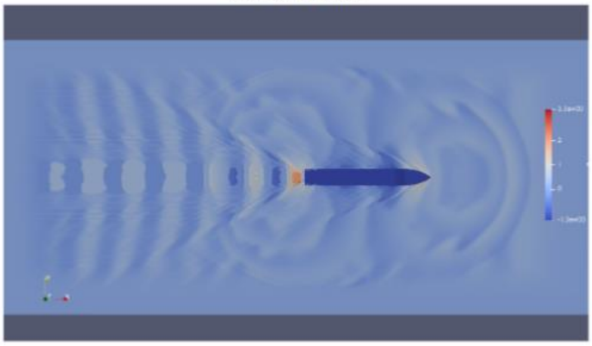

(c) SeaQuantum X200-R

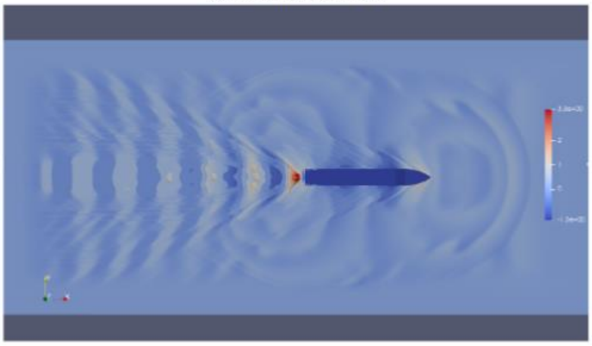

(d) SeaQuantum X200-S

Fig.8: Estimated Kelvin waves with the corresponding surface elevation in metres for the New Product, SeaQuest Endura-S, SeaQuantum X200 (R and S).

4.2. Steady resistance for various surface and various Froude numbers

The steady resistance result for the various cases is shown in Fig.10. The results are shown for Smooth Reference, SeaQuest Endura (R and S), and SeaQuantum X200 (R and S). Non-dimensional viscous drag coefficients are shown for five Froude numbers. In general, the total viscous drag force increases as the speed increases which corresponds to an increase in Froude number. This is because the faster the ship moves, the larger the wetted surface and the higher the wall shear stresses. The viscous forces not shown here show a similar pattern. However, the use of the drag coefficients which show a decrease with respect to increasing Froude number has been preferred in this paper since non-dimensional value can be easily used in comparing various results from various research.

The Smooth Reference drag coefficients range from 1.25E-03 to 1.34E-03, Table III. The New Product coated surface shows the lowest drag coefficient which ranges from 1.19E-03 to 1.27E-03. This corresponds to a reduction of around 5% in resistance estimation from the standard Smooth Reference. The SeaQuantum X200-R coated surface gives the highest drag coefficient. This represents approximately 25% increase in drag coefficient compared to the Smooth Reference case. However, the SeaQuest Endura-R shows around 10% increase in drag coefficient. The SeaQuest Endura-S and SeaQuantum X200-S show drag coefficient close to Smooth Reference but higher than the New Product coated surface.

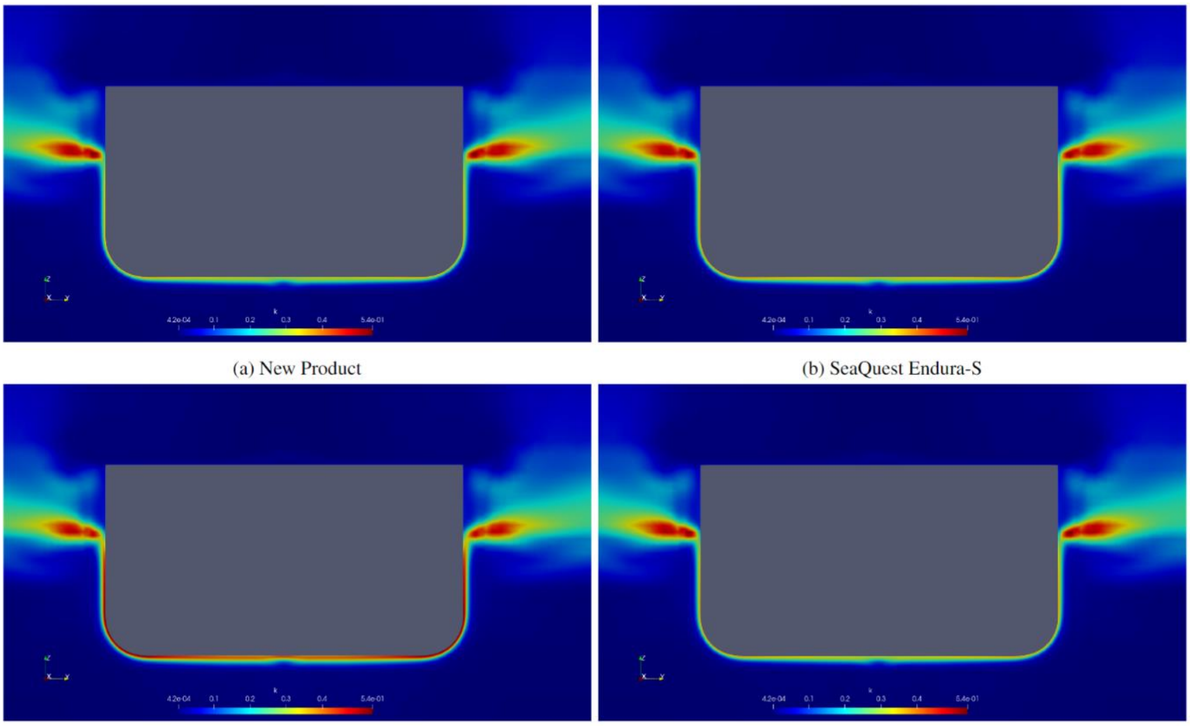

(a) New Product (b) SeaQuest Endura-S

(c) SeaQuantum X200-R (d) SeaQuantum X200-S

Fig.9: Estimated TKE for the New Product, SeaQuest Endura-S, SeaQuantum X200 (R and S) view for a cut at mid-section of the KCS ship

Table III: Percentage change in viscous drag for various surface coatings

Fn	*Smooth Ref.*	*SeaQuest Endura-R*	*SeaQuest Endura-S*	*SeaQuantum X200-R*	*SeaQuantumX200-S*	*New Product*
0.20	1.34E-03	9.79%	-0.07%	24.58%	-1.52%	-5.17%
0.24	1.30E-03	9.67%	0.52%	25.41%	-0.88%	-4.98%
0.26	1.28E-03	9.64%	0.75%	25.58%	-0.66%	-4.86%
0.28	1.26E-03	9.76%	1.00%	26.14%	-0.50%	-4.79%
0.30	1.25E-03	9.75%	1.16%	26.99%	-0.28%	-4.63%

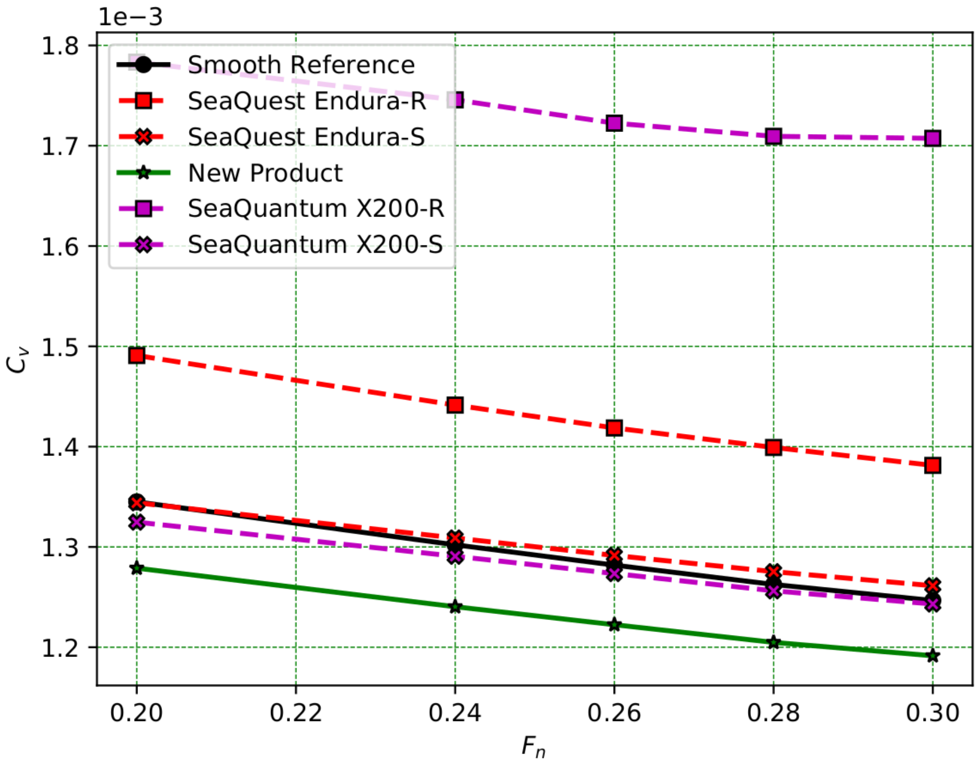

Fig.10: Estimated viscous resistance at various Froude numbers for the smooth reference, new product, SeaQuest Endura (Rough and Smooth) and SeaQuantum X200 (R and S).

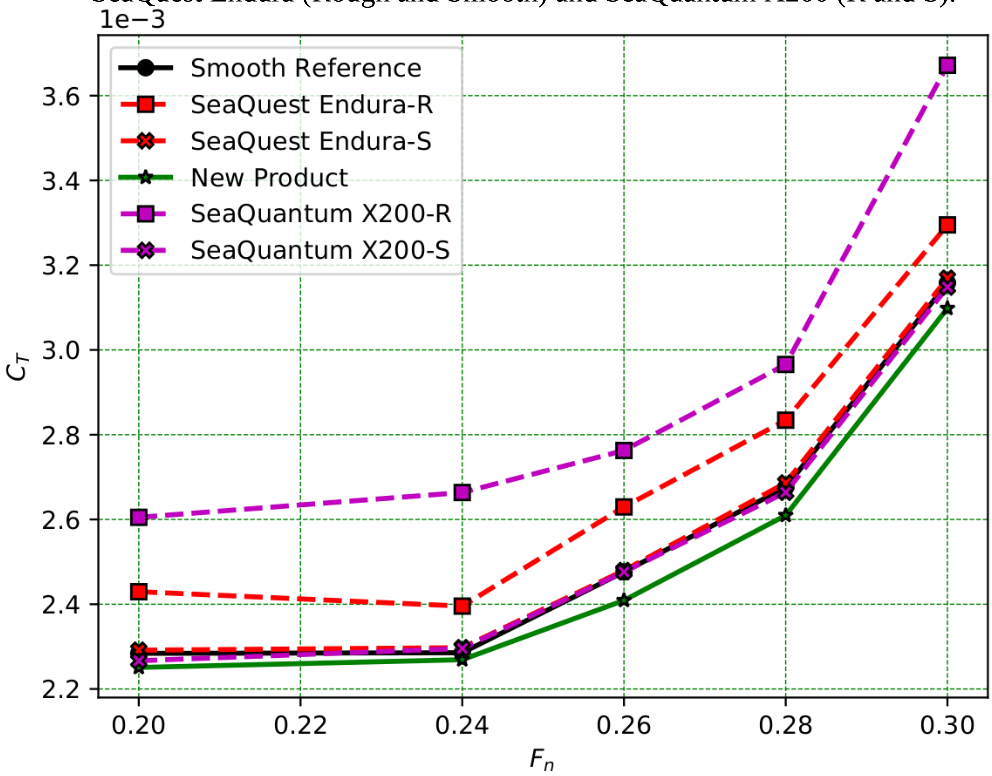

Fig.11: Estimated total resistance at various Froude numbers for the smooth reference, new product, SeaQuest Endura (Rough and Smooth) and SeaQuantum X200 (R and S).

The total resistance coefficient is shown in Table IV and Fig.11. The results show increasing resistance with increasing Froude number. This is because the pressure resistance increases with increasing Froude number. As expected, the smooth SeaQuantum-S and SeaQuest-S are closer to the Smooth Reference total resistances while the New Product shows the lowest total resistance. Like viscous drag result, the

SeaQuantum X200-R gives the highest total drag increase which is given in the range of 13 % compared to smooth reference.

Table IV: Percentage change in total drag for various surface coatings

Fn	*Smooth Ref.*	*SeaQuest Endura-R*	*SeaQuest Endura-S*	*SeaQuantum X200-R*	*SeaQuantum X200-S*	*New Product*
0.20	2.28E-03	5.99%	0.33%	12.32%	-0.77%	-1.48%
0.24	2.29E-03	4.59%	0.52%	14.20%	0.44%	-0.72%
0.26	2.48E-03	5.83%	0.13%	10.37%	0.00%	-2.79%
0.28	2.68E-03	5.59%	0.39%	9.78%	-0.44%	-2.53%
0.30	3.16E-03	4.16%	0.36%	13.99%	-0.31%	-1.93%

5. Conclusions

The present work investigates large container ship viscous resistance using experimental and numerical simulation. Frictional resistances from different coatings are measured and their corresponding roughness function are used in numerical computation. The full-scale resistance is estimated in steady-state condition without incoming head or oblique waves. The results are presented with respect to various Froude number. Since propulsion has not been included, fixed velocity has been specified instead of propulsive power. The findings are summarized as follows:

- The new roughness length scale offers a more nuanced analysis of its impact on flow phenomena. By capturing a broader range of roughness characteristics, it contributes to more accurate predictive capabilities of the in-house CFD model.
- Highest resistances are obtained for SeaQuantum X200-R which can be attributed to the underlying roughness introduced deliberately to simulate dry-dock coating application.
- SeaQuest Endura-S and SeaQuantum X200-S have resistance close to Smooth Reference case.
- The lowest resistance is found in the newly developed coated termed here as New Product. The lowest resistance observed for this coating can be attributed to its unique hybrid composition, silk-like surface finish, optimized surface energy, and the controlled laboratory conditions in which it is applied.

The use of steady resistance simulation has been able to give a general quantification of viscous drag coefficient for the various coatings analysed. However, a complete hydrodynamic performance is required to conclusively quantify the various effects of these different surfaces. Further studies such as sea keeping and free sailing under head or oblique might be necessary to supplement the present work.

References

CLAUSER, F.H. (1956), *The Turbulent Boundary Layer*, in Advances in Applied Mechanics, Elsevier, pp.1-51

DEMIREL, Y.K.; TURAN, O.; DAY, S. (2015), *Experimental Determination of Added Hydrodynamic Resistance Caused by Marine Biofouling on Ships*, 4th Int. Conf. Advanced Model Measurement Technology for Maritime Industry (AMT'15), Istanbul

DEMIREL, Y.K.; TURAN, O.; A. INCECIK, A. (2017), *Predicting the Effect of Biofouling on Ship Resistance using CFD,* Applied Ocean Research 62, pp.100-118

GRAY-STEPHENS, A.; TEZDOGAN, T.; DAY, S. (2019), *Strategies to Minimise Numerical Ventilation in CFD Simulations of High-Speed Planing Hulls,* ASME 2019 38th Int. Conf. on Ocean, Offshore and Arctic Engineering

ITTC (1978), *1978 ITTC Performance Prediction Method:Resistance and Propulsion Committee of the 29th ITTC*, Ch. 7.5 – 02- 03 – 01.4., p.19

KIOSIDOU, E.D.; LIAROKAPIS, D.E.; TZABIRAS, G.D.; PANTELIS, D.I. (2017), *Experimental Investigation of Roughness Effect on Ship ResistanceUsing Flat Plate and Model Towing Tests,* J. Ship Research 61/2, pp.1-16

LARSEN, B.E.; FUHRMAN, D.R. (2018), *On the over-production of turbulence beneath surface waves in Reynolds-averaged Navier–Stokes models,* J. Fluid Mechanics 853, pp.419-460

LIGRANI, P.M.; MOFFAT, R.J. (1968), *Structure of transitionally rough and fully rough turbulent boundary layers*, J. Fluid Mechanics 162, pp.69-98

MONTY, J.P. (2005), *Developments in Smooth Wall Turbulent Duct Flows,* University of Melbourne, p.272

MURPHY, E.A.K.; BARROS, J.M.; SCHULTZ, M.P.; FLACK, K.A.; STEPPE, C.N.; REIDENBACH. M.A. (2018), *Roughness effects of diatomaceous slime fouling on turbulent boundary layer hydrodynamics*, Biofouling 34/9, pp.976-988

SCHULTZ, M.P.; FINLAY, J.A.; CALLOW. M.E.; CALLOW, J.A. (2000), *A Turbulent Channel Flow Apparatus For The Determination Of The Adhesion Strength of Microfouling Organisms,* Biofouling 15(4), pp.243-251

SCHULTZ, M.P.; FLACK, K.A. (2013), *Reynolds-Number Scaling of Turbulent Channel Flow,* Physics of Fluids 25(025104), pp.1-13

SCHULTZ, M.P.; WALKER, J.M.; STEPPE, C.N.; FLACK, K.A. (2015), *Impact of Diatomaceous Biofilms on the Frictional Drag of Fouling-Release Coatings,* Biofouling 31/9-10, pp.759-773

SHAPIRO, T.A. (2004), *The Effect of Surface Roughness on Hydrodynamic Drag and Turbulence*, USNA Trident Scholar project report, USNA-1531-2, p.59

YEGINBAYEVA, I. (2017), *An Investigation into Hydrodynamic Performance of Marine Coatings 'In-Service' Conditions*, Newcastle University

YEGINBAYEVA, I.; AAS, V.E.; BRINK, A. (2022), *New measurement facility: Enhanced skin-friction measurement over large-scale plates in a channel flow*, 7th HullPIC Conf., Tullamore

Simulation of Fuel Oil Consumption of Ships Based on Big Data Analysis by OCTARVIA Web Applications

Naoto Sogihara, National Maritime Research Institute, Tokyo/Japan, sogihara@m.mpat.go.jp
Mariko Kuroda, National Maritime Research Institute, Tokyo/Japan, kuroda@m.mpat.go.jp
Tatsuya Akamatsu, Ocean Network Express, Singapore, tatsuya.akamatsu@one-line.com
Tetsuo Yanagida, Monohakobi Technology Institute, Tokyo/Japan, tetsuo_yanagida@monohakobi.com
Yoshihiko Sugimoto, Mitsui O.S.K. Lines, Tokyo/Japan, yoshihiko.sugimoto@molgroup.com
Ryu Ito, Kawasaki Kisen Kaisha, Tokyo/Japan, ito.ryu@jp.kline.com

Abstract

The International Maritime Organization has entered the EEXI and CII into force in 2023. This makes it increasingly important to predict and evaluate the fuel oil consumption of ships in operation. OCTARVIA project, where stakeholders in Japanese maritime cluster participated, developed three web applications: EAGLE-OCT.-web, SALVIA-OCT.-web, and OCTARVIA-web. This paper describes the overview of each web application and presents the analysis of sensor data collected onboard for evaluating ship performance in service and simulation of the fuel oil consumption in its lifecycle considering the effect of weather, fouling, and aging.

1. Introduction

The International Maritime Organization has been continuously discussing environmental regulations: EEDI, which began in 2013, covers ship performance at the design stage, while EEXI and CII, which has begun in 2023, cover ship performance at the operational stage. Stricter environmental regulations require shipyards to design ships with superior operational performance, and ship operators are under pressure to implement fuel-efficient operations.

In general, ships are subject to disturbances such as waves and wind during operation, so in order to satisfy the environmental regulations, it is necessary to develop technologies for evaluating ship performance in actual seas that take disturbance effects into account in the ship's performance in calm water. In addition, for CII, it is necessary to evaluate the performance in actual seas considering the effects of vessel fouling and aging. In order to comply with environmental regulations, it is preferable to evaluate ships around the world using the same method. However, there is no international standard for in-service performance evaluation.

OCTARVIA project, a joint research project by the Japanese Maritime Cluster, is conducting research and development with the aim of establishing international standards for evaluating the ship performance in a calm sea and actual seas, as well as the life cycle fuel consumption of main engines. The results of the project have been packaged as a web application with a view to promoting social implementation. This makes it possible to evaluate the performance using the method developed in the project anywhere in the world, as long as there is an Internet connection. In this paper, we introduce the web application and present an example of its application.

2. Web applications developed by OCTARVIA project

The intended users of the web application developed for the project include not only shipyards, but also shipping companies and makers. For this reason, consideration was given so that users who do not have detailed hull form data or model test data can also use the applications.

OCTARVIA project built three web applications, as shown in Table I. These web applications are available on the cloud service of the National Maritime Research Institute (NMRI Cloud, https://cloud.nmri.go.jp/portal/pub/top) and can be used after creating a user account and completing the usage procedures. There is a paid version with full functionality and a trial version with limited functionality, and the trial version can be used free of charge.

Table I: Web applications developed by OCTARVIA project.

Web application	Function
EAGLE-OCT.-web	Simple estimation of parameters required for evaluation of ship performance in actual seas
SALVIA-OCT.-web	Evaluation of ship performance using onboard monitoring data
OCTARVIA-web	Simulation of ship performance in service and fuel oil consumption from main engine during its lifecycle

The relationship between the three applications is shown in Fig. 1. EAGLE-OCT.-web estimation results can be used as input for SALVIA-OCT.-web and OCTARVIA-web. Added resistance due to waves and wind, as well as that due to oblique navigation and steering, estimated by OCTARVIA-web, can be used in SALVIA-OCT.-web. In addition, it is possible to input the performance in calm water, which is the evaluation result of SALVIA-OCT.-web, to OCTARVIA-web and evaluate the performance under arbitrary sea conditions. Between the applications, data can be exchanged in JSON format, which allows users to run web applications smoothly. Furthermore, SALVIA-OCT.-web can acquire onboard monitoring data from ShipDC and hindcast data from POLARIS database by Japan Weather Association via API connection.

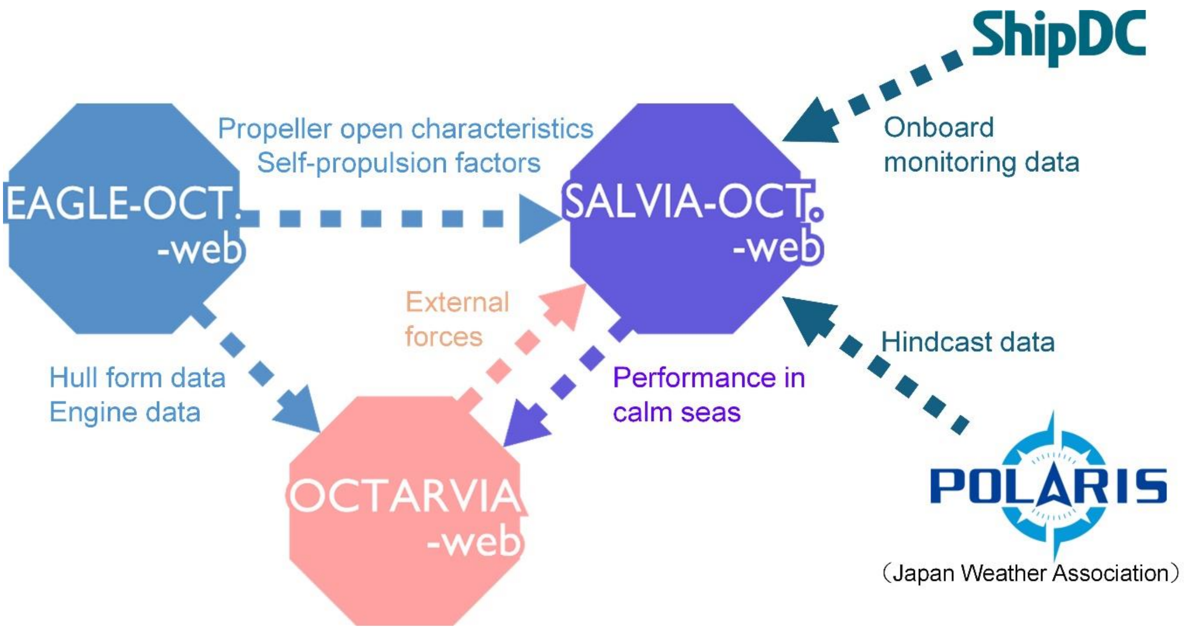

Fig.1: Relationship between the three applications

2.1. EAGLE-OCT.-web

EAGLE-OCT.-web is an application for simple estimation of parameters required for evaluation of ship performance in actual seas, such as hull shape, propeller open characteristics, and self-propulsion factors, based on ship principal particulars. The inputs and outputs of this application are shown in Table II. Some of the output is shown in Fig.2. The ship type can be selected from container ship, car carrier, bulk carrier, and tanker, and the hull shape is estimated based on the mother ship type for each ship type installed to the application. The self-propulsion factors are estimated by regression equations derived from the tank test database. Propellers are determined by a simple design function implemented in the application. The details of the estimation can be found in *Sogihara et al. (2019)*.

Table II: Inputs and outputs of EAGLE-OCT.-web

Input	Output
✓ Ship type (Container ship, PCC, bulk carrier, and tanker are available.) ✓ Length overall, length between perpendiculars, maximum breadth ✓ Draft at mid, fore, aft in design full and operation condition ✓ Design speed ✓ Propeller diameter ✓ Transmission efficiency and gear ratio of main engine ✓ MCR of main engine and engine revolution at MCR	✓ Sectional data (draft, half breadth, and area), waterplane ✓ Blockage coefficient （C_B, C_P etc.） ✓ Superstructure parameters ✓ Longitudinal and vertical center of gravity ✓ Height of transverse metacenter and natural roll period ✓ Radius of gyration (pitch, roll, and yaw) ✓ Self-propulsion factors ✓ Propeller open characteristics

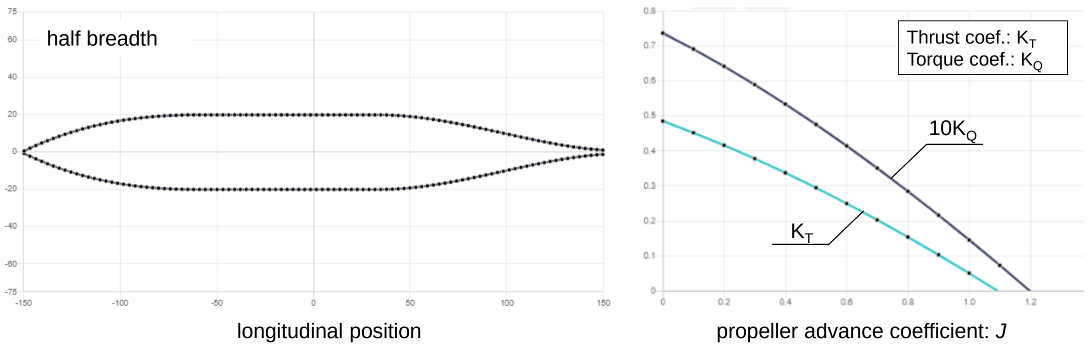

Fig.2: Output examples of EAGLE-OCT.-web (left: waterplane, right: propeller open characteristics)

2.2. SALVIA-OCT.-web

SALVIA-OCT.-web is an application for evaluating ship performance using onboard monitoring data. The application is characterized by data filtering based on the apparent slip ratio and by the resistance criteria method (called ‘RCM’), developed, *Sakurada et al. (2020)*, and validated, *Sogihara et al. (2021)*, in the project, which is an evaluation method using the rate of increase in resistance. Another feature of this application is that it outputs quality information, defined by data scattering, for the evaluation results.

The evaluation target in this application is mainly the ship performance in a calm sea. In addition, the application can also evaluate the ship performance in actual seas. Furthermore, by using onboard monitoring data collected over a long period of time, including dock to dock, the application can assess changes in ship performance over time due to fouling and aging.

The onboard monitoring data, which is the principal inputs to this application, should include the items shown in Table III. For those items that are automatically measured on board, it is recommended to use the average value over a certain period of time. Not only the mean value but also the standard deviation can be entered, and data filtering on the standard deviation is also possible. Instantaneous values can also be used, but it should be noted that there is a concern that the data scattering may increase.

Fig.3 shows the results of this application's evaluation of the ship performance in a calm sea. Fig.4 indicates the evaluation of the time variation of the rate of increase of engine output at a constant ship speed.

Table III: Recommended items in the standard monitoring method

Item	Instrument, data source	allowable error
Ship speed over ground	GPS	2%
Course over ground	GPS	
Ship speed through water	Doppler log	1%
Shaft horsepower	Shaft horsepower meter	0.5%
Engine revolution	Revolution counter	1%
Heading angle	Gyro compass	
Wind	Anemometer	Relative wind speed: 5% Relative wind direction: 5°
Sea state	Wave data (hindcast or nowcast data is available), onboard measurement (radar, visual observation, etc.)	Wave height: 0.1m Wave direction: 5°
Rudder angle	Rudder angle indicator	
Draft	Visual observation at departure	
Longitudinal radius of gyration	Measured value or simplified estimation	

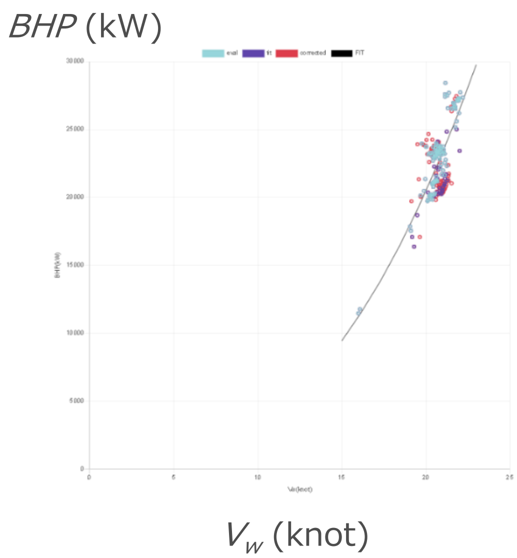

Item	Value	Remark
Pass Grade	Pass	Pass : power curve obtained by the straight procedure G1 : power curve by the initial criterion of δR for the fitting data G2 : power curve by the initial criterion of δR for the fitting data with b_n=3 G3 : power curve by no filtering of δR for the fitting data with b_n=3

Fig.3: Evaluation of the ship performance in a calm sea. (upper: relationship between ships speed and engine output, lower: quality information output)

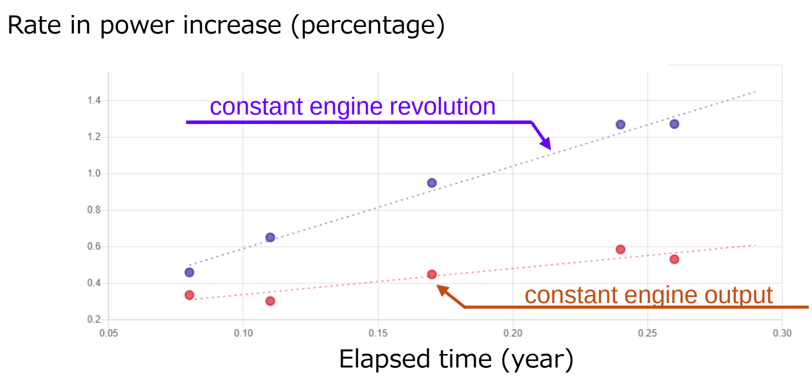

Fig.4: Time variation of the rate of increase of engine output

2.3. OCTARVIA-web

OCTARVIA-web is an application for simulating the ship performance in service and fuel oil consumption from main engine during its lifecycle and has the three calculation modes shown in Table IV.

Table IV: Calculation modes in OCTARVIA-web.

Mode	Function
Prediction	Short-term prediction of ship speed and fuel consumption in arbitrary sea conditions
Index	Calculation of total fuel oil consumption throughout its lifecycle from main engine
Simulation for fouling and aging effect	Estimating increase in power under constant ship speed in a calm sea

The main function of the Prediction mode is the short-term prediction of ship speed and fuel consumption in arbitrary sea conditions, which can be used in the design phase to accurately predict the ship performance in actual seas and to design hull forms that consume less fuel. For example, the relationship between energy-saving effects and sea conditions can be quantitatively evaluated by adopting a hull form with less resistance increase in waves or a superstructure with less wind resistance.

For the estimation of added resistance in waves, the method of *Tsujimoto et al. (2015)* is adopted, in which the diffraction component dominant in the short wavelength is modified in a practical way to ensure accuracy. Based on the frequency response function of added resistance in regular waves, added resistance in short crested irregular waves is calculated considering the directional spectrum of ocean waves, as shown in Fig.5. For the estimation of wind force coefficient including added resistance in wind, the regression formulae by *Fujiwara et al. (2006)*, which is based on the results of wind tunnel tests on a large number of hull forms, is adopted. Wind force coefficient is calculated as indicated in Fig.6. Since both methods have been recognized as having the highest accuracy by the ITTC's expert committee, *ITTC (2014)*, the incorporation of these methods ensures the accuracy of the application estimates. Furthermore, if the user has model test data on added resistance in waves or that in wind, it can be used as input, allowing for more accurate performance evaluation.

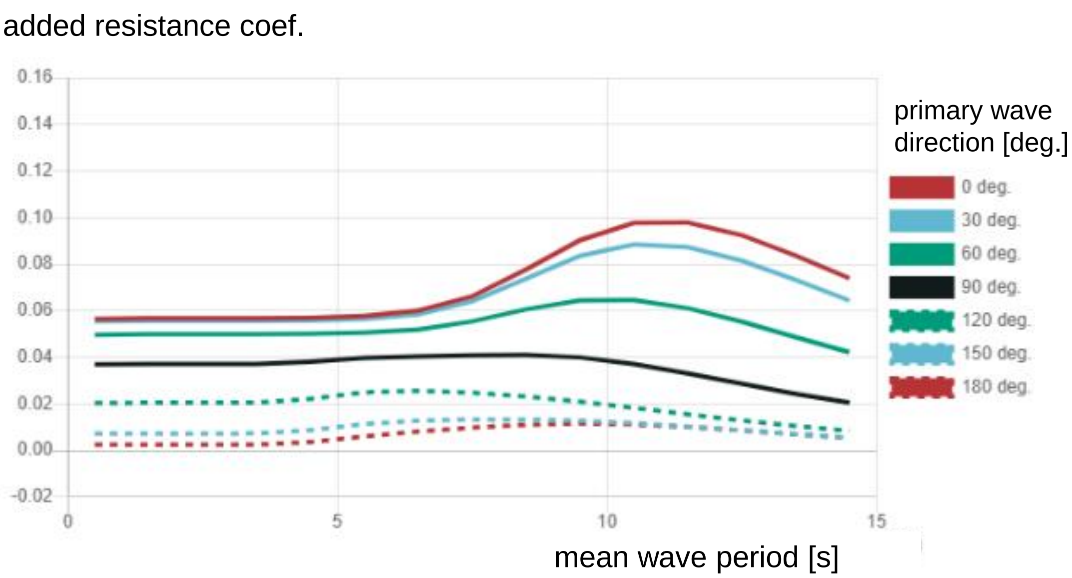

Fig.5: Added resistance in short crested irregular waves

When estimating fuel consumption, the user can select the operation mode of the main engine: constant main engine speed, fuel index control, constant main engine power, or constant ship speed. The application implements governor control, which allows the user to estimate fuel consumption taking into account the decrease in main engine revolution due to torque rich in rough weather.

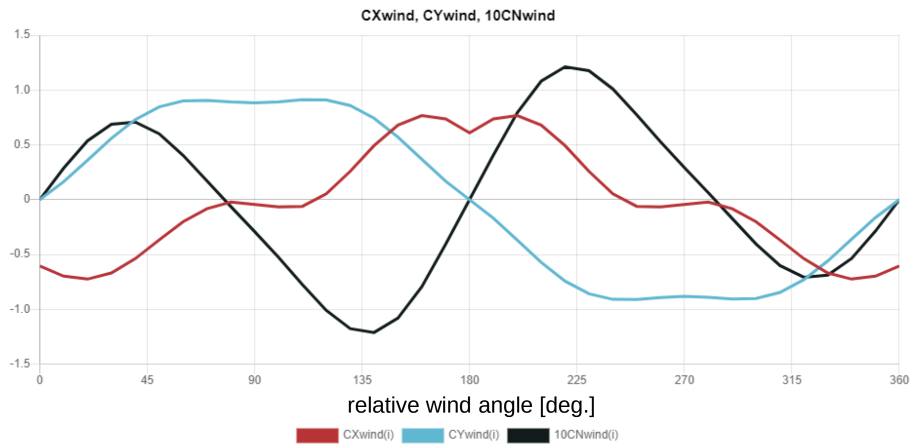

Fig.6: Wind force coefficient. (including starboard and port side)

Some of the calculations in the Index mode overlap with those in the Prediction mode; the Index mode allows long-term prediction of fuel consumption using the occurrence probability of weather on a user-selected route, based on the performance prediction for the weather defined in the EC scale in Table V prepared for this application. Seven different routes can be selected for this application, and the occurrence probability of weather for each route is available, *Kuroda and Sugimoto (2022)*. Fig.7 shows the occurrence probability of weather in West Pacific Ocean. In addition, the user can directly input the occurrence probability.

Table V: Evaluation conditions

EC	True wind speed U [m/s]	Significant wave height H [m]	Mean wave period T [s]
1	4.4	1.25	4.3
2	6.9	2.00	5.5
3	9.8	3.00	6.7
4	12.6	4.00	7.7
5	15.7	5.50	9.1
6	19.0	7.00	10.2

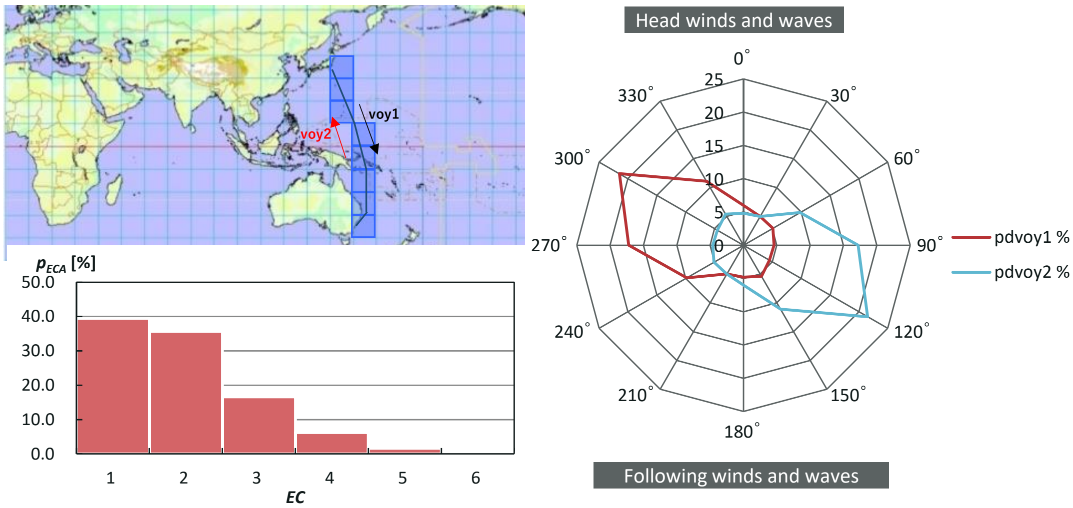

Fig.7: Route and occurrence probability of weather in West Pacific Ocean

In the Index mode, the above long-term forecasting includes a function to calculate the fuel consumption of the main engine over the ship's life cycle by taking into account the effects of hull and propeller fouling during operation and the effects of aging on the hull and main engine, *Kuroda and Sugimoto (2021)*. The time variation of fuel oil consumption throughout ship’s life can be calculated. This function can be used to investigate the effects of paint differences and dock intervals on the main engine fuel consumption over the lifecycle. It can also be used for vessel allocation planning, as the impact of different routes on main engine fuel consumption over the life cycle can be evaluated to determine which route the vessel should be deployed on.

3. Simulation of fuel oil consumption based on onboard monitoring data analysis

Fig.8 shows the flowchart of FOC simulation based on onboard monitoring data analysis. It should be emphasized that the performance in a calm sea used in the simulation is evaluated by SALVIA-OCT.-web using onboard monitoring data, which means that input the accurate performance in a calm sea enables an accurate evaluation of performance in actual seas. Shipyards don't necessarily have to use EAGLE-OCT.-web since they usually have the detail data of hull form and model test data. On this respect, *Sogihara et al. (2023)* reported that the evaluation using EAGLE-OCT.-web was in close agreement with the evaluation using the aforementioned detailed data from the shipyard. This means that Performance in a calm sea evaluated by EAGLE-OCT.-web is accurate enough.

In this section, performance prediction in actual seas and simulation of fuel oil consumption in lifecycle from main engine is presented, using the evaluated performance in a calm sea of Cape-Size bulk carrier following the flowchart in Fig.8.

3.1 Performance prediction in actual seas

Performance in a calm sea of the bulk carrier based on onboard monitoring data, which is fundamental performance for predicting performance in actual seas, results in Fig.9. This performance evaluation uses 5000 data measured with one hour interval. In the figure, ‘corrected’ means the corrected data for wind and waves whilst ‘fit’ and ‘eval’ denotes the data of resistance increase rate 50% and 10% from still water, respectively. ‘FIT’ is the resultant power-curve as output of SALVIA-OCT. The power-curve shown in Fig.9 is input for OCTARVIA-web.

The performance in actual seas is calculated by solving equilibrium equations expressing the external forces acting on a ship. After solving the equilibrium equations, the relationship between propeller revolution (equivalent to engine revolution in cases of low-speed diesel) and engine output and that between ship speed and engine output are obtained. Taking the engine characteristics into consideration, ship speed and fuel oil consumption are obtained as shown in Fig.10 for the bulk carrier in full and ballasted condition.

3.2 Simulation of fuel oil consumption in lifecycle

Based on the results above, simulation of fuel oil consumption in lifecycle can be conducted to estimate the effect of different paints on the fuel oil consumption. The methodology and formulation of the simulation is explained by *Sogihara et al. (2022)*, and this paper mentions the summary. The simulation considers the fouling and aging effect, specifically, resistance increase due to the fouling and aging for hull and decrease of propeller efficiency due to fouling. This means that performance prediction in actual seas is conducted for each time step in assumed lifecycle period. For each time step, multiplying the performance indicated in Fig.10 by occurrence probability of weather shown in Fig.8 yields the expected speed and fuel oil consumption, which is carried out for both full and ballasted condition. Based on the expected value for both conditions, the expected value is calculated. Integrating the expected value at each time step throughout lifecycle yields fuel oil consumption in lifecycle.

Fig.11 shows time variation of the expected fuel oil consumption with three different paints (excellent, normal, poor, obtained as product of performance in actual seas and occurrence probability of weather in West Pacific Ocean. From this figure, it can be seen that different paint performance has a different tendency to increase fuel consumption.

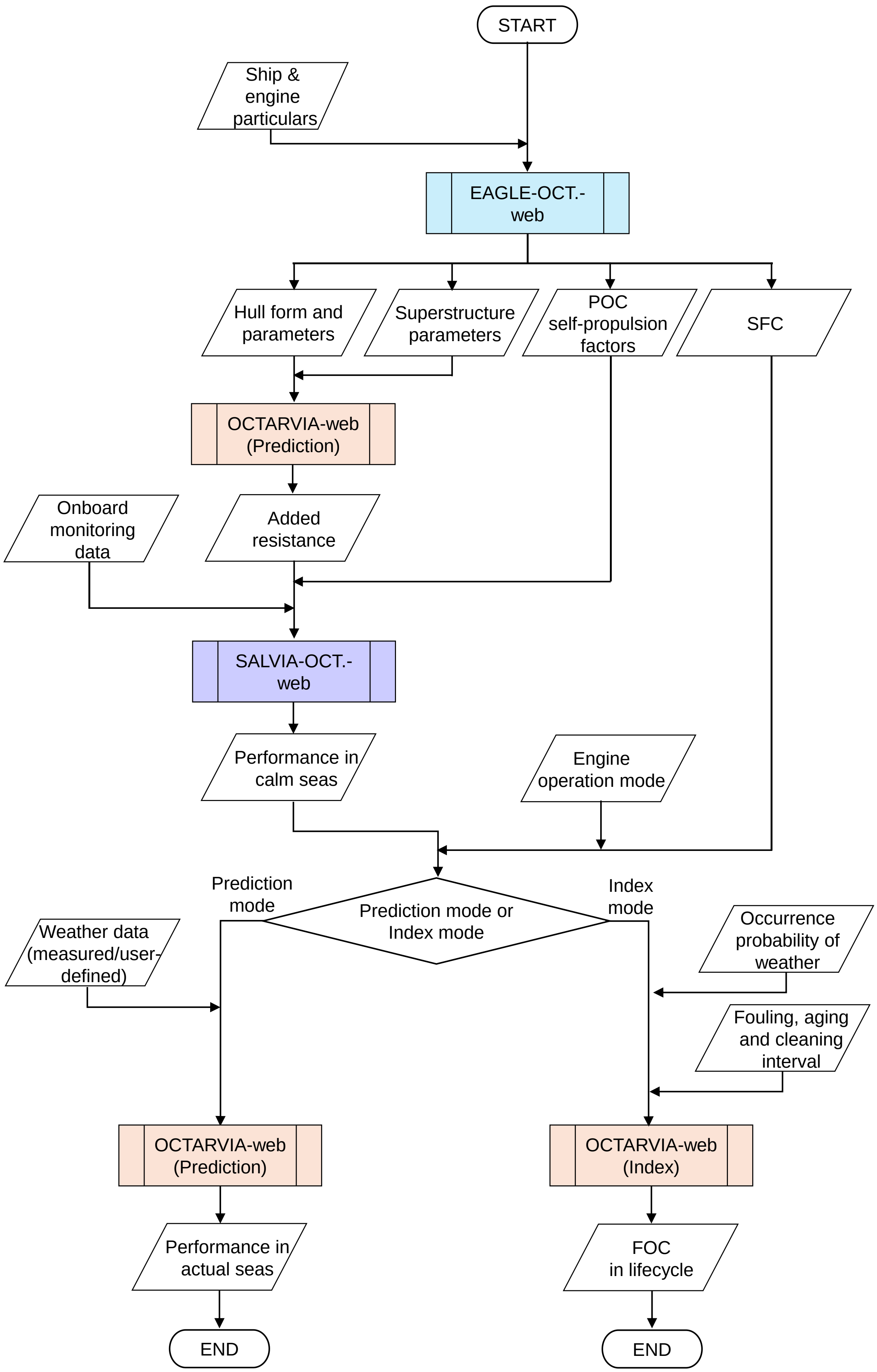

Fig.8: Flowchart of FOC simulation based on onboard monitoring data analysis

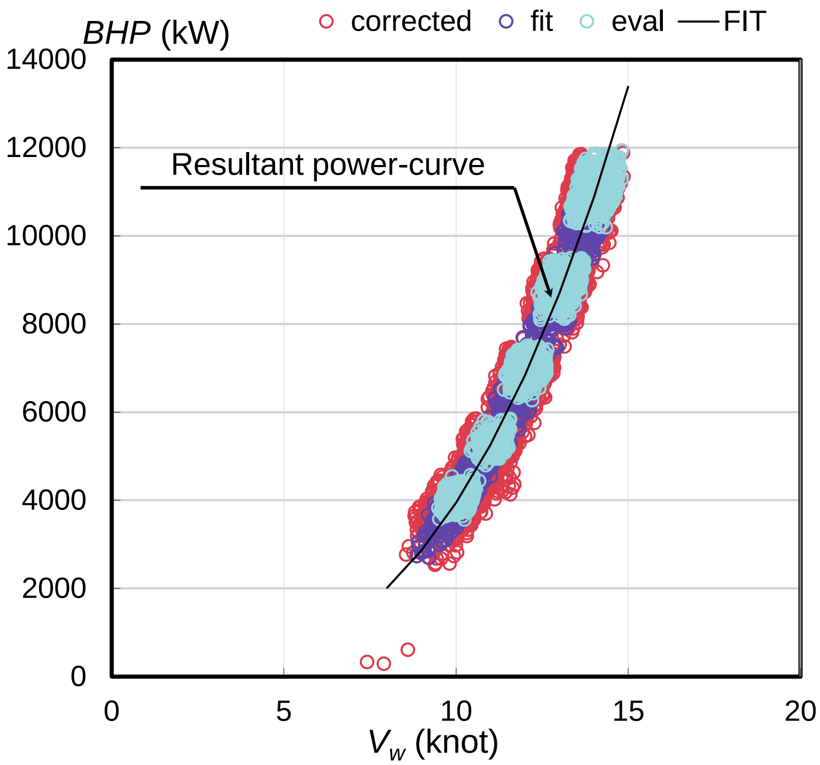

Fig.9: Performance in a calm sea based on monitoring data of Cape-size bulk carrier

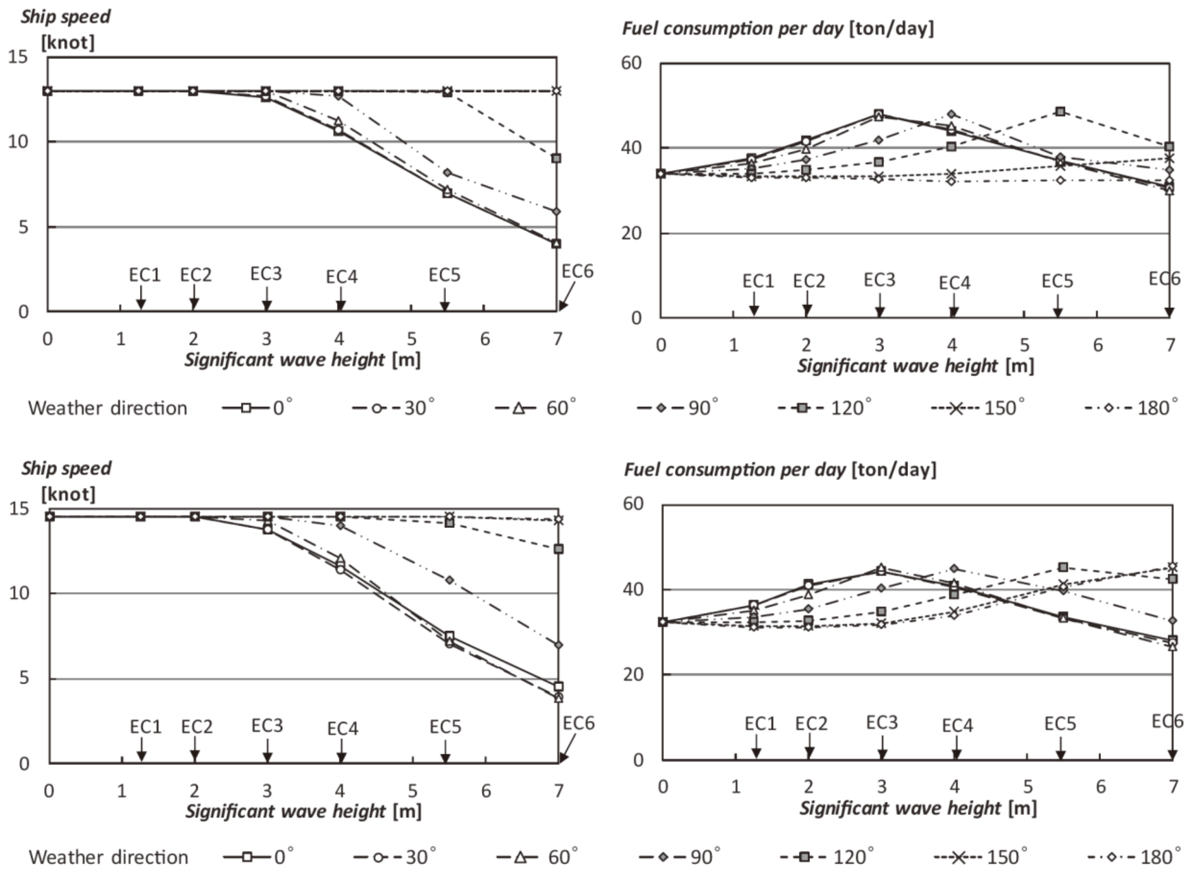

Fig.10: Ship speed and fuel oil consumption, *Kuroda and Sugimoto (2021)*, (top: design full load condition, bottom: ballasted condition)

Fig.12 shows total fuel oil consumption from main engine in lifecycle as a result of intergeneration of time variation of fuel oil consumption in Fig.11. Fig.12 indicates that the fuel oil consumption from main engine differs depending on the paint performance. The fuel saving effect in lifecycle due to the use of excellent paint can be quantitatively evaluated, which is expected to predict an improvement of CII ranking.

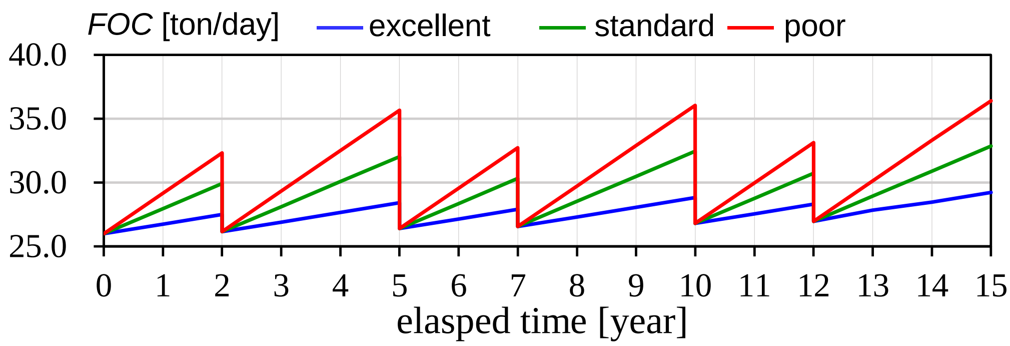

Fig.11: Time variations of expected values (left: ship speed, right: fuel oil consumption per day)

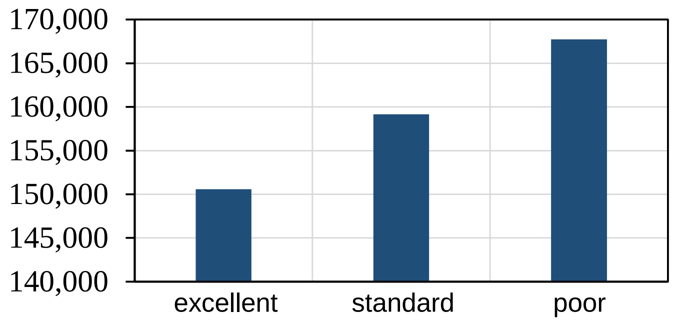

Fig.12: Total fuel oil consumption [ton] in lifecycle of the cape-size bulk carrier

4. Conclusions

This paper provides an overview of the three web applications developed in OCTARVIA project and their application examples. These applications enable accurate performance evaluation even in the absence of detailed hull form data or model test data only if onboard monitoring data is available. Therefore, not only shipyards, but also shipping companies and makers can conduct various performance evaluations using onboard monitoring data.

The performance in a calm sea obtained from the evaluation based on onboard monitoring data can not only be used for the applications presented in this paper but also for hull design and for voyage planning. Additionally, it is useful for evaluating the fuel saving effect due to the measures such as introducing excellent paints or optimizing maintenance plan on dock interval. It can also be used in the evaluation of EEXI and CII and can be utilized as a measure to comply with IMO regulations.

Acknowledgement

This study was carried out as part of the Initiative on Evaluation of Ship Performance in Actual Seas, the “OCTARVIA Project phase 2” a Japan Maritime Cluster Collaborative Research project. The authors are grateful to all the parties concerned who discussed the content of this study in the working groups.

References

FUJIWARA, T.; UENO, M.; IKEDA, Y. (2006), *Cruising performance of a large passenger ship in heavy sea*, ISOPE2006, San Francisco

KURODA, M.; SUGIMOTO, Y. (2021), *Development of the Evaluation Method for Life Cycle Ship Performance*, J. Japan Society of Naval Architects and Ocean Engineering 34, pp.19-28

KURODA, M.; SUGIMOTO, Y. (2022), *Evaluation of Ship Performance in terms of Shipping Route and Weather Condition*, Ocean Engineering 254

ITTC (2014), *Specialist Committee in Performance in Ships in Service*, Proceedings of the 27th ITTC, Copenhagen, pp.606-611

SAKURADA, A.; SOGIHARA, N.; TSUJIMOTO M. (2020), *Development of a Filtering Method for the Evaluation of Performance in Calm Sea Based on Onboard Monitoring Data*, Journal of Japan Society of Naval Architects and Ocean Engineering 31

SOGIHARA, N.; KURODA, M.; SAKURADA, A.; YOKOTA, S.; TSUJIMOTO, M. (2019), *UNITAS: Tool for supporting evaluation of ship performance in actual seas*, Papers of National Maritime Research Institute 19/1, pp.101-122

SOGIHARA, N.; SAKURADA, A.; TSUJIMOTO, M. (2021), *Validation of Filtering Method for Evaluating Ship Performance in Calm Sea Using Onboard Monitoring Data*, Journal of Japan Society of Naval Architects and Ocean Engineering 33

SOGIHARA, N.; KURODA, M.; TSUJIMOTO, M.; SATO, H. (2022), *Lifecycle Assessment of Fuel Oil Consumption of a Ship in Service*, 7th HullPIC Conf., Tullamore, pp.36-49

SOGIHARA, N.; AKAMATSU, T.; YANAGIDA, T.; SANO, H.; ITO; R. (2023), *Simplified and Accurate Models of Correction for Wind and Waves on Onboard Monitoring Data -Effects on Evaluation of Ship Performance in a calm sea-*, 8th HullPIC Conf., Pontignano, pp.36-49

TSUJIMOTO, M.; SOGIHARA, N.; KURODA, M.; SAKURADA, A. (2015), *Development of a ship performance simulator in actual seas*, OMAE2015, Newfoundland

Long-term Verification of ALS and WAPS Systems

Eivind Ruth, DNV AS, Oslo/Norway, Eivind.Ruth@dnv.com
Johanna Tranell, DNV AS, Oslo/Norway, Johanna.Tranell@dnv.com
Olav Rognebakke, DNV AS, Oslo/Norway, Olav.Rognebakke@dnv.com
Uwe Hollenbach, DNV, Hamburg/Germany, Uwe.Hollenbach@dnv.com

Abstract

Reducing the GHG emissions from shipping will be an important contribution to limiting global warming. DNV is investing significantly in building knowledge about energy-saving technologies to build transparency and trust in the performance and value of such systems. The aim is to increase the uptake in the industry, to facilitate the transition to a more sustainable future. Two such energy saving technologies are Air Lubrication Systems (ALS) and Wind Assisted Propulsion Systems (WAPS). These two technologies can usually be switched on and off during normal operation. This paper elaborates on methods and challenges when assessing the long-term performance of such on-off energy saving technologies. Test procedures and how to compute savings are addressed. The paper discusses factors contributing to uncertainty in the saving estimates, ways of reducing the uncertainty and methods for quantifying the uncertainty. DNV develops procedures for such assessments to build confidence in the actual performance.

1. Introduction

IMO has taken an active role in fighting climate change. Since 2011 various legislations have been put into force affecting the fleet of vessels trading globally, *IMO (2024)*. Requirements to energy efficiency are getting continuously stricter and the cost of fuel is expected to drastically increase. Solutions for which there was previously no economical initiative to explore become more attractive. Examples of such energy saving technologies are ALS (Air Lubrication Systems) and WAPS (Wind Assisted Propulsion Systems).

Currently ~160 ALS systems are installed and 280 are on order, https://www.clarksons.net/wfr/fleet. Some of the larger vendors are Silverstream, Mitsubishi, HHI and Samsung. The systems work by exploiting different physical principles. Some systems reduce resistance by introducing air bubbles in the boundary layer, whereas others try to obtain an air layer or cavity avoiding contact between water and hull. More information on the different solutions can be found in e.g. *Lee (2017)*, *De Freitas (2018)* and *Mizokami (2019)*. Some literature is published on the performance of the systems. The evaluation methods vary from CFD to model tests and full-scale tests. Most of the presented results from full-scale tests are from sea trails, e.g. *Lee et al. (2017)*, *De Fereitas et al. (2018)* and *Mizokami and Kuroiwa (2019)* and few consider in-service performance.

Several WAPS technology solutions are today available for commercial vessels, either as retrofits or part of newbuilding. These can be categorized as Flettner rotor, rigid wingsail, soft or hybrid wingsail, soft sail, suction sail and kite. There are currently 36 WAPS systems installed and 51 in the orderbook, https://www.clarksons.net/wfr/fleet, with Flettner rotor as the most installed system today. The WAPS installed are supplied from designers like Norsepower, Anemoi Marine and Econowind. While many sources focus on performance prediction using model tests, CFD or other methods, e.g. *Bataille et al. (2023)*, *Eggers et al. (2023)* and *Eide et al. (2023)*, the published work related to full-scale verification of WAPS have in the past years mainly been focused on short-term assessment using sea trial procedure, such as *Werner et al. (2021,2022)*. There are a few published long-term performance verification reports of WAPS using in-service measurements, such as *Hurford (2019)*, however these are still restricted to single vessel cases and with less focus on the methodology for best industry practice.

When assessing the performance of energy saving technologies, the proof of the pudding is the full-scale in-service performance. Most energy saving technologies give small savings, which are difficult to distinguish from measurement noise and the effect of other modifications. However, ALS and WAPS are expected to yield savings in the higher range and could be possible to verify. Still the effect of the system can be difficult to assess in "before and after" assessments due to difference in vessel condition, vessel operation and environmental conditions. Methods trying to correct the results back to a reference condition usually show a significant scatter, even when a significant number of parameters like vessel speed, engine power, draft, trim and weather condition are considered. A major benefit of the ALS and WAPS systems are that they can be switched on and off relatively quickly. The idea presented herein is to exploit this property by comparing a measurement just before and just after the switch to estimate the relative saving. This will eliminate the need for corrections due to vessel condition, vessel operation and environmental conditions by assuming that the conditions are the same since the measurements are close in time. This assumption needs to be checked as part of the performance evaluation. As most corrections can be removed from the equations, the uncertainty in the savings estimate can be reduced. The purpose of the procedure developed by DNV is to assess the in-service performance of the systems from full scale in-service measurements. Done properly, the procedure should give a good understanding of the saving with respect to normal operation and CII.

This paper sets out by discussing alternative methods to quantify the relative saving, followed by a recommended test sequence. Further, a virtual speed is introduced to improve the speed through water estimate. Corrections and filtering are discussed and finally saving computations including uncertainty estimates are presented. The paper outlines the ideas behind the DNV procedures for assessment of ALS and WAPS performance which when matured will be developed into formal DNV recommended practices.

2. WAPS benefit by reduced power or increased speed?

"What is the power saving of the energy saving system?" is one of the first questions asked when considering an energy saving technology. For most systems providing smaller saving up to 5-10% this is indeed the right question to ask and in theory, the reduced engine power used should be easy to observe while keeping the same speed. For vessels with WAPS, however, the power benefit may be significantly larger making it difficult to maintain vessel speed due to operational restrictions on the engine (e.g. it is not possible to sufficiently reduce RPM). Instead, part of the WAPS benefit is extracted as vessel speed gain. Since it then is unrealistic to operate at the same vessel speed in on and off condition, there is a need for two different methods of quantifying the performance. Firstly, a method of quantifying the power saving (method 1) when the vessel can reduce the engine power and maintain same speed, and secondly, a method when the ship increases the vessel speed (method 2). For the latter, it is not relevant to evaluate the on power at the off speed, i.e. the power difference between on and off conditions at the off speed. Instead, the power per distance sailed (closely related to tonne fuel per nautical mile) should be evaluated.

While method 2 is always applicable, there are restrictions for when method 1 should be used. In the case of significantly increased vessel speed (method 2), the saving due to speed change is only linear in speed, whereas when correcting to the same vessel speed (method 1) the saving is roughly proportional to speed cubed. Hence, taking out the benefit in terms of reduced energy consumption (at same vessel speed) gives larger savings than taking it out in increased vessel speed. The saving in terms of power per sailed distance can always be evaluated (and neither speed nor power need to be same in on and off condition), however, the power saving should only be evaluated when the speed difference between the on and off condition is small, e.g. less than 1 [kn], to avoid too much influence of the (uncertain) speed correction on the results.

3. Test sequence

The main benefit of the on and off approach is that the measurements that are compared are close in time such that the non-monitored disturbances are as similar as possible. Hence, it is desirable that the measurements in on and off condition are conducted as close in time as possible. However, when starting and stopping the energy saving system, some time is required to obtain stationary conditions.

Hence it is recommended to follow a particular sequence when performing the measurements:

1. Start approach: Turn energy saving technology on and set constant RPM. Start logging.
2. Wait for sufficient time (approach time) for vessel to reach stationary conditions.
3. End approach/Start measurement: No actions.
4. Wait for sufficient time (measurement time) to get a good measurement.
5. End measurement: No actions.
6. Wait for some time to avoid influence of switching on measurements.
7. Switching instance: turn off energy saving technology. Adjust to new constant RPM if necessary.
8. Wait for some time to avoid influence of switching on measurements.
9. Start approach: No actions.
10. Wait for sufficient time (approach time) for vessel to reach stationary conditions.
11. End approach/Start measurement: No actions.
12. Wait for sufficient time (measurement time) to get a good measurement.
13. End measurement: No actions.
14. Wait for some time to avoid influence of switching on measurements.

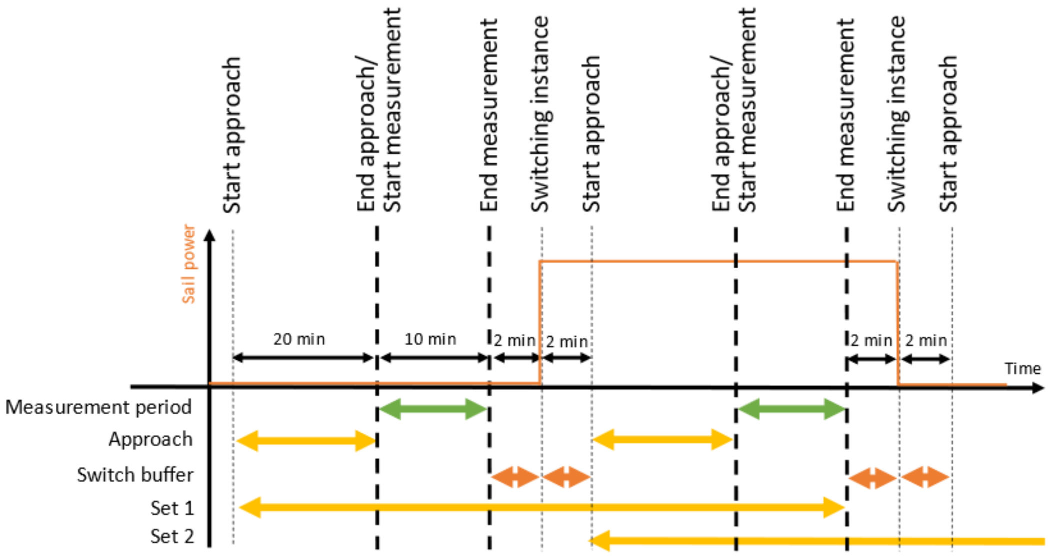

Fig.1: Test procedure for vessel of ~64 000 tonnes

A "Set" is defined as one on and one off condition immediately after each other, including the approach leading up to the first measurement. This sequence is also shown in Fig.1. For both ALS and WAPS systems, the onset of the system is faster than the response of the vessel to the change in forces. Hence, the approach time will be dominated by the vessel size. As a rule of thumb, it is recommended that the approach time is at least:

$$T_{\text{approach, minimum}}\ [\text{min}] = 0.5\sqrt[3]{\nabla[\text{tonne}]}$$

∇ is displacement. The measurement time needs to be sufficient to get a good and stable reading. For further postprocessing the measurements are averaged over the measurement period and 10 min is found to be a good trade-off between accuracy and need to minimize time between measurement periods. The switching buffer is included to ensure that switching does not affect the approach and measurement periods. Also note that several sets may be obtained consecutively by looping the procedure.

4. Virtual speed

Independently of whether the benefit is taken out in terms of reduced power or increased speed, a good speed measurement is key to reducing uncertainty. Traditional measurements of speed through water are known to be unreliable and the highly accurate GPS speed does not include currents. Experience has shown that using the propeller for measuring the speed through water may give a better estimate as both RPM and torque measurements are much more reliable. The virtual speed has many similarities to the more traditional slip value and can be found by taking the Kq curve from the e.g. EEDI technical file and shift horizontally to fit all measured Kq-Js values (Js is the advance number with respect to vessel speed without any wake correction). Then for a measurement period, the vessel speed can be estimated by computing the Kq value and interpolate on the shifted EEDI Kq curve to determine Js, which again can be used to determine the vessel speed. The estimated change in speed (which is more important than the speed itself) from this approach is expected to be quite good. Note that for vessels with ALS, this system may affect the propeller wake and a separate Kq fit may be needed with the system on and off.

5. Corrections and filtering

The idea behind the on-off procedures is that the vessel conditions should be same in the on and off condition and the only difference should be if the energy saving technology is enabled or not. Hence, a minimum of filtering and corrections is necessary. Still some filtering should be done to ensure that there is no human induced changes or major change in the environment. It is suggested to only use tests conducted in deep water with constant shaft speed, constant vessel heading, constant vessel speed and without large changes in wind forces. The parameters should be constant throughout the set with exception of RPM, which should be constant from start approach to switching instance.

In case the power saving is to be computed, method 1, a correction for the difference in ship speed is necessary. For WAPS, if the off condition is obtained by idling the sail, i.e. a physical adaption set-up where the sail is left upright, but in a position to obtain a fictious “no-sail” condition, correction due to wind resistance should be done to the off measurements. No other corrections should be applied.

6. Savings computation

The saving computation consist of two main steps: computation of saving in each set, and computation of the average long-term saving. The saving in all sets need to be computed in the same way, either as power saving or saving per nm, as discussed above. The procedure is elaborated below.

6.1. Power saving (method 1)

In this case the on and off measurements need to be corrected to the same vessel speed to estimate the power gain. In practice, we correct the on measurement to the speed of the off measurement as seen in Fig.2.

The relative saving at the off speed is computed as:

$$x_i = \frac{P_{\text{shaft, on, i}} + P_{\text{speed, i}} + P_{\text{EST, i}}}{P_{\text{shaft, off, i}}} - 1$$

where P_{shaft}, is measured shaft power, P_{speed}, is power correction due to speed difference between on and off (where a negative number indicates a larger speed in the on condition), P_{EST} is the power required by the energy saving technology (e.g. to rotate a Flettner rotor or pump air under the hull), x is the relative saving (negative value means energy saved with system on) and i indices the different sets.

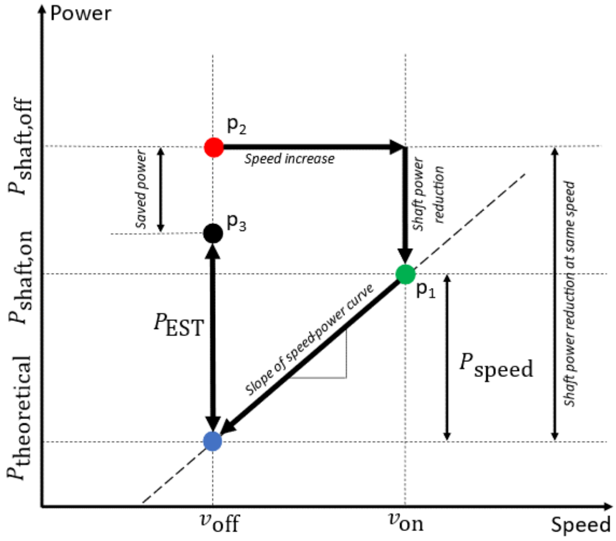

Fig.2: Correction of speed gain to power gain

Applying this method gives larger benefit of speed increase than the saving per nm method as the power typically vary with speed cubed.

6.2. Saving per distance sailed (method 2)

In this case the power per distance sailed (approximately tonne fuel per nm) is the measure of efficiency:

$$z_i = \frac{P_{\text{shaft, i}}}{v_{\text{i}}}$$

where z_i is the power per meter and v_{i} is the vessel speed. The relative saving between the on and off condition is computed as:

$$x_i = \frac{z_{\text{on, i}}}{z_{\text{off, i}}} - 1 = \frac{P_{\text{shaft, on, i}} \cdot v_{\text{off, i}}}{P_{\text{shaft, off, i}} \cdot v_{\text{on, i}}} - 1$$

6.3. Uncertainty

Independently of whether the saving is computed as power saving or saving per nm, the uncertainty analysis is the same. If we assume the saving estimates from each set is normally distributed (experience shows that this is the case) the mean value follows a student-t distribution and the estimated 90% confidence interval of the saving, $[\hat{x}_{0.05}, \hat{x}_{0.95}]$, can be determined as:

$$w_i = \frac{P_{shaft,off,i}}{\sum_n P_{shaft,off,i}}$$

$$\bar{x} = \sum_n x_i w_i$$

$$s_x = \sqrt{\left(\frac{\text{n}}{n-1}\right) \sum_n w_i (x_i - \bar{x}_i)^2}$$

$$\hat{x}_{0.05} = \bar{x} + t_{0.05,n-1} \frac{s_x}{\sqrt{n}}$$

$$\hat{x}_{0.95} = \bar{x} + t_{0.95,n-1} \frac{s_x}{\sqrt{n}}$$

where n is the number of sets, and w_i is the set weight. An important feature of using the 90% confidence interval as the measure rather than simply taking the mean is that the minimum savings estimate is likely to improve with more measurements as the confidence in the mean increases. This favours doing more measurements and including them in the statistics.

6.4 Other effects and benefits

In addition to the savings computed by the on-off methodology, both ALS and WAPS may be subject to other effects that are not captured in the method discussed here. ALS systems could on long term affect the fouling, see e.g. the white paper *Kidd et al. (2023)* which shows reduced fouling for ALS systems. ALS systems may also affect the flow around the propeller as the water around the propeller may contain air from the ALS system. This can affect the radiated underwater noise, onboard noise and the water density experienced by the propeller. In addition, the change of friction along the underwater hull due to the air may result in a different propeller wake than without ALS. For WAPS systems, vessels are reported to have benefits in terms of reduced ship motions, especially in roll. Furthermore, the weather routing is likely to be different with and without WAPS, which makes the two cases less comparable. In a practical case of a vessel with WAPS using the described method, the voyage will likely be routed for the purpose of exploiting the WAPS benefits, and the off condition will incorrectly be assumed to travel the same route. In addition, for both kind of systems, it would be possible that ship design and cargo capacity may be different adding additional complexity to true evaluations.

7. Fuel savings

The savings discussed above are purely related to the power savings and not fuel consumption. To get there the main and auxiliary engine specific fuel oil consumption as a function of shaft speed and torque needs to be considered. Some of the sail systems can be operated with no or negligible power input. This is different for example for the suction sails where electric power is needed for the fan drive, or for the rotor sails where an electric motor is engaged spinning the rotors. Even larger consumers of electric power are the compressors required by air lubrication systems. The net fuel savings depend very much on how the electric power for the above consumers is generated.

In case a shaft generator is engaged the specific fuel oil consumption is that of the main engine. Just small mechanical and/or electrical losses need to be considered in the gear unit (if any) and in the electric switchboard(s).

In case auxiliary diesel engines are engaged the difference in the specific fuel oil consumption between main engine and auxiliary diesel engines needs to be considered. At best the additional power demand of WAPS/ALS is so small that still one generator set can provide the necessary power at a beneficial utilization of the auxiliary diesel (e.g., at 70% MCR).

A more unfavourable case would be that the additional power demand by WAPS/ALS requires engagement of a second auxiliary diesel, and both auxiliary diesels are running at a low utilization (e.g., at 40% MCR). In such a case the specific fuel oil consumption of the auxiliary diesels running at constant rpm may increase significantly. Auxiliary diesels running at variable rpm would improve the situation a bit.

8. Conclusions

For verification purpose using actual operational data from in-service measurements, ALS and WAPS as energy saving technologies have the advantageous characteristics of easily being turned on and off within a short period. Being able to compare measurements with and without the energy saving technology close in time eliminates or reduces uncertainties related to changes in operational and environmental conditions. Hence, a performance assessment of the systems from full-scale in-service measurements based on on-off tests should give a good understanding of the energy savings.

Due to the potentially significant power contribution from WAPS, vessels operating with such a system may exploit the benefit by increasing the vessel speed and not only reducing power. If the vessel cannot reduce the engine RPM sufficiently, it is not realistic to compare an on and off case at the "off" vessel speed. This calls for an alternative assessment method compared to when a vessel exploits the benefit by reducing the engine RPM and keeping constant vessel speed. The work described in this paper suggests evaluating the power per distance sailed and the power saving, respectively. For both methods, a relative saving (of power or power per distance sailed) can be computed.

Typical speed through water measurements are usually uncertain or unreliable. Since a good speed measurement is key to reducing uncertainty in a performance assessment, it is proposed in this work to use a so-called virtual speed based on the propeller and measurements of its RPM and torque.

In addition to the above-described benefits of using on-off tests, the procedure significantly reduces the number of necessary corrections to the measurement data. Since the vessel and environmental conditions are assumed to be constant, only minimum filtering is needed during measurement periods. Furthermore, in case of a WAPS unit, which is left raised during an off condition (so-called idling mode), corrections due to wind resistance should be applied. In general, the low number of corrections needed reduces the result uncertainty.

Despite many benefits of using on-off test for performance assessment, there are some effects of the systems that are difficult to capture in the procedure described. For WAPS, weather routing plays an important role, and the off cases will incorrectly be assumed in environmental conditions sought by a weather routing algorithm optimised for the on cases. For both systems, ship design and cargo capacity may be different from the vessel not having installed the systems. Further limitations of the procedure are that the savings computed are purely power savings, not fuel or CO2 savings. For such a quantification, the main and auxiliary engine specific fuel oil consumption must be considered. How the required power to run the systems is generated can affect the net fuel savings of the systems, and hence a fuel consumption assessment may be necessary.

Acknowledgement

This work is carried out as part of the DNV Sustain and DNV TechHub projects aiming at reducing global GHG emissions.

References

BATAILLE, J.; BLAYO, C.; SERGENT, P. (2023), *PERFO: Methodology benchmark for wind assisted propulsion ship performance estimation*, Wind Propulsion Conf., London

DE FREITAS, L.; SILBERSCHMIDT, N.; PAPPAS, T.; JOHANNESON, J. (2018), *Full scale applications of air lubrication for reduction of ship frictional resistance*, RINA Conf., London

EGGERS, R.; KISJES, A.S. (2023), *WISP2 project on wind propulsion performance prediction methods and maneuvering,* Wind Propulsion Conf., London

EIDE, K.; ÖSTMAN, A.; ALTERSKJÆR, A. (2023), *Validation of performance prediction program against cyber-physical model tests*, Wind Propulsion Conf., London

HURFORD, A. (2019), *D2.7 Vessel Performance Final Report (Q1-Q6) for HDV Marine Flettner Vessel Performance Monitoring,* Data Analysis and System Modelling Project, Lloyd's Register

IMO (2024), *IMO's work to cut GHG emissions from ships,* https://www.imo.org/en/MediaCentre/HotTopics/Pages/Cutting-GHG-emissions.aspx

KIDD, B.; CONNOLLY, D.; DUBOIS, A. (2023), *Exploring Synergy between energy saving solutions for the maritime industry, A Collaborative white paper by AkzoNobel and Silverstream Technologies*, White Paper

LEE, J.; KIM, J.; KIM, B.; JANG, J.; McSTAY, P.; RAPTAKIS, G.; FITZPATRICK, P. (2017), *Full scale applications of air lubrication for reduction of ship frictional resistance*, SNAME Maritime Convention, SMC 2017

MIZOKAMI, S.; KUROIWA, R. (2019), *Installation of air lubrication system for ro-pax ferry and verification of its effect in actual seas based on onboard measurement data*, J. Jpn. Soc. Naval Archit. Ocean Eng 29, pp.1-9

WERNER, S.; NISBET, J.; HÖRTEBORN, A.; NIELSEN, R. (2021), *Speed Trial Verification for a Wind Assisted Ship*, RINA Int. Conf. Wind Propulsion, London

WERNER, S.; NISBET, J.; OLSSON, F. (2022), *Sea trial methodology for wind assisted ships*, 7th HullPIC Conf., Tullamore, pp.124-140

Estimation of Wind, Waves and Fouling Effect on Ships from Full Scale and Hindcast Data

Dimitris Georgousis, Vessel Performance Solutions, Lyngby/Denmark, dge@vpsolutions.dk
Kristian Nielsen, Vessel Performance Solutions, Lyngby/Denmark, kbn@vpsolutions.dk
Jakob Petersen, Vessel Performance Solutions, Lyngby/Denmark, jbp@vpsolutions.dk
Alexandr Adveev, Vessel Performance Solutions, Lyngby/Denmark, ala@vpsolutions.dk
Eirini Arvanitaki, Vessel Performance Solutions, Athens/Greece, ear@vpsolutions.dk
Sergey Tuymetov, Vessel Performance Solutions, Lyngby/Denmark, set@vpsolutions.dk

Abstract

Assessment of vessel performance requires estimating various types of added resistance to the calm water resistance, with the most significant caused by the presence of wind, waves and fouling of the hull and propeller. In this paper, the performance prediction system VESPER is applied to the estimation of added resistance for two fleets, one of bulkers and one of containerships. Firstly, the bias and error of measurements from ship-mounted anemometers is investigated. The measured wind speeds were corrected for the anemometer height and compared with hindcast data. Two different pairs of anemometer heights and wind shear exponents were used and the Mean Bias Percentage Error (MBPE) between the anemometer and hindcast data was evaluated. The study showed an overestimation of wind speed from the anemometers due to flow acceleration by the presence of the superstructure and the ship itself. The acceleration was higher for containerships compared to bulkers. Also, for both fleets the acceleration was higher for side winds. Additionally, the change of the average Confidence Interval of the calculated total added resistance is presented after applying corrections for wind, waves and currents, using both the above wind data sets with and without corrections. For both fleets, the effect of fouling was calculated significantly higher compared to the effect of the weather. Finally, the SPAWAVE method was applied to quantify the effect of waves, which, relative to the total added resistance, was calculated stronger for the bulkers compared to the containerships, while the effect of the wind was similar between the two ship types.

1. Introduction

The fuel efficiency and performance of vessels concerns the whole shipping industry due to environmental, regulatory and financial issues. High resistance during sailing increases the fuel cost and CO_2 emissions. Efficient methods to reduce the resistance of the ship are sailing with optimum trim, installing energy saving devices, voyage optimization, sailing with clean hull and polished propeller etc. Avoiding sudden increases in fouling is advantageous for both the environment and shipping companies' finances, which is the reason for the necessity of frequent monitoring of the ship's fouling resistance. Estimating the resistance due to fouling requires to estimate firstly the resistance due to wind and waves as accurately as possible.

The wind resistance rarely overcomes 10% of the total resistance according to *Aage (1968)*. The longitudinal force is generally considered the largest part of the total wind resistance. However, *Berlekom (1981)* points out that the induced resistance from the increased ruder angle can be of the same magnitude as the longitudinal force for strong winds. *Berlekom (1981)* also mentions that the wave resistance is also of the same magnitude. Numerous wind tunnel investigations have been carried out by many, such as *Blendermann (1994)*, *Aage (1968)* and *Berlekom (1981)*, who provided wind drag coefficients for various vessel types. Wind coefficients collected by *STA-JIP (2013)* and coefficients estimated by the method of *Fujiwara (2005)* have also been adopted by *ITTC (2014)*. For the estimation of the wind force, equally important to the wind coefficients is the relative wind climate input, which can be erroneously measured from anemometers due to flow disturbances.

In the last few decades, a lot of effort with increased accuracy has been done in the prediction of wave added resistance with numerical methods by utilization of strip theory, e.g. *Amini-Afshar and Bingham*

(2021) or Rankine source panel codes and CFD. Although some of these methods are easily applicable during conceptual ship design, they are not so convenient in daily performance monitoring. Fortunately, numerous empirical and semi-analytical methods have been developed, which although have questionable accuracy, they are still robust and easily applied. A simple formula capturing the resistance due to diffraction was developed by *Kreitner (1939)*. STAWAVE, adopted by *IITC (2014)*, captures both the resistance from the diffracted and radiated waves but only for head waves. SPAWAVE developed by *Grin (2022)* within the SPA-JIP project, SNNM developed by *Liu and Papanikolaou (2020)* within the EU SHOPERA project and the DTU design tool developed by *Nielsen (2015)* and *Martinsen (2016)* are some of the wave resistance estimation methods for arbitrary heading angles, which have been widely validated.

2. Ship Resistance

As a ship sails through calm sea, many forces act on it, such as the viscous, the wave making, the air and appendage resistance. The speed – power curves in calm water are usually obtained by CFD, towing tank tests or sea trials. However, when the ship sails under a specific sea condition, added power, Fig.1, is required to overcome the additional resistance acting on the ship:

$$R_{TW} = R_T + \Delta R_W \qquad (1)$$

where R_{TW} is the total resistance under specific sea conditions

R_T is the total resistance under calm sea

ΔR_W is the added resistance

Added resistance is caused due to the effects of wind and waves, fouling on the hull, sailing in shallow water and differences between the sailing conditions of the ship throughout the calm water resistance and the added resistance estimation. The latter differences correspond to the water temperature and salt content, the displacement and the trim.

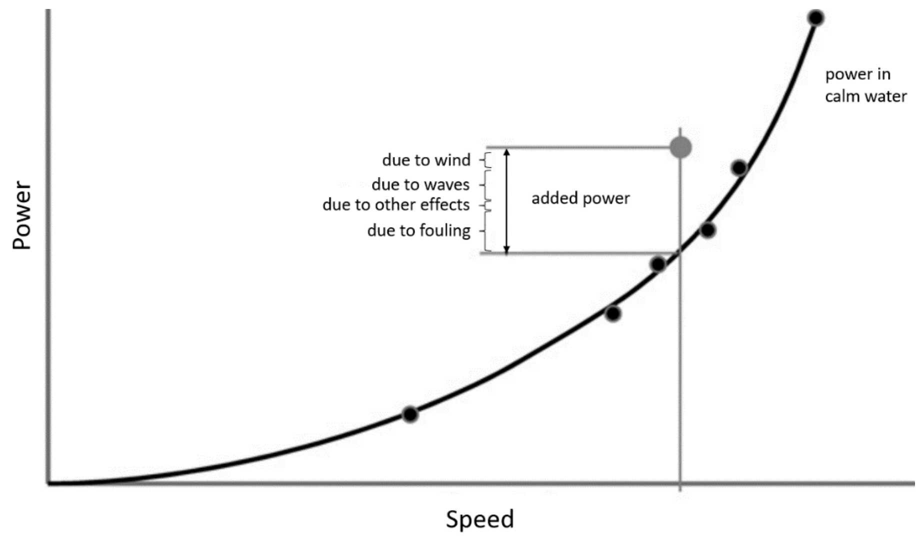

Fig.1: Added power required to sail in specific weather conditions and power curve in calm water

3. Vesper – Performance Prediction modelling

In this study the vessel's performance monitoring software VESPER has been used to estimate the various types of resistances. VESPER is a state-of-the-art system that interfaces various types of data such as noon, autolog, AIS and hindcast data and outputs reports related to main engine, auxiliary engine, compliance reports, hull and propeller performance among other features. Fig.2 shows a typical output of Vesper, which is the history of added resistance due to fouling.

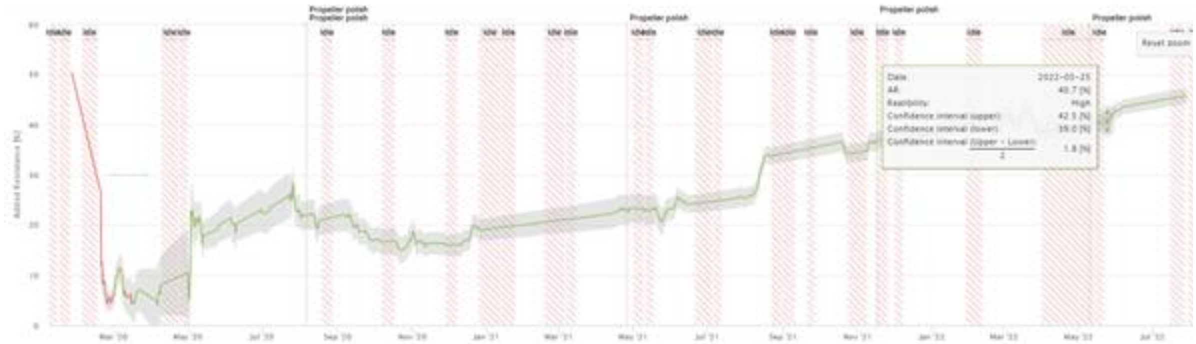

Fig.2: Example of a vessel’s added resistance due to fouling

The prediction of a vessel’s fouling resistance is based firstly on measuring the power (or fuel consumption) at a specific draft and speed, then correcting for the various types of added resistance (due to operational or environmental effects) and finally subtracting the power corresponding to the calm water resistance at the same speed and draft. The residual power is the one needed to overcome the resistance due to fouling of the hull and propeller.

The applied corrections of the measured power due to the wind and wave resistance are also described in this section, since their magnitude is much higher than the other added resistance types, *Berlekom (1981)*. The wind resistance is calculated by:

$$R_{AA} = \frac{1}{2}\rho_A V_R^2 C_X(\gamma) A_T - \frac{1}{2}\rho_A V_S^2 C_X(0) A_T \qquad (2)$$

where ρ_A is the air density,
V_R the relative wind speed,
V_S the ship’s speed,
C_X the wind resistance coefficient,
γ the relative wind direction,
A_T the maximum transverse section exposed to the wind

Kreitner (1939) proposed a simple correction formula for the resistance due to waves, in the range of ±45° off bow, using only wave height and ship dimensions. The formula has been slightly modified with correction factors to account for all wave directions:

$$R_{AW} = 0.64 \xi_W^2 \frac{B^2 C_B \rho_W}{L} C_{XX} \qquad (3)$$

where ξ_W is the wave height,
B the ship’s beam,
C_B the block coefficient,
ρ_W is the water density,
L the ship’s length,
C_{XX} the correction factor for all wave headings.

This method for estimation of resistance due to waves, employed by *ITTC (2005)*, captures the force due to the diffraction of the incident waves but omits the effect of the radiated waves due to the ship’s motion. ITTC recommends the use of the model for wave heights only up to 2 m. *Bhushan (2021)* compared recently developed more sophisticated models with this simplistic one, concluding that it achieves comparable accuracy for low wave heights. In the study the SPAWAVE method is also utilized, which is an empirical method validated with numerous model tests. The method, developed by *Grin* (2022), captures both the force due to the diffraction of the incident waves and due to the radiated waves from the ship's motion in all wave directions. Additionally, since the method was developed under the service performance analysis JIP, *SPA-JIP (2008)*, there is no wave height limitation.

4. Description of databases

The constructed databases for the data analysis and resistance calculations consist of autolog data from two fleets, one of bulkers and one of containerships. The averages of the fleet's particulars, which have been weighted according to the size of each class, are summarized in Table I.

Table 1. Weighted averages of vessels' particulars and other properties

	Bulkers	Containerships
L_{PP}	192.4 m	342.6 m
L_{OS}	198.4 m	357.7 m
B	32.1 m	48.7 m
C_B	0.8	0.64
T_{design}	11.4 m	14.2 m
$T_{operational}$	10.1 m	13.8 m
V_{design}	14.8 kn	23.4 kn
$V_{operational}$	12.1 kn	16.2 kn
$H_{superstructure}$	15.2 m	33.6 m
$B_{superstructure}$	21.1 m	31.7 m
DWT_{design}	47980 t	123392 t (13217 TEU)
MCR	9340 kW	54915 kW

The autolog signals of the speed over ground, speed through water, course over ground, draft aft and fore, relative wind speed and direction, fuel consumption, power and rpm are utilized in this study. To avoid unnecessary scatter, the autolog signals are filtered by detecting stable periods, as described by *Montazeri (2019)*. The stationary periods are identified by the theory of probability of detection of a change in the mean and standard deviation. Finally, the stationary periods are averaged for timespan of 1 hour. The bulkers database consists of about 65000 stable periods, from 54 vessels of 17 classes, covering about 3 years, while the signals from the containerships produced around 80000 datapoints, from 31 vessels of 5 classes, covering about 6 years.

Hindcast data have been introduced at the timestamps and positions of the autolog measurements for comparison with anemometer data. The parameters of the hindcast data used in this analysis as well as the corresponding time and spatial resolution are summarized in Table II.

Table II: Resolution of Hindcast data

	Time resolution	Spatial resolution
True wind	6 hours	0.125°
Significant height	6 hours	0.125°
Currents	24 hours	0.083°

5. Correlation of Anemometer Readings with Hindcast Data

This section describes the analysis of the data from the two wind sources i.e., anemometer and hindcast. It is assumed that although the hindcast wind data may be biased to parameters relevant to the mathematical modelling or to the historic wind measurements included in them, they are not subject to biases related to vessels' operational profile. Thus, the hindcast data can be utilized as reference for identifying the biases' origins of the anemometer readings, such as the presence of the superstructure and of containers or the anemometer's location.

5.1. Anemometer height correction

The autolog readings from the on-board anemometer, located mostly on the top of the superstructure, measure the apparent wind speed and direction. The true wind vector is determined from these 2 signals combined with the speed over ground and the course over ground signal (from GPS), due to lack of the heading signal. The calculated true wind speed is finally corrected with Eq.(4) for the wind speed profile considering the anemometer height.

$$U_z(z_{ref}) = U_z(z)\left(\frac{z_{ref}}{z}\right)^{\alpha} \qquad (4)$$

where $U_z(z)$ is the wind speed measured at height z,

z_{ref} is the reference height (typically 10m),

α wind shear exponent (typically 0.143).

The direction of the true wind relative to the North from the hindcast models is compared with the same parameter from measurements of one vessel's anemometer in Fig.3. These measurements cover 2 years. A shift of ±360° was applied, where it was necessary, at the hindcast wind direction before being compared with the one from anemometer. For instance, a 330° angle from hindcast was converted to -30°, so that when compared against a 20° angle from anemometer, leads to a difference of 50° instead of 310°. Thus, the axis corresponding to the hindcast direction ranges from -180° to 540°.

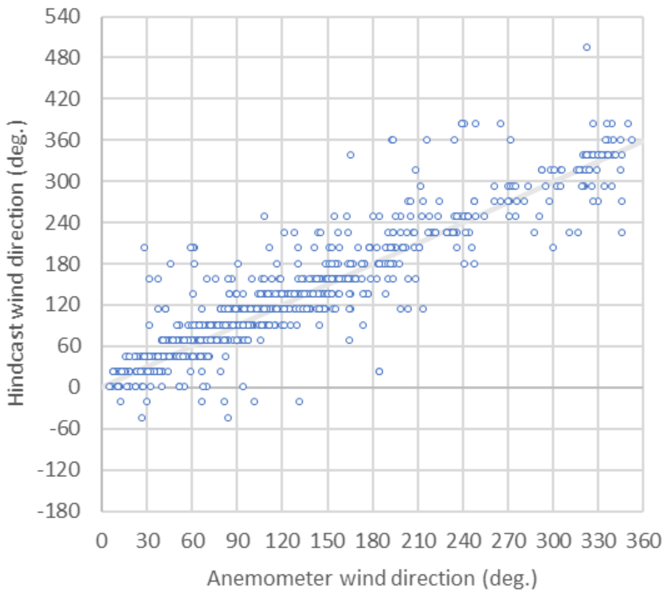

Fig.3: Comparison of true wind direction between hindcast and anemometer

In Fig. 4, two sets of autolog datapoints from the same vessel were converted to true wind speed and are compared with the true wind speed from hindcast. One set corresponds to the autolog datapoints without correction for the height of the anemometer, while the other set with correction.

The Mean Bias Percentage Error (MBPE) and the Mean Absolute Percentage Error (MAPE) were used as metrics for the assessment of the anemometer signals accuracy from the measurements of the whole two fleets.

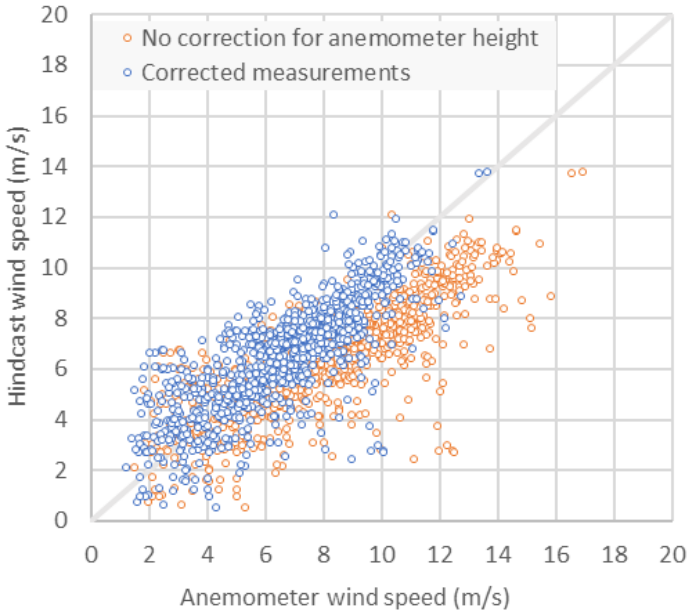

Fig.4: Comparison of wind speed from anemometer (with and without correction for the anemometer height) with the wind speed from hindcast source

$$MBPE = \frac{1}{n}\sum_{i}^{n}\left(\frac{y_i - x_i}{y_i}\right) \tag{5}$$

$$MAPE = \frac{1}{n}\sum_{i}^{n}\left|\frac{y_i - x_i}{y_i}\right| \tag{6}$$

where x_i is the wind speed from anemometer,
y_i is the wind speed from hindcast data,
n is the number of datapoints.

For the correction of the wind speed for the anemometer height, *ITTC (2021)* recommends $\alpha = 1/9$, while *ITTC (2014)* recommends $\alpha = 1/7$ for the wind shear exponent. The anemometer data analysis led to lower error compared to hindcast data with use of the latter exponent combined with the higher anemometer height.

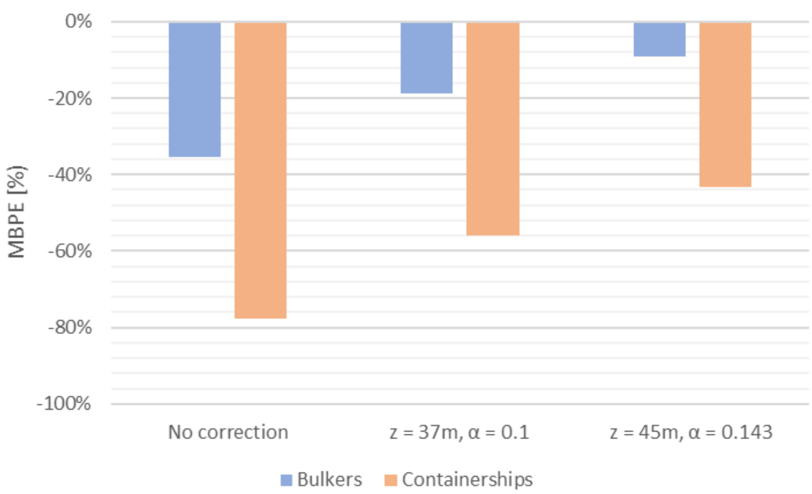

Fig.5: Sensitivity analysis of the correction of the wind speed readings for the anemometer height

However, the higher exponent value may compensate for the wind acceleration unwantedly not only due to height from the sea level, but due to other effects. The MBPE from the anemometers of the containerships are higher compared to the ones corresponding to the bulkers. The presence of containers may accelerate the wind, a behavior that can be noticed in Fig.5. The negative sign of the MBPE outlines that the measured wind speed is higher compared to the hindcast wind speed.

5.2. Directional bias of anemometer

This subsection attempts to show the biases of the anemometer due to its location and the presence of the superstructure or other features, which can be observed by looking into the dependence of the wind speed error against the direction of the true wind relative to the ship's heading, shown in Fig.6. A wind angle of 0° signifies head wind.

It was observed that numerous anemometers of some containerships showed significantly higher error compared to other containerships. It is unknown where these large differences in the errors originate between some ships. The almost double error was observed in vessels of same classes, thus generalized assumptions for the error's source are avoided, i.e. due to the location of anemometer or ship's geometry. Although the containerships' general arrangements documents were available, the location of the anemometer was not identifiable. Additionally, the possibility of different convention between the anemometers' readings is low since the dataflow was from the same installed equipment and API. Other possible sources may lie to the containers' configuration, or poorly calibrated anemometers etc. Thus, the containerships dataset has been separated into two datasets. The error analysis for the containerships is applied twice. Once at the whole fleet and once at the fleet without the above-mentioned anemometers, which is marked as "Containerships*" in Fig.6.

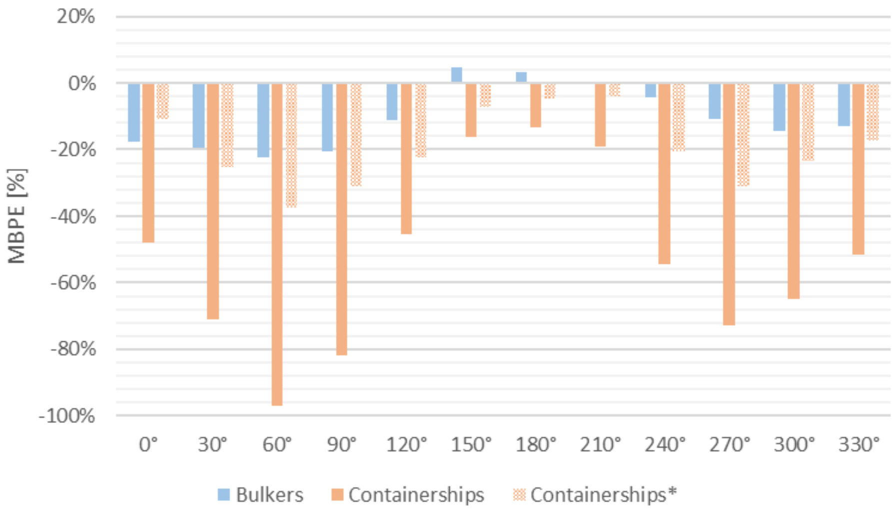

Fig.6: Dependence of true wind speed error against hindcast wind direction (relative to the heading)

The readings from the bulkers' anemometers show accelerated wind speed mostly for head and beam winds, which could originate from the presence of the superstructure. Wind speed measurements, from both bulkers and containerships, show lower discrepancy from the hindcast wind speed when the wind is coming from the stern, 150°-210° relative to the ship's heading. At this region, there is no acceleration of the wind speed for bulkers, while there is still slight acceleration for containerships. The presence of containers at the aft could explain this behavior.

Wind direction measurements, from both bulkers and containerships, show higher deviance from the hindcast wind direction when the wind is coming from 60°-90° and 240°-270° relative to the ship's heading, as illustrated in Fig.7. In this analysis, the anemometers of all the bulkers are mounted at the right side of the mast, for someone observing it from the fore, which is seen in Fig.8. Thus, the location of the anemometer either on the left or the right side of the mast may cause this behavior, meaning that the mast itself may cause not negligible distortion of the wind. Timeseries from two anemometers on the same vessel have shown discrepancy of 14° after change of 30° of a vessel's heading, *Stephens (2011)*.

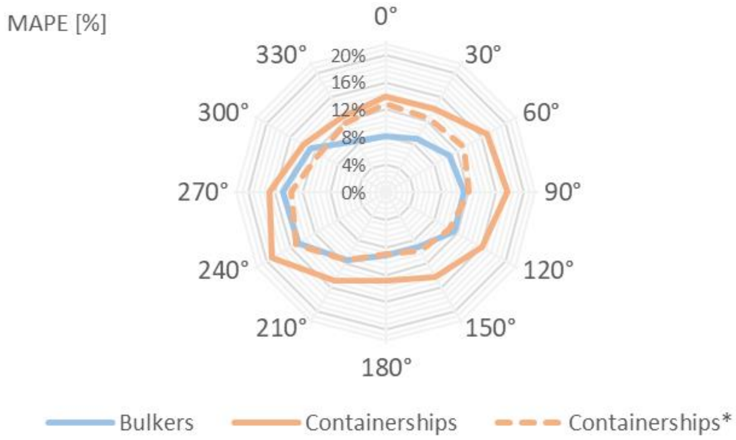

Fig.7: Anemometer-hindcast true wind direction error against hindcast true wind direction (relative to heading)

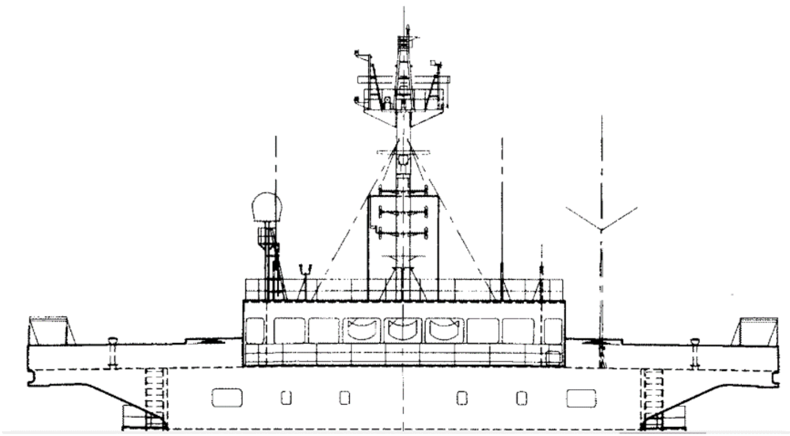
Fig.8: Typical frontage of the bulkers' superstructure's top

The errors shown in Fig.6 and Fig.7 are fully coupled since they correspond to true wind values, which has been converted from the relative wind readings. The relative wind speed readings' errors directly affect the calculation of the true wind direction, while the relative wind direction readings errors directly affect the calculation of the true wind speed as well.

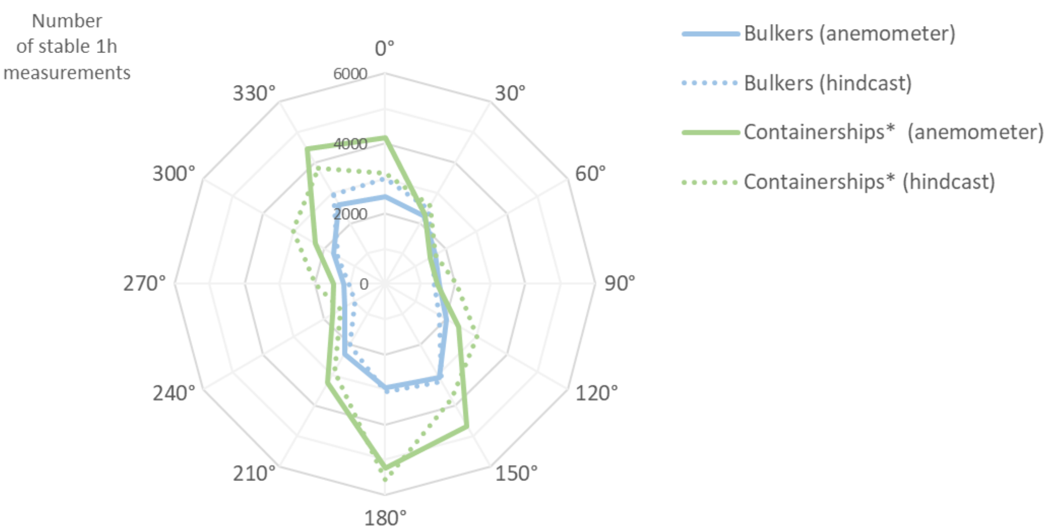

Fig.9: Distribution of measurements of 1-hour stable period against hindcast true wind direction (relative to heading)

Fig.9 shows the distribution of the stable periods of the measurements relative to the relative wind angle. Stable measurements of the wind coming from starboard and port side are significantly rarer, indicating that the mast distorts the flow significantly. Sudden gusts are also considered unstable throughout the process of detecting stable periods. Fig.6, Fig.7 and Fig.9 point out that the signals are more stable for tail winds.

6. Results and Discussion

The added resistance estimation by VESPER, similarly to other performance monitoring systems, is subject to scatter, which is introduced, among other sources, from the sensor errors or the inaccuracy of numerical weather data. It is necessary to quantify the prediction's scatter, so that the increase or decrease of the prediction's reliability can also be quantified by altering data inputs or resistance models i.e., wind climate from anemometer and hindcast or with and without currents involved.

In section 3, Fig.2 shows the history of the estimated added resistance by Vesper, which is calculated with linear regression from the population of the historic autolog stable periods points. The result is accompanied with a 95% confidence interval:

$$CI = \bar{x} \pm z\frac{s}{\sqrt{n}} \qquad (7)$$

where $\bar{x}$ is the mean of the added resistance points,
z is the value for the 95% confidence level,
s is the standard deviation of the added resistance points,
n is the amount of datapoints.

Correcting the total added resistance for the added resistance due to wind, waves, currents etc., decreases the scatter and consequently the CI. The average change of CI of the total added resistance of all linear trends after applying these corrections are summarized in Fig.10.

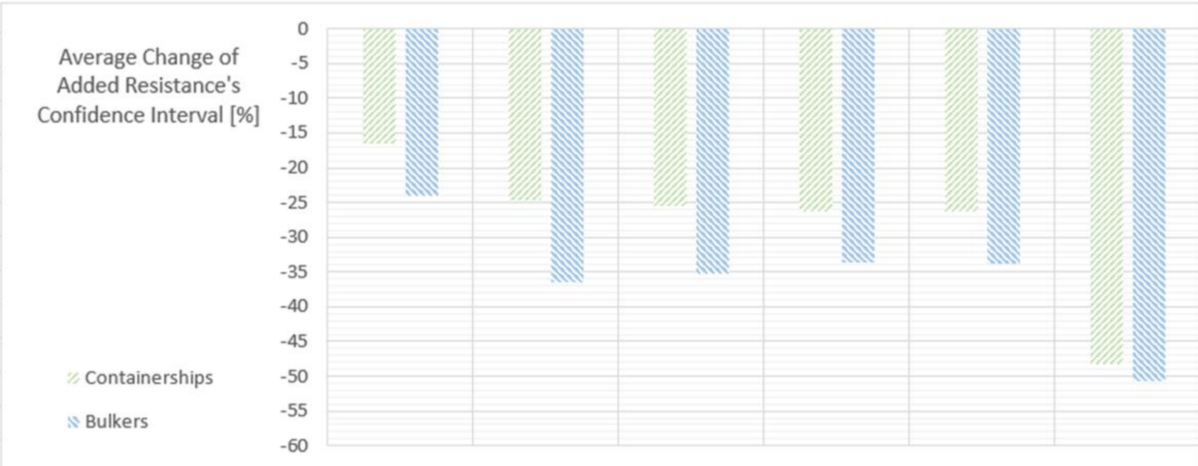

Currents correction	No	No	No	No	No	Yes
Wind correction	Yes	Yes	Yes	Yes	Yes	Yes
Wave correction	No	Yes	Yes	Yes	Yes	Yes
Wind source	Anemometer	Anemometer	Anemometer	Hindcast	Hindcast	Hindcast
Wave source	Hindcast	Hindcast	Hindcast	Hindcast	Hindcast	Hindcast
Anemometer height correction	no	no	α=0.143	-	-	-
Wind coefficients	Berlekom	Berlekom	Berlekom	Berlekom	ITTC	Berlekom

Fig.10: Change of the average Confidence Interval of the total added resistance after applying corrections for the various added resistance types

In performance systems, the severe weather (above 5 BF) is often filtered out when the wind and wave resistance is estimated. However, in the current analysis this filtration is not applied, so that the amount of datapoints between anemometer and hindcast weather are the same to avoid a biased CI score. Additionally, when the ships are sailing in severe weather the autolog signals become unstable. These unstable periods have been already filtered out, as explained in section 3. Thus, around 95% of the remaining autolog wind speed dataset is up to 5 BF. The same percentage accounts for the corresponding hindcast weather, which can be extracted from Fig.1 and Fig.2 in the Appendix.

Correcting firstly for the wind, then correcting for both wind and waves, and finally also adding the currents, decreases the CI respectively by 24%, 36.4% and 50.6% for bulkers. The corresponding decreases for containerships are 16.5%, 24.7%, 48.3% and are depicted in Fig.10 from the pair of columns number 1, 2 and 6. The corresponding decreases for containerships are 16.5%, 24.7%, 48.3% and are depicted in Fig.10 from the pair of columns number 1, 2 and 6. Using wind data from the bulkers' anemometers without correcting for the anemometer height led to 36.4% decrease of CI, while with correction leads to only 35.2%. The latter value was expected to be higher and possible reasons should be investigated further. Similarly, the correction for the anemometer height led to only 0.7% further reduction of CI for containerships ending up to 25.5%. The use of hindcast wind decreased further the CI to 26.4% for containerships, while the opposite behavior appeared for bulkers. A behavior which also should be investigated further. Finally, *STA-JIP (2013)* collected wind resistance coefficients for various ship types and drafts, which has also been adapted by *ITTC (2014)*, presented in Fig.A-3 and Fig.A-4 in appendix.

A magnitude comparison between the resistances due to wind, waves and fouling is also described in this section. The ratio of these types of resistance to the total added resistance is depicted in Fig.11. In this analysis, hindcast wind has been chosen to avoid the over-measured anemometer readings. Although around 90% of the hindcast waves are 2 m or less, as shown in Fig.A-2 in Appendix, the *Kreitner (1939)* wave resistance method was considered less reliable for the resistance magnitude comparison, so the SPAWAVE method was used instead, which has no wave height limit.

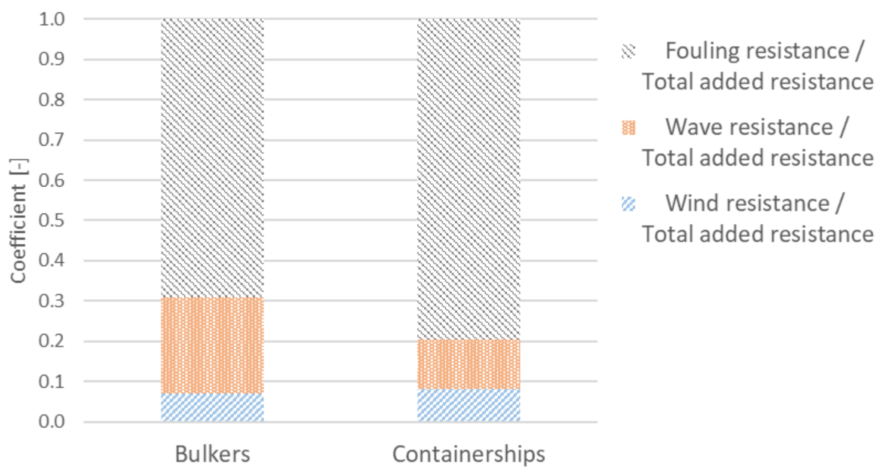

Fig.11: Ratios of resistance types to the total added resistance

For both bulkers and containerships, the resistance due to fouling is significantly higher than the other two types. The speed-power curves, which are usually extracted from the sea trials, could be underestimated, leading to direct overestimation of fouling resistance and underestimation of wind and wave resistance. Moreover, when the weather is severe the autolog signals are unstable, thus these periods are also filtered out. The absence of these periods also leads to underestimation of the ratio of the resistance due to weather to total added resistance, as well as to overestimation of the ratio of fouling resistance to the added resistance. Even if this is the case, the result of this analysis points out the importance of keeping the vessels' hulls clean and propellers polished.

Additionally, the ratio of wind resistance to wave resistance, which is not affected from the baseline, is about 0.65 for the containerships, while for the bulkers the ratio is about 0.3. *Molland et al. (2011)* provided proportions of wind and wave resistances with increasing BN only in head seas. In his analysis also, the ratio of the effect of head wind to head waves on containerships is higher compared to other ship types. The windage area of this study's containerships is multiple times wider compared to the bulkers, which partially explains the higher wind to wave resistance ratio. Additionally, Fig.A-3 and Fig.A-4 in Appendix, depict the wind coefficients proposed by *ITTC (2014)* for the two ship types. These coefficients are product of wind tunnel tests, where a bulker of 280k tons deadweight and a containership of 6800 TEU capacity were analyzed. According to these graphs, the wind forces on the containerships, either against or in favor to the sailing route, are stronger when the ships sail ballast without containers. This contradicts *Andersen (2012),* who analyzed the impact of various containers' configurations (streamlined fore or aft, semi loaded or fully loaded etc.) with wind tunnel tests. The sizes of these two ships, of which the coefficients were adopted by ITTC, is not similar with the vessels' size used in this study. Therefore, in this part of the study the coefficients proposed by *Berlekom (2013)* are used.

Apart from the higher wind resistance of the containerships, their wave resistance is also lower, which is explained partially by these ships' shape. *Liu and Papanikolaou (2017)* showed that lower beam to draft ratio is related with higher maxima of wave added resistance. This ratio is indeed lower for the containerships, however more investigation should be carried out to see how close the location of the maxima is to the operational wave spectrum. Additionally, *Grin (2022)* showed the maxima of wave added resistance are also higher for ships with wider beams and shorter lengths, which agrees with the geometry of the two fleets.

Both SPAWAVE and SNNM methods estimate higher added resistance due to waves for higher sailing speed. The operational speed of the containerships is higher than the speed of the bulkers. However, it seems that the ships' shape had higher impact compared to their operational speed profile in the matter of wave added resistance. Averages of the particulars of the two fleets are summarized in Table I.

Finally, the total added resistance was estimated at 41.1% for bulkers and 33.7% for containerships. These values are significantly higher than both the widely used 15% sea margin and the proposed sea margins by *Harvald (1983)* for specific routes, ranging from 12% to 30%.

7. Conclusions

In the present study, autolog data combined with hindcast weather data from two fleets, one of bulkers and one of containerships, were inputted into the performance prediction system VESPER to estimate the resistance of ships due to wind, waves and fouling.

Firstly, a comparison of wind data originated from anemometers and hindcast models was carried out. The relative wind from the anemometers readings was converted firstly to true wind, then the wind speed was corrected for the anemometer height and finally was compared with the corresponding hindcast wind speed. For the correction, two different pairs of anemometer heights and wind shear exponents were used and the MBPE between the anemometer and hindcast values for each pair was presented. Between, the two corrections the major one led to lower MBPE, which points out the widely known overestimation of wind speed from the anemometers due to flow distortion. The acceleration of the wind due to the presence of the superstructure and the ship itself, was higher for the containerships compared to the bulkers. The presence of the containers may accelerate further the wind. The acceleration of the true wind speed was plotted against its angle relative to the ship's heading to illustrate dependencies. It was shown for both bulkers and containerships, that the acceleration was higher for side winds, less intense for head winds and even lower for tail winds. A similar MAPE analysis was repeated between the measured wind angle and the hindcast wind angle, where the same dependency of the error with the relative wind angle was found. This originated from the coupling of the true wind speed and direction during the conversion from relative wind. This dependency was also present at the distribution of the population of the stable wind measurements. A potential reason for the error dependency with the relative wind angle could be the location of the anemometer either at the right or left side

of the mast, with the mast provoking further distortion to the wind.
The added resistance of the two fleets was also estimated using VESPER's performance module. The estimation was combined with a reliability analysis to show the impact to the scatter, firstly by correcting for the effects of the wind, waves and currents and then without corrections. Correcting for these effects reduces the scatter significantly. In the case of containerships, the hindcast wind data were found to be slightly more reliable compared to anemometers' readings. This was not the case for the bulkers, which indicates the fact that the anemometers' readings from the bulkers are more reliable compared to the containerships' readings and also addresses that the need for improved hindcast wind data for further analysis.

In addition, the magnitudes of the resistances due to wind, waves and fouling were also compared. It was found that the fouling effect was significantly higher than the wind and waves effect in the ship's performance. Additionally, the wave resistance was around 50% higher compared to the wind resistance for containerships and tripled for bulkers, which is a result of these ships shape. Finally, the resistance due to fouling was predicted more than double compared to the resistance due to weather, which could partially originate from a potential underestimation of the ship's efficiency during sea trials. However, these sea margins were calculated significantly higher compared to the widely used sea margin of 15%, which points out the need for frequent monitoring of the hull and propeller degradation and for measures against them.

8. Future Work

The focus of the current study was to increase the accuracy of performance prediction to such a degree, so that drop in performance can be identified immediately after it occurs. Potential improvements in the modelling, such as the method of *Fujiwara (2005)* for providing vessel and size specific wind coefficients, should be investigated. Recently developed robust wave resistance methods, alternative to the SPAWAVE method, should also be assessed scatter-wise with Vesper. Alternative hindcast weather providers for wind, wave and currents should also be tested. Finally, the quantified bias of the anemometers' readings with the relative wind angle seems to be consistent for containerships and bulkers, which makes these measurements correctable, *Thornhill (2020)*.

Acknowledgement

The authors thank the Society of Naval Architects and Marine Engineers (SNAME) for their permission to reprint the current paper, since the paper was originally presented in at SOME, Athens, Mach 2023.The authors also thank the data owners, which although preferred to be anonymized, they gave full permission to their fleets' data based on their drive for improving vessel performance predictions.

References

AMINI-AFSHAR, M.; BINGHAM, H. (2021), *Added resistance using Salvesen-Tuck-Faltinsen strip theory and the Kochin function,* Appl. Ocean Res. 106

AAGE, C. (1971), *Wind Coefficients for Nine Ship Models,* SSPA

ANDERSEN, I. (2013), *Wind loads on post-panamax container ship,* Ocean Eng. 58

BERLEKOM, W. (1981), *Wind Forces on Modern Ship Forms-Effects on Performance,* SSPA

BHUSHAN, T.; ANDERSEN, P. (2021), *Comparison of added resistance methods using digital twin and full-scale data,* Ocean Eng. 229

BLENDERMANN, W. (1994), *Parameter identification of wind loads on ships,* J. Wind Eng. Ind. Aerody.

BOOM, H.; HUISMAN, H.; MENNEN, F. (2013), *New Guidelines for Speed/Power Trials*, Hansa Int. Maritime Journal

FUJIWARA, T.; UENO, M.; IKEDA, Y. (2005), *A New Estimation Method of Wind Forces and Moments acting on Ships on the basis of Physical Component Models*, J. Jasnaoe

GRIN, R. (2022), *SPAWAVE, An Empirical Method to Predict Wave Added Resistance in all Wave Directions*, SNAME 14th IMDC Conf.

HARVALD, S. (1983), *Resistance and Propulsion of Ships*, Ocean Engineering

ITTC (2014), *Preparation, Conduct and Analysis of Speed/Power Trials*, ITTC Recommended Procedures and Guidelines

ITTC (2002), *Analysis of Speed/Power Trial Data*, ITTC Recommended Procedures and Guidelines

KREITNER, J. (1939), *Heave, pitch and resistance of ships in a seaway*, Trans. RINA 87

LIU, S.; PAPANIKOLAOU, A. (2020), *Regression analysis of experimental data for added resistance in waves of arbitrary heading and development of a semi-empirical formula*, J. Ocean Eng.

MONTAZERI, N.; PETERSEN, J.B.; HANSEN, S.V. (2019), *Autolog data processing for vessel performance application*, 4th HullPIC Conf., Gubbio

MOLLAND, A.; TURNOCK, S.; HUDSON, D. (2011), *Ship resistance and propulsion*, Cambridge University Press

THORNHILL, E.; WALL, A.; McTAVISH, S.; LEE, R. (2020), *Ship anemometer bias management*, Ocean Engineering

STEPHENS, R. (2011), *Wind feedforward: blowing away the myths*, 4th Dynamic Positioning Conf.

Appendix

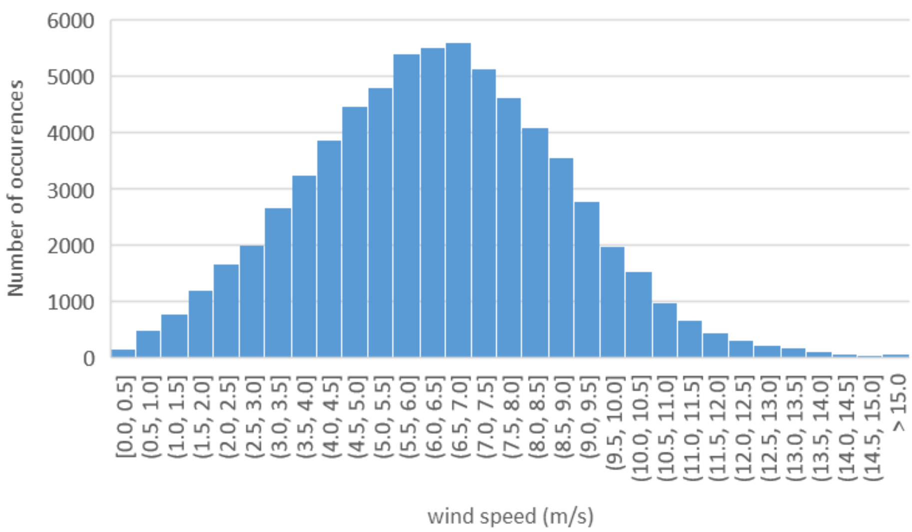

Fig.A-1: Distribution of hindcast true wind speed, introduced at the bulkers' autolog positions (after the filtration of the anemometers' unstable periods)

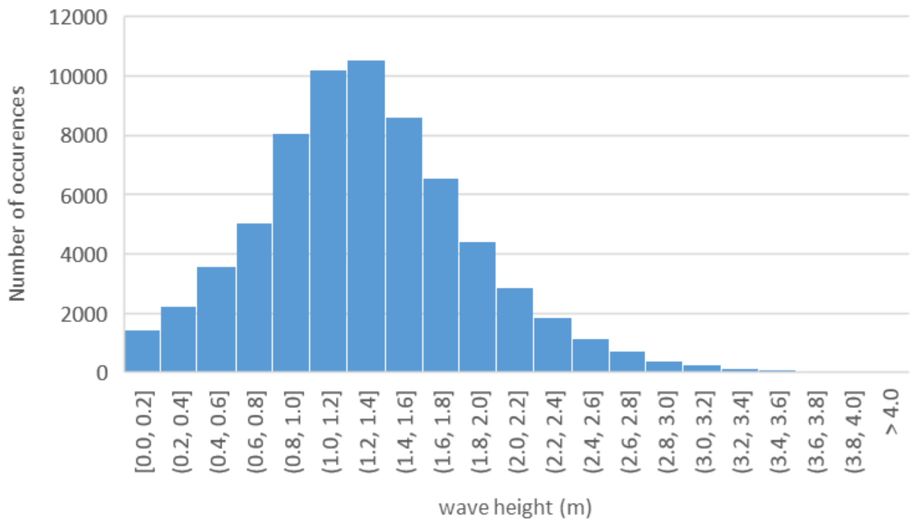

Fig.A-2: Distribution of hindcast wave height, introduced at the bulkers' autolog positions (after the filtration of the anemometers' unstable periods)

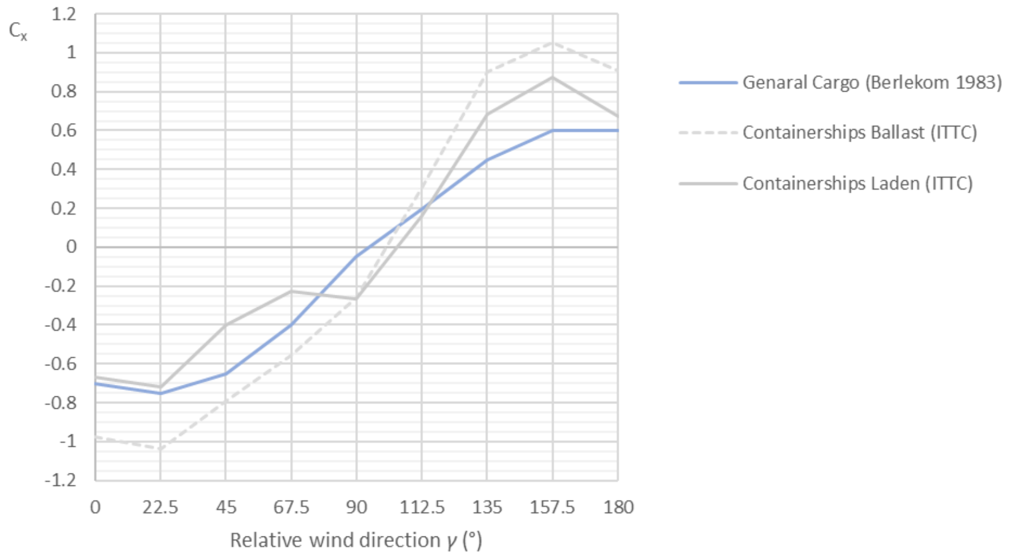

Fig.A-3: Wind coefficients of containerships and general cargo ships

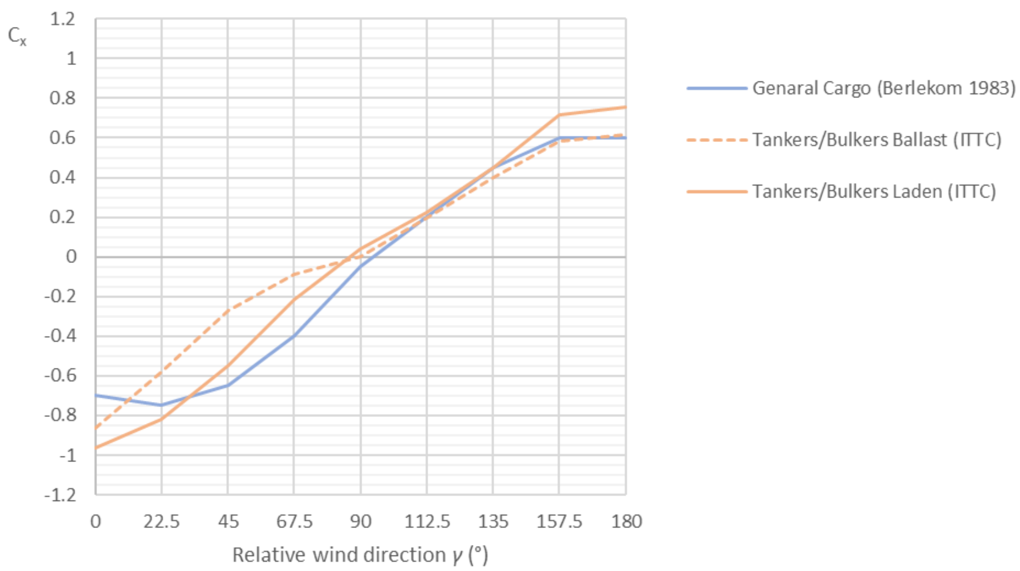

Fig.A-4: Wind coefficients of bulkers and general cargo ships

Modelling Annual CO_2 Emissions for the Global Containership Fleet: Hempel Model

Andrea Farkas, Hempel, Zagreb/Croatia, afar@hempel.com
Ditte Gundermann, Hempel, Lyngby/Denmark, digu@hempel.com
Mads Raun Bertelsen, Hempel, Lyngby/Denmark, madb@hempel.com
Gerasimos Kyprianou, Hempel, Athens/Greece, gkyp@hempel.com

Abstract

The shipping industry is facing a great challenge in the task of curbing down CO_2 emissions in order to achieve carbon neutrality. In the last few years, a lot of mitigations measures were proposed and implemented, but the determination of their overall mitigation potential has still remained complicated. The complexity of this determination lies in the fact that the operational performance of ships is affected by various influential parameters. A model that can reliably predict fuel consumption and CO_2 emissions based on real operational profiles is required for the evaluation of various mitigations measures. In this paper, a comprenhensive model that can be used in a bottom-up approach for predicting annual CO_2 emissions based on Automatic Identification System (AIS) data is proposed. The proposed model accounts for ship performance in real service conditions and models the fuel consumption and CO_2 emissions of both main and auxiliary engines. The modelled annual CO_2 emissions are validated by comparison with the actual annual CO_2 emissions obtained with Data Collection System (DCS) for several ships with different out of dry-dock timings. Thereafter, a case study is prepared in which developed model is used to estimate CO_2 emissions in 2024 for ships which will be dry-docked in the begining of 2024 with the hypothesis that they will have the same operational profile as they had in 2023. Two scenarios are analysed including antifouling protection using mid-tier self-polishing copolymer and low friction coatings.

1. Introduction

The shipping industry is facing a great challenge in the task of curbing down CO_2 emissions in order to achieve carbon neutrality. The International Maritime Organization (IMO) has proposed several required technical regulative which require from both design and operational point of view important modifications in order to successfully achieve its fulfilment. In addition, EU has implemented several policies and measures, including the Emissions Trading System (ETS) and the EU Monitoring, Reporting, and Verification (MRV) system, *Kim et al. (2023)*. Starting from 2023, reporting carbon intensity indicator (CII) is mandatory, while EU ETS came into force in January 2024. Both these measures directly evaluate real sailing conditions of ships and in that way operational performance of ship can be monitored, in comparison to design-based indicators, which evaluate ship energy efficiency only from design or nominal point of view, *Kalajdžić et al. (2023)*.

In the last few years, a lot of mitigations measures were proposed and implemented, but the determination of their overall mitigation potential has still remained complicated.

There are many studies in the literature which evaluate the mitigation potential of various measures, *Ahn et al. (2017)*, *Gatin and Kalajdžić (2022)*, *Werner et al. (2022)*. However, the most of studies in the literature evaluate measures potential in design condition, rather than for real operational conditions. This can be explained with the existence of only design-based indicators, which has led to the fact that shipowners have put more emphasis in minimizing their ship index levels rather than reducing fuel and energy consumption, *Barreiro et al. (2022)*. With the introduction of measures which directly monitor operational performance of a ship, it is logical to assume that more effort will now be placed to evaluate actual energy savings from certain mitigation measure, rather than only evaluate its potential for design conditions. This will add the complexity in the determination of mitigation potential for certain measures, since operational performance of ship is affected by various influential parameters. For this, a model that can reliably predict fuel consumption and CO_2 emissions based on real operational profiles is required.

The bottom-up approach for the prediction of CO_2 emissions in shipping industry represents an approach of calculating annual CO_2 emissions based on ships activity, while the top down approach is fuel-based, *You and Lee, (2022)*. In the last few years, bottom-up approach is considered to be more accurate than top-down approach for the prediction of annual CO_2 emissions of ship fleet, especially in combination with Automatic Identification System (AIS) data, *Johansson et al., (2017)*.

A detail review of bottom-up approaches for the prediction of fuel consumption and CO_2 emissions is presented in *Kim et al. (2023)*. The authors listed the most important models proposed in the literature for this prediction and summarized the methods used for the prediction of ship resistance in calm water, fouling effects, weather effects and propulsive efficiency. The most of models in the literature use Holtrop-Mennen method for the prediction of ship resistance in calm water, *Holtrop and Mennen (1982)*, while for the prediction of propulsive efficiency several methods are used including *Holtrop and Mennen (1982)*, *Bernitsas et al. (1981)*, Emerson's formula, *Kristensen and Lützen (2012)*, OpenProp, combining values from sea trial reports and from similar ships. Fouling effects are often either neglected, or in some cases are applied as constant factor of 9%, *Smith et al. (2014)* and *Faber et al. (2020)*, or 10% *Tvete et al. (2020)*, *Guo et al. (2022)*. In more sophisticated model referred as MariTEAM, fouling effects are related to ship age, *Olmer et al. (2017)*, *Bouman et al. (2016)*, *Muri et al. (2019a,b)*, *Dale (2020)*, *Kramel et al. (2021)*. The explanation of accounting for fouling effects is given in *Kim et al. (2023)*, with the application of average hull roughness (AHR) which changes due to ship age and time since dry-dock (DD). The relationship between AHR, ship age and time since DD is modelled with equation proposed by *Stenson (2015)* is used for the prediction of AHR, while *Steen and Aarsnes, (2014)* equation is used for prediction of increase in frictional resistance coefficient. However, due to missing information about coating specification as well as biofouling management plan, authors have applied yearly average increase in AHR. This basically simplified fouling, mechanical and aging effects into yearly increase of AHR, with the inclusion of AHR reduction in DD. This means that fouling and aging effects are depending only on ship age and not on time since DD. Weather effects are mostly accounted either using sea margin, or separated in wind effects which are then accounted using *Blendermann (1996)* or *Fujiwara (2006)* approach and in wave effects which are accounted using ITTC recommendations, *ITTC (2017)*, method proposed by *Liu and Papanikolaou (2020)* or *Kim et al. (2022)*. After brake power is obtained, fuel oil consumption (FOC) of main engine (ME) is calculated using specific fuel oil consumption (SFOC) which can depend on the engine load or be constant, depending on the model. Finally, auxiliary engine (AE) consumption is estimated mostly using *IMO (2014)*, since information about installed AE power is usually missing.

In this paper, a comprehensive model that can be used in a bottom-up approach for predicting annual CO_2 emissions of containerships based on AIS data is proposed. The proposed model accounts for ship performance in real service conditions and can be used for the prediction of the fuel consumption and CO_2 emissions of both main and auxiliary engines. To the best of the authors knowledge, this model represents the first model which accounts for fouling and aging effects separately. Namely, fouling effects are modelled depending on speed loss/power increase values for different coatings and time since DD. In addition, for low friction coatings an out of dock power saving is also included. The modelled annual CO_2 emissions are validated by comparison with the actual annual CO_2 emissions obtained with Data Collection System (DCS) for several ships with different out of dry-dock timings. What is more, predicted power for propulsion is compared on timestamp level, as well as within speed power plots in order to further demonstrate its prediction capabilities. After an extensive validation study, a case study which demonstrates the application of model to identify total benefit of low friction coating is presented.

2. Materials and Methods

This section briefly presents the material and methods used for the prediction of annual CO_2 emissions. Firstly, input data is specified and then methods used in the prediction of calm water resistance, weather effects, fouling and aging effects, propulsion efficiency, FOC/CO_2 emission for propulsion and remaining FOC/CO_2 emission are presented.

2.1. Materials

The prediction of annual FOC and CO_2 emission of ship using bottom-up approach generally requires three types of data: ship dynamic data, technical information and environmental data, *Kim et al. (2023)*. Within this study ship dynamic data is obtained from AIS data provided by https://www.vesseltracker.com/, a leading provider of global AIS ship movements and maritime information services, having around 250,000 users all over the globe from multiple sectors, and tracking more than 170,000 ships every day. Technical information consists of ship's main particulars and specifications of ME. During the development of model, specifications of AE are used as well, in order to more accurately predict the emissions during time in port basin and berthing. The data used for technical information is obtained from https://maritime.ihs.com and https://www.clarksons.com/. Environmental data including wave conditions and sea temperatures at the time and location the ship is sailing is obtained from https://data.marine.copernicus.eu/products. The voyage trajectory completion is made by AIS data provider, while missing data handling in terms of technical info is mostly solved by using info from both data providers. However, if some technical data is still missing it can be estimated using relationships amongst ship's main particulars.

2.2. Methods

In order to predict CO_2 emission from the described input data several predictions should be made. In general, total resistance of a ship when sailing is consisted of:

$$R_{Total} = R_T + R_{AA} + R_{AW} + \Delta R$$

R_T is the total resistance of a ship in calm water condition, R_{AA} is the added resistance due to wind, R_{AW} is the added resistance in waves and ΔR is the added resistance due to fouling and aging.

R_T is predicted using *Holtrop and Mennen (1982)*, however wetted surface area is obtained from equation presented in *Kristensen and Bingham (2017a)* and correlation allowance coefficient is used either from *Holtrop and Mennen (1982)* or *Kristensen and Bingham (2017a)*, whichever is smaller. Also resistance of appendages and additional pressure resistance of immersed transom stern are neglected. The validity of this slightly modified *Holtrop and Mennen (1982)* approach is demonstrated in the prediction of sea trial results, after propulsive efficiency is also modelled. This comparison is made for various ship types, loading conditions including ballast, design and scantling draught and at various speeds. The results of comparison demonstrated the validity of the approach. In Fig.1. the comparison of sea trial results and the obtained results are presented for both design and scantling draught of two containerships.

In this study, added resistance due to wind is accounted for using margin 2.5% of R_T instead of modelling the added resistance due to wind, which would depend on several input variables. This value is taken from *Kim et al. (2023)*, where the authors demonstrated the average portions of ship resistance components within ship total resistance. This was decided due to two important considerations: first one being the fact that added resistance in wind is not that important component of total resistance, and second one being that several input variables cannot be precisely determined using input data. Therefore, it is not certain whether the modelling of added resistance due to wind would improve the overall prediction of FOC/CO_2 emission that much. Within future work this prediction could be improved using environmental data and one of the methods proposed in the literature, such as *Blendermann (1996)* or *Fujiwara (2006)* approach.

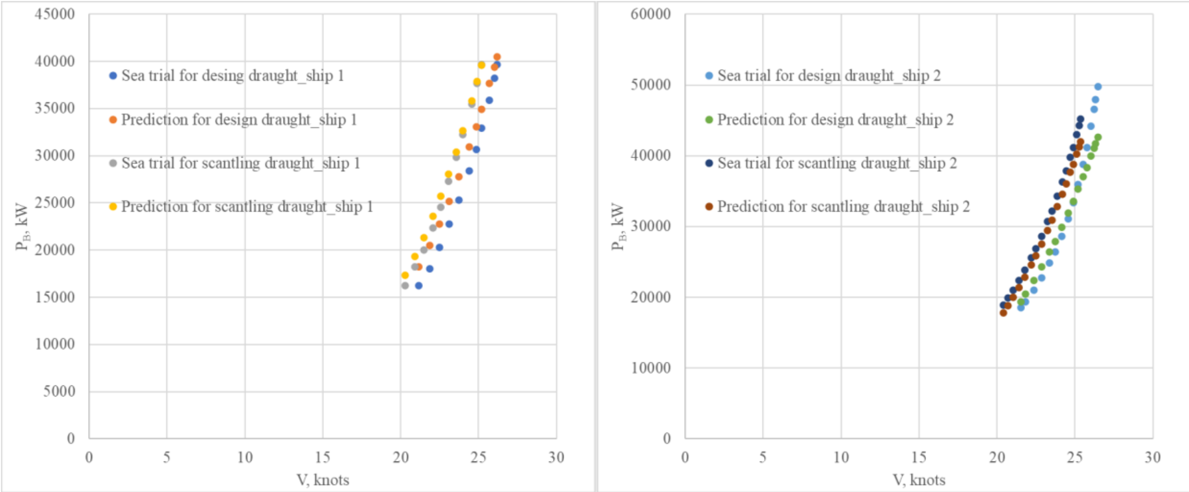

Fig.1: Comparison of the obtained results with sea trial results

The added resistance in waves is predicted using STAwave-1 presented in *ITTC (2017)*. Although this method is limited to only head waves, it can still provide relatively good results with only few inputs. However, it is obvious that the ship during its voyage will encounter waves from various directions which will then lead to wrong prediction of added resistance in waves. STAwave-1 was developed for short head waves which have high encounter frequency. For such waves, the impact of motions caused by the waves can be disregarded, and the primary factor influencing added resistance is the wave reflection of the hull at the waterline. Therefore, this method is only suitable for lower significant wave heights and for small heave and pitch during the sail. What is more, added resistance in waves within this method is not affected by ship speed.

Due to all simplifications, it was clear that prediction of added resistance in waves for tankers and bulk carriers is not accurate as it usually provided too high values of R_{AW} in comparison with R_T. Therefore, it was decided to limit the applicability of Hempel model for the prediction of annual CO_2 emission to only containerships for which more reliable results of R_{AW} are obtained which are within limits presented by *Kim et al. (2023)*.

Taking into account that the added resistance in waves is much more important resistance component within ship total resistance than added resistance due to wind, in future development of Hempel model for the prediction of annual CO_2 emission, the prediction of R_{AW} will be improved. From the literature review there are several models which could be implemented for such prediction, for example *Kim et al. (2022)* which combines *Liu and Papanikolaou (2020)* and *Lang and Mao (2021)* methods. This will allow the application of developed model to various ship types and the improvement in the prediction of the annual CO_2 emission. Currently, within Hempel model for other ship types than containerships, sea margin approach is used for the prediction of weather effects, but those results are not presented in this paper.

The added resistance due to aging and fouling effects are separately accounted. Aging effects are determined according to *Gundermann and Dirksen (2016)* and they depend on ship age, while fouling effects are accounted using speed loss/power increase values for every given coating and aside from coating they are dependent on time since DD. If there is no information about which coating is applied on a certain ship, then it is assumed that low tier self-polishing copolymer (SPC) coating is applied. What is more, for low friction coatings, an out of dock power saving is added, *Sfiris et al. (2023)*. An out of dock power saving accounts for smoothness of low friction coatings which causes lower initial required power after its application, *Bertelsen and Meseguer Yebra (n.d)*. In the literature there are several studies which demonstrates the potential benefits of low friction coatings over SPC coatings as presented in *Schultz (2004), Demirel (2015), Farkas et al. (2021).*

In order to predict required power for propulsion i.e., brake power at given speed, propulsive efficiency has to be determined:

$$\eta_P = \eta_H \eta_O \eta_R \eta_M$$

η_H is the hull efficiency, η_O is the propeller open water efficiency, η_R is the relative rotative efficiency and η_M is the mechanical efficiency.

Constant values η_R=1 and η_M = 0.98 are taken, as done in *Kristensen and Lutzen (2012)* and *Kim et al. (2023)*. For the prediction of hull efficiency, wake fraction and thrust deduction fraction are calculated using both *Holtrop and Mennen (1982)* and *Kristensen and Bingham (2017a)*. Namely, *Holtrop and Mennen (1982)* approach is prioritized, however if unreasonable values for wake fraction or thrust deduction fraction are obtained, then those values are determined using *Kristensen and Bingham (2017a)*. During the determination of propulsive efficiency, important input variable is propeller diameter which is modelled using either 70% of draught value, or equations presented in *Kristensen and Lutzen (2012)*, which are different for various ship types. An additional check is adopted in this step using the relationship between MCR, propeller nominal rotation rate and propeller diameter. Propeller open water efficiency is determined using the equations presented in *Kristensen and Lutzen (2012)*, which approximate Wageningen B series. Within the calculation of η_O the most important parameter is propeller load which is determined for R_{Total} within this study. After the brake power is determined it is checked whether it is above limit of specified engine load, as done in *Kim et al. (2023)*.

In order to predict FOC per hour for a given speed, brake power has to be multiplied with SFOC, which is within this study modelled using equation presented in *Kristensen and Binghman (2017b)*, and it depends on engine load. Since this equation is developed for marine diesel/gas oil (MDO/MGO), it is assumed that ship is using this fuel and therefore CO_2 emission is estimated using:

$$CO_2\ emission = FOC \cdot C_F$$

C_F is the carbon conversion factor equal to 3.206 t CO_2 / t fuel.

To complete prediction of annual FOC/CO_2 emission, AE consumption has to be modelled. During ship sail, AE consumption is estimated using *IMO (2014)*. For consumption during anchorage in port basin and berthing ME and AE loads presented in *Budiyanto et al. (2022)* are used. This has enabled the estimation of annual FOC and CO_2 emission for a given ship. The code is developed in Python and as an input it only requires the list of IMO numbers for which results are required. For a given IMO number and one year, FOC and CO_2 emissions are estimated on both yearly level and for every four hour throughout whole year. This estimation takes on average around 0.1 CPU hours per ship.

3. Results and discussion

Within this section the developed model is validated by comparison of the modelled required power used for propulsion, FOC used for propulsion, and annual CO_2 emissions with the ones from in-service data and with the actual annual CO_2 emissions obtained with DCS for several containerships with different out of DD timings. After the validity of developed model is demonstrated, a case study is prepared in which Hempel model is used to estimate CO_2 emissions in 2024 for ships which will be dry-docked in the beginning of 2024 with the hypothesis that they will have the same operational profile as they had in 2023. Two scenarios are analyzed including antifouling protection using mid-tier SPC and low friction coatings.

3.1. Validation of Hempel model for annual CO_2 emission

Validation of Hempel model is carried out using three different comparisons:

a) Required power used for propulsion is compared within speed-power plots and on timeseries level
b) FOC/CO_2 emission used for propulsion on annual level
c) Total annual CO_2 emission

In total data from 40 different containerships is compared for 2022: data from 23 containerships is used for a), data from 10 containerships is used for b) and data from 17 containerships is used for c).

3.1.1. Required power used for propulsion

To demonstrate the validity of power prediction method within Hempel model, modelled values are compared with the ones from in-service data on timeseries level as well as in speed-power plots. In total, data from 23 containerships are compared, which have different time since DD, coatings as well as different sizes. Due to extensiveness of the obtained results, within Fig.2. speed-power plot is presented for four ships, while in Fig.3. required power for propulsion on timeseries level is provided for those ships as well. Table I presents the characteristics of compared ships in Figs.2. and 3. To demonstrate results of validation for all ships, a power function is fitted to in-service data and modelled data. Thereafter, these equations are used for the calculation of required power for propulsion for average speed in 2022 and relative deviations are obtained and presented in Table I.

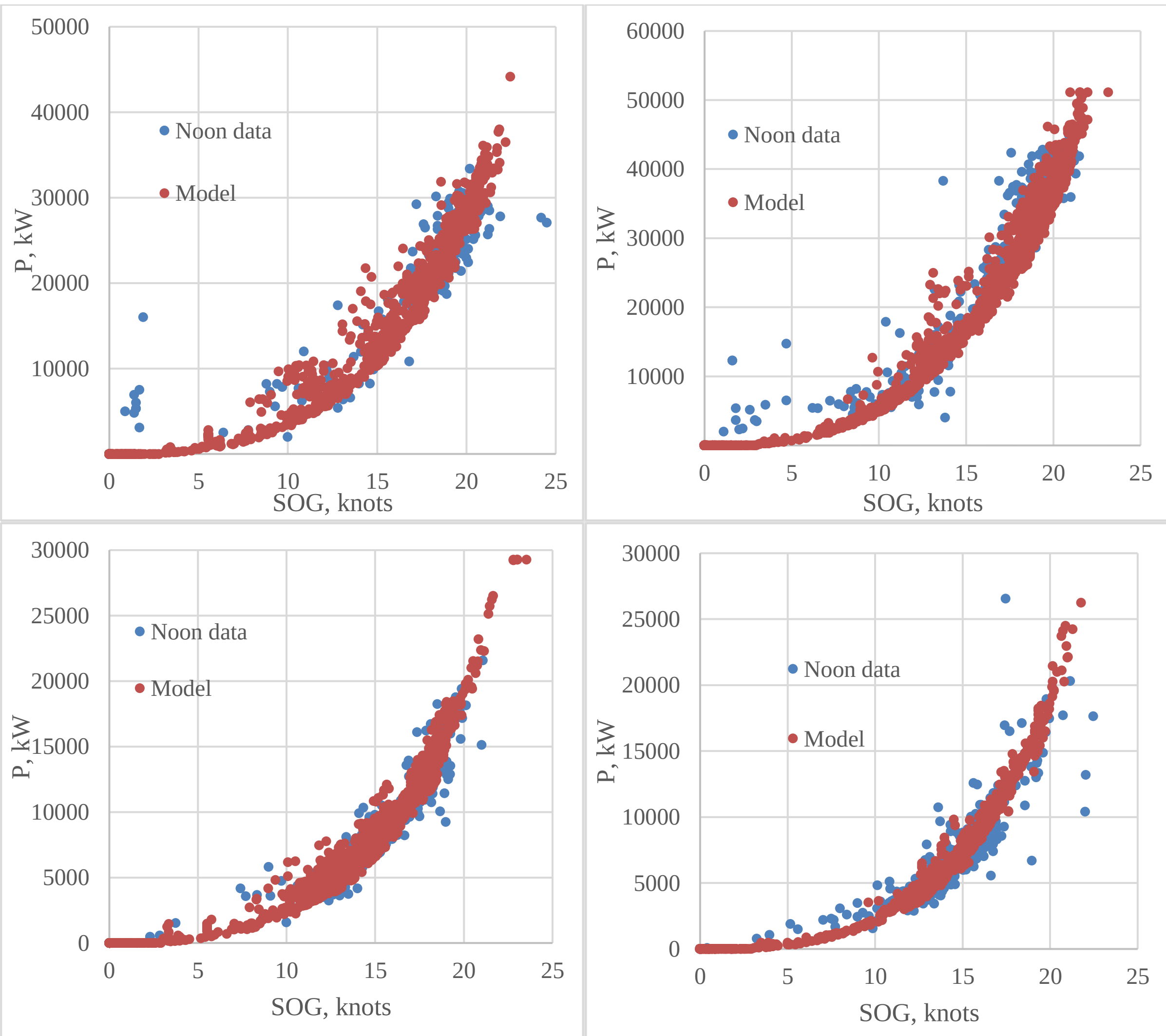

Fig.2: Speed-Power plots for Ship A (upper left), Ship B (upper right), Ship C (lower left) and Ship D (lower right)

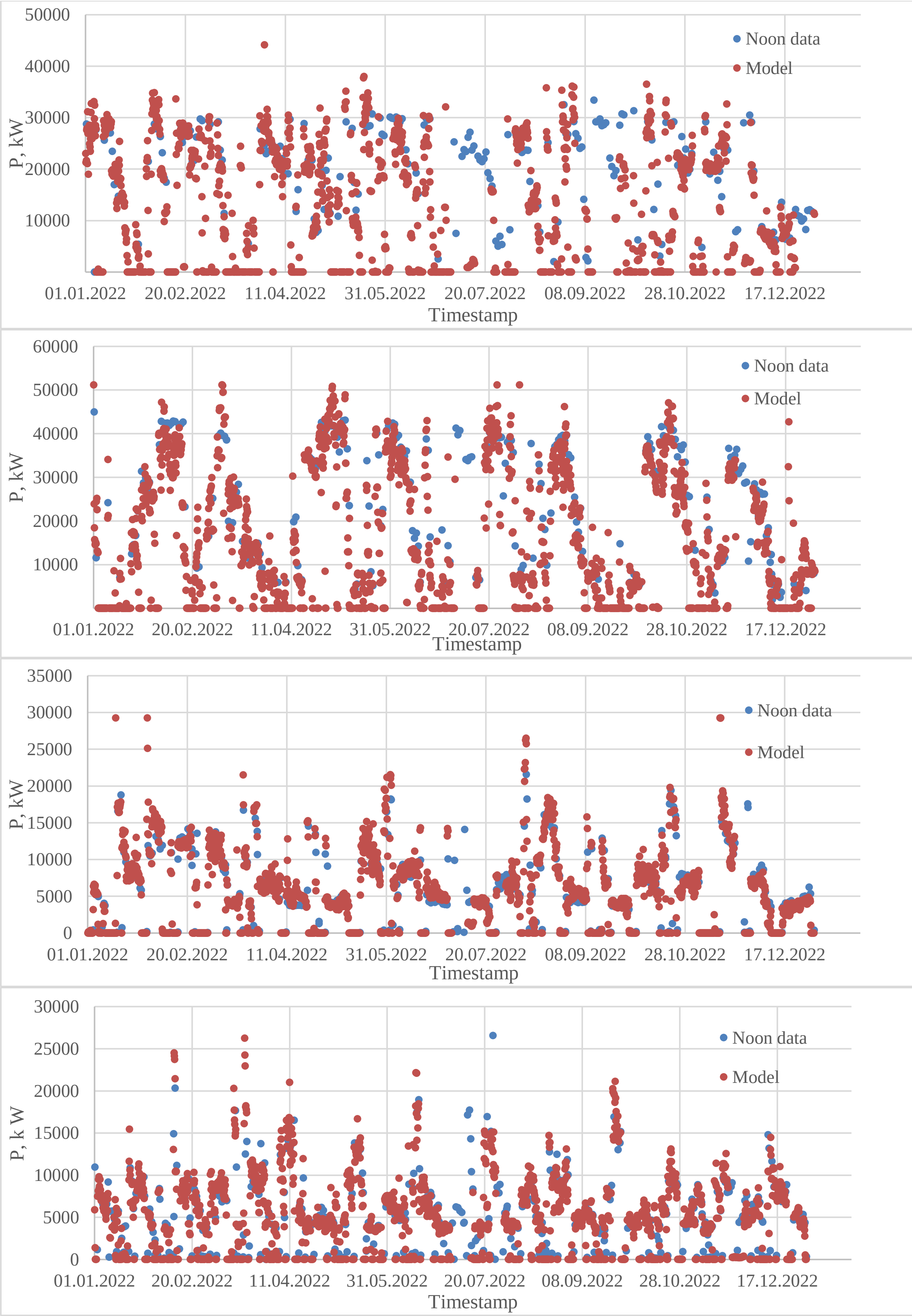

Fig.3: Required power for propulsion timeseries for Ship A (first), Ship B (second), Ship C (third) and Ship D (fourth)

As can be seen from Table I, containerships of different sizes are compared with varying age, time since DD and different antifouling coating applied. The results of comparison show that there is no clear tendency in the predictions, in the sense that there is no correlation between relative deviation and any of the input variables, like age of vessel, type of coating, time since DD, etc. Based on the comparison, it can be concluded that Hempel model can yield minor deviations at some moments in time. However, it seems that the model is capable of adequately capturing required power used for propulsion both on timeseries level, but as a speed-power relationship, as well.

Table I: The characteristics of compared ships and obtained relative deviations (RD)

Ship	Coating	Months since DD in mid 2022	Age in 2022	Ship size	RD,%
A	Low friction coating	39	8	8000-11999 TEU	-1.23
B	Mid-tier SPC	18	7	8000-11999 TEU	-0.95
C	Low friction coating	13	16	3000-7999 TEU	-0.73
D	Low friction coating	13	16	3000-7999 TEU	1.38
E	Low friction coating	38	13	8000-11999 TEU	2.92
F	Mid-tier SPC	8	16	8000-11999 TEU	4.15
G	Low friction coating	13	11	8000-11999 TEU	10.76
H	Mid-tier SPC	15	12	8000-11999 TEU	17.1
I	Low friction coating	33	13	8000-11999 TEU	-8.17
J	Mid-tier SPC	22	7	17000+ TEU	-9.39
K	Null => Low-tier SPC	9	1	12000-16999 TEU	3.11
L	Null => Low-tier SPC	7	1	12000-16999 TEU	3.15
M	Mid-tier SPC	6	0	12000-16999 TEU	-6.14
N	Low friction coating	10	21	3000-7999 TEU	1.61
O	Low friction coating	8	16	3000-7999 TEU	1.39
P	Low friction coating	9	16	3000-7999 TEU	-0.60
Q	Low friction coating	13	14	2000-2999 TEU	9.38
R	Mid-tier SPC	51	14	2000-2999 TEU	-10.25
S	Mid-tier SPC	21	11	8000-11999 TEU	-19.17
T	Low friction coating	24	7	8000-11999 TEU	-1.63
U	Low friction coating	10	6	12000-16999 TEU	-13.21
V	Low friction coating	8	6	8000-11999 TEU	-13.34
W	Null => Low-tier SPC	41	10	8000-11999 TEU	-11.85

3.1.2. FOC/CO_2 emission used for propulsion on annual level

After the validity of Hempel model in the power prediction is demonstrated, a comparison of FOC/CO_2 emission used for propulsion on annual level, distance sailed, as well as the transport work obtained using Hempel model and in-service data is made for 10 containerships, Table II. Transport work is calculated in the same way as attained CII, however annual CO_2 emission for propulsion is used instead of annual total CO_2 emission.

Table II: The obtained RD for annual distance, FOC/CO_2 and transport work

Ship	RD in annual distance,%	RD in annual FOC/CO_2,%	RD in transport work,%
W	-0.82	-7.59	-6.83
U	4.66	5.29	0.60
V	6.39	3.15	-3.04
T	4.14	15.10	10.53
O	3.12	-10.78	-13.48
N	0.64	-1.73	-2.35
C	2.29	5.20	2.84
D	3.24	1.53	-1.65
P	8.04	1.34	-6.21
S	3.90	-4.92	-8.49

Discrepancies in the prediction of annual distances can be attributed to AIS data. It is obvious that due to possible discrepancies in operational conditions within in-service and AIS data, annual FOC/CO_2

emission will also be affected. Other cause of discrepancy is for sure caused by all assumptions applied in Hempel model. Considering this, it can be concluded that reasonable agreement between obtained results using Hempel model and in-service data is achieved, Table II. The prediction of annual FOC/CO_2 emission of containership enables the possibility of evaluating the mitigation potential of various measures, as well as the analysis of possible fuel savings and payback period (PP). Thus, in this study the mitigation potential of low friction coating is demonstrated and possible financial gains are provided in subsection 3.2.

3.1.3. Total annual CO_2 emission

After the validity of power prediction and annual FOC/CO_2 emission used for propulsion is successfully presented, the comparison between total annual CO_2 emission obtained using Hempel model and in-service data is made for 17 containerships. The comparison is made for annual distance, annual CO_2 emissions and attained CII in terms of RD between result obtained using Hempel model and in-service data, Table III.

Table III: Characteristics of compared ships and obtained RD for annual distance, annual CO_2 emissions and attained CII

Ship	Coating	Months since DD in mid 2022	Age in 2022	Ship size	RD in annual distance,%	RD in annual FOC/CO_2,%	RD in attained CII,%
1	Null => Low-tier SPC	19	26	2000-2999 TEU	-6.47	7.4	14.8
2	Low-tier SPC	36	23	1000-1999 TEU	-1.17	8.7	10.0
3	Low friction coating	10	21	3000-7999 TEU	-2.07	-6.1	-4.1
4	Null => Low-tier SPC	15	16	3000-7999 TEU	-1.38	5.0	6.5
5	Low friction coating	13	16	3000-7999 TEU	0.95	-2.2	-3.1
6	Low friction coating	8	16	3000-7999 TEU	0.48	-3.8	-4.2
7	Mid-tier SPC	16	15	2000-2999 TEU	-4.77	4.2	9.4
8	Null => Low-tier SPC	9	16	1000-1999 TEU	-6.48	-14.3	-8.4
9	Null => Low-tier SPC	45	14	3000-7999 TEU	-6.61	-0.7	6.3
10	Low friction coating	37	13	3000-7999 TEU	-0.56	-1.4	-0.8
11	Null => Low-tier SPC	14	11	8000-11999 TEU	-0.18	-4.9	-4.8
12	Null => Low-tier SPC	14	11	2000-2999 TEU	-2.95	-11.8	-9.1
13	Null => Low-tier SPC	15	11	12000-16,999 TEU	-8.45	-2.6	6.4
14	Low friction coating	9	10	12000-16,999 TEU	-3.48	3.8	7.5
15	Null => Low-tier SPC	5	10	12000-16,999 TEU	-6.01	-2.2	4.0
16	Null => Low-tier SPC	6	10	12000-16,999 TEU	4.45	14.3	9.4
17	Mid-tier SPC	35	8	3000-7999 TEU	-3.80	3.1	7.2

From the obtained results of comparison, it can be concluded that Hempel model can reliably predict total annual CO_2 emission of containership using the available input data. Current models in the literature are mostly validated only for power used for propulsion on ship level, and not for total CO_2 emissions, or they are validated for total CO_2 emission but not on ship level. The validation on ship level is usually made for only limited amount of in-service data and number of ships, which highlights the importance of this study, where quite extensive validation study is presented. Therefore, it can be concluded that the proposed model for power prediction and energy consumption of containership fleet can contribute to valuable insights related to potential savings of mitigation measures, but also in the bottom-up analysis of the global containership fleet.

3.2. Case study – benefits of low friction coatings

After an extensive validation of Hempel model, which can be used for the prediction of annual FOC/CO_2 emission, the developed model is used to demonstrate the benefits of low friction coating over the mid-tier SPC coating. In total, 88 containerships are analyzed representing ships which will be dry-docked in the beginning of 2024. We assumed that the analyzed ships will have the same operational profile as in 2023. To demonstrate benefits in terms of saved fuel/CO_2 emissions, containerships of various sizes, age, average operational speed, and activity levels are investigated, Table IV. In addition, PP is determined for every containership by considering obtained financial savings due to saved fuel costs, purchasing and DD costs, *Sfiris et al. (2023)*. An average MDO price of 760 $/t is used within the calculations, which is MDO price in the mid-January 2024 in Rotterdam, https://shipandbunker.com/prices#MGO. In order to calculate PP, annual FOC savings should be evaluated, because the possible savings will increase with time since DD is increasing, due to speed loss/power increase values for different coatings. Namely, power increase will be higher for the mid-tier SPC coatings than for the top-tier silicone coating, and this relative difference amongst coatings will be more pronounced for longer time since DD. Also, an out-of-dock power reduction is also important, but this benefit is constant during entire DD period and does not depend on time since DD. Aside from the fuel savings which are present due to the application of low friction coating, new regulative – EU ETS will also affect PP. Namely, if one of the analyzed ship will have certain port call within EU through entire DD period, it will have to pay carbon tax and in that sense ship which has low friction coating will emit less CO_2 and pay less tax, which will again reduce PP. This is not taken into the consideration within current case study.

Table IV: The characteristics of containerships in case study

Average operational speed ($V_{average}$) in 2023, knots	Activity in 2023	Age in 2024	Ship size, TEU
7.7 – 20.8	0.284 – 0.839	5, 10, 15, 20	368 - 23756

On average annual fuel/CO_2 emission savings for analyzed containership fleet is slightly above 7%, with higher savings reaching to 8.9% for ships with higher operational speeds and activity levels. Since higher operational speeds and activity levels are mostly related to larger vessels, it can be concluded that benefits of low friction coatings are more pronounced for them. In terms of PP, 77 of 88 analyzed ships have PP of 12 months or lower, which demonstrates high financial savings which are obtained by application of low friction coating. Remaining ships have PP within second year of DD period, while there is only one ship with PP equal to 25 months. The higher PP are related to lower operational speeds, mostly below 10 knots and lower activity levels.

To further analyze the impact of input variables on PP, statistical analysis is carried out. Correlations between the dependent (PP) and the independent variables ($V_{average}$, activity, design speed (V), wetted surface area (S), DWT, block coefficient (C_B), length between perpendiculars (L_{PP}), width (B) and draught (T)) are expressed through the Pearson's correlation coefficient. Partial correlations between the dependent and each of the independent variables controlling for the other independent variables are presented in Table V.

Within Table V the Pearson's correlation coefficients between all the variables are presented. All correlations are found to be statistically significant at $p<0.01$. The high correlation obtained between S, ship's main particulars and DWT demonstrate that those variables practically convey the same information. Namely, wetted surface area is estimated using these variables, so these results are expected and obvious. Interestingly, the correlation between average operational speed with design speed is not that high, which indicates that they may convey different information. This can be explained with the fact that some vessels apply slow steaming, which then causes that average operational speed is significantly lower than design speed.

Table V: Correlation matrix and partial correlations of the dependent and independent variables

	$V_{average}$	Activity	S	Age	DWT	C_B	L_{PP}	B	T	V	PP
$V_{average}$	1	0.554	0.571	-0.029	0.517	-0.272	0.625	0.576	0.663	0.680	-0.873
Activity		1	0.449	-0.089	0.409	-0.041	0.501	0.429	0.451	0.391	-0.678
S			1	-0.220	0.991	0.084	0.985	0.988	0.939	0.630	-0.557
Age				1	-0.268	-0.053	-0.163	-0.265	-0.112	0.183	-0.027
DWT					1	0.133	0.957	0.979	0.899	0.552	-0.507
C_B						1	0.006	0.013	-0.060	-0.100	0.184
L_{PP}							1	0.973	0.954	0.702	-0.603
B								1	0.940	0.623	-0.556
T									1	0.770	-0.661
V										1	-0.675
PP*	**-0.812**	**-0.477**	-0.147	-0.107	-0.134	-0.113	-0.150	-0.133	-0.227	-0.228	1

* - Partial correlations (controlling for the effect of $V_{average}$ or Activity).

In order to understand better the nature of the interdependencies of the variables, partial correlations are also calculated. The partial correlation of the variables with PP controlling for the effect of the other variables are presented in the last row of Table V. The partial correlation of average operational speed with PP remains significantly high, evidencing that the correlation of these two variables does not depend on the effect of other variables. The same applies to the correlation between activity and PP, while other partial correlations are not significant, meaning that partial correlation of these variables with PP depends on the effect of other variables.

Fig.4.shows the dependency of PP on each input variable. For almost all input variables clear trend can be seen, Fig.4., the higher values of input variables are causing reduction in PP, which can be also seen from Table V. For input variables block coefficient and age no clear trend can be noticed, and for the rest of input variables power function seems to adequately describe the trend. For ship's main particulars, wetted surface area and DWT it seems that there is a certain threshold, after PP is always lower than certain limit. This can be of particular importance, because for such containerships the application of low friction coatings seems more profitable than for other containerships which have lower input variables than this threshold. As already written, the input variables average operational speed and activity have the highest partial correlation with PP, Table V. With the analysis of the obtained results it has been found that PP will be within first year of DD period, if average operational speed is above 11.6 knots and activity level is above 60%, regardless of all other input variables.

This case study demonstrates that for larger containerships, or for containerships which sail on average above 11.6 knots and have activity level above 60%, PP will be within the first year after DD, which presents high financial benefits of applying the low friction coatings in DD in comparison to the application of mid-tier SPC.

The obtained fuel savings due to the application of low friction coating are not only important in terms of financial savings, but also from regulative perspective as well. Currently, if a vessel would get a D-rating 3 years in a row or E rating for one year, shipowner is obliged to submit a SEEMP Part III Corrective Actions Plan before DCS Statement of Compliance can be issued. This requirement can be even stricter after revision of the regulations from IMO in 2025. Amongst the analyzed 88 ships, 47 ships will be obliged to submit a SEEMP Part III Corrective Actions Plan during DD period, if mid-tier SPC coating is applied in DD and no additional mitigation measure is considered. However, if low friction coating is applied in DD, only 22 ships will be obliged to submit a SEEMP Part III Corrective Actions Plan during DD period, meaning that for 25 ships application of low friction coating is sufficient mitigation measure for the entire DD period. This highlights the importance of considering low friction coatings as a very valuable measure for mitigation GHG emissions.

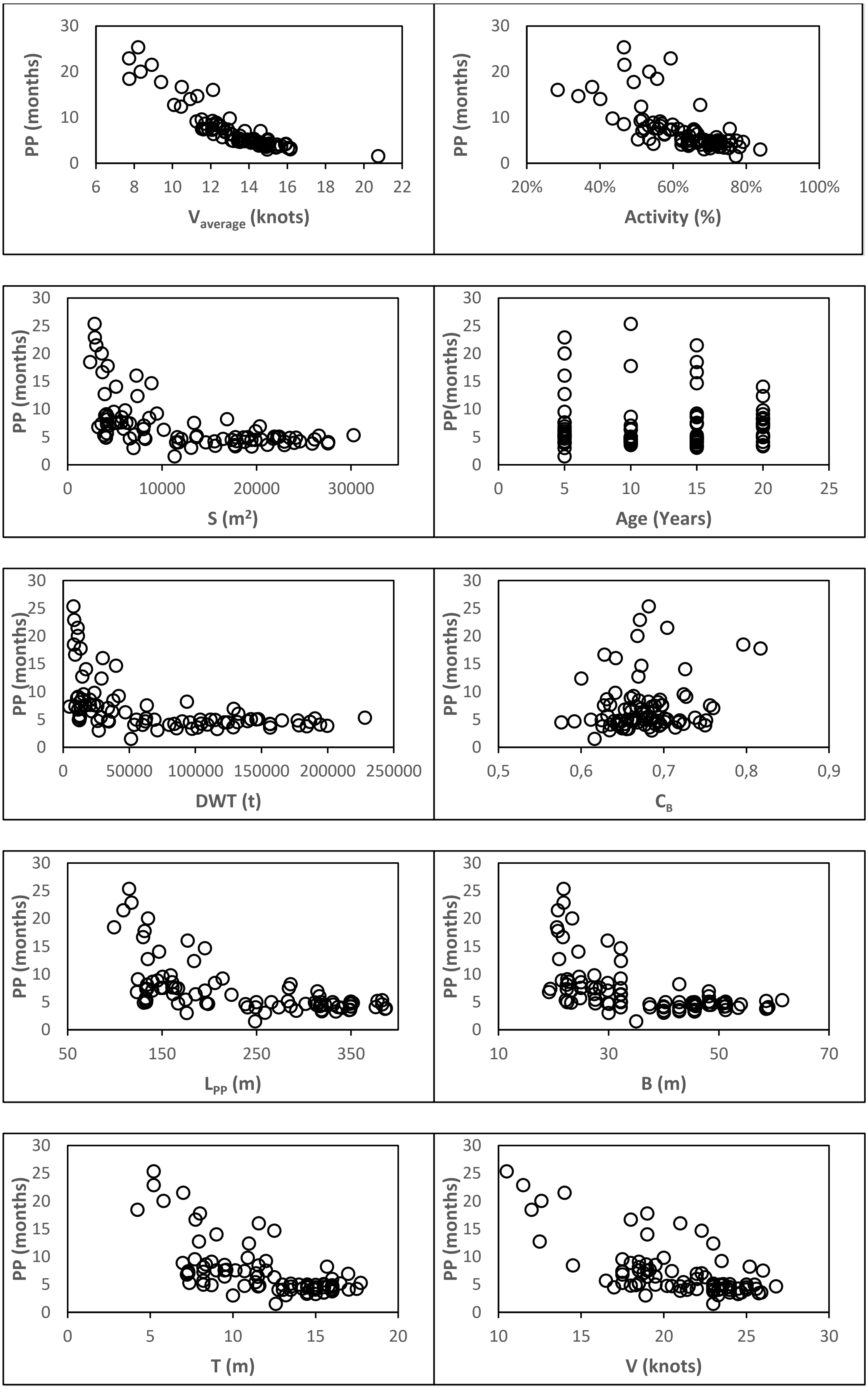

Fig.4: Dependency of PP and input variables

4. Conclusions

This study presents a comprehensive model for predicting annual CO_2 emissions of containerships based on AIS data. It accounts for ship performance in real service conditions and can be used for the prediction of the fuel consumption and CO_2 emissions of both main and auxiliary engines. The proposed model is validated by comparison with the actual annual CO_2 emissions obtained with Data Collection System (DCS) for several containerships. What is more, predicted power for propulsion is compared on timestamp level, as well as within speed power plots in order to further demonstrate its prediction capabilities. The developed model can be applied for the evaluation of mitigation potential of various measures. Since this evaluation is based on real service conditions it can provide more accurate actual savings than the evaluations obtained for certain conditions, most often design conditions.

A case study which demonstrates the benefits of low friction coatings is prepared, and 88 containerships which will be dry-docked in the beginning of 2024 are analyzed. To demonstrate benefits of low friction coatings in terms of saved fuel/CO_2 emissions over the mid-tier SPC, containerships of various sizes, age, average operational speed and activity levels are investigated. In addition to, PP is calculated for every analyzed ship to further emphasize the financial benefits of the low friction coatings. It has been shown that on average annual fuel/CO_2 emission savings for analyzed containership fleet is slightly above 7% of total consumption, with higher savings reaching to 8.9% for ships with higher operational speeds and activity levels. The obtained savings represent very valuable performance gain as well as the reduction of CO_2 emissions. This is even more important because of the three main reasons:

1) The application of low friction coatings does not have any additional side effects, such as slow steaming which causes slowing down of the transport process.
2) The obtained savings are calculated for real service conditions and not for design conditions, for which mitigation potential is usually higher. Furthermore, the obtained reductions in CO_2 emissions are presented as savings of total ship emissions, which include both ME and AE emissions. This is of particular importance, because in the literature other mitigation measures are often investigated by evaluation of their possible gains only in terms of reduction of CO_2 emission used only for propulsion.
3) In terms of PP, it is demonstrated that the most of the analyzed ships have PP within the first year of DD period, which demonstrates high financial savings due to the application of low friction coating.

With statistical analysis it has been demonstrated that the most influential variable on PP is an average operational speed followed by activity level. The impact of other input variables on PP is also investigated and it has been demonstrated that for ship's main particulars, wetted surface area and DWT there is an certain threshold after PP will be lower than certain limit. It has been demonstrated that larger containerships, or for containerships which sail on average above 11.6 knots and have activity level above 60%, will have PP within the first year of DD period. This highlights financial benefits of applying the low friction coatings in DD in comparison to the application of mid-tier SPC.
Aside from the financial benefits related to the application of low friction coatings, the benefits from regulative perspective are also demonstrated. Thus, it has been estimated that 47 out of 88 investigated ships will be obliged to submit a SEEMP Part III Corrective Actions Plan during DD period, if mid-tier SPC coating is applied in DD and no additional mitigation measure is considered. However, if low friction coating is applied in DD this will be sufficient mitigation measure for 25 out of 47 ships for the entire DD period. This highlights the importance of considering low friction coatings as a very valuable measure for mitigation GHG emissions.

-References

AHN, J.; YOU, H.; RYU, J.; CHANG, D. (2017), *Strategy for selecting an optimal propulsion system of a liquefied hydrogen tanker*, Int. J. Hydrogen Energy 42(8), pp.5366-5380

BARREIRO, J.; ZARAGOZA, S.; DIAZ-CASAS, V. (2022), *Review of ship energy efficiency*, Ocean Eng. 257

BERNITSAS, M.M.; RAY, D.; KINLEY, P. (1981), *KT, KQ and efficiency curves for the Wageningen B-series propellers*, University of Michigan, Ann Arbor

BERTELSEN, M.R.; MESEGUER YEBRA, D. (n.d), *HEMPAGUARD - Evidence of performance gains*, HEMPEL, https://www.hempel.com/-/media/Files/Global/PDF/Resource-centre---Marine/Technical-papers/Hempaguard---Performance-and-evidence.pdf

BLENDERMANN, W. (1996), *Wind loading of ships collected data from wind tests tunnel in uniform flow*, IfS report 574, University Hamburg

BOUMAN, E.A.; LINDSTAD, H.E.; STROMMAN, A.H. (2016), *Life-cycle approaches for bottom-up assessment of environmental impacts of shipping*, SNAME Maritime Convention

BUDIYANTO, M.A.; HABIBIE, M.R.; SHINODA, T. (2022). *Estimation of CO2 emissions for ship activities at container port as an effort towards a green port index*, Energy Reports 8, pp.229-236

DALE, T. (2020), *Development of simplified methods for ship powering performance calculations*, Master's thesis, NTNU, Trondheim

DEMIREL, Y.K. (2015), *Modelling the roughness effects of marine coatings and biofouling on ship frictional resistance*, PhD thesis, University of Strathclyde, Glasgow

FABER, J.; HANAYAMA, S.; ZHANG, S.; PEREDA, P.; COMER, B.; HAUERHOF, E.; SCHIM VAN DER LOEFF, W.; SMITH, T.; ZHANG, Y.; KOSAKA, H.; et al. (2020), *Fourth IMO GHG Study*, Int. Mar. Org., London

FARKAS, A.; DEGIULI, N.; MARTIĆ, I.; VUJANOVIĆ, M. (2021), *Greenhouse gas emissions reduction potential by using antifouling coatings in a maritime transport industry*, J. Cleaner Production 295

FUJIWARA, T. (2006), *A new estimation method of wind forces and moments acting on ships on the basis of physical components models*, J. Japan Society of Naval Arch. and Ocean Eng. 2, pp.243-255

GATIN, I.; KALAJDŽIĆ, M. (2022), *Energy Saving Devices Performance Assessment Using CFD*, 7th HullPIC Conf., Tullamore, pp.30-35, http://data.hullpic.info/HullPIC2022_Tullamore.pdf

GUNDERMANN, D.; DIRKSEN, T. (2016), *A Statistical Study of Propulsion Performance of Ships and the Effect of Dry Dockings, Hull Cleanings and Propeller Polishes on Performance*, 1st HULLPIC Conf., Castello di Pavone, pp. 282-291, http://data.hullpic.info/HullPIC2016.pdf

GUO, B.; LIANG, Q.; TVETE, H.A.; BRINKS, H.; VANEM, E. (2022), *Combined machine learning and physics-based models for estimating fuel consumption of cargo ships*, Ocean Engineering 255

HOLTROP, J.; MENNEN, G.G.J. (1982), *An approximate power prediction method*, Int. Shipb. Progress 29(335), pp.166-170

IMO (2014), *MEPC 66/21 - 2014 Guidelines on the Method of Calculation of The Attained Energy Efficiency Design Index (EEDI) for New Ships*, Annex 5, page 1

ITTC (2017), *Recommended procedures and guidelines, preparation, conduct and analysis of speed/power trials*, Int. Towing Tank Conf.

JOHANSSON, L.; JALKANEN, J.P.; KUKKONEN, J. (2017), *Global assessment of shipping emissions in 2015 on a high spatial and temporal resolution*, Atmosph. Environ. 167, pp.403-415

KALAJDŽIĆ, M.; VASILEV, M.; MOMČILOVIĆ, N. (2023), *Inland waterway cargo vessel energy efficiency in operation*, Brodogradnja 74(3), pp.71-89

KIM, Y. R.; STEEN, S.; KRAMEL, D.; MURI, H.; STRØMMAN, A.H. (2023), *Modelling of ship resistance and power consumption for the global fleet: The MariTEAM model*, Ocean Eng. 281

KIM, Y.; ESMAILIAN, E.; STEEN, S. (2022), *A meta-model for added resistance in waves*, Ocean Eng. 266

KRAMEL, D., MURI, H., KIM, Y., LONKA, R., NIELSEN, J.B., RINGVOLD, A.L., BOUMAN, E.A.; STEEN, S.; STRØMMAN, A.H. (2021), *Global shipping emissions from a well-to-wake perspective: the MariTEAM model*, Environ. Science & Technology 55(22), pp.15040-15050

KRISTENSEN, H.O.; BINGHAM, H. (2017a). *Prediction of Resistance and Propulsion Power of Ships*, https://gitlab.gbar.dtu.dk/oceanwave3d/Ship-Desmo/-/blob/master/Report%204%20-%20Resistance%20and%20Propulsion%20Power%20-%20June%20%202017.pdf

KRISTENSEN, H.O.; BINGHAM, H. (2017b). *Energy demand and exhaust gas emissions of marine engines*, https://gitlab.gbar.dtu.dk/oceanwave3d/Ship-Desmo/-/blob/master/Report%205%20-%20Energy%20demand%20and%20emissions%20of%20marine%20engines%20-%20May%202017.pdf

KRISTENSEN, H.O.; LÜTZEN, M. (2012), *Prediction of resistance and propulsion power of ships*, Clean Shipping Currents 1(6), pp.1-52

LANG, X.; MAO, W. (2021), *A practical speed loss prediction model at arbitrary wave heading for ship voyage optimization*, J. Marine Science and Application 20(3), pp.410-425

LIU, S.; PAPANIKOLAOU, A. (2020), *Regression analysis of experimental data for added resistance in waves of arbitrary heading and development of a semi-empirical formula*, Ocean Eng. 206

MURI, H.; STRØMMAN, A.H.; RINGVOLD, A.L.; LONKA, R.; BOUMAN, E. (2019a), *Influence of weather on emissions from the global shipping fleet*, Geophysical Research Abstracts 21

MURI, H.; STRØMMAN, A.H.; RINGVOLD, A.L.; LONKA, R.; LINDSTAD, E.; BOUMAN, E.A.; (2019b), *A new emission inventory of the global maritime fleet; the effect of weather*, AGU Fall Meeting Abstracts, pp.A21W–2637

OLMER, N.; COMER, B.; ROY, B.; MAO, X.; RUTHERFORD, D. (2017), *Greenhouse gas emissions from global shipping, 2013–2015 Detailed Methodology*, Int. Council on Clean Transportation, Washington/DC, pp.1-38

SCHULTZ, M.P. (2004), *Frictional resistance of antifouling coating systems*, J. Fluids Eng. 126, pp.1039-1047

SFIRIS, P.; DEMIREL, Y.K.; AVLONITIS, V.; PAGONI, S., (2023). *Navigating Energy Efficiency Dilemmas in the CII Era*, 8th HULLPIC Conf., Pontignano, pp. 171-187, http://data.hullpic.info/HullPIC2023_Pontignano.pdf

SMITH, T.W.; JALKANEN, J.-P.; ANDERSON, B.; CORBETT, J.J.; FABER, J.; HANAYAMA, S.; O'KEEFFE, E.; PARKER, S.; JOHANSSON, L.; ALDOUS, L.; RAUCCI, C.; TRAUT, M.; ETTINGER, S.; NELISSEN, D.; LEE, D.S.; NG, S.; AGRAWAL, A.; WINEBRAKE, J.J.; HOEN, M.; CHESWORTH S.; PANDEY, A. (2014), *Third IMO GHG study 2014*., Int. Mar. Org., London

STEEN, S.; AARSNES, J.V. (2014), *Experimental methods in marine hydrodynamics*, Lecture Notes

STENSON, P. (2015), *Predicting the rough and the smooth*, The Naval Architect, pp.36–38

TVETE, H.A.; GUO, B.; LIANG, Q.; BRINKS, H. (2020), *A modelling system for power consumption of marine traffic*, 39th Int. Conf. Offshore Mechanics and Arctic Eng.

WERNER, S.; NISBET, J.; OLSSON, F. (2022), *Sea Trial Methodology for Wind Assisted Ships*, 7th HullPIC Conf., Tullamore, pp.124-140, http://data.hullpic.info/HullPIC2022_Tullamore.pdf

YOU, Y.; LEE, J.C. (2022), *Activity-based evaluation of ship pollutant emissions considering ship maneuver according to transportation plan*, Int. J. Naval Architecture and Ocean Eng. 14

Enhancing Linear Models Vessel Performance Prediction through Domain-Informed Feature Engineering and Data Pre-processing

Georgios Papachristou, METIS Cyberspace, Athens/Greece, giorgos.papachristou@metis.tech
Georgios Antonopoulos, METIS Cyberspace, Athens/Greece, giorgos.antonopoulos@metis.tech
Angeliki Dimitrokalli, METIS Cyberspace, Athens/Greece, angeliki.dimitrokalli@gmail.com
Andreas Doulgeridis, METIS Cyberspace, Athens/Greece, andreas.doulgeridis@metis.tech
Elpida Loizou, METIS Cyberspace, Athens/Greece, elpida.loizou@metis.tech
Georgios Manditsios, METIS Cyberspace, Athens/Greece, georgios.manditsios@metis.tech

Abstract

Vessel hydrodynamic performance is a critical factor influencing operational costs and environmental impact, making accurate prediction of power demand a crucial aspect for all stakeholders involved. Conventional approaches often employ more complex machine learning models, but this paper challenges the notion that linear models cannot achieve comparable performance. Their simplicity, robustness, and well-understood theoretical foundations make them a valuable tool for predictive applications that require extrapolation capabilities. By leveraging careful feature engineering based on Marine domain knowledge and data pre-processing, we demonstrate that linear models can effectively predict required power and associated fuel consumption, under varying operational and external weather conditions. The problem formulation intentionally refrains from treating the task as a time-series problem, aligning with specific applications where the inclusion of the time factor as an input feature is not feasible by design. Extensive testing across a diverse range of vessel types validates the effectiveness of this approach, achieving comparable accuracy to more sophisticated models like Gradient Boosting Trees and Neural Networks. These findings highlight the potential of linear models in maritime predictive analytics, enabling a wide range of applications. This research underscores the importance of careful feature engineering and data pre-processing in enhancing predictive performance. Future research should explore broader applications and mitigation of identified limitations.

1. Introduction

The maritime industry has been undergoing a significant transformation over the past two decades. In view of stricter regulations concerning environmental preservation, maritime stakeholders are focused on efficient vessel monitoring. The hydrodynamic performance of ships plays a critical role, influencing both operational costs and greenhouse gas emissions. With the rise of Internet of Things (IoT) solutions and high-frequency data collection, ship operators have access to vast amounts of data, enabling more effective vessel monitoring and performance prediction, *Gupta (2011), N.N. (2022).*

Traditionally, ship performance prediction has relied on methods ranging from analytical approaches based on design draft and computational fluid dynamics (CFD) to machine learning (ML). While complex ML models (e.g., neural networks) have gained popularity for their ability to handle non-linear relationships in data, there is growing evidence that simpler, interpretable models can be comparably effective with proper feature engineering, *Gupta (2022), Kriezis (2022)*.

This study shall demonstrate that linear models, when properly engineered with domain-specific features based on cleaned data, can predict effectively vessel performance under varying operational and external weather conditions with comparable accuracy to more sophisticated models. The analysis was based on 2 years' data from 100 vessels, predominantly bulk carriers, and tankers. This extensive data collection allows comprehensive validation and testing across a diverse range of vessel types and operating conditions, ensuring the generalizability and robustness of the findings.

In summary, this study aims to bridge the gap in maritime predictive analytics by leveraging the strengths of linear models in conjunction with sophisticated feature engineering and data pre-processing techniques. The results have the potential to offer ship operators a more accessible, efficient, and environmentally friendly approach to vessel performance monitoring and prediction.

1.1. Pre-processing framework

In the context of in-service ship performance, the current industry standard has been ISO 19030, *ISO (2019)*. It provides an initial framework for collecting, storing, cleaning and validating measurements, that is essential to ensure the quality and reliability of available data, *Chen et al. (2023)*. These processes are not free of criticism as employed methods regarding data filtering have been characterized as strict, *Valchev et al. (2022)*, and may lead to a misrepresenting dataset, *Farkas et al. (2020)*. In the context of this paper, data pre-processing will mainly focus on the methods used to rule out erroneous measurements, mainly distortions, disturbances, spikes, drop-outs, and null values, *Dalheim and Steen (2020a)*, which are potentially present to the acquired data. This process is an invaluable part of any meaningful analysis.

Data preparation includes extracting, compiling, screening, and validating the data to give it a structure, format, and quality suitable for further processing, *ISO (2015)*. For the present study, all examined vessels were equipped with a continuous data acquisition system, with a sampling rate of 15 seconds. All acquired measurements are retrieved, synchronized, and compiled in a tabular format and sorted sequentially based on the timestamp, using a 1-minute average.

High-frequency data introduces additional considerations due to the inherent unreliability of certain sensors, *Skamagkas (2022)*. For instance, even with regular cleaning and calibration speed logs and draft transducers remain sensitive to changes in speed and external conditions due to their operating principles, i.e., Doppler and Venturi effects respectively, *Gupta (2022), Dalheim and Steen (2021)*, requiring extensive validation before analysis. Another challenge arises from the use of weather hindcast data, which are retrieved with a 1-hour resolution and are linearly interpolated in space and time over the vessel's course. This process can be further affected by drifting or missing GPS latitude values, *Karagiannidis (2019)*, potentially compromising the accuracy and completeness of the weather data obtained from third-party providers. To address these issues, validation and imputation mechanisms are employed by the monitoring system to fill out missing or nonsensical values, which are beyond the scope of this paper. A method to correct acquired draft values inspired by the work of *Gupta (2021)* is used in our pre-processing framework.

Another consideration is the physical systems properties that are being analyzed, and the context in which the data will be used, *Karagiannidis (2019)*. This study aims to accurately predict the power requirements of the analyzed vessels under the diverse external influences they encounter during operation. A ship is a slow-moving system and can be assumed to be in a state of equilibrium, but is not free from transitional states or external phenomena i.e., accelerations/decelerations, ballasting operations, maneuvering, wind gusts, etc., *Gupta et al. (2021)*. Therefore, it is necessary to identify non-stationary behavior for an unbiased interpretation of the data, *Dalheim and Steen (2020a)*.

The final pre-processing framework employed in the present study includes the setting of domain, asset, and operational lower and upper limits, filtering, weather criteria, and a stationary check to further rule out acceleration related measurements. Upper and lower domain wise limits were set for each parameter, to rule out outliers depending on their natural significance. Asset specific limits were set based on vessels' characteristics and equipment (e.g., Main engines MCR). A layer of operational limits was also implemented to avoid numerical errors, or operations not associated (i.e., non-sailing conditions, rudder angle, shallow waters) with intended predicted operation, *Coraddu et al. (2019)*.

The next layer, which includes established criteria of ISO 19030 was then applied by splitting the dataset into 10-minute non-overlapping consecutive blocks and implementing Chauvenet's criterions in and with use of stipulated validation criteria as per ISO 19030. When the data of one parameter was null or invalid according to Chauvenet's criterion, the complete data point was marked as invalid (i.e., all measurements with the same timestamp). If a data point was marked as invalid according to the validation criteria, then the entire data block was marked as invalid. Unsteady samples remaining were filtered out by the use of a sliding-window quasi-steady filter based on the work of *Dalheim and Steen (2020a)*, with appropriate window length and sensitivity parameters for each quantity, *Dalheim and Steen (2020b)*.

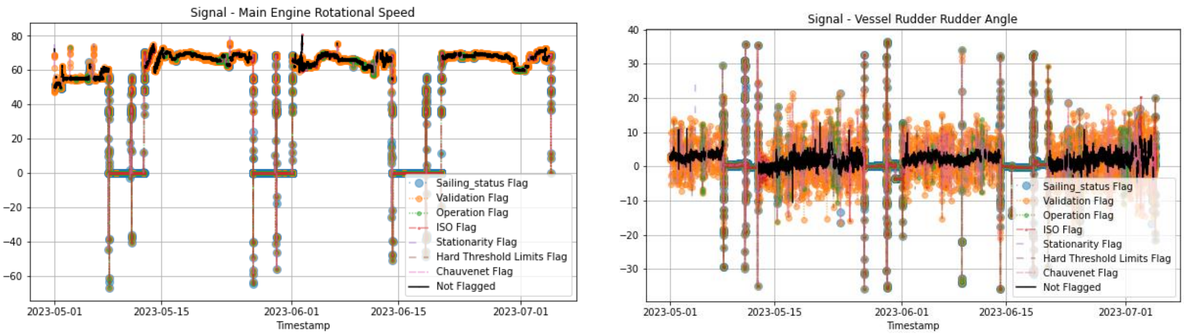

Fig.1: Pre-processing framework data flagging examples for timeseries data from different signal perspective, Rotational Speed (left plot) and Rudder Angle (right plot).

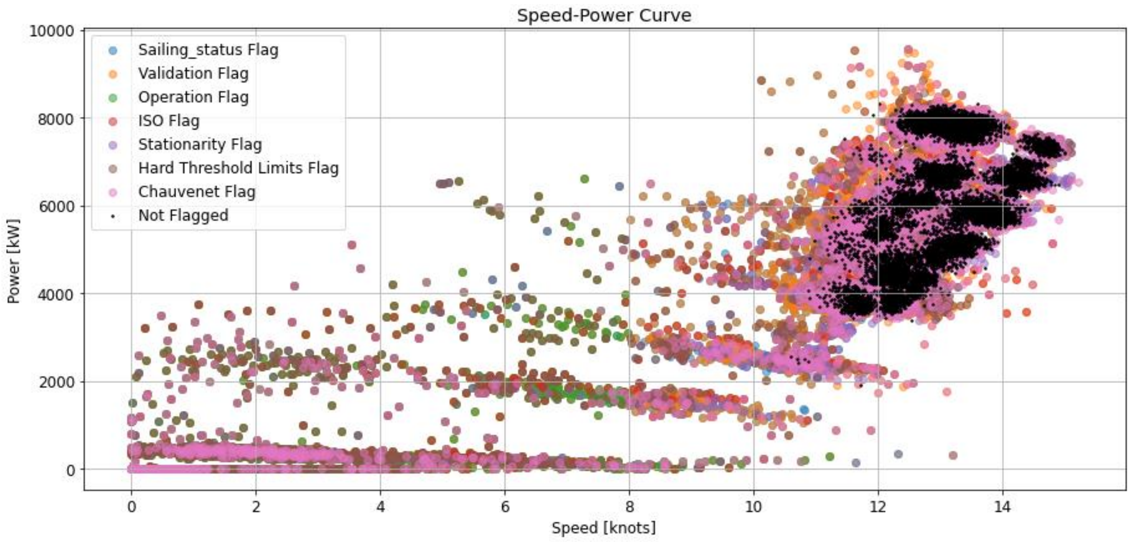

Fig.2: Pre-processing framework data flagging areas from Speed-Power perspective. Black markers represent the remaining datapoints (not flagged). The colored markers are the excluded (flagged) datapoints; colored according to the flagged method.

Environmental conditions based filtering in ISO 19030 has been criticized as strict, *Valchev et al. (2022)*, imposing an upper limit to wind speed of 4BF independent of ship characteristics, *Sogihara (2019)*; on the other hand, greater wind speeds have been associated with inconsistent and unreliable measurements, *Coraddu et al. (2019)*. This limitation is established since wind waves directly correlate with wind speed. Given the absence of a correction method for added wave resistance in the current standard, setting this limit is a logical precaution against exaggerated sea states. Of course, the absence of wind generated waves does not necessarily mean the absence of swell which can be a significant part of the added wave resistance, *Tsarsitalidis and Rossopoulos (2018)*. Data from studied vessels revealed that a notable part of their operation lies outside the above limit and the intended prediction capabilities of the developed features. To this end, *ISO (2015)* proposed limits were employed, which are applied in relation to the ship's length and include effects of both wind generated waves and swell, in line with *Park et al. (2018)*. In addition, a directional filter was applied for waves as proposed by *Carchen et al. (2019)*, where a strictness parameter is employed so that head seas have a more relaxed filtering, since effects on wake from following seas can be misleading.

1.2. Draft Correction

Draft measuring sensors are not calibrated, nor designed to accurately measure the draft of a moving ship. Moreover, the response of a ship to external waves further distorts the pressure sensor measurements, inferring noise in following calculations. In the context of employing sensor data for our research correcting the rather noisy and unreliable during operation, draft measurements are significant, as along with speed, are the most prominent contributors in the calm-water resistance of slow-steaming ships. To counteract those effects, present in the acquired data, a method to identify the non-sailing periods was employed and draft measurements coinciding with those periods were interpolated, resulting in a smooth signal during sailing periods, with satisfactory results. The resulting draft was further validated against the measured by limiting the mean absolute percentage error (MAPE) according to a well-defined threshold, but further validation against other sources (e.g., Noon Reports), and refinement is needed to identify plausible inaccuracies.

The results are illustrated in Fig.3, where the corrected daft during sailing is represented by continuous green sections, against the raw measurements of the sensors in orange. The corrected draft and trim were used for the estimation of draft dependent quantities, based on regression equations of their hydrostatic data or well-known methods used in preliminary design process.

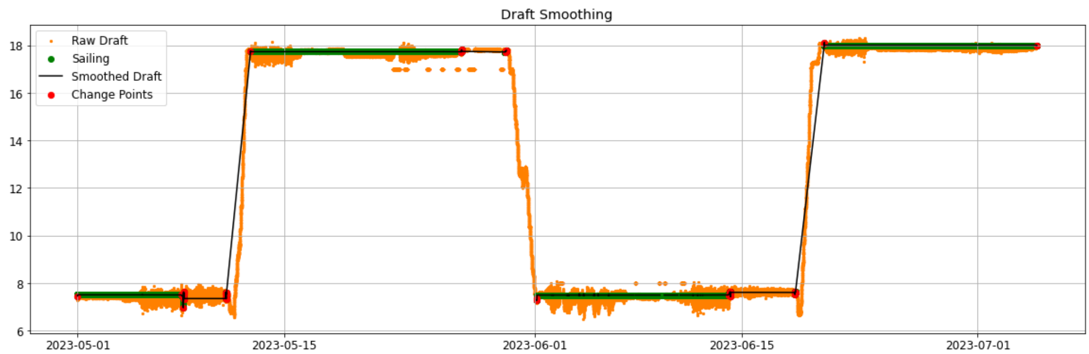

Fig.3: Preprocessing: Draft smoothing

2. Modeling Methodology

A shaft power prediction model based on external conditions is a common regression modeling task in the maritime industry. This type of modeling involves identifying the statistical relationship between a dependent variable (shaft power) and a set of independent variables (e.g., ship speed, draft, weather conditions). While machine learning (ML) incorporates a vast and diverse range of models and implementations, this study selects one model from each main family: linear, tree-based, and neural networks.

Table I: Machine Learning model families with Python implementations used in this paper

Estimator Family	Algorithm	Implementation (library)
Linear	Linear Regression **(lr)**	sklearn
Tree based	Gradient Boosting Trees **(gbt)**	LightGBM
Neural Network	Multi-layer Perceptron **(mlp)**	sklearn

2.1. Linear Model Assumptions

In statistical modeling, there is an unknown mapping function from input (e.g. the set of the independent variables) to the output (i.e. the target variable Y) as the following:

$$Y = f(X) + \varepsilon$$

where f is the mapping function and ε is the residuals error.

To estimate the unknown function, a statistical model needs to be fitted over the training data. In linear models, some assumptions are typically made for the underlying relationship between the X and Y. Generally, when the function f characterized by assumptions regarding its form, then it pertains to a parametric model. These underlying assumptions are linearity, homoscedasticity, residuals normality and absence of multicollinearity.

Linearity means that the model forces the prediction to be a linear combination of features. In other words, a change in the response Y associated with one-unit change in predictors X_j is constant, regardless of the value of X_j, *James et al. (2023)*. The study examines sets of predictors ranging from simpler to more complex, developed through feature engineering detailed in Section 4, building on existing research, *Gupta (2022)*, *Kriezis (2022)*, and introducing novel physics-based features (Section 4.4). The linearity assumption between all the study features and the target (shaft power) is given by Pearson correlation coefficient Fig.4.

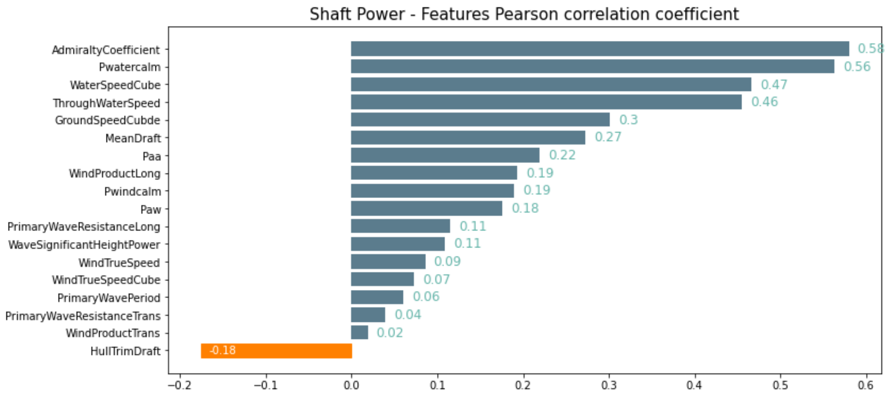

Fig.4: Pearson correlation coefficient (PCC) between Main Engine Power and features. The plot is calculated for cleaned data over 100 vessels for 2-year period. Bars are sorted based on the Pearson Correlation value

Homoscedasticity means that the error terms exhibit constant variance. To evaluate this assumption, comparing diagrams of actual versus fitted values which is a common practice to assess alignment. In Fig.4, from the leftmost to the rightmost plots, the models present decreasing homoscedasticity. Specifically, in the right-hand plot the depicted model demonstrates a lack of constant variance evidenced by the divergence between the actual and predicted values.

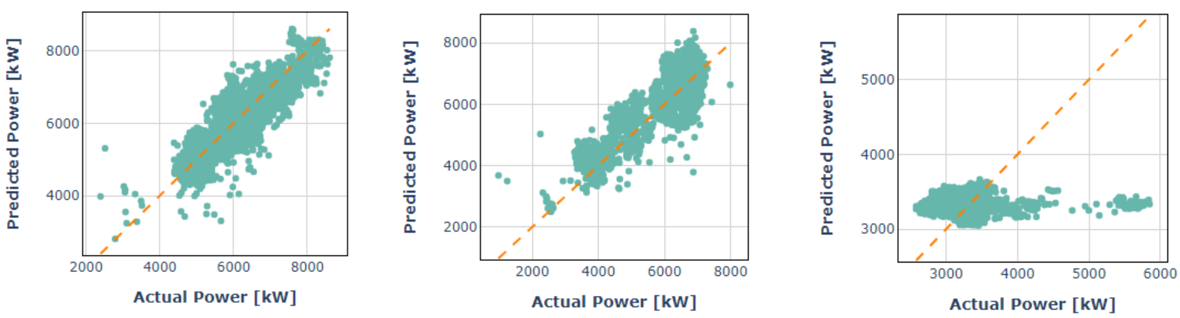

Fig.4: Actual vs Predicted Power plot (Homoscedasticity detection) across three different ships

Additionally, Fig.5. (right) depicts a common scenario observed in vessels operating at constant main engine power. This behavior while potentially achieving low error metric (e.g. MAPE) signifies a non-generalizable model. No homoscedastic residuals (heteroscedastic) are a strong indicator of linear models' lack of generalization across the range of the target variable (Shaft Power in our case). However, achieving homoscedasticity is challenging in non-linear problems characterized by complex patterns.

Residuals normality is another assumption for linear models. In Fig.6, the plots depict the assumption of normal distribution of the residuals. In the left plot the assumption of the normal distribution is validated compared to models from different ships.

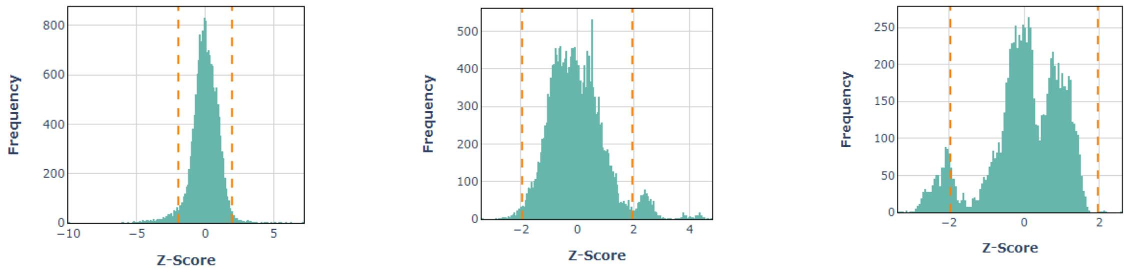

Fig.6: Residuals Normality across three different ships. The left plot has a close to normal distribution compared to other ships.

Finally, the multicollinearity assumption refers to the situation in which the variables in a regression might be correlated with each other. The primary techniques for multicollinearity detections are Pearson Correlation Coefficient, Variance inflation factor and eigenvalue method, *Noora (2020)*. In this study Pearson Correlation is used, Fig.7.

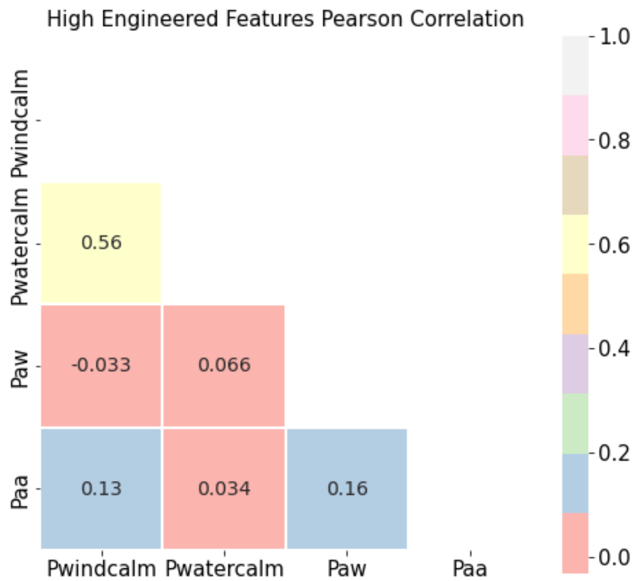

Fig.5: Pearson Correlation Coefficient for Highly Engineered Features

3. Feature Engineering

This section outlines an incremental feature engineering approach. Prior studies have demonstrated that models employed only raw signals, such as Vessel Through Water Speed, Draft Trim etc. have poor goodness of fit, *Kriezis (2022)*. This phenomenon is particularly pronounced in linear estimators due to the inherent non-linear relationship between features and the target variable. To demonstrate the effectiveness of feature engineering in transforming non-linear effects into linear relationships and enhancing model performance, this study places a particular emphasis on linear models.

3.1. Scenario - No Engineered

This scenario contains only raw features, without any transformation. (Raw features are signals without any transformations. However, they are not pure high frequency signals. As they have pass through our pre-processing framework. Moreover, sources such Draft or Trim have an extra processing level for corrections and smoothing.) This model will be used as a baseline model. The feature-set is based on other research, *Kriezis (2022)*, and is inspired from generalized formulas for vessel performance, *Gupta (2022)*. No grid search or statistical feature selection techniques are applied, rather domain expertise and insights from past studies. Table II gives the selected features.

Table II: No engineered feature-set

Scenarios	**Feature**	**Formula**
No Engineered [baseline]	Draft Mean	D_{mean}
	Draft Trim	D_{trim}
	Through Water Speed	V_w
	True Wind Speed	V_{wind}
	Combined Wave Sign. Height	H_p
	Combined Wave Period	T_p

The features represent a combination of operational-related features, and measures of weather external conditions for wind and sea. For sea state, we either treat waves as separate components, divided into wind waves and swell, or use the combined wave characteristics, *Lakshmynarayanana (2017)*. All relevant measurements are directly obtained from the weather provider. The model intentionally excludes directional features, such as wind or wave angle (0˚- 360˚), due to their non-linear relationship with the target variable. Employing these features directly can lead to model degradation and suboptimal performance.

3.2. Scenario - Light Engineered

The starting point of feature engineering in maritime industry, is based on the widely accepted speed-power law. This law assumes a relation $P \approx \mathrm{V}^{\mathrm{c}}$ where $c \approx 3$ when the speed is around the design draft, *MAN ES (2023)*. However, it's important to mention that other studies have proven that the previous law tends to underestimate the power in lower speeds, *Berthelsen (2021)*. Features from other studies, *Kriezis (2022),* were selected, Table III.

Table III: Light engineered feature-set

Scenarios	**Feature**	**Formula**
Light Engineered	Draft Mean	D_{mean}
	Through Water Speed Cube Power	V_w^3
	True Wind Speed Cube Power	V_{wind}^3
	Combined Wave Sig. Height	H_s
	Combined Wave Period	T_p

3.3. Scenario - Middle Engineered

Middle engineered models introduce more advanced features by encapsulating the ship's form characteristics providing insights about the hydrodynamic behavior of the ship. The Admiralty coefficient summarizes the relationship between speed, power and displacement, *Gupta et al. (2021),* in near calm weather conditions. The generalized form of admiralty coefficient is:

$$P = \nabla^{\mathrm{m}} V_w^n \qquad (1)$$

with the most common values be $m = \frac{2}{3}$ and $n = 3$.

However, the speed-power relationship of ships with modern hulls cannot be described well by this formula, *Gupta et al. (2021)*, and various studies have attempted estimate the m, n factors, with one data-driven method proposed by *Berthelsen (2021)*. The approach is based on high frequency data, achieved by sorting speed data and finding the change points in the signal where the slope of speed-power alters. In this scenario, complexity of the model is minimized by employing only a few essential features and utilizing the original admiralty factors. The features are inspired by theoretical formulas for wave and wind resistance as described in *Dekeyser (2022)*. Table IV gives the selected features.

Table IV: Middle engineered feature-set

Scenarios	**Feature**	**Formula**
Middle Engineered	Admiralty Coefficient	$\nabla_{mean}^{\frac{2}{3}} V_w^3$
	Wind Product (long.)	$V_{windrel} \cos(\theta_{rel})$
	Wind Product (trans.)	$V_{windrel} \sin(\theta_{rel})$
	Wave Power (long.)	$H_p^2 T_p \cos(a_{rel})$
	Wave Power (trans.)	$H_p^2 T_p \sin(a_{rel})$

3.4. Scenario - Highly Engineered

Highly engineered features are based on ship resistance theory. This approach integrates empirical formulas which can transform nonlinear effects to linear. This type of modeling is targeted for a parametrical model e.g. a linear estimator, driven to follow linear model assumptions (section 2.1). The generated set will be a collection of features based on calm conditions and weather added resistances. The ship power resistances can be modeled according to ISO 19030:

$$R_{total} = R_{Calm} + R_{AA} + R_{AW} + R_{AH} + R_{Others} \tag{2}$$

R_{Calm} is the ship resistance in calm water conditions, R_{AA}, R_{AW} are the added resistances due to wind and waves and R_{AH} is the added resistance due to increase in hull friction and R_{Others} includes other losses due to other effects e.g. steering. The calm resistance can be split into:

$$R_{calm} = R_{viscous} + R_{wmaking} + R_{acalm} \tag{3}$$

with,

$$R_{viscous} = C_{viscous} \frac{1}{2} \rho_w S V_w^2 \tag{4}$$

and

$$R_{wavemaking} = C_{wmaking} \frac{1}{2} \rho_w S V_w^2 \tag{5}$$

and

$$R_{acalm} = \frac{1}{2} \rho_a A_{XV} C_{AA}(0°) V_G^2 \tag{6}$$

$R_{viscous}$ is the hull viscous (friction) resistance, $R_{wmaking}$ is the wave making resistance and R_{acalm} is the air resistance caused by ship moving through calm air. To overcome this fundamental difficulty to satisfy the similarity laws, a major (first) assumption was made by Froude that the frictional and the wave-making resistances are independent, and the frictional-resistance coefficient depends only on the Reynolds number. The wave-making or residual resistance coefficient depends only on the Froude number.

$$C_{viscous} = f_1\left(\frac{V_w L}{v}\right) \tag{7}$$

and

$$C_{wmaking} = f_2\left(\frac{V_w}{\sqrt{gL}}\right) \tag{8}$$

V is the vessel through water speed, L is the length between perpendiculars, g is the gravity acceleration, v is the kinematic viscosity. For wave-making we generalize the term by creating a polynomial function (3rd power) of Froude number:

$$f_2\left(\frac{V}{\sqrt{gL}}\right) = A_0 C_f F_n^3 + A_1 C_f F_n^2 + A_2 C_f F_n^1 + A_3 C_f \tag{9}$$

For added wind resistances, R_{AA} following ISO 19030 is:

$$R_{AA} = \frac{1}{2}\rho_a A_{XV} C_{AA}(\theta_{rel}) V_{windrel}^2 - \frac{1}{2}\rho_a A_{XV} C_{AA}(0°) V_G^2 \tag{10}$$

In ship modeling the wave resistance is the most challenging factor to model. But due to high complexity, non-linear factors and stochastic effects, we need to simplify the problem and create a generic formula with the most important factors. In bibliography there are plenty of methods for modeling this term. For this study we choose to use the formula, *Hansen (2011):*

$$R_{AW} = 0.64 g H_S^2 C_B \rho_w \frac{B^2}{3L_{OA}}(2 + \cos(\alpha_{rel})) \tag{11}$$

The shaft power needed for moving the ship with a certain speed through water is based on a simplified formula which includes propeller efficiency and mechanical efficiencies (shaft, gearbox):

$$P_{shaft} = f(R_{total} V_w) \tag{12}$$

P_{calm} represents the needed power to overcome the calm-water resistances. R_{AA}, R_{AW} are the added resistances due to wind and waves, P_{AH}. To simplify our study, we did not formulate the P_{AH}, P_{Others} with extra features, because these terms have high complexity due to ship-specific factors, *DeKeyser and Mittendorf (2022)*. Table V gives the selected features are.

Table V: Highly engineered features mathematical formulas summary

Features	**Analytical Formula**
P_{wcalm}	$((f_1\left(\frac{VL}{v}\right) + f_2\left(\frac{V}{\sqrt{gL}}\right))\frac{1}{2}\rho_w S V_w^2)\, V_w$
P_{acalm}	$(\frac{1}{2}\rho_a A_{XV} C_{AA}(0°) V_G^2) V_w$
P_{AA}	$\left(\frac{1}{2}\rho_a A_{XV} C_{AA}(\theta_{rel}) V_{windrel}^2 - \frac{1}{2}\rho_a A_{XV} C_{AA}(0°) V_G^2\right) V_w$
P_{AW}	$(0.64 g H_S^2 C_B \rho_w \frac{B^2}{3L_{OA}}(2 + \cos(\alpha_{rel}))) V_w$

4. Evaluation Framework

The evaluation phase includes models' accuracy and access the predictive and generalization ability as the overall quality of the results. A suboptimal evaluation, in terms of test dataset selection, can include biases and false results. In this study, an extensive evaluation framework is selected in terms of number of ships, types, and testing periods. An arbitrary sample of 100 ships of a diverse range of vessel types with bulk carriers and tankers representing the majority, followed by other categories such as vehicle carriers and container ships. A period of two years was selected for giving various patterns in our models for training and testing phase

In the framework setup, the target was to define how to generalize our models and simulate a near real world training-test setup. This is achieved by a "sliding window" format by using a re- smaller re-train period than train period, Fig.8. This setup is more computationally intensive compared to a "tumbling window" but it's unbiased to start-end of the training-test periods; every data point has been included either as training or test. In time-related problems models are re-trained frequently by keeping the balance between data drift effect (i.e. Hull Fouling in our problem) and re-training cost. We intentionally avoided traditional cross-validation techniques with random folds or data shuffling due to the risk of data leakage. This leakage can lead to overfitting and subsequently, poor performance in real-world deployment.

To comprehensively assess model fit we employed several error metrics which are not biased from target scale. The study primary metric is the MAPE, used to evaluate the accuracy of a prediction of a model by measuring the average percentage difference of the predicted value from the actual values:

$$\mathrm{MAPE} = \frac{1}{N}\sum_{i=1}^{N}\left|\frac{P_i - \hat{P}_i}{\hat{P}_i}\right| \tag{13}$$

As secondary metric we used the Root Mean Squared Percentage Error (RMSPE). The RMSPE measures the accuracy of the model through comparison of the predicted with the actual values by calculating the average of the squared percentage differences between them:

$$\mathrm{RMSPE} = \sqrt{\frac{1}{n}\sum_{i=1}^{n}\left(\frac{P_i - \hat{P}_i}{P_i}\right)^2} \tag{14}$$

MAPE and RMSPE are complement metrics. MAPE is more sensitive to smaller values and RMSPE is more sensitive to larger values.

Another metric for linear models' goodness of fit is the R-squared (R^2). R-squared is very valuable for linear models but it's not suitable for non-linear models. In this study we want to compare the goodness of fit not only of linear models but also for nonlinear, *Spiess (2010)*. In conclusion, the performance of our models can be evaluated by calculating a single statistic, such as the 95th percentile of the error distribution of MAPE, or by visualizing the distribution of MAPE values across multiple evaluation windows for different ships.

Evaluation framework configuration was determined as much closer to a real-time implementation. The training period was selected for having a balance between data variability and time-related factors such as fouling effect. Since the number of rows in the test data varies across windows and ships, it is more representative to use a weighted metric for evaluation. Our weights are integers, giving us the ability to obtain a natural weighted metric by simply repeating elements.

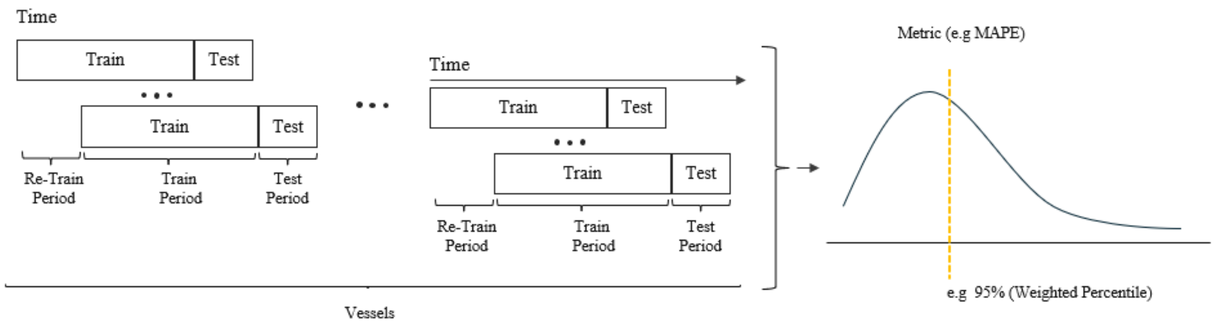

Fig.8: Evaluation framework scoring across test windows and ships. Evaluation framework configuration is total period of 730 days, train period 180 days, test period 15 days and re-train period 15 days.

4.1. Evaluation Results

Evaluation results can be highly correlated with the test dataset specifics and could be biased from extreme rare conditions. To address this issue, bad weather conditions were excluded, as described in Section 2.1. This decision not only removes conditions that are difficult or impossible to model but also reduces the potential for evaluation process biases. MAPE was chosen as the primary metric for evaluation due to its ease of interpretation compared to RMSPE. Additionally, two percentiles (50^{th} and 95^{th}) were used to provide more comprehensive and informative conclusions.

Gradient Boosting Trees (GBT) model is tested only for a subset of feature engineering scenarios, only middle, highly engineered features. This estimator is a computationally intensive algorithm and comparable slower. For future study a more extensive set of runs can be done also in GBT models. The following table summarizes the MAPE score for test, train:

Table VI: Gradient Boosting Trees run results. The results were sorted based on test 95th MAPE percentile. In all gbt tests used the same configuration, learning rate: 0.1, estimators: 200, alpha: 2 lambda: 2

Features	**Train MAPE 95%**	**Test MAPE 95%**	**Test MAPE 50%**	**Train Time (secs)**
Highly Eng.	0.075	0.223	0.080	120-140
Middle Eng.	0.042	0.247	0.083	120-140

Multi-layer Perceptron (MLP) is the selected model for Neural networks (NN). This type of model consists of an input layer, hidden layers, and an output layer. The input layer has the size of the number of input features, while the hidden layer depends on the specific complexity of the problem. The output layer is comprised of a single node responsible for generating the final prediction value. In numerous applications, the optimal number of hidden layers and nodes is determined through a grid search of various configurations. However, in this study, we opted to utilize a structure established from prior research, *DeKeyser (2022)*. Neural networks (NN) are highly sensitive to hyperparameters values. While a comprehensive and computationally demanding evaluation framework was employed for this study, grid search with cross-validation for NN hyperparameter tuning was excluded due to time constraints and computational limitations. Instead, the model configuration was chosen through a combination of prior research, *DeKeyser (2022)*. The cases in Table VII were taken place.

Table VII: Multi-layer Perceptron run results. The results were sorted based on test 95^{th} MAPE percentile. In all mlp tests used the same configuration hidden layers (64, 32, 16, 8), Max Iterations: 1000, Activation: Relu, Solver Adam, Alpha: 0.001.

Features	**Train MAPE 95%**	**Test MAPE 95%**	**Test MAPE 50%**	**Train Time (secs)**
Highly Eng.	0.081	0.219	0.079	60-70
Middle Eng.	0.238	0.331	0.126	1-2

For solver, the Adam method is selected as it is a fast and low memory solver; this decision significantly accelerated the testing procedure. Middle Eng. Runs trained was stopping after few epochs with no improving, as a result the training time be extremely fast for middle engineer features. On the other hand, by using the highly engineering features there was significant improvement in model performance and training time.

Table VIII: Linear models run results. Runs are sorted based on test 95^{th} MAPE percentile. 50^{th} MAPE was also presented only for test dataset

Features	**Train MAPE 95%**	**Test MAPE 95%**	**Test MAPE 50%**	**Train Time (secs)**
Highly Eng.	0.110	0.218	0.071	0.05-0.010
Middle Eng.	0.128	0.242	0.085	0.05-0.010
Light Eng.	0.133	0.259	0.089	0.010-0.015
Raw Features [baseline]	0.140	0.265	0.095	0.05-0.010

To implement the linear regression model, a standard linear regression estimator was employed. Additionally, a standard scaler was utilized alongside the estimator. As linear regression was significantly faster estimator than MLP and GBT, we conducted various runs. The cases examined are presented in Table VIII. Table IX summarizes the best models for each estimator family.

Table IX: Best estimator results. Runs are sorted based on test 95th MAPE percentile. 50th, 95th RMSPE is also provided

Runs	Train MAPE 95%	Test MAPE 95%	Train RMSPE 95%	Test RMSPE 95%
lr **(Highly Eng.)**	0.110	0.217	15.48	24.81
mlp **(Highly Eng.)**	0.081	0.219	12.24	25.71
gbt **(Highly Eng.)**	0.075	0.223	10.38	25.85

Applying feature engineering led significant improvement to model fitting; highly engineered model significantly outperforms the other feature engineering techniques. Linear models have slightly lower test scores (MAPE & RMSPE) and better ratio between train-test dataset. Conversely, Gradient Boosting Trees show a sign of overfitting, with lower train scores and larger test score gaps.

Given the significant disparity between the 50th and 95th percentiles, we decided to visualize its distribution to gain a more comprehensive understanding of model performance. The following plot visualizes the distribution of MAPE scores for each model's test data. A lower area under the curve and a more left-skewed distribution indicates superior model fit. This visualization provides additional insights beyond percentile-based metrics, offering a broader perspective on model performance consistency.

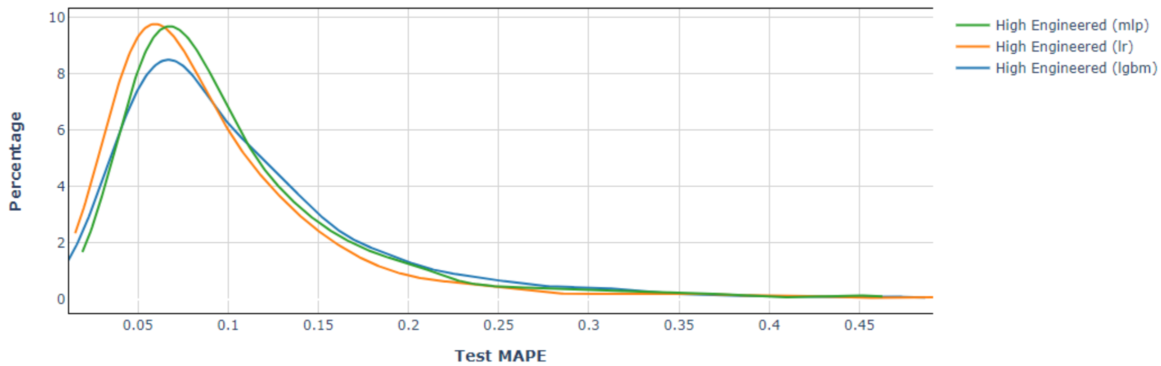

Fig.6: MAPE Score distribution across best feature engineered model for Linear Regression, Multilayer Perceptron and Gradient Boosting Trees

While MAPE and RMSPE are valuable performance metrics, they mark potential prediction underestimation and overestimation patterns. To identify these patterns, additional plots are necessary. Plotting actual vs. predicted power and non-absolute residuals can offer clearer insights. Analyzing data from multiple vessels, with varying power scales, necessitates normalization for meaningful comparison. In Fig.10 we have the actual vs predicted and residuals ratio

$$Residual\ Ratio = \frac{Actual - Predicted}{Actual} \tag{17}$$

for the highly engineered model for each family. Notably, a consistent underperformance pattern is present in low powers and an overestimate at high powers.

This pattern was possibly caused from the operational profile of the ships. Captains often reduce speed during unfavorable weather conditions and tend to operate at high speeds with lower drafts, such as in ballast condition. **Fehler! Verweisquelle konnte nicht gefunden werden.** further supports this established behavior.

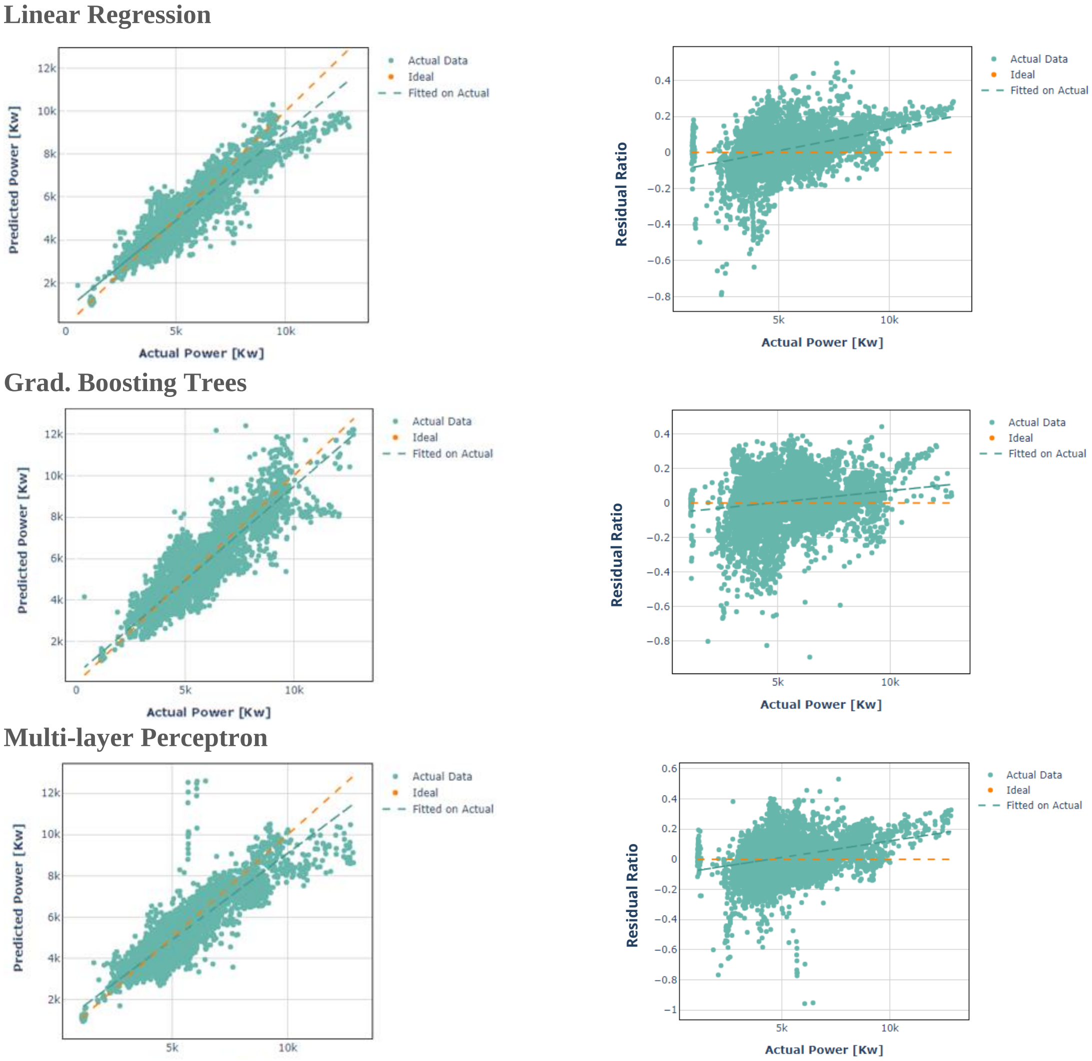

Fig.7: Different model families evaluation plots for all Vessels. For each family, the left plot presents actual-prediction and the right the residual ratio (Actual-Predicted)/Actual across Actual Main Engine Power

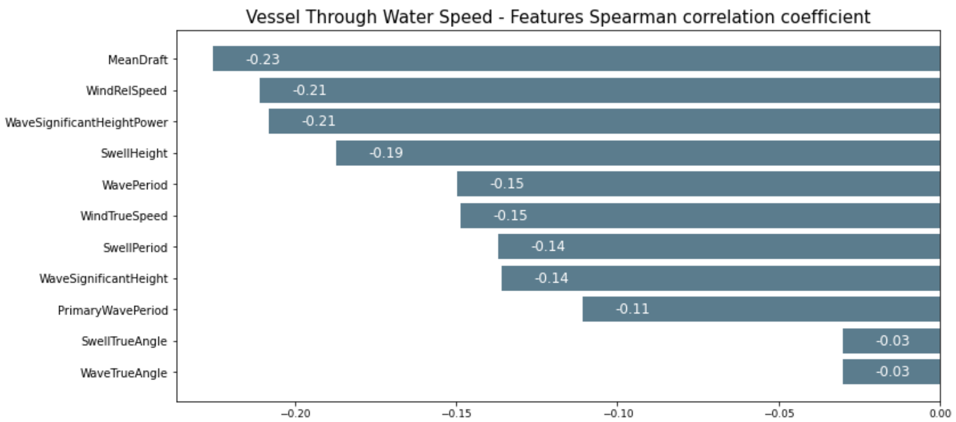

Fig.11: Vessel Through Water Spearman Correlation with Weather signals and draft

The correlation values presented here are derived from diverse vessel types over a long period after applying the data cleaning procedures detailed in (section 1). This cleaning process excluded high impactful weather conditions, which consequently lowered the correlation between weather conditions and speed.

4.2. Identified limitations

The previous analysis encompassed an extensive evaluation on multiple training-test datasets for a significant number of vessels, utilizing a sliding window approach. Within this overview, we highlight several vessel behavioral patterns that notably influence the outcomes. These examples are intended solely to demonstrate the comparative performance of various modeling approaches namely Gradient Boosting Trees, Multilayer Perceptron Regressor, and Linear Regressions underscoring their identified limitations in the context of this study. These observations are offered for the reader's consideration, without delving into a detailed analysis, and will inform future research directions and analyses.

Our analysis provides insights into the challenges of modeling vessel behavior, especially when extrapolating speeds beyond the typical operational range and addressing constant power patterns. When training data is limited to a narrower speed range, models struggle to accurately predict conditions outside of this range. Gradient Boosted Trees, for example, demonstrate difficulties in extrapolating to unseen speeds, leading to static predictions that fail to account for increased power demands at higher speeds. In contrast, linear regression models show better extrapolation capabilities under the assumption of a linear speed-power relationship, yet they can overestimate power requirements in certain scenarios.

Furthermore, the study highlights the issue of modeling constant main engine power across diverse operational patterns. A model trained on a very narrow range of power values. This pattern affects model generalization and prediction accuracy in cases with main engine power out of seen range. This limitation is observed across various modeling approaches, indicating a common challenge in accurately capturing the nuanced relationship between speed and power across different vessel behaviors. The analysis underscores the importance of considering a wide array of operational conditions and the inherent limitations of current modeling techniques in predicting vessel performance under unrepresented or extreme conditions.

This study's predictive model encounters a significant limitation by not incorporating hull fouling, a factor critical for understanding variations in a ship's fuel efficiency and power requirements. The model's training over a two-year period without accounting for hull condition changes or cleaning events introduces substantial inaccuracies, given the complex, multi-variate nature of hull fouling influenced by factors such as idle time and sea temperature, *Uzun et al. (2019)*. This complexity necessitates a sophisticated analytical approach that goes beyond time-related deterioration estimates.

Additionally, the model's predictive accuracy is further compromised by aleatoric and epistemic uncertainties, including the variability in operational conditions and a lack of comprehensive knowledge on maintenance schedules and load variations, *Kiachopoulos (2020), Ventikos and Psaraftis (2013)*. Future improvements should focus on integrating data on hull condition, maintenance activities, and environmental factors to refine the accuracy of power demand and fuel consumption predictions, underscoring the need for collaborative data collection efforts within the maritime industry.

5. Conclusion

The motivation of this study stems from the lack of extensive analysis of linear estimators in the maritime domain. While linear models are often employed as benchmark models in other studies, they are generally used without the benefit of extensive feature engineering. This study aims to bridge this gap by exploring the potential of linear models in maritime applications, leveraging their strengths in interpretability, low computational demands, and predictable extrapolation.

Evaluation framework strategy was computationally intensive limiting our scope of testing parameters train-test ratio, hyperparameter tuning etc. Our study scope does not focus on the estimator side leaving out hyper-parameters fine-tuning. Instead, extra focus is given on data processing and features engineering, especially for linear models. The lack of fine-tuning could significantly affect high configurable estimators (Gradient Boosting Trees, Multi-layer Perceptron) compared to a few hyper-parameters (or none) linear model.

This study underscores the importance of meticulous data cleaning, while striving to prevent over-cleaning and preserving essential noise patterns that influence model performance. Incremental feature engineering with various features built upon other studies and mathematical formulas helped to understand the nature of the problem. Highly engineered, physics-based features, not only improved performance across model families but made the linear models outperform non-linear estimators.

While recognizing the nonlinearity nature of our problem, we acknowledge that neural networks have the potential to overperform linear models' performance given certain considerations. These include extensive hyperparameter tuning, access to a large dataset, and potentially an expanded feature set, particularly if linear assumptions do not constrain feasible feature engineering. However, when dealing with limited, noisy, or poorly engineered datasets, linear models can exhibit enhanced prediction capabilities, especially in extrapolation regions.

Several comparative studies, including work by *N.N. (2022), Gkerekos (2019), Ferreira (2022),* have evaluated the performance of similar model families, demonstrating that high-variance models like neural networks outperform linear models. However, it's crucial to recognize that different studies, due to variations in evaluation processes, dataset size and composition, can yield contrasting results. This study emphasizes the importance of considering the specific context of each study when interpreting its findings. Notably, when we account these inherent differences, the evaluation results across these studies show a level of proximity, suggesting the possibility of comparable performance under relevant conditions.

References

BERTHELSEN, F.H.; NIELSEN, U.D. (2021), *Prediction of ships' speed-power relationship at speed intervals below the design speed*, Transportation Research Part D: Transport and Environment, https://www.sciencedirect.com/science/article/pii/S1361920921002947?via%3Dihub

CARCHEN, A.; ALTAR, M.; TURKMEN, S.; PAZOUKI, K.; MURPHY, A.J. (2019), *Ship Performance Monitoring Dedicated to Biofouling Analysis: Development on a Small Size Catamaran*, Applied Ocean Research 89, pp.224-236

CHEN, G., CAI, J.; RYTTER, N.; LÜTZEN, M. (2023), *A practical data quality assessment method for raw data in vessel operations*, J. Marine Science and Application

CORADDU, A.; LIM, S.; ONETO, L.; PAZOUKI, K.; NORMAN, R.; MURPHY, A.J. (2019), *A novelty detection approach to diagnosing hull and propeller fouling*, Ocean & Marine Engineering

DALHEIM, Ø.Ø.; STEEN, S. (2020a), *A computationally efficient method for identification of steady state in time series data from ship monitoring*, Ocean Engineering and Science 5, pp.333-345

DALHEIM, Ø.Ø.; STEEN, S. (2020b), *Preparation of in-service measurement data for ship operation and performance analysis*, Ocean Engineering 212

DALHEIM, Ø.Ø.; STEEN, S. (2021), *Uncertainty in the real-time estimation of ship speed through water*, Ocean Engineering 235

DEKEYSER, S.; MOROBÉ, C.; MITTENDORF, M. (2022), *Towards Improved Prediction of Ship*

Performance: A Comparative Analysis on In-service Ship Monitoring Data for Modeling the Speed–Power Relation, https://arxiv.org/pdf/2212.13061.pdf

FARKAS, A.; DEGIULI, N.; MARTIC, I.; DEJHALLA, R. (2020), *Impact of Hard Fouling on the Ship Performance of Different Ship Forms*, J. Marine Science and Engineering 8/748

FARKAS, A.; SONG, S.; DEGIULI, N.; MARTIĆ, I.; DEMIREL, Y.K. (2020), *Impact of biofilm on the ship propulsion characteristics and the speed reduction*, Ocean Engineering 199

FERREIRA, R.D.S.; DE LIMA, J.V.D.; CAPRACE, J.D. (2022), *Comparative analysis of machine learning prediction models of container*, Ocean Engineering 255

GKEREKOS, C.; LAZAKIS, I.; THEOTOKATOS, G. (2019), *Machine learning models for predicting ship main engine Fuel Oil Consumption: A comparative*, Ocean Engineering 188.

GUPTA, P.; RASHEED, A.; STEEN, S. (2022), *Ship performance monitoring using machine-learning*, Ocean Engineering 254

GUPTA, P.; TASKAR, B.; STEEN, S.; RASHEED, A. (2021), *Statistical modeling of Ship's hydrodynamic performance indicator*, Applied Ocean Research 111

HANSEN, S.V.; PETERSEN, J.; JENSEN, J.; LUTZEN, M. (2011), *Performance Monitoring of Ships*, DTU Mechanical Engineering

ISO (2015), *ISO 15016 - Guidelines for the assessment of speed and power performance by analysis of speed trial data*, Int. Standard Org., Geneva

ISO (2016), *ISO 19030 - Measurement of changes in hull and propeller performance*, Int. Standard Org., Geneva

JAMES, G.; WITTEN, D.; HASTIE, T.; TIBSHIRANI, R.; TAYLOR, J. (2023), *An Introduction to Statistical Learning with Applications in Python*, Springer

KARAGIANNIDIS, P. (2019), *Data-driven Ship Propulsion modeling with applications in the Performance Analysis and Fuel Consumption prediction*, Diploma Thesis, NTUA, Athens, https://dspace.lib.ntua.gr/xmlui/bitstream/handle/123456789/49260/Thesis_Karagiannidis_Pavlos.pdf

KARAGIANNIDIS, P.; THEMELIS, N. (2021), *Data-driven modelling of ship propulsion and the effect of data pre-processing on the prediction of ship fuel consumption and speed loss*, Ocean Eng. 222

KIACHOPOULOS, T.; KYRIAKOULIS, N.; GRITZALIS, D. (2020), *Addressing aleatoric and epistemic uncertainty in maritime risk assessment*, Risk Analysis, pp.584-600

KRIEZIS, A. (2022), *Ship Power Prediction Using Machine Learning*, Massachusetts Institute of Technology

LAKSHMYNARAYANANA, P.A.; HUDSON, D. (2017), *Is Wave Height Necessary to Determine Ship Performance in Calm Water from Measurements?*, 3rd HullPIC Conf., Redworth

MAKRIDAKIS, S.; SPILIOTIS, E.; ASSIMAKOPOULOS, V. (2018), *Statistical and Machine Learning forecasting methods: Concerns and ways forward*, Public Library of Science 13(3), pp.1-26

MAN ES (2023), *Basic Principles of ship propulsion*, MAN Energy Solutions

MITTENDORF, M. (2023), *Data-driven Prediction of Added Resistance on Ships in Waves*, PhD thesis, DTU, Lyngby, https://backend.orbit.dtu.dk/ws/portalfiles/portal/331584676/PhD_Thesis_Malte_Mittendorf.pdf

N.N. (2022), *Resistance and Powering of Ships*, US Naval Academy, https://www.usna.edu/NAOE/_files/documents/Courses/EN400/02.07%20Chapter%207.pdf

NOORA, S. (2020), *Detecting Multicollinearity in Regression Analysis*, American J. Applied Mathematics and Statistics, pp.39-42, http://article.sciappliedmathematics.com/pdf/ajams-8-2-1.pdf

PARK, B.J.; SHIN, M.S.; LEE, G.J.; KI, M.S. (2019), *Application of an ISO 15016:2015 based Method in Analysing Ship's Performance*, 4th HullPIC Conf., Gubbio

PARK, B.J.; SHIN, M.S.; KI, M.S.; LEE, G.J.; LEE, S.B. (2018), *Ideas on How to Improve ISO 19030 based on the Results of Applying to Field Data*, 3rd HullPIC Conf., Redworth

REIMER, K. (2021), *How to Achieve Peformance Optimization Potential Considering High-Quality Data: An ISO 19030 Use Case with an Exemplary Vessel-Specific Trim Map*, Ocean Engineering 235

SCHULTZ, M.P.; BENDICK, J.A.; HOLM, E.R.; HERTEL, W.M. (2011), *Economic impact of biofouling on a naval surface ship*, Biofouling, pp.87-98

SKAMAGKAS, A. (2022), *An Application of Delphi Method on Vessel Performance, Monitoring & Optimization*, Thesis, University of Piraeus

SOGIHARA, N.; YONEZAWA, T.; ISHIGURO, T.; SUGIMOTO, Y.; MASUYAMA, S.; MIENO, H.; SHIMADA, M.; MATSUBARA, Y. (2019), *Introduction of OCTARVIA Project: Project for Ship Performance in Actual Seas*, 4th HullPIC Conf., Gubbio

SPIESS, A.N.; NEUMEYER, N. (2010), *An evaluation of R2 as an inadequate measure for nonlinear models in pharmacological and biochemical research: A Monte Carlo approach*, BMC pharmacology

TOWNSIN, R.L. (2003), *The ship hull fouling penalty*, Biofouling, pp.9-15

TSARSITALIDIS, V.; ROSSOPOULOS, S. (2018), *ISO 19030 - The Good, the Bad and the Ugly*, 3rd HullPIC Conf., Redworth

UZUN, D.; DEMIREL, Y.K.; CORADDU, A.; TURAN, O. (2019), *Time-dependent biofouling growth model for predicting the effects of biofouling on ship resistance and powering*, Ocean Engineering 191

VALCHEV, I.; CORADDU, A.; KALIKATZARAKIS, M.; GEERTSMA, R.; ONETO, L. (2022), *Numerical methods for monitoring and evaluating the biofouling state and effects on vessels' hull and propeller performance: A review*, Ocean Engineering 251

VENTIKOS, N.P.; PSARAFTIS, N.H. (2013), *A survey on the ship hull fouling penalty*, Ocean Engineering, pp.97-106

XIE X.W.; SUN, B.Z.; LI, X.H.; OLSSON, T.; MALEKI, N.; AHLGREN, F. (2023), *Fuel Consumption Prediction Models Based on Machine Learning and Mathematical Methods*, J. Marine Science and Engineering

Navigating a Sustainable Future with Wind-Assisted Ship Technology: NAPA, Norsepower and Sumitomo's Collaborative Journey

Naoki Mizutani, NAPA, Kobe/Japan, naoki.mizutani@napa.fi
Naoyuki Nakadozono, NAPA, Kobe/Japan, naoyuki.nakadozono@napa.fi
Akihiko Masutani, Sumitomo Heavy Industries Marine & Engineering, Yokosuka/Japan, akihiko.masutani@shi-g.com
Yuji Arai, Sumitomo Heavy Industries Marine & Engineering, Yokosuka/Japan, yuji.arai@shi-g.com
Takeshi Aono, Sumitomo Heavy Industries, Yokosuka/Japan, takeshi.aono@shi-g.com
Ville Paakkari, Norsepower, Helsinki/Finland, ville.paakkari@norsepower.com

Abstract

NAPA, Norsepower, and Sumitomo Heavy Industries Marine & Engineering collaborated in a project to validate emissions reduction potential of wind propulsion and voyage optimization. In the initial stage of ship design phase, individual vessel performance and voyage conditions are meticulously considered using NAPA's voyage simulation technology which is a unique blend of hydrodynamic modeling technology and big data analytics for which data generated by Norsepower and Sumitomo are given. The results of this project include evaluations for reduction of CO_2 emissions compliance with Carbon Intensity Indicator (CII) and EU-ETS regulations, along with a cost impact analysis. In this project, the simulation model is refined to incorporate nuanced changes in vessel performance in real sea conditions equipped with wind propulsion systems. This leads to the development of an enhanced voyage simulation and optimization tool that contributes to the improved performance of wind-assisted ships. Looking forward, the three companies aim for commercialization post-2024, and their collaboration extends towards designing and developing carbon-neutral ships, optimizing operations, and fostering partnerships with maritime companies to promote a sustainable future.

1. Introduction

The maritime industry's journey towards decarbonization is sharply accentuated by the International Maritime Organization's (IMO) ambitious targets. In an environment where new technologies and solutions such as alternative fuels are shrouded in uncertainty, wind-assisted ship technology emerges as a practical and immediate approach to decarbonization. In addition, the EU Emissions Trading System (EU-ETS) influences the economics of shipping by increasing operational costs while also promoting the acceleration of decarbonization efforts.

This project aims to meticulously evaluate the role of wind-assisted ships in enhancing both the environmental sustainability and economic efficiency of maritime operations, capitalizing on advanced voyage simulation and optimization technologies.

The project entails a comprehensive assessment of the viability of wind-assisted ships in actual maritime operations, with a focus on both economic and environmental impacts. It refines our virtual voyage simulation and optimization technologies, tailoring them specifically for wind-assisted ships to augment their operational effectiveness.

The objective of this study is to explore the feasibility and practicality of wind-assisted ships in promoting decarbonization within the maritime sector. We investigate how voyage simulation is instrumental in evaluating operational performance and economic viability at the design stage, and how voyage optimization can further contribute to reducing CO_2 emissions and fuel consumption in wind-assisted ship operations. This exploration sets the stage for a future where sustainable maritime practices are not just envisioned but realized.

2. Methodology

2.1. Simulation platform

In this project, NAPA Fleet Intelligence and its related technologies are used. NAPA Fleet Intelligence is a ship performance monitoring and voyage optimization platform that utilizes a ship-specific performance model and various data such as Automatic Identification System (AIS), weather, current, nautical charts, and performance-related data from ships, including automation signals and/or noon reports, as shown in Figs.1 and 2. NAPA Fleet Intelligence's voyage optimization feature, also known as weather routing, has the potential to reduce ship emissions by optimizing voyages for any sea passage.

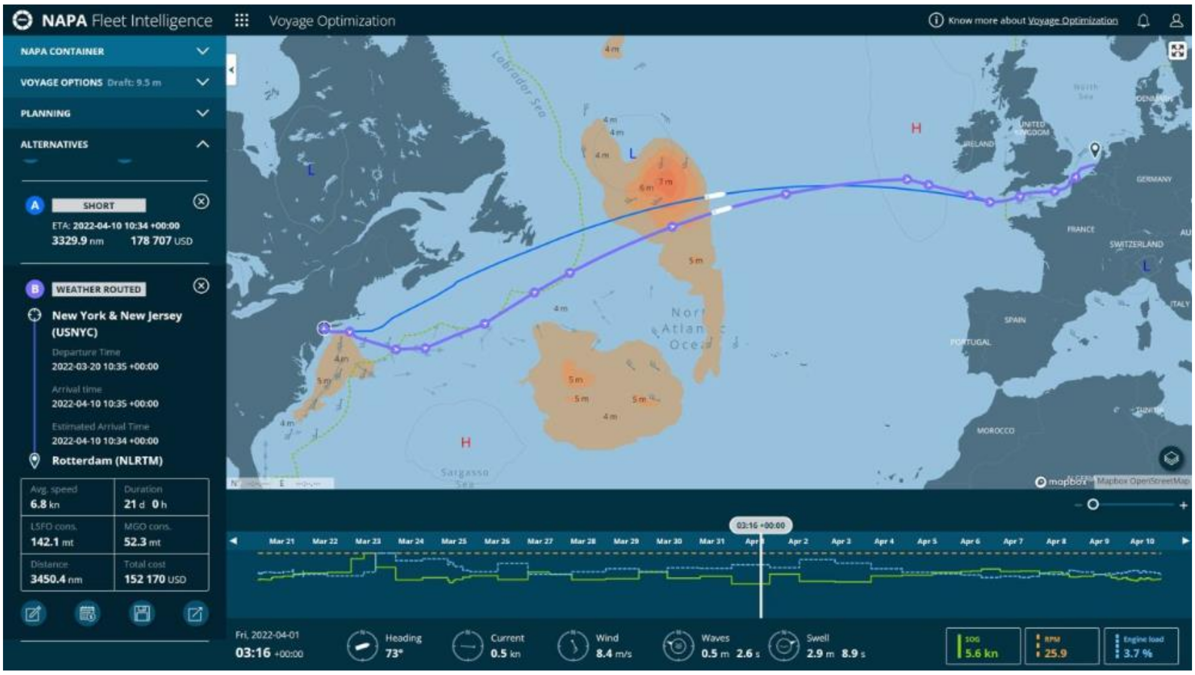

Fig.1: NAPA Fleet Intelligence for voyage simulation and voyage optimization

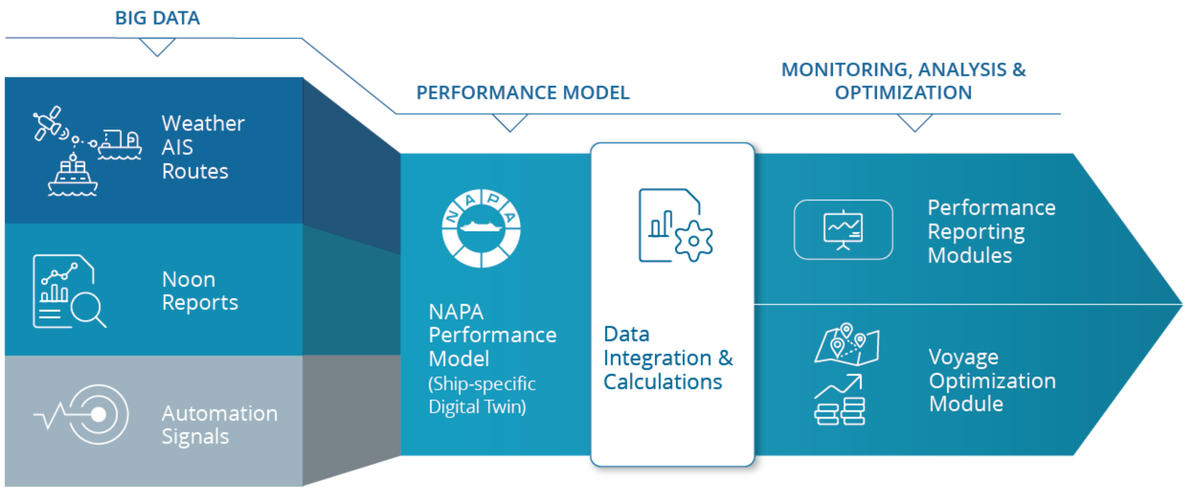

Fig.2: NAPA Fleet Intelligence concept

In NAPA Fleet Intelligence, the subject ship's fuel consumption and CO_2 production are simulated based on the ship-specific model and the given operational conditions: route, speed, loading condition, water depth, current, wave and wind conditions.

All the forces acting on the ship are calculated with hydrodynamics models as shown in Fig.3. Quartering waves and wind cause a drifting angle to ship's propagation, which needs to be balanced by the rudder. The rudder forces are also included in the model together with the hydrodynamic coefficients accounting for the additional resistance due to the drift angle.

Factoring in all the above-mentioned forces, the required thrust to propel the ship at a given speed is calculated by solving the force balance. The thrust is calculated considering the propulsion arrangement, including propeller diameter, pitch ratio, thrust deduction, and wake factor. Then the required propeller revolutions per minute (rpm) and the corresponding required power from the main engine are calculated. Finally, based on these calculations, the fuel consumption and CO_2 production are determined.

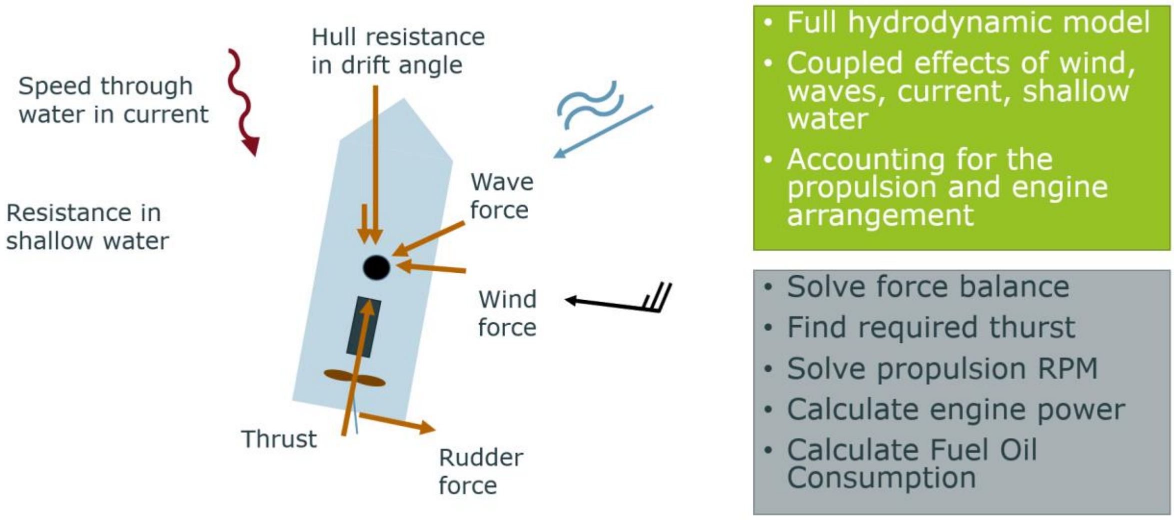

Fig.3: Calculation of required propulsion power for each timestamp

2.2. Rotor sail model

Rotor sails are large cylindrical sails that use Magnus effect to create thrust for the ship utilizing the prevailing wind. The sails are rotated with an electrical motor, and the rotation of the sail surface, together with the wind, results in a pressure differential which pushes the ship forward. This enables the reduction of power required by the propeller propulsion system while maintaining the same operational speed, thus reducing the fuel consumption and the related emissions of the ship. Alternatively, the propeller propulsion power can be kept constant, and the ship speed can be increased. The benefit of using rotor sails is their very high lift production capability compared to the conventional sails making the rotor sails very compact in size while still providing sufficient thrust forces at sufficient scale for ship propulsion.

Fig.4: VLOC Sea Zhoushan equipped with five Norsepower Rotor Sails™

The Norsepower Rotor Sails (NPRS) utilize the working principle described above. As of writing (Q1 2024), there are seven large cargo ships sailing with Norsepower Rotor Sails and the current production backlog is expected to more than double the number in coming 12 months. The performance of the sails has been extensively validated by third parties, including NAPA, over the years through using both sea-trial type tests and long-term data collection and analysis, *Norsepower (2023)*.

As mentioned, the rotor sails exhibit very high lift production capability, making them a particularly interesting technology for weather routing. By making relatively small deviations in the course over ground, the benefits of wind propulsion can be significantly improved. Previous research has shown that the weather routing can potentially double the savings from wind propulsion, *Mason et al. (2023),* and that this effect is more pronounced for high lift devices compared to passive devices, *Dupuy et al. (2023).*

For reliable fuel saving estimation and optimization, understanding the performance of the sails on a given ship is crucial. While the sea-trial procedures and the long-term measurement campaigns mentioned earlier have been crucial for validating the overall performance, a need for high-frequency performance data has emerged to further improve and optimize not only the technical performance of the sails but also the operational performance of the ship. Thus, providing accurate, real-time and full-scale measurements of the rotor sail performance is highly important. For this purpose, Norsepower Sentient Control™ (NPSC) was developed. This tool combines real-time performance measurement with smart control features and enables individual control of the sails to optimize both the aerodynamics of the sail system and their impact on the hydrodynamic behavior of the vessel. In this study, only aerodynamics data collected from NPSC were considered, as the hydrodynamic optimization was conducted using the method described chapter 2.3.

The ship can significantly influence the flow field around it, especially in the vicinity of the ship where the anemometers are typically located. In their review of three sea trials of wind assisted ships, *Werner et. al. (2022)* assessed the uncertainty of the wind measurement as among the largest error sources in measuring the thrust produced by wind propulsion. Therefore, relying solely on ship anemometer data may not provide a sufficient basis for analysis. The solution deployed for the purpose of this paper is to use non-intrusive measurements of the freestream wind conditions using LIDAR technology, and to couple that with high-frequency measurements on the sails. With this approach, assessing the effectiveness of the sails in "undisturbed wind conditions" becomes possible. This enables reliable mapping of the sail performance onto the weather statistics. An example of such measurements is detailed in *Dupuy et al. (2023)*.

For the purpose of this paper, the standard performance model of rotor sails was tuned using the aerodynamic data collected from the NPSC and LIDAR measurements as described above.

2.3. Rotor control system

The force generated by sails contributes not only to propulsive force enhancing thrust performance but also introduces a lateral force acting as drag, which deteriorates propulsive power. This lateral force, dependent on sail configuration, can induce a yaw moment (weather helm), necessitating rudder steering for course keeping, yet this action heightens propulsive drag due to the rudder adjustment.

To address this issue, Sumitomo Heavy Industries, Ltd. has devised a system capable of managing the yaw moment through the independent manipulation of rotor sails, facilitating course keeping with minimal counter-steering required. Consequently, the independent control of each rotor sail is effective to reduce CO_2 emissions, Fig.5.

In an effort to validate this concept, a model test was conducted as shown in Fig.6, verifying that rotor sails can effectively control the yaw moment, Fig.7.

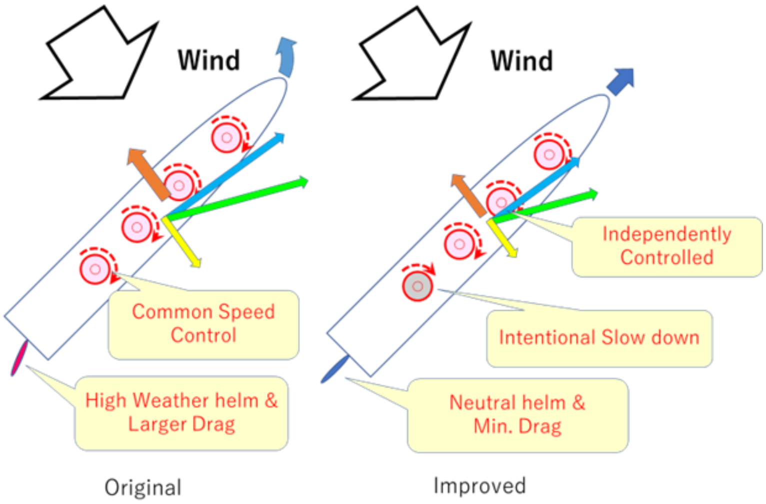

Fig.5: Concept of Rotor control system

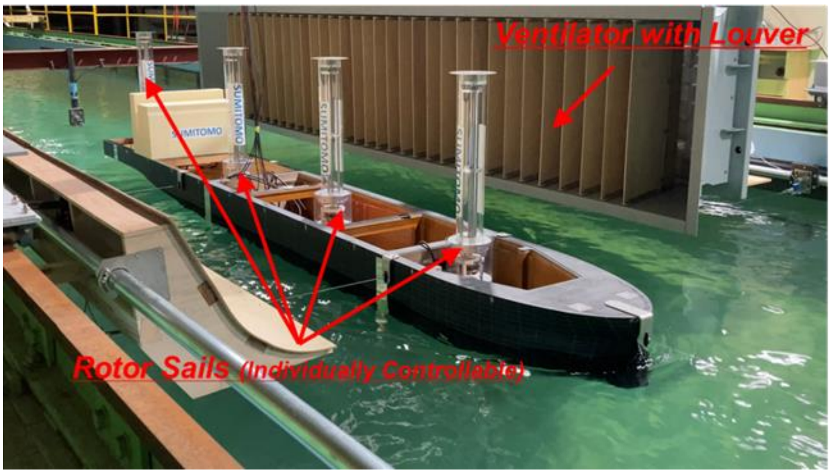

Fig.6: Model test for Rotor control system

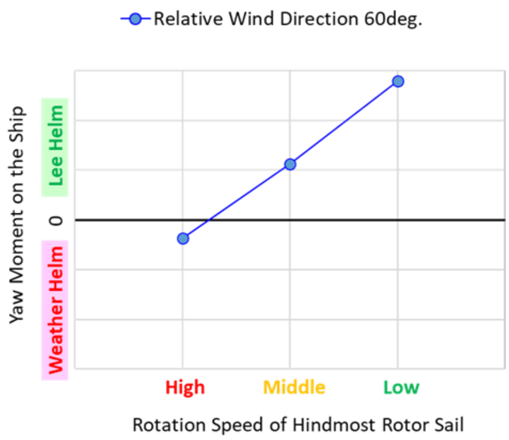

Fig.7: Model test result of Rotor control system

2.4. Integrated ship performance model and voyage simulation

NAPA Fleet Intelligence develops a ship performance model based on actual design information such as hull resistance, wind resistance, self-propulsion factors, propeller characteristics, specific fuel consumption of main engine, wave added resistance, among others, for a subject ship. This model is further enhanced by integrating the previously mentioned rotor sail model and control system for comprehensive voyage simulations. The generated propulsive and lateral forces by the rotors are calculated based on the apparent wind angle and speed encountered by the ship. The project's ship performance model logic diagram is illustrated in Fig.8.

In this project, voyage simulations are conducted utilizing the NAPA Fleet Intelligence platform, incorporating an integrated ship performance model along with global weather, current data, and nautical charts. This approach enables the creation of realistic "virtual" voyage simulations for a specific ship.

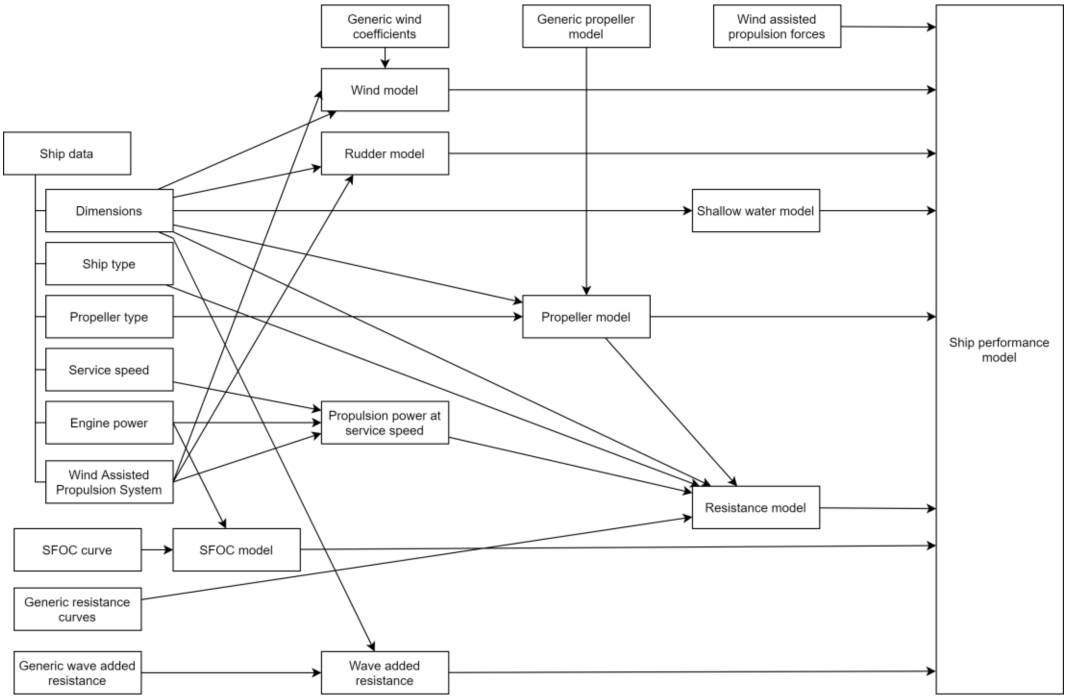

Fig.8: NAPA ship performance model logic diagram

2.5. Case study scenarios and evaluation method

The project encompasses three distinct studies, the themes of which are outlined in Table I.

Table I: Study themes

	Theme	Used Model
Study 1	Evaluates the decarbonization effectiveness and economic viability of rotor sails [**Annual**]	1, 2
Study 2	Evaluates the decarbonization effectiveness and economic viability of rotor sails [**Seasonal**]	1, 2
Study 3	Investigates the impact of rotor sails' lateral forces and the control of yaw moments	2, 3, 4

In the studies, a Panamax tanker equipped with four rotor sails undergoes voyage simulations across various scenarios. The ship and rotor sail specifications are detailed, with four distinct ship performance models (Model 1 through 4) utilized to evaluate rotor effects, lateral forces, and yaw moment control, as depicted in Fig.9. Model 1 represents a ship without any rotor sails. Model 2 showcases the ship with four rotor sails (rotor A, B, C and D) operating at uniform rotational speeds, omitting lateral force considerations. Model 3, similar to Model 2, includes lateral force considerations, inducing a yaw moment necessitating rudder action for balance. Model 4, while similar, differentiates by adjusting the rotational speed of the rear rotor (D) to counteract the yaw moment, potentially reducing rudder usage.

Ship model configuration

Ship type	: Panamax Tanker
Length over all	: 229 m
Breadth	: 32.3 m
Design Draft	: 11.3 m
Deadweight	: 77,000 t
Main engine power	: 7,170 kW
Service speed	: 14.1 kn

Wind assisted device configuration

Device type	: Flettner rotor
Specification	: 30 m(H) x 5 m(D) x 4 pcs

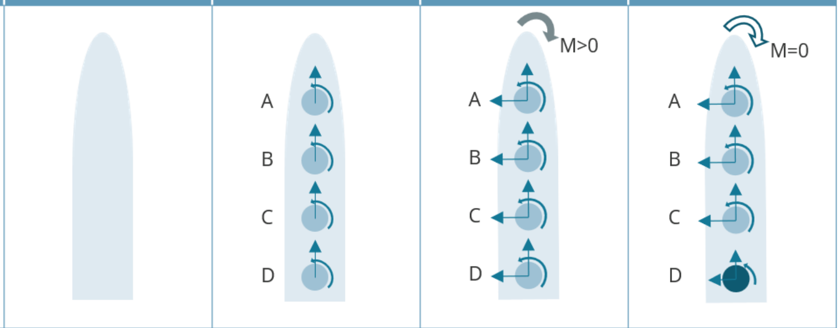

Ship model	**1**	**2**	**3**	**4**
Rotor	No	4 x Identical rotating speed (A=B=C=D)	4 x Identical rotating speed (A=B=C=D)	A=B=C: Identical rotating speed D: Independent speed control
X-force	-	X	X	X
Y-force moment calculated	-	-	X	X
Moment control	-	-	-	X (Cancelled)
Rudder	No	No	Yes	Yes
Counter rudder action due to Rotor induced force / moment	Only hull wind moment is taken into account for counter rudder angle	Same as Model 1		The rotor moment is forced to zero i.e. no counter rudder angle due to rotors

Fig.9: Performance models for simulation

The operational profile of the ship, including routes, loading conditions, and departure/arrival time, is clearly outlined in the studies. This encompasses routes between Europe and North America (Route 1 and 2), Japan and Australia (Route 3 and 4), and Singapore and Africa (Route 5 and 6), with departures on the 1st and 15th of each month to lessen the impact of daily weather variations. Annually, this results in 24 voyages per route for one year. Route specifics, like duration and draft, are detailed in Fig.10. Notably, some voyages encountered errors due to adverse weather and those voyages are excluded from the studies. For each voyage, the following four cases are studied:

(a) without rotor sails and without route optimization (short route)
(b) without rotor sails but with route optimization
(c) with rotor sails but no route optimization (short route)
(d) with rotor sails and route optimization

Studies 1 and 2 focus on assessing the decarbonization effectiveness and economic impact of wind-assisted ships with rotor sails over one year and each season, respectively, through voyage simulations departing on the 1st and 15th of every month in 2022, using actual weather data. Study 3 aims to refine the simulation model by incorporating Sumitomo's newly developed rotor control method, which addresses the rotors' lateral forces and neutralizes the yaw moment induced by the rotors. This enhancement also leverages Norsepower's rotor sail characteristics, refined through measured data. In the Study 3, a selected route is re-evaluated using this advanced simulation model.

		Voyages*	Departure port	Arrival port	Duration (days)	Draft (m)
North America ⇔ Europe	Route 1	24	Amsterdam	New York	11	11.3
	Route 2	24	New York	Amsterdam	11	5.66
Japan ⇔ Australia	Route 3	24	Chiba	Port Botany	16	14.0
	Route 4	24	Wandoo	Yokohama	14	14.0
Singapore ⇔ Africa	Route 5	24	Escravos	Singapore	28	14.0
	Route 6	24	Singapore	Luanda	25	13.1

* Simulation was done for the voyages that depart on the 1st and 15th of every month in 2022. There were some error voyages due to bad weather.

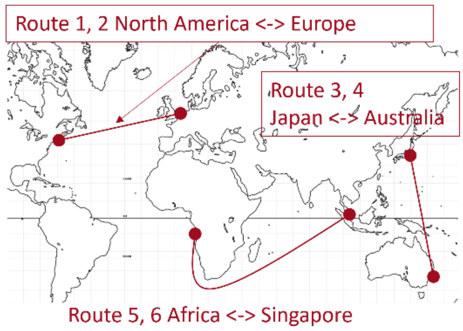

Fig.10: Studied routes and operational conditions

Evaluations in this project are conducted by comparing various metrics such as fuel oil consumption (FOC), CO_2 emissions, distance traveled, fuel cost, and Carbon Intensity Indicator (CII) across cases (a) through (d).

The project employs specific assumptions and methodologies for simulations and evaluation as described below:

1) The energy requirements and CO_2 emissions associated with operating rotor sails are not included in the simulations.
2) CII is calculated not as an annual metric but on a per-voyage basis, excluding fuel consumptions related to auxiliary engines and port operations. Therefore, in this study, the CII is determined by dividing the CO_2 emissions produced by the main engine during the voyage by the voyage's distance and the ship's deadweight.
3) In Studies 1 and 2, lateral forces and yaw moments induced by rotor sails are not considered. However, in Study 3, these factors are taken into account.
4) For fuel cost saving calculations, the following pricing and allowance are used:
    a. LSFO (Low Sulfur Fuel Oil) price = 710.5 USD/ton
    b. MGO (Marine Gas Oil) price = 1002 USD/ton
    c. EU-ETS allowance = 100 USD/ton
5) In the Emission Control Area (ECA), MGO is selected as fuel for the main engine.
6) Nowcast weather and current forecasts are utilized for weather routing optimization.
7) The optimization target is to minimize the fuel cost for the planned voyage without altering the departure and arrival time.

3. Results

3.1. Study 1 Effectiveness of decarbonization and economics of rotor sails (Annual)

Study 1 conducts voyage simulations for six predefined routes and operational conditions as described in Fig.10, spanning a one-year period in 2022. A summary of these routes—comparing simulation results for a year between a conventional ship (case (b), without rotor sails, incorporating weather routing) and a wind-assisted ship (case (d), with rotor sails and weather routing)—is presented in Fig.11.

From the results of Study 1, it is anticipated that average Fuel Oil Consumption (FOC) savings and CO_2 reductions will range from approximately 10 to 30%, with average fuel cost savings of about 16k to

37k USD per voyage and CO_2 emission reductions between 72 to 165 tons per voyage, depending on the route.

For Route 1 and Route 2, which include a European port (Amsterdam), the expected reduction in EU-ETS allowance costs is estimated to be about 6.1k to 7.8k USD per voyage, assuming an allowance cost of 100 USD per ton of CO_2 and 100% adoption from 2027 onwards.

Evaluated FOC/CO2/Cost savings (mean)

		Route 1	Route 2	Route 3	Route 4	Route 5	Route 6
From		Amsterdam	New York	Chiba	Wandoo	Escravos	Singapore
To		New York	Amsterdam	Port Botany	Yokohama	Singapore	Luanda
Conventional-Opt vs Wind assisted-Opt							
FOC difference	LSFO	-30 t	-52 t	-37 t	-23 t	-52 t	-48 t
	MGO	-8 t	2 t	-	-	-	-
CO2 difference		-121 t / -19 %	-155 t / -32 %	-117 t / -17 %	-72 t / -14 %	-165 t / -10 %	-151 t / -13 %
FO Cost difference		-30 k$	-34 k$	-27 k$	-16 k$	-37 k$	-34 k$
Attained CII / Required CII (2024)		A (0.46 ⇒ 0.37)	A (0.35 ⇒ 0.24)	A (0.39 ⇒ 0.34)	A (0.35 ⇒ 0.30)	A (0.48 ⇒ 0.42)	A (0.39 ⇒ 0.34)

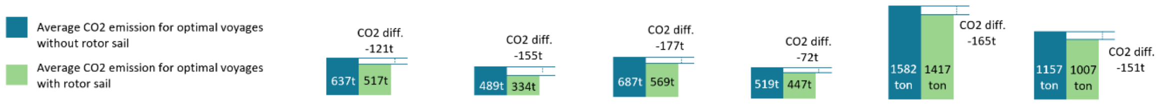

Reference (Conventional-base cases)	Route 1	Route 2	Route 3	Route 4	Route 5	Route 6
# of voyages	19 voyages	24 voyages	24 voyages	24 voyages	24 voyages	23 voyages
Duration / voyage	11.0 days	11.0 days	16.0 days	14.0 days	28.1 days	25.0 days
Draft	11.28 m	5.66 m	14.00 m	14.00 m	14.00 m	13.10 m
Distance / voyage	3348 nm	3362 nm	4351 nm	3627 nm	8086 nm	7196 nm
Average speed	12.7 knot	12.7 knot	11.3 knot	10.8 knot	12.0 knot	12.0 knot

** LSFO 710.5 USD/ton, MGO 1002 USD/ton*

Fig.11: Summary of simulations for Study 1 (conventional ship (b) vs wind-assisted ship (d))

Figs.12 and 13 present examples of one-year simulation results. The comparison across cases (a), (b), (c), and (d) reveals that rotor sails significantly reduce CO_2 emissions, and weather routing can further enhance this effect, enabling greater CO_2 reductions and FOC savings as routes are optimized for better rotor sail performance, particularly with "good wind" conditions, characterized by strong wind blowing from the side of the ship.

This study reveals that the average CO_2 reduction across six routes over one year is 17.5% when comparing ships equipped with rotor sails and weather routing (case (d)) against those without rotor sails but with weather routing (case (b)). Furthermore, the average impact of weather routing on CO_2 reduction for these routes and simulation cases over one year is 10.8% for ships with rotor sails (comparing case (d) to (c)) and 6.3% for ships without rotor sails (comparing case (b) to (a)).

Route 1: Amsterdam – New York (for 1 year)

Average evaluation, Results of all cases are included, Draft: 11.30 m

Case			Avg Distance (nm)	Avg Speed (kn)	Avg LSFO (ton)	Avg MGO (ton)	Avg CO2 (ton)	Avg Cost (k$)
(a)	Conventional	Base	3,348	12.7	115	98	676	180
(b)		Optimal	3,424	13.0	132	69	637	163
(c)	Wind assisted	Base	3,348	12.7	98	87	588	157
(d)		Optimal	3,457	13.1	102	61	517	133

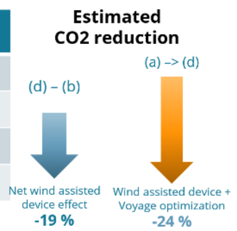

Sample routes
2022.02.01 ~ 2022.12

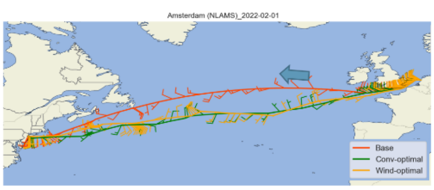

19 cases' results comparison for apparent wind
(spent time in % (SOG>5knot))

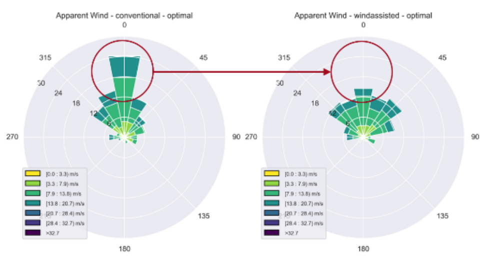

Fig.12: Example case result (Route 1: Amsterdam to New York)

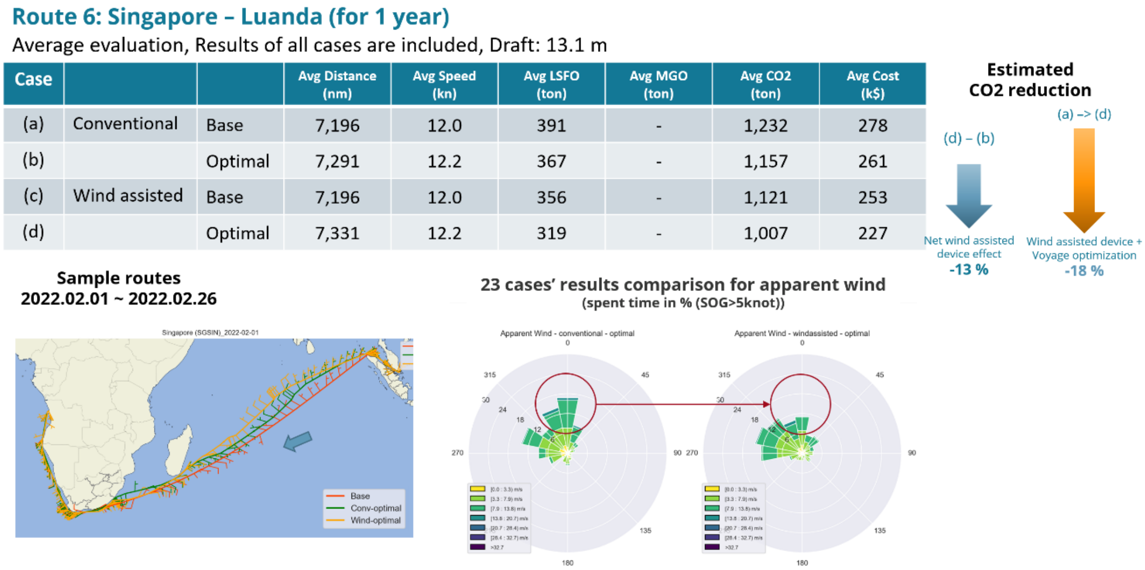

Case			Avg Distance (nm)	Avg Speed (kn)	Avg LSFO (ton)	Avg MGO (ton)	Avg CO2 (ton)	Avg Cost (k$)
(a)	Conventional	Base	7,196	12.0	391	-	1,232	278
(b)		Optimal	7,291	12.2	367	-	1,157	261
(c)	Wind assisted	Base	7,196	12.0	356	-	1,121	253
(d)		Optimal	7,331	12.2	319	-	1,007	227

b

Fig.13: Example case result (Route 6: Signapore to Luanda)

3.2. Study 2 Effectiveness of decarbonization and economics of rotor sails (Seasons)

Study 2 conducts voyage simulations for six predefined routes and operational conditions as outlined in Fig.10, covering each season (Spring, Summer, Autumn, and Winter) of 2022. A summary of these routes—seasonal simulation results comparing a conventional ship (case (b), without rotor sails, with weather routing) with a wind-assisted ship (case (d), with rotor sails, with weather routing)—is presented in Table II.

The effectiveness of wind-assisted ships varies, with FOC savings and CO_2 reductions ranging from 5% to 42% in this study, depending on the routes, and seasonal variations within the same route are evident, Fig.14. This study finds that the benefits of wind-assisted devices, such as rotor sails, are more pronounced in winter than in summer, owing to stronger winds and routes optimized for such conditions. The definition of seasons varies between the northern and southern hemispheres, Fig.14.

Table II: Anticipated seasonal and route-specific CO_2 reductions and FOC savings achieved through rotor sails and voyage optimization (Comparison between case (b) and case (d))

		Spring	Summer	Autumn	Winter
Route 1: Amsterdam – New York	CO_2	-24%	-12%	-17%	-22%
	LSFO	-37mt	-27mt	-18mt	-32mt
	MGO	-13mt	+3mt	-15mt	-13mt
Route 2: New York – Amsterdam	CO_2	-30%	-21%	-32%	-42%
	LSFO	-46mt	-40mt	-57mt	-62mt
	MGO	-1mt	+10mt	+7mt	-7mt
Route 3: CHIBA – Port Botany	CO_2	-21%	-14%	-11%	-22%
	LSFO	-46mt	-30mt	-23mt	-48mt
Route 4: Wandoo – Yokohama	CO_2	-15%	-14%	-12%	-14%
	LSFO	-25mt	-22mt	-21mt	-24mt
Route 5: Escravos – Singapore	CO_2	-12%	-5%	-9%	-16%
	LSFO	-61mt	-24mt	-46mt	-79mt
Route 6: Singapore – Luanda	CO_2	-15%	-11%	-11%	-15%
	LSFO	-53mt	-40mt	-41mt	-57mt

The benefit of wind assisted device in (actual) winter season is bigger than one in summer
One of reasons is stronger wind in the winter season

	Route 1	Route 2	Route 3	Route 4	Route 5	Route 6
From	Amsterdam	New York	Chiba	Wandoo	Escravos	Singapore
To	New York	Amsterdam	Port Botany	Yokohama	Singapore	Luanda
CO2 difference: Conventional-Opt vs Wind assisted-Opt						
Actual summer*	-75 t / -12 %	-98 t / -21 %	-97 t / -14 %	-67 t / -14 %	-75 t / -5 %	-128 t / -11 %
Actual winter*	**-143 t / -22 %**	**-217 t / -42 %**	**-153 t / -22 %**	-76 t / -14 %	**-250 t / -16 %**	**-181 t / -15 %**

Bigger benefit in winter

*** Definition of actual seasons**

Route 1, 2, 3 and 4
- Spring 3/B ~ 5/E
- **Summer** 6/B ~ 8/E
- Autumn 9/B ~ 11/E
- **Winter** 12/B ~ 2/E

Route 5 and 6 (**South hemisphere**)
- Autumn 3/B ~ 5/E
- **Winter** 6/B ~ 8/E
- Spring 9/B ~ 11/E
- **Summer** 12/B ~ 2/E

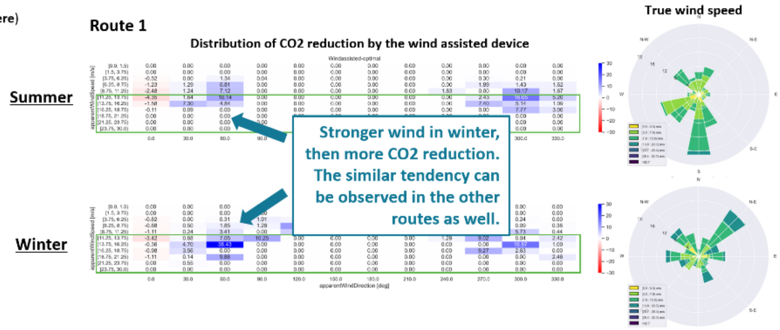

Fig.14: Comparison of CO_2 reduction between summer and winter in different routes

Fig.15 illustrates the cost savings and Carbon Intensity Indicator (CII) ratings for Route 1 (Amsterdam to New York) across each season, serving as a representative example. Following the methodology of Study 1, a one-year simulation demonstrates anticipated significant cost savings due to fuel efficiency and CO_2 reduction. Furthermore, the CII rating is expected to improve correspondingly.

Evaluated FOC/CO2/Cost savings (mean)

		Spring*	Summer*	Autumn*	Winter*
From		Amsterdam			
To		New York			
Conventional-Opt vs Wind assisted-Opt					
FOC difference	LSFO	-37 t	-27 t	-18 t	-33 t
	MGO	-13 t	3 t	-15 t	-13 t
CO2 difference		-158 t / -24 %	-75 t / -12 %	-105 t / -17 %	-143 t / -22 %
FO Cost difference		-40 k$	-16 k$	-28 k$	-36 k$
Attained CII / Required CII (2024)		A (0.48 ⇒ 0.37)	A (0.44 ⇒ 0.39)	A (0.45 ⇒ 0.38)	A (0.46 ⇒ 0.36)

*** Definition**
Seasons are defined with departure time,
i.e.

Spring 3/B ~ 5/E
Summer 6/B ~ 8/E
Autumn 9/B ~ 11/E
Winter 12/B ~ 2/E

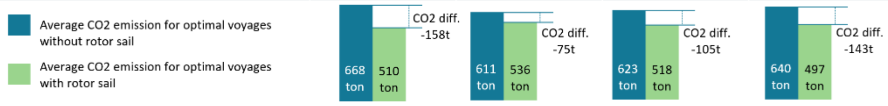

Reference (Conventional-base cases)				
# of voyages	6 voyages	6 voyages	3 voyages	4 voyages
Duration / voyage	11.0 days	11.0 days	11.0 days	11.1 days
Draft	11.28 m	11.28 m	11.28 m	11.28 m
Distance / voyage	3348 nm	3348 nm	3348 nm	3348 nm
Average speed	12.7 knot	12.7 knot	12.7 knot	12.6 knot

** LSFO 710.5 USD/ton, MGO 1002 USD/ton*

Fig.15: Cost savings and CII ratings of Route 1 (Amsterdam to NewYork) for each seasons (conventional ship (b) vs wind-assisted ship (d))

Detailed results for Route 1 across each season are illustrated in Figs.16 to 19. These findings indicate that wind-assisted ships utilizing weather routing encounter more favorable winds, enhancing the efficiency of wind-assisted devices, such as rotor sails. Consequently, CO_2 reductions of 12% to 24% are anticipated on this route, varying by season.

Average evaluation, Results of all cases are included, Draft: 11.30 m

Case			Avg Distance (nm)	Avg Speed (kn)	Avg LSFO (ton)	Avg MGO (ton)	Avg CO2 (ton)	Avg Cost (k$)
(a)	Conventional	Base	3348	12.7	130	102	736	194
(b)		Optimal	3427	13.0	128	83	668	174
(c)	Wind assisted	Base	3348	12.7	105	85	603	160
(d)		Optimal	3465	13.1	91	70	510	134

Estimated CO2 reduction

(d) – (b)

Net wind assisted device effect

-24 %

Sample routes
2022.03.01 ~ 2022.03.12

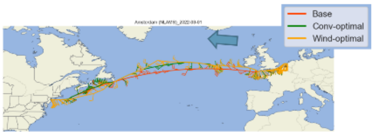

6 cases' results comparison for apparent wind
(spent time in % (SOG>5knot))

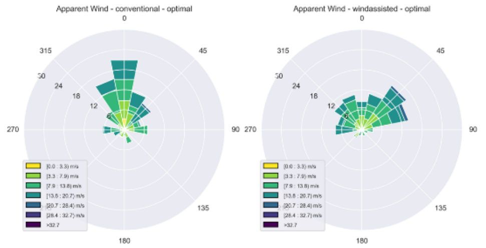

Fig.16: Example results [Spring] for Route 1 (Amsterdam to NewYork)

Average evaluation, Results of all cases are included, Draft: 11.30 m

Case			Avg Distance (nm)	Avg Speed (kn)	Avg LSFO (ton)	Avg MGO (ton)	Avg CO2 (ton)	Avg Cost (k$)
(a)	Conventional	Base	3348	12.7	99	92	606	162
(b)		Optimal	3416	12.9	131	62	611	155
(c)	Wind assisted	Base	3348	12.7	92	88	572	154
(d)		Optimal	3437	13.0	104	65	536	139

Estimated CO2 reduction

(d) – (b)

Net wind assisted device effect

-12 %

Sample routes
2022.06.01 ~ 2022.06.12

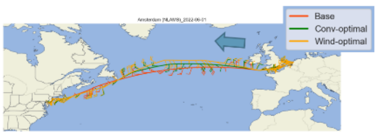

6 cases' results comparison for apparent wind
(spent time in % (SOG>5knot))

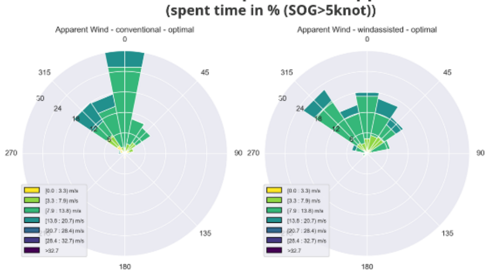

Fig.17: Example results [Summer] for Route 1 (Amsterdam to NewYork)

Average evaluation, Results of all cases are included, Draft: 11.30 m

Case			Avg Distance (nm)	Avg Speed (kn)	Avg LSFO (ton)	Avg MGO (ton)	Avg CO2 (ton)	Avg Cost (k$)
(a)	Conventional	Base	3348	12.7	106	91	626	167
(b)		Optimal	3428	13.0	139	58	623	157
(c)	Wind assisted	Base	3348	12.7	89	84	551	148
(d)		Optimal	3464	13.1	121	43	518	129

Estimated CO2 reduction

(d) – (b)

Net wind assisted device effect

-17 %

Sample routes
2022.09.01 ~ 2022.09.12

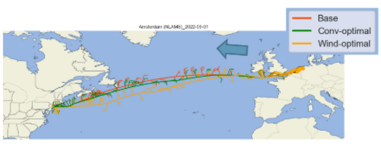

3 cases' results comparison for apparent wind
(spent time in % (SOG>5knot))

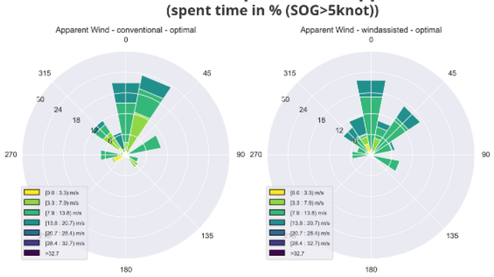

Fig.18: Example results [Autumn] for Route 1 (Amsterdam to NewYork)

Average evaluation, Results of all cases are included, Draft: 11.30 m

Case			Avg Distance (nm)	Avg Speed (kn)	Avg LSFO (ton)	Avg MGO (ton)	Avg CO2 (ton)	Avg Cost (k$)
(a)	Conventional	Base	3348	12.6	124	105	726	193
(b)		Optimal	3428	13.0	135	67	640	163
(c)	Wind assisted	Base	3348	12.7	103	91	616	164
(d)		Optimal	3472	13.2	103	54	497	127

Estimated CO2 reduction

(d) – (b)

Net wind assisted device effect
-22 %

Sample routes
2022.12.01 ~ 2022.12.12

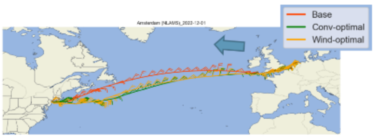

4 cases' results comparison for apparent wind
(spent time in % (SOG>5knot))

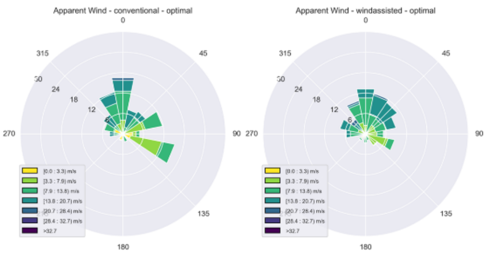

Fig.19: Example results [Winter] for Route 1 (Amsterdam to NewYork)

3.3. Study 3 Effect of rotors' lateral force consideration and yaw moment control

Study 3 incorporates rotor-induced lateral forces to simulate more realistic conditions. Furthermore, this study assesses the efficacy of Sumitomo's technique for neutralizing yaw moments by adjusting the speed of the fourth rotor (D). The investigation unfolds in two phases. Initially, the basic behavior of each simulation model depicted in Fig.9 is analyzed under ideal conditions. Subsequently, mirroring the approach of Studies 1 and 2, voyage simulations for Route 3 are undertaken, with a particular emphasis.

Calculation conditions for basic behavior analysis

Draft	: 11.28 m
Ship Speed Over Ground	: 11.7 kn (6.0 m/s)
Course Over Ground	: 0°
True Wind Speed	: 6.0 m/s
True Wind Direction	: 90° (from aside of the ship)
Wave	: No wave

Ship model	2	3
Rotor	4 x Identical ratating speed (A=B=C=D)	4 x Identical ratating speed (A=B=C=D)
X-force	X	X
Y-force (moment calculated)	-	X
Moment control	-	-
Calculation results at windDirection = 90 deg (Y force: positive is pointing to the starboard)		
FOC / FOC (Model 1)	0.69	0.76
Drift angle [deg]	0.09	0.42
totalXforce [kN]	-327.4	-361.1
totalYforce [kN]	0.0	0.0
totalMoment [kN*m] except rudder	3320.4	19420.2
rudderXForce [kN]	-6.9	-40.4
rudderYForce [kN]	23.0	134.6
windPropulsionXForce [kN]	138.8	138.7
windPropulsionYForce [kN]	0.0	-207.6
windPropulsionYawMoment [kN*m]	0.0	8153.2
windXForce [kN]	-23.3	-23.4
windYForce [kN]	-50.4	-50.0
windMoment [kN*m]	1047.6	1042.0

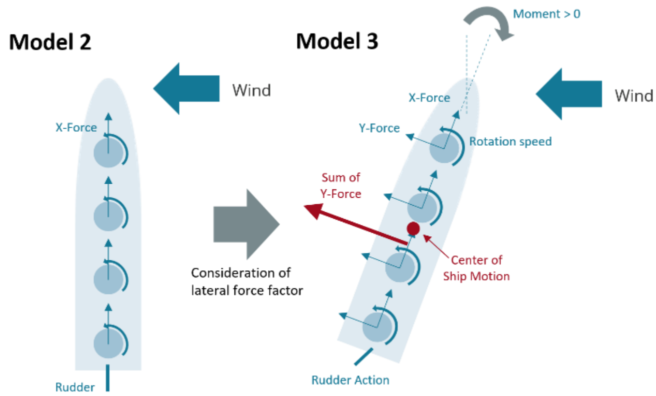

Fig.20: Effect of rotor sails with lateral force component

3.3.1 Effect of rotor sails with lateral force component

Simulations for Models 2 and 3 are conducted under ideal conditions (no waves) for comparison. Both models equip four identical rotors; however, Model 3 accounts for the lateral force induced by the rotors, whereas Model 2 does not.

Fig.20 illustrates that considering the lateral force of rotors leads to 7 percentage points increase in Fuel Oil Consumption (FOC) compared to the original ship without rotor sails (Model 1). This phenomenon can be elucidated as follows: Incorporating the rotor's lateral force into the model generates lateral forces and yaw moments. Subsequently, rudder action is required to neutralize these moments, necessitating additional propulsion power. Furthermore, the drift angle increases to counteract the lateral forces, causing a change in the ship's heading. This adjustment modifies the ship's angle relative to the wind, allowing it to balance the wind pressure against the rotor-induced lateral forces, effectively reducing them to zero.

3.3.2 Effect of rotor sails with yaw moment control

Simulations for Models 3 and 4 are conducted under ideal conditions (no waves) for comparison. Model 3 is equipped with four identical rotors, while Model 4 has three identical rotors and one controlled rotor designed to neutralize the yaw moment induced by the rotors.

Fig.21 illustrates that accounting for the lateral force of rotors leads to 2 percentage points decrease in Fuel Oil Consumption (FOC) compared to the original ship without rotor sails (Model 1). This reduction can be attributed to the controlled operation of the fourth rotor (D), which neutralizes the yaw moment, thereby reducing the need for rudder action and, consequently, the overall power requirement.

Ship model	3	4
Rotor	4 x Identical ratating speed (A=B=C=D)	A=B=C: Identical rotating speed D: Independent speed control
X-force	X	X
Y-force (moment calculated)	X	X
Moment control	-	X (Cancelled)
Calculation results at windDirection = 90 deg (Y force: positive is pointing to the starboard)		
FOC / FOC (Model 1)	0.76	0.74
Drift angle [deg]	0.42	0.55
totalXforce [kN]	-361.1	-350.3
totalYforce [kN]	0.0	0.0
totalMoment [kN*m] except rudder	19420.2	14332.0
rudderXForce [kN]	-40.4	-29.8
rudderYForce [kN]	134.6	99.3
windPropulsionXForce [kN]	138.7	139.0
windPropulsionYForce [kN]	-207.6	-209.4
windPropulsionYawMoment [kN*m]	8153.2	0.0
windXForce [kN]	-23.4	-23.5
windYForce [kN]	-50.0	-49.8
windMoment [kN*m]	1042.0	1039.8

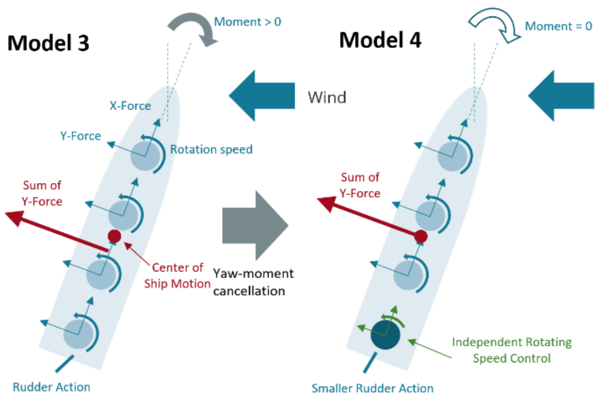

Fig.21: Effect of rotor sails with yaw moment control

3.3.3 Effect of lateral force & yaw moment control

A comparison is made between Model 1 (the original ship without rotor sails) and Model 4 (equipped with rotor sails, incorporating lateral force and yaw moment control).

The findings suggest that rotor sails, when considering lateral force and implementing yaw moment control, can achieve a 26% reduction in Fuel Oil Consumption (FOC) under the specified ideal conditions, as depicted in Fig.22.

Ship model	1	4
Rotor	No	A=B=C: Identical rotating speed D: Independent speed control
X-force	-	X
Y-force (moment calculated)	-	X
Moment control	-	X (Cancelled)
Calculation results at windDirection = 90 deg (Y force: positive is pointing to the starboard)		
FOC / FOC (Model 1)	1.00	0.74
Drift angle [deg]	0.09	0.55
totalXforce [kN]	-466.2	-350.3
totalYforce [kN]	0.0	0.0
totalMoment [kN*m] except rudder	3320.4	14332.0
rudderXForce [kN]	-6.9	-29.8
rudderYForce [kN]	23.0	99.3
windPropulsionXForce [kN]	0.0	139.0
windPropulsionYForce [kN]	0.0	-209.4
windPropulsionYawMoment [kN*m]	0.0	0.0
windXForce [kN]	-23.3	-23.5
windYForce [kN]	-50.4	-49.8
windMoment [kN*m]	1047.6	1039.8

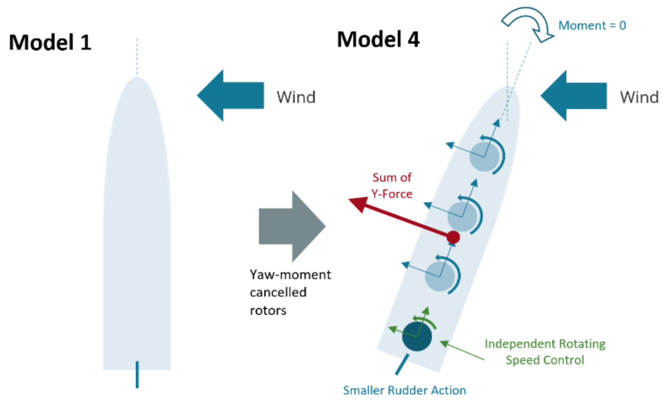

Fig.22: Effect of rotor sails with lateral force component and yaw moment control

3.3.4 Evaluation in actual sea condition by voyage simulation

Upon analyzing the basic behavior of each simulation model under ideal conditions (no wave), voyage simulations for an example route (Route 3: Chiba to Port Botany) using Spring 2022 weather conditions are conducted. The outcomes are depicted in Figs.23 and 24, summarized as follows. While this section focuses on the reduction of CO2 emissions, it is important to note that the strategies and findings discussed herein also contribute to FOC savings.

1) Effects of considering lateral force from rotors

When comparing CO_2 emissions from ships equipped with rotor sails under two scenarios - one disregarding the lateral force (Model 2, a simplified condition) and the other taking it into account (Model 3, an actual condition) - it emerges that CO_2 emissions in the actual condition exceed those in the simplified by an average of 11%. This discrepancy arises because the rotor's yaw moment necessitates additional rudder actions, which in turn increases the ship's drift angle. As a result, the ship requires more propulsion power, leading to higher CO_2 emissions.

2) Effects of yaw-moment control on rotors

In an analysis comparing CO_2 emissions between ships equipped with rotor sails, including those with lateral force alone (Model 3) and those with both lateral force and controlled yaw-moment rotor sails (Model 4), it is observed that CO_2 emissions for ships employing yaw-moment control exhibit an average decrease of 4%. The implementation of yaw-moment control significantly reduces the necessity for rudder actions, thereby lowering the required power and, consequently, diminishing CO_2 emissions.

3) Benefits of installing yaw-moment controlled rotors

When comparing conventional ships (Model 1) to those outfitted with yaw-moment controlled rotor sails (Model 4), an average reduction in CO_2 emissions of 18% is observed. This underscores the substantial environmental advantages of integrating yaw-moment controlled rotor sails into ship design.

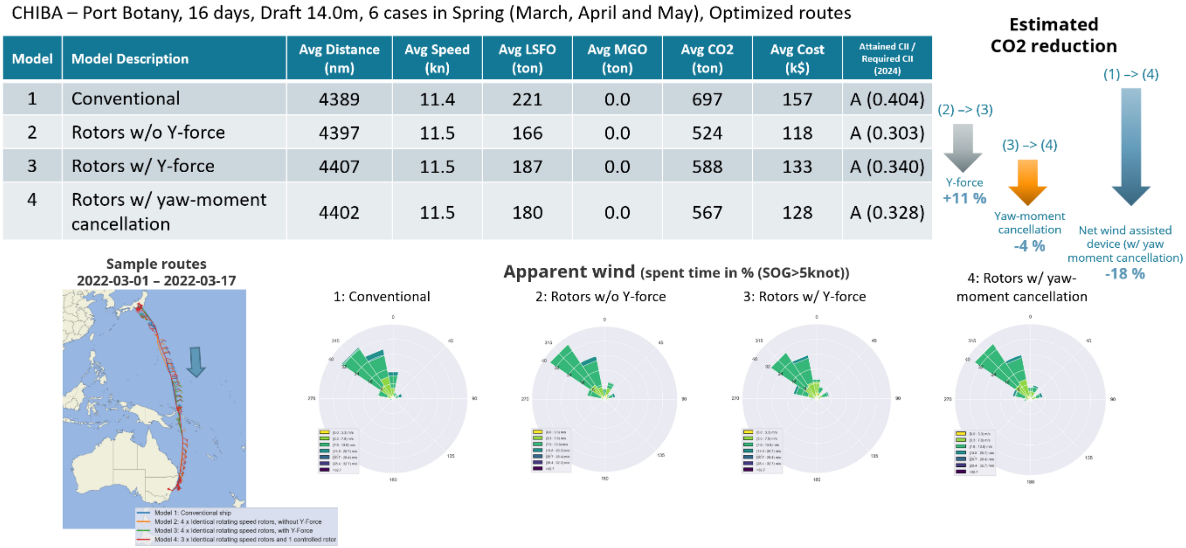
CHIBA – Port Botany, 16 days, Draft 14.0m, 6 cases in Spring (March, April and May), Optimized routes

Model	Model Description	Avg Distance (nm)	Avg Speed (kn)	Avg LSFO (ton)	Avg MGO (ton)	Avg CO2 (ton)	Avg Cost (k$)	Attained CII / Required CII (2024)
1	Conventional	4389	11.4	221	0.0	697	157	A (0.404)
2	Rotors w/o Y-force	4397	11.5	166	0.0	524	118	A (0.303)
3	Rotors w/ Y-force	4407	11.5	187	0.0	588	133	A (0.340)
4	Rotors w/ yaw-moment cancellation	4402	11.5	180	0.0	567	128	A (0.328)

Fig.23: Comparison of effectiveness of CO_2 emission and fuel cost between the models by voyage simulations for Route 3 (Chiba to Port Botany)

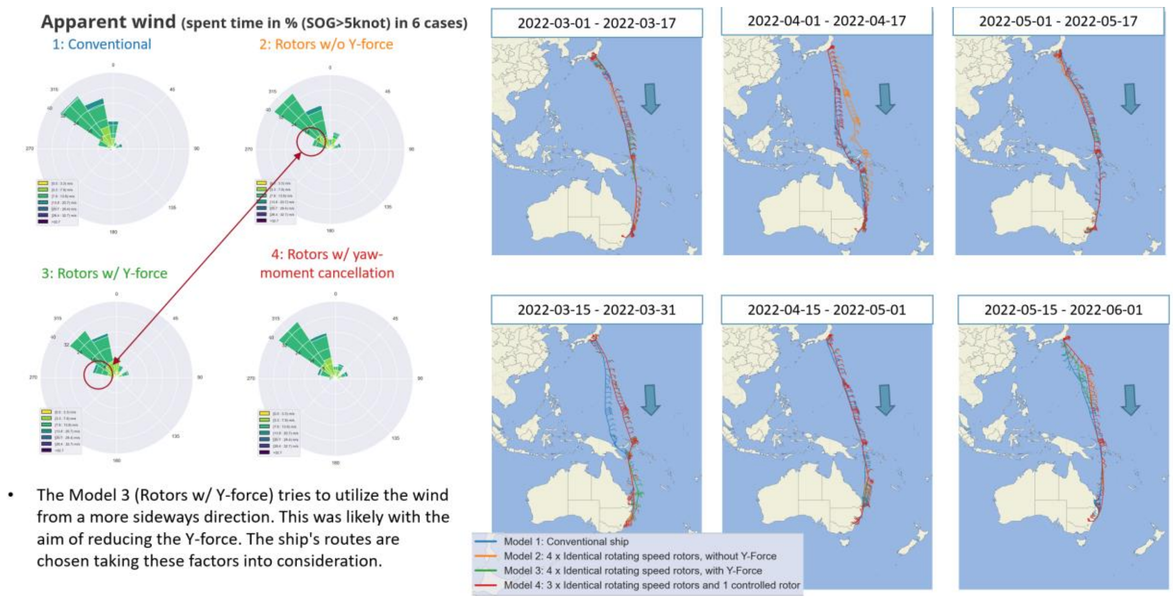

Fig.24: Comparison of optimized route and encountered wind between the models by voyage simulations for Route 3 (Chiba to Port Botany)

3.4. Discussion

3.4.1. Effects of lateral force and yaw-moment control in Study 1 and 2

In Study 1 and 2, ship equipped with rotor sails without considering the lateral force (Model 2, a simplified condition) is used. As more realistic conditions are analyzed in Study 3 by considering lateral force and with yaw-moment control, this allows for an estimation of its effects.

As depicted in Table II, the utilization of Model 2 yields a CO_2 emissions reduction of 21% for Route 3 in Spring. Evaluating voyages under more realistic conditions (incorporating lateral force from rotors) and with yaw moment control (Model 4) indicates a modification in CO_2 emissions reduction by 3 percentage points (from 21% to 18%). Similar variations in CO_2 emissions reduction are anticipated for other routes as well.

3.4.2. Effect of CO_2 emissions by energy required to operate rotor sails

The energy requirements and CO_2 emissions associated with operating rotor sails are not explicitly included in the simulations for this project. However, the energy required for operating the four rotor sails is approximately estimated to average 107 kW. With an example Specific Fuel Oil Consumption (SFOC) of 200 g/kWh for the auxiliary engine, the fuel consumption is projected to be about 0.5 ton/day (MGO), leading to CO_2 emissions of approximately 1.6 tons/day.

With the voyage on, for example, Route 3 in Spring lasting 16 days, the total CO_2 emissions are calculated at 25.6 tons. Given this, the average Fuel Oil Consumption (FOC) savings and CO_2 reductions are anticipated to be impacted by about 3 percentage points (comparison between case (b) and case (d)). Estimating in the same manner, similar variations in FOC savings and CO_2 emissions reduction are anticipated on the other routes.

3.4.3. Provisional estimations of FOC savings and CO_2 reductions

Upon considering the discussions regarding the impacts of lateral force and yaw-moment control as investigated above, and factoring in the CO_2 emissions attributable to the energy required for operating rotor sails, it is conjectured that the anticipated average FOC savings and CO_2 reductions observed in Studies 1 and 2 might see a slight adjustment, within the range of a few percentage points. Considering these figures represent preliminary estimates, further detailed discussions are warranted for a more definitive evaluation.

4. Conclusions

To assess the effectiveness of wind-assisted ships and optimize their performance in terms of decarbonization and economic efficiency, we present a simulation system that leverages NAPA Fleet Intelligence's voyage simulator, Norsepower's refined rotor sail model, and Sumitomo's rotor control logic.

In this project, a Panamax tanker equipped with and without four rotor sails is analyzed under various operational conditions, such as routes, loading conditions, and seasons. The case studies are conducted through simulations that utilize actual historical weather data and certain assumptions. The key findings, implications, and future directions of the studies are summarized as follows.

1) Key findings
    - Rotor sails combined with voyage optimization (weather routing) can yield CO_2 reductions and fuel savings ranging from 10% to 30%, contributing significantly to compliance with CII and EU-ETS regulations and facilitating EU-ETS allowance cost savings.
    - Voyage optimization (weather routing) enhances the performance of ships with rotor sails, with expected FOC savings and CO_2 reduction in the range of 5% to 10%.
    - Implementing a yaw moment control system can decrease CO_2 emissions by an additional about 4 percentage points compared to ships operating all four rotors at the same speed without this control system.

2) Implications of the study
    - Voyage simulations play an indispensable role in assessing the variability of savings from wind-assisted devices across different ships (type and size), device configuration, their trading areas, loading conditions, voyage schedules, and seasons (weather). By incorporating a tuned performance model and realistic operational conditions, these simulations offer comprehensive insights into decarbonization and economic benefits, including environmental performance and Return on Investment (ROI) analysis, thereby aiding stakeholders in making informed decisions about adoption and in designing optimal wind-assisted ships.

3) Future directions
   - Further enhancements and development of the system are crucial, including validating and refining the performance model and rotor control system, alongside developing simulation-based ship design tools.
   - It is imperative to conduct experiments and trials to ascertain the system's efficacy in enhancing economic viability, reducing emissions, and improving safety in shipping operations.
   - Advancing actual implementations and contributing to the maritime industry's efforts towards decarbonized shipping are key priorities.

Acknowledgement

This project received support from Sumitomo Heavy Industries, Ltd. Appreciation is extended to our colleagues at NAPA, Sumitomo Heavy Industries Marine & Engineering, and Norsepower for their insights and expertise, which were invaluable to the project. Special thanks are given to Masahiko Tanigawa and Kana Dohi from NAPA Japan for their exceptional project management, to Kouki Wakita for analysis support, and to Claus Stigler, Dr. Helong Wang, and Kimmo Laaksonen from NAPA, Yoshinori Tagaya and Kahori Amano from Sumitomo Heavy Industries Marine & Engineering, and Severi Sarsila from Norsepower, for their invaluable advice that significantly enhanced the manuscript.

References

AHOKAS, M., (2019), *Analysis of voyage optimization benefits for different shipping stakeholders*, Master's thesis, Aalto Univ., https://aaltodoc.aalto.fi/items/7713c886-644d-4213-bed1-7fe9f2502c09

ARAI, Y.; DOHI, K.; PAAKKARI, V. (2023), *NAPA's Virtual Voyage Simulation of Wind Assisted Ships in Design Phase*, NAPA User Meeting 2023, Helsinki

ASHIDA, T.; MIZUTANI, N.; PAKKANEN, P.; VÄISÄNEN, A.; MANDERBACKA, T. (2019), *Performance Monitoring Insight at MOL*, 4th HullPIC Conf., Gubbio

DUPUY, M.; LETOURNEL, L.; PAAKKARI, V.; RONGÈRE, F.; SARSILA, S.; VUILLERMOZ, L. (2023), *Weather Routing Benefit for Different Wind Propulsion Systems*, J. Sailing Technology 8(01), pp.200-217

HARANEN, M.; MYÖHÄNEN, S.; CRISTEA, D.S. (2017), *The Role of Accurate Now-Cast Data in Ship Efficiency Analysis*, 4th HullPIC Conf., Gubbio, pp.25-38, http://data.hullpic.info/HullPIC2016.pdf

MARIMON GIOVANNETTI, L.; OLSSON, F.; ALEXANDERSSON, M.; WERNER, S.; FINNSGÅRD, C. (2020), *The Effects of Hydrodynamic Forces on Maneuvrability Coefficients for Wind-Assisted Ships*, 39th Int. Conf. Ocean, Offshore & Arctic Engineering (OMAE2020)

MASON, J.; LARKIN, A.; BULLOCK, S.; VAN DER KOLK, N.; BRODERICK, J.F. (2023), *Quantifying voyage optimisation with wind propulsion for short-term* CO_2 *mitigation in shipping*. Ocean Eng. 289

NORSEPOWER (2023), *Norsepower Performance Data at glance*, Norsepower

PAAKKARI, V.; WANG, H.; STIGLER, C. (2022), *Voyage optimization with wind propulsion*, Int. Conf. Computer Applications in Shipbuilding (ICCAS), Yokohama

WERNER, S.; NISBET, J.; OLSSON, F. (2022), *Sea Trial Methodology for Wind Assisted Ships*, 7th HullPIC Conf., Tullamore

Lost in Interpretation – The User Interfaces in Hull Condition Monitoring

Falko Fritz, Albis Marine Performance, Hamburg/Germany, falko.fritz@albis-mp.com

Abstract

This paper discusses the role of the user interfaces in hull condition monitoring. Data needs to be transformed into information and made available to people. Algorithms and automatic data processing have come a long way already, but in the end it's still humans who take decisions. These decisions influence both the quality of hull condition monitoring and its monetary success. The practical experiences with designing the user interfaces and using various information channels are presented and compared.

1. Introduction

The value of vessel performance management lies in the decisions that are based on the displayed data. Many applications of hull condition monitoring and other assisting software tools eventually get dismissed because the information provided is not implemented in the decision-making processes and thereby fails to make profit. Three routines contributing to a working solution are discussed in the following chapters.

- User interfaces for data input,
- User interfaces for data output,
- User interfaces for sensor calibration and maintenance.

The customers of performance management solutions will only use the systems as intended if all three interfaces are designed to ensure the reliability of the data and information. However, this paper cannot even scratch the surface of methods to create high quality user interfaces in general. Delving deeper into the entire topic, e.g. regarding visual design, usability and user guidance would be far beyond its scope. Therefore, it will only highlight selected aspects where the interpretation of information is crucial, and which are particularly relevant for vessel performance monitoring.

2. Manual Data Entries on Board

Most performance monitoring solutions take data into account that are not automatically recorded by sensors and cannot be gathered from third party sources like e.g. weather data. Some ship owners even rely completely on Noon Report based systems, where manually entered forms are the predominant source of information. In other cases, only e.g. the draft information, the fuel consumption, M/E load or shaft power could be data that are entered by the crews.

Noon reports contain a mix of different types of information. General voyage information, miscellaneous remarks, etc., plus two types of values that can be used for performance evaluations, either as additional information to sensor data or exclusively if no high frequency measurements are available.

- Values that describe the specific point in time, typically noon local time, like e.g., vessel position, weather conditions, momentary engine load, fuel remaining on board, distance to next destination, etc.
- Values that describe the period since last report, like e.g., distance run, steaming time, fuel consumption, etc.

These two value types do not create a common dataset. If the vessel did not operate in similar conditions over the complete reporting period, which usually is not the case, the M/E power at noon and the fuel consumption rate over the last 24 h cannot be used to assess the M/E efficiency. Likewise, the weather conditions at noon might say very little about the influences of swell and waves on the fuel consumption.

Furthermore, at least in the experience of Albis, many ship owners and operators still use their own noon reporting procedures that do not even specify exactly what should be entered in some of the available fields. This concerns the above distinction between momentary data and averages since last report, but also the units in some cases. For instance, wind, swell and waves directions can be given in reference to true north in degrees, or as an angle relative to ship heading, or even as a 45° sector noted with the digits 1-8. There have been examples where different crews on the same vessel used the same entry fields to fill in either a sector 1-8 or an angle 0-359° since no unit was clearly defined in the field description. Of course, this may easily lead to the misinterpretation of data in the following evaluation.

Thankfully, this issue has been addressed in recent years. Initiatives to standardize noon report entries and align them with ISO 19848, *ISO (2018),* are on their way, e.g. conducted by the Smart Maritime Network, *SMN (2023)*. However, it must be expected that it will take many years before a standardized format will be established in a larger share of the shipping industry.

3. Information Screens and Reports

3.1 Data Screens on Board

Of all the interfaces discussed in this paper, the screens displaying measurement data on board the vessels are the easiest ones to interpret, at least in the experience of Albis. As long as the information "only" concerns vessel performance and is not crucial information for the ship's safety, the readings are either used for good purpose or simply ignored if they seem implausible. Consequently, poorly calibrated sensors or errors are mostly discovered by the evaluation routines on shore, rather than reported by the vessels' crews. An example of that kind is shown in chapter 4.

3.2 Online Tools and Reports for Office Use

Reports and information dashboards accessed by the office staff are probably the most important ones in the decision-making processes. It is therefore essential that the information shown is interpreted correctly.

For the purpose of hull condition monitoring, data must be normalized to account for different ship speeds, drafts, etc., as also described in ISO 19030, *ISO (2016)*. Consequently, the propulsion power, ship speed or M/E fuel consumption rate used as a parameter to track the development may not be the actual power, speed or consumption of the most recent ship operation. It is an extrapolated value which may be close to the latest recordings if the vessel operates near reference conditions, but it might just as well not be. Fig.1 shows an exemplary hull condition monitoring report where the overconsumption is stated in percent and as an absolute value in metric tons per day, assuming the vessel is operating at the reference conditions listed at the bottom of the report page.

In the discussions Albis had with customers, there have been numerous occasions where this necessity was not understood at first. The reliability of the data was questioned or even straight out denied because the reported normalized values for some vessel did not agree with the real power, speed or consumption that were known to the person reading the report. The difference between raw data and normalized results is evident to those who frequently work with analysing measurements or who did so during an education in applied science or engineering. But many decision makers in shipping may not have that kind of background. Presented results may be misinterpreted if they are not explained. But detailed, written explanations are often not read, at least in the experience of Albis. Therefore, a close contact between the evaluation service provider and the customer is essential.

There are some factors that improved this communication in recent years, though. First, more and more ship owners and operators created dedicated positions to assess the efficiency of their fleet in their organizations. Second, the widespread introduction of video conferencing with MS Teams and similar tools made it a lot easier to arrange short, productive meetings with the involved people all across the globe. Creating a common understanding, discussing how to interpret results and which conclusions to draw from them is a lot easier now than it was a decade ago.

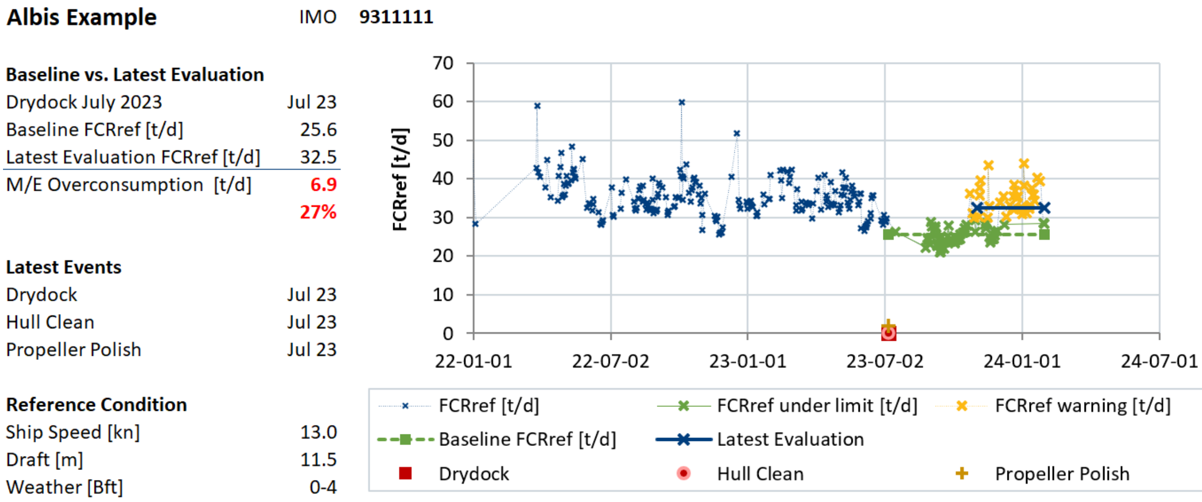

Fig.1: Exemplary hull condition monitoring report

4. Data Interpretation for Sensor Calibration and Maintenance

In a company that also manages the quality of sensor outputs, a noticeable share of data interpretation is done for the purpose of device calibrations and maintenance. While the calibration is a standardized process, the fault finding when sensors show implausible results can be more time consuming. Fig.2 illustrates such an example.

In this case, the fuel temperature and mass flow rates are shown in the booster circulation, before the main engine (M/E Inlet) and after it (M/E Outlet). This setup allows for the evaluation of fuel meter accuracy every time the main engine is off, when it consumes no fuel and the shaft revolutions counter shows zero. The inlet and outlet fuel meters should read the same circulation flow rates in that condition, *Fritz (2023)*. However, in the example in Fig.3, the inlet has a lower reading than the outlet, meaning that more fuel flowed out of the pipe than into it, which of course cannot be true.

This error is easy to detect in the data. Understanding the problem and resolving the issue are separate matters, though, and the latter cannot be achieved without getting technicians and the crew on board involved. In this particular case the fuel meters themselves did not show any signs of malfunction. Instead, it proved that a bypass valve started leaking and fuel evaded the inlet flowmeter, causing its readings to differ from the outlet mass flow. In maintenance cases like this, the correct interpretation of data often relies on detailed information regarding the sensor installation and reliable communication with the crews.

5. Conclusion

The benefit of vessel performance management systems may get lost in interpretation. The potential to misinterpret information hides in numerous places. The manual data entries on board only deliver high quality input when the exact intended content of the entry field is clear. To ensure that the decision-makers can confidently and appropriately respond to the evaluation results in their offices, it is essential to facilitate their ability to accurately identify the best solutions for their organization. This in turn requires robust procedures to calibrate and maintain sensors properly, so that the feed of raw data into all subsequent evaluation steps is not corrupted from the very start. Thankfully, the ability to reach these goals increased significantly over the recent years, and it continues to do so. In response to new

IMO and EU regulations that require a heightened emphasis on energy efficiency, the maritime industry is adapting by integrating new skills into their teams. Ship owners and operators seize the opportunity to utilize new technologies effectively and efficiently. The breakthrough of video conferencing offers the tool required to tap into this new potential and draw the right conclusions, between people.

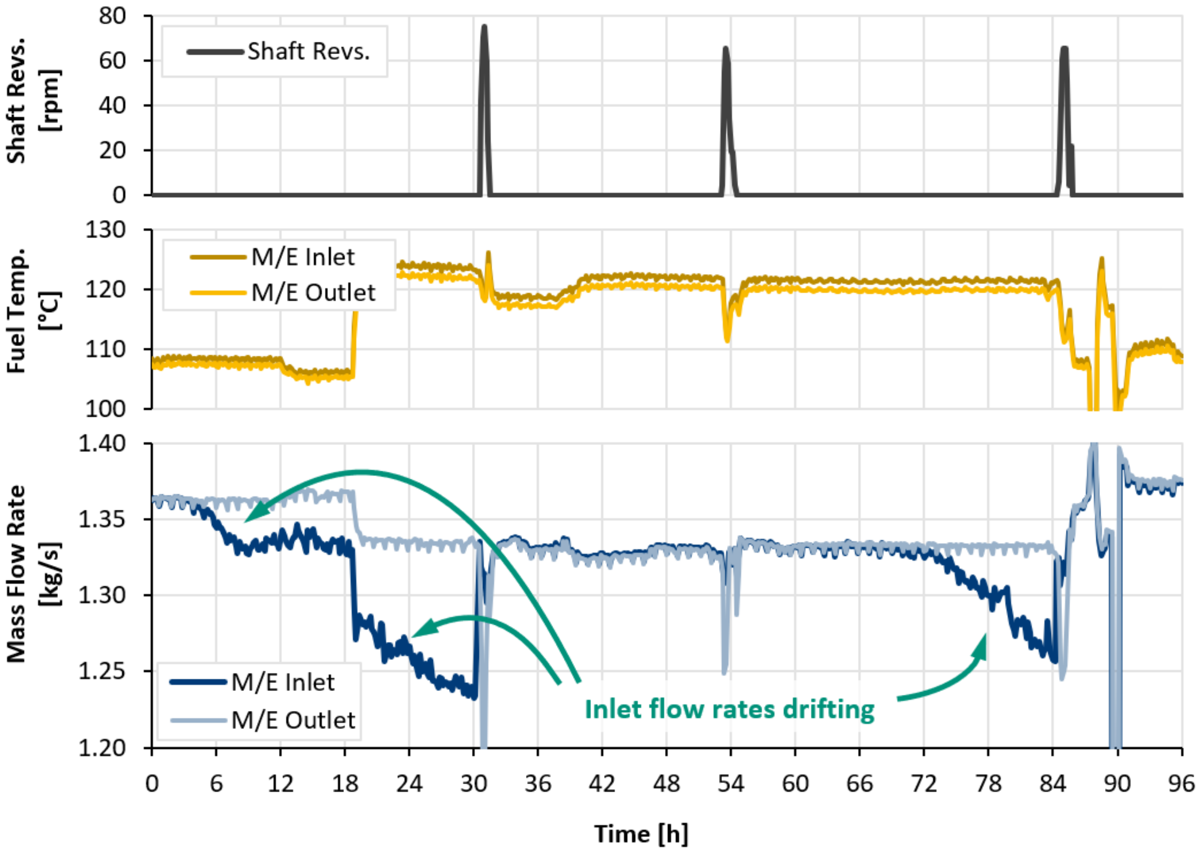

Fig.2: Exemplary fuel meter data, showing implausible inlet fuel meter results

References

FRITZ, F. (2023), *Data Recording on Board – Are We Getting it Wrong from the Start?*, 8th HullPIC Conf., Pontignano, pp.62-69, http://data.hullpic.info/HullPIC2023_Pontignano.pdf

ISO (2016), *ISO 19030 - Ships and marine technology — Measurement of changes in hull and propeller performance — Part 1: General principles*, Int. Standard Org., Geneva

ISO (2018), *ISO 19848 - Ships and marine technology — Standard data for shipboard machinery and equipment*, Int. Standard Org., Geneva

SMN (2023), *A Standardised Dataset for Vessel Noon Reports*, Smart Maritime Network, https://smartmaritimenetwork.com/wp-content/uploads/2023/01/SMN-SVD-for-Noon-Reports-White-Paper.pdf

Applying Analytical Hierarchy Process for Data Quality Analysis in Maritime Industry

Emir Ejder, DFDS, Istanbul/Turkey, emiejde@dfds.com
Hasan Göler, DFDS, Istanbul/Turkey, hagol@dfds.com
Frederik H. Berthelsen, DFDS, Copenhagen/Denmark, frber@dfds.com
Şahin Üsküdarlı, DFDS, Istanbul/Turkey, sausk@dfds.com

Abstract

The study analyzes the importance of data quality in the maritime industry and its impact on the efficiency of ship operations. Based on critical criteria such as communication, data entry, and voyage setup, 15 vessels with low error rates were selected and evaluated using the Analytic Hierarchy Process (AHP) methodology. According to the analysis results, the performance of each of these vessels according to the criteria is expressed as a percentage. These scores show how effective each vessel is regarding data quality and operational efficiency. In particular, the accuracy of data entry processes has a decisive impact on the overall quality of voyage reporting. The study's findings emphasize the importance of data quality management and continuous improvement activities in the maritime industry and show that improvements in this area contribute to the effectiveness of operational decision-making processes. This study provides important insights for developing data quality strategies in the maritime industry and provides a basis for adopting sustainability-oriented approaches in the industry.

1. Introduction

The maritime industry is a critical component of global trade and requires decision-making processes based on high quality data. Ship operations and management require decisions based on accurate and reliable data. This data is used in many areas from route planning to fuel consumption optimisation, maintenance, and repair to cargo management. Therefore, data quality directly affects the effectiveness of these decisions and contributes greatly to the overall performance of the maritime industry. Ship management has a complex and dynamic structure, especially at the international level. This structure is shaped by various factors such as laws, environmental regulations, and safety standards of different countries. All these factors require ship operators to maintain high quality standards in data management and analysis processes. This paper aims to comprehensively address the data quality practices for a maritime fleet and the existing data entry errors.

The assessment and improvement of data quality in the maritime industry is one of the most critical elements of this field. At the centre of this study is the user evaluation of data entry practices using the Analytic Hierarchy Process (AHP). AHP is an effective tool for managing complexity in decision-making processes and has been used in this research to objectively assess data quality in the maritime industry. The method is designed to determine the relative importance of different criteria and to establish a hierarchy among them. This systematic approach allows for an in-depth analysis of the data quality issues faced in the maritime industry and a clear understanding of the impact of each of these issues on overall data quality. This application of AHP provides valuable insights into the development of data management strategies and emphasises the critical role of methodological approaches at the heart of strategic decision-making.

Consistent and accurate data obtained in the maritime sector enables healthy and proper reporting in regulatory processes such as IMO (International Maritime Organisation) DCS (Data Collection System) and EU (European Union) MRV (Monitoring, Reporting, and Verification). These processes impose an obligation on ship operators to carefully monitor and report environmental impacts. This is especially vital for tracking critical environmental factors such as carbon emissions. Effective reporting plays a key role in achieving sustainability targets and reducing environmental impact in the industry. Thus, the implementation of regulations such as IMO DCS and EU MRV makes a significant contribution to improving data management and reporting practices in the maritime sector. These regulations encourage continuous improvement of data quality in the industry, while at the same time raising standards of environmental compliance and transparency. This process contributes significantly to the adoption of a more sustainable and environmentally sensitive business approach in the maritime sector.

Technological developments and industry innovations contribute greatly to the improvement of data quality in the maritime industry. This study specifically investigates how technology affects data quality and how this quality can be further improved in the future. Emerging technologies are enabling data collection and processing in ship management to become more effective and efficient, *Le et al. (2020).* For example, advanced sensor technologies and satellite communications enable more accurate and reliable data collection processes in the maritime industry, *La Ferlita et al. (2013).* These advances contribute to the continuous improvement of data quality, making decision-making processes more reliable and effective. These technological innovations open new horizons for strategic decision-making and operational efficiency in the maritime sector.

In this research, 15 vessels with the lowest error rate based on the number of voyages have been carefully selected to gain in-depth insights into data quality in the maritime industry. The main criterion for the selection of these vessels is to focus on the importance of providing accurate and reliable data in the industry. This accurate and reliable data plays a critical role in improving operational efficiency. Furthermore, the collection of this data points to the potential for a wide range of usability, such as operational optimizations, training modules. In the maritime industry, such data management has been observed to facilitate and improve regulatory compliance and reporting processes. In the light of technological advances and sectoral innovations, these processes are expected to contribute to the sustainable and safe development of the sector. The research aims to provide comprehensive guidance on how to develop data management strategies in the maritime sector and sheds light on the steps to be taken in this field.

2. Materials and Methodology

2.1. Methodology of the study

The methodology of this study requires a detailed and comprehensive approach to the assessment of data quality in the maritime industry. The framework of study is presented in Fig.1. Research process includes vessels selected from the different Business Units (BUs) in DFDS. It focussed on identifying the vessels with the lowest number of errors compared to the number of voyages. This selection process is designed to provide an objective assessment of the data quality performance of the vessels.

A scoring system ranging from 1 to 9 was used in the vessel comparison and evaluation process. This scoring system aims to comprehensively assess the data quality performance of each vessel. This evaluation process assesses the data quality performance of the vessels based on several criteria.

Fig.1: The framework of study

2.2. Analytic Hierarchy Process

Analytic Hierarchy Process (AHP) is a multi-criteria decision analysis method developed by Dr Thomas L. Saaty in the late 1970s to solve decision-making problems. AHP allows decision makers to evaluate a set of alternatives according to predetermined criteria and make the most appropriate choice, *Wang et al. (2022)*. The basic principles of this method are to establish a three-level hierarchy of objectives, criteria, and alternatives; to determine their importance by making pairwise comparisons between criteria and alternatives; to calculate priorities for criteria and alternatives using the values obtained from pairwise comparisons; and to check the consistency of decision makers' evaluations and to revise these evaluations if necessary.

A detailed examination of the causality of each index was subjected to multiple rankings using the AHP approach. To determine the ranking of the importance of the indicators, expert judgement was used. The judgement matrix based on 1 to 9 scale is presented in Table I. In the analysis of the hierarchical analysis, the stages vary: each higher-level criterion is subjected to pairwise comparisons with its sub-criteria, and the scale used in these comparisons serves as comparison statements, *Bike and Ruichang (2023).*

Table I: Explanation of the 1 to 9 Scale in AHP Methodology

Significance Level	Definition of given values
1	Equally significant
3	Moderately significant
5	Significantly strong
7	Very significantly strong
9	Utterly significant
2, 4, 6, 8	Values intermediate to the principal ones

The AHP results express the performance of each ship according to the main criteria in a measurable and comparable way. These percentage scores clearly show the level of achievement in the criteria and the level of data quality and operational efficiency of the different vessels. The evaluation of the AHP analysis provides an objective and quantitative basis for decision-making processes, thus enabling more informed and data-driven decisions to be made in data quality management and improvement efforts. The AHP methodology provides a scientific and objective assessment to ship evaluation in terms of data quality and this approach contributes significantly to improving the efficiency of data quality strategies and operational decisions within the industry. The main criteria and sub-criteria are:

- Voyage Setup: Date & Time Inconsistency, Port & Route Inconsistency, Voyage Report Type, Missing Voyage, and Distance-Timeline Accuracy Match.
- Data Entry: Fuel Consumption Errors, MVS & Manual Cargo entry, Energy Consumption and Ballast Entry.
- Communication: Forum Responses, Explanation Section and Speed of Action.

These criteria and sub-criteria are important factors to consider when evaluating the performance of our vessels and the quality of voyage reporting. Through the AHP method, it is possible to select the best ship by systematically addressing these criteria and sub-criteria.

- Voyage Setup: Voyage setup involves the correct creation of voyages on voyage creating systems. This assesses whether the vessel is in line with the previous voyage, whether the port of arrival and departure are correctly selected and the effectiveness of the voyage planning in general.
- Data Entrance: Accurate and complete data entry prevents incorrect analysis and decisions,

which improves operational efficiency and decision-making processes. In addition, accurate data entry enables critical operational factors such as energy and fuel consumption to be accurately monitored and evaluated.

- Communication: Communication evaluates the effectiveness of communication between the ship's crew and Vessel Performance Management. Effective communication facilitates fast and accurate decision making, as well as timely response and coordination.

3. Case Study

During the research, detailed data analysis was carried out for a 40-week period between 1 January and 20 October 2023. During this period, the voyage reporting software was updated, and proactive measures were developed to minimise error rates. During the analysed time, 23,225 voyages belonging to a total of 60 vessels were analysed and a total of 2,691 errors were detected in these voyage reports. The detailed distribution of the detected errors is presented in Fig.3. This analysis plays a critical role in determining the type and frequency of errors encountered in ship operations and planning strategic interventions to reduce these errors.

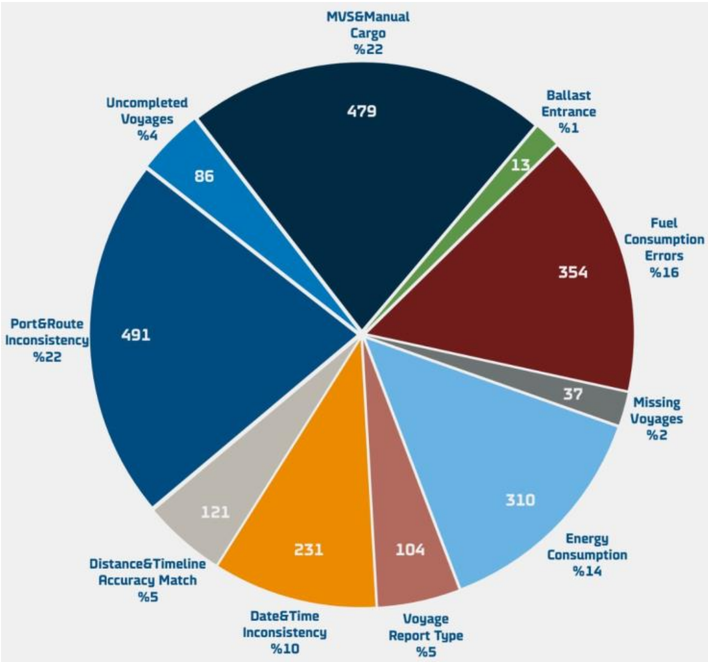

Fig.3: The total number of errors for each type

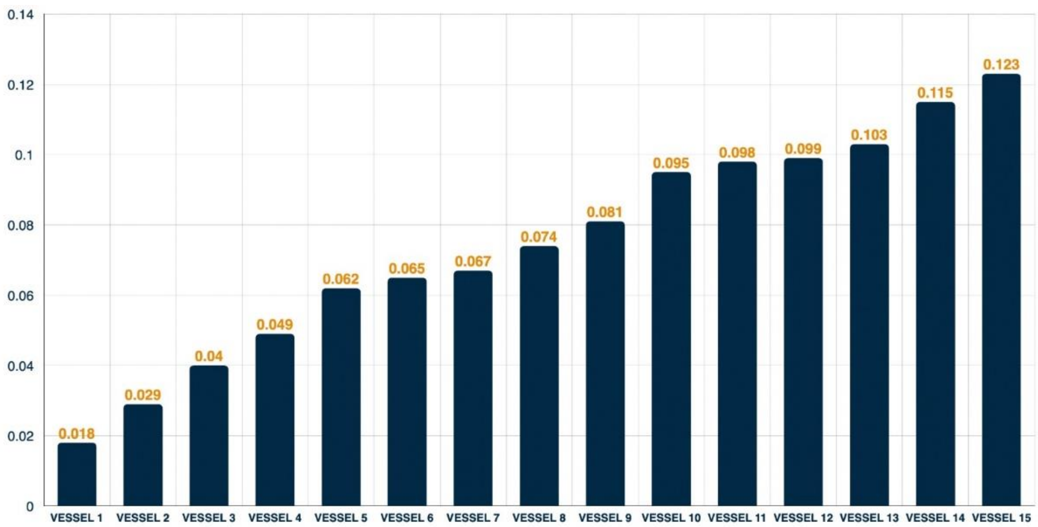

Fig.4: 15 vessels with the lowest error ratio

In order to emphasise the importance of data quality and to make an in-depth assessment by error types, the top 15 vessels with the lowest number of errors compared to the number of voyages in terms of data quality parameters among the different Business Units (BUs) in DFDS were identified for the base case and shown in Fig.4.

The number of faults and their distribution according to faults for the 15 vessels analysed are presented in Fig.5. The fault distribution of the vessels serves as a key reference point for analysing the intensity and types of faults.

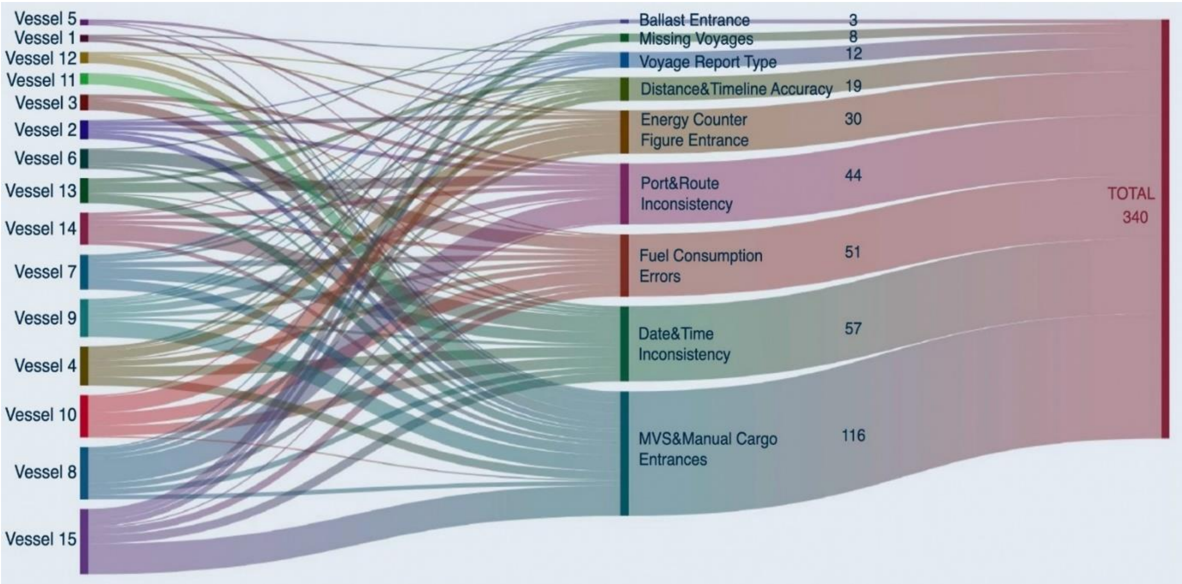

Fig.5: 15 vessels distributions with the lowest error number

4. Results and Discussions

Fig.6 highlights the three main criteria on which the vessel data quality assessment process is based and illustrates the importance of identifying the main factors through judgement from the DFDS vessel performance team in the selection of these criteria; the decision-making software based on the Analytic Hierarchy Process (AHP) was used to build the model and determine the weighting of each factor. The Vessel Performance Superintendents in DFDS decided which parameters were more important than others and calculated the relative importance of each factor using a comparison matrix.

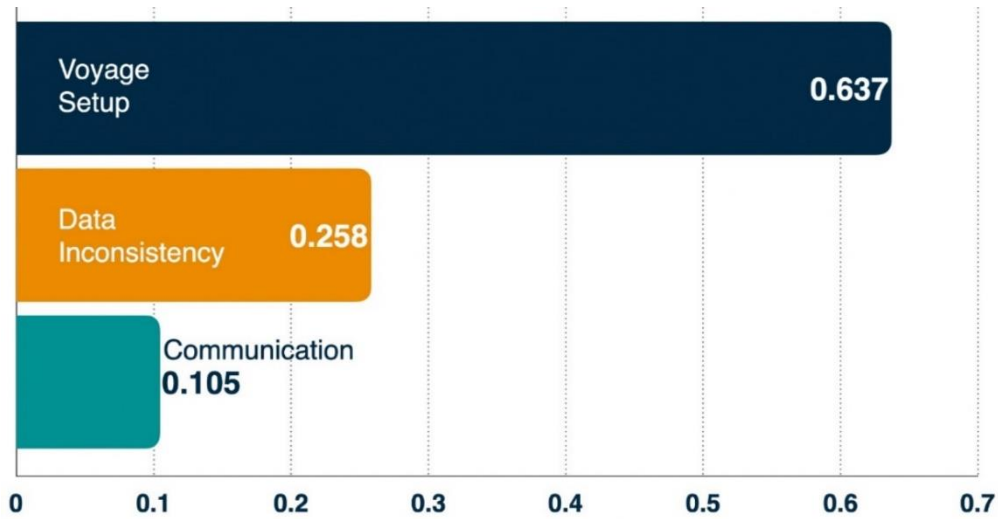

Fig.6: Main criteria weights

Fig.6 demonstrates that the factor 'Voyage Setup' has the highest degree of importance in the AHP model regarding ship errors, with a score of 0.6370. This high importance of voyage setup is due to its capacity to assess whether the voyages are set up correctly, whether the ship is compatible with the previous voyage, whether the ports of arrival and departure are chosen correctly, and the effectiveness of voyage planning in general. The 'Data Entry' factor is ranked second in the overall priority ranking with a score of 0.2583. This importance of data entry stems from the fact that accurate and complete data entry improves operational efficiency and decision-making processes by preventing incorrect analyses and decisions. It also enables critical operational factors such as energy and fuel consumption to be accurately monitored and evaluated. The 'Communication' factor has the lowest importance rating, with a score of 0.1047. This communication facilitates timely intervention and coordination of operational processes, enabling fast and accurate correction of erroneous data. The Consistency Ratio (CR) of the table is 0.0332 and it's quite acceptable for AHP studies. CR is a validation parameter for AHP studies. If the ratio is higher than ‘0.1’ there is a mistake in terms of experts' answers in comparison matrixes. The decision matrix of the study was ensured with the help of the DFDS vessel performance team. Following the determination of rankings, the scores for each scheme are presented. Finally, the rankings are established and the outcomes for each system are presented in Table II.

Table II: The weighted normalized matrix of each vessel

	Error Ratio	Voyage Setup	Data Entrance	Communication	Overall
VESSEL 1	0.018	0.97564	0.45913	0.00916	0.741036
VESSEL 2	0.029	0.73534	0.17221	0.28336	0.542563
VESSEL 3	0.04	0.94117	0.45912	0.11343	0.729992
VESSEL 4	0.049	0.58820	0.45912	0.40161	0.535325
VESSEL 5	0.062	0.85291	0.68877	0.93197	0.818790
VESSEL 6	0.065	0.70591	0.45911	0.04882	0.573366
VESSEL 7	0.067	0.67647	0.51657	0.13765	0.578694
VESSEL 8	0.074	0.44121	0.00010	0.28067	0.310463
VESSEL 9	0.081	0.08829	0.68873	0.35303	0.271103
VESSEL 10	0.095	0.23542	0.00010	0.13075	0.163678
VESSEL 11	0.098	0.70593	0.68875	0.98541	0.730754
VESSEL 12	0.099	0.94117	0.97564	0.9952	0.955733
VESSEL 13	0.103	0.23539	0.45912	0.01861	0.270486
VESSEL 14	0.115	0.23540	0.17224	0.33047	0.229040
VESSEL 15	0.123	0.02436	0.45911	0.17607	0.152542

The examination of Table II provides a detailed analysis of the vessels' data quality efficiency and error management. Based on the error rates, the base case provides an overall assessment of their operational efficiency. At the same time, the results of the Analytic Hierarchy Process (AHP) reveal variations in data quality as the specific weights of faults are considered.

The base case analysis provides an important indicator of efficiency, particularly for Vessel 1, where a low error rate (0.018) and a high number of voyages indicate that this vessel is highly operationally efficient. In contrast, the overall performance of Vessel 1 in the AHP evaluation stands out with a relatively high score (0.741036), indicating that it still performs at a high level when considering the weighted criteria of the AHP. It reveals that Vessel 1 manages its voyages effectively and minimises critical errors in operational processes.

On the other hand, Vessel 12 ranks highest in the AHP analysis with an overall performance of (0.955733) and exceeds the fleet standards, especially in the categories of Data Entrance (0.97564) and Communication (0.9952). It shows that Vessel 12 performs much more effectively than the number of errors and manages the weighted errors better.

Vessel 5 has shown a significant increase in its overall performance (0.818790) with its outstanding performance in the AHP analysis, especially in Communication (0.93197), indicating the impact of communication and reporting skills on error management and that these competencies play a decisive role in overall operational performance.

This benchmarking analysis shows that it is possible to achieve lower error rates by creating competition between vessels. Detailed benchmarking has been identified as a critical method to understand the error management capabilities of ships and to use this information to improve the system. Identifying ships' susceptibility to errors and developing training programmes to target these weak points can minimise operational risks and significantly improve maritime safety. Furthermore, the data obtained can guide the identification of specific areas that need to be prioritised in crew training and enrich the content of the training received by the ship's crew before joining. Thus, this study provides a basis for developing strategies to reduce error rates in the maritime industry and provides a reference point for future research.

5. Conclusion

The study focuses on data quality in the maritime industry and analysing errors in this area. Based on criteria such as Communication, Data Entry and Voyage Setup, a detailed analysis of 15 vessels with low error rates has been conducted. This analysis aims to identify errors in data entry processes and their potential impact on voyage reporting. Updates to voyage reporting software address the errors identified in this analysis and aim to improve the accuracy of data entry processes. The addition of time zone options, a more detailed definition of voyage legs and adjustments to reporting types are designed to make the data entry process more precise and accurate. In addition, revisions to validation processes and flexibilities in user rights support the integrity of the reporting process by allowing the correction of data entry errors. This study highlights the impact of accuracy in data entry processes on the quality of voyage reporting, and the updates to voyage reporting system represent steps to improve this accuracy. These improvements improve the overall quality of voyage reporting and contribute to the efficiency of operational processes. This analysis contributes to developing data management strategies in the maritime industry by providing essential insights into areas of focus for improving data entry processes.

References

BIKE, Z.; RUICHANG, W. (2023), *Construction of equipment evaluation index system of emergency medical rescue based on Delphi method and analytic hierarchy process*, In Ain Shams Eng. J. 14/2

LA FERLITA, A.; QI, Y.; DI NARDO, E.; EL MOCTAR, O.; SCHELLIN, T.E.; CIARAMELLA, A. (2023), *A Comparative Study to Estimate Fuel Consumption: A Simplified Physical Approach against a Data-Driven Model*, J. Marine Science and Engineering 11(4)

LE, L.T.; LEE, G.; KIM, H.; WOO, S.H. (2020), *Voyage-based statistical fuel consumption models of ocean-going container ships in Korea*, Maritime Policy and Management 47(3), pp.304–331

WANG, H.; XU, C.; DI, R.; XU, Z. (2022), *Analytic hierarchical process with stochastic uncertainty: A case study of governmental audits in China*, Information Sciences 608, pp.1072–1092

Cost-Benefit Analysis of Ship's Hull Maintenance Scenarios in the Kattegat and Danish Strait Route

Youngrong Kim, Chalmers Univ. of Technology, Gothenburg/Sweden, youngrong.kim@chalmers.se
Maria Lagerström, Chalmers Univ. of Technology, Gothenburg/Sweden, maria.lagerstrom@chalmers.se
Lena Granhag, Chalmers Univ. of Technology, Gothenburg/Sweden, lena.granhag@chalmers.se
Erik Ytreberg, Chalmers Univ. of Technology, Gothenburg/Sweden, erik.ytreberg@chalmers.se

Abstract

This study conducts a cost-benefit analysis of various hull maintenance scenarios using the support tool HullMASTER. The analyses provide examples of a ship operating in the Kattegat-Danish Strait. This study indicates that increased hull roughness due to biofouling and hull maintenance, compared to hydraulically smooth hulls, can escalate operational and socio-environmental costs by 6 and 7.2 times. Among the evaluated coatings, non-biocidal foul-release coatings are identified as the most sustainable option by reducing climate change and health damage, and biocide release into the ocean. It also highlights the importance of proper maintenance and the need for sustainable long-term planning.

1. Introduction

The accumulation of marine organisms on a ship's hull, known as ship biofouling, decreases the operational efficiency of vessels, increases fuel consumption, and consequently elevates costs for shipping companies, *Schultz (2007)*. Furthermore, it has severe implications for human health and marine ecosystems due to the increased exhaust emissions and the release of toxic substances from anti-fouling paints applied to hulls, *Ytreberg et al. (2021)*. As a result, the appropriate management of ship biofouling has emerged as a critical task in ship operations.

The determination of an optimal hull management strategy is a complex process influenced by several factors, including the ship's size, operational profile, and sailing area, *Kim et al. (2022)*. Moreover, shipowners must consider not only the increased operational costs resulting from hull management strategies but also their implications for climate change, human health, and the marine environment. To address these concerns, it is essential to apply life cycle cost analysis to assess the economic performance and social impact of various technologies, enabling shipowners to select the most sustainable hull maintenance strategy.

In response to this challenge, *Oliveira et al. (2022)* developed HullMASTER (Hull MAint-nance STrategies for Emission Reduction), a tool designed to assist shipowners, operators, and other stakeholders in evaluating the economic and environmental costs of various ship hull maintenance strategies. Expanding on this work, in this paper, we employ HullMASTER to simulate various hull management scenarios for a ship navigating the Kattegat and Danish Strait and conduct an economic, social, and environmental cost-benefit analysis accordingly. Through this, we aim to understand how variations in hull management strategies affect costs in these water areas and propose sustainable hull management strategies that minimize the operational costs for shipowners while contributing to social and environmental protection.

2. HullMASTER: Decision Support Tool for Hull Maintenance Strategies

HullMASTER is a tool designed to calculate and compare the operational, societal, and environmental costs of various hull maintenance strategies, such as the type of coating, docking frequency, in-water cleaning frequency, and hull treatment procedures applied to a specific ship. The operational costs include additional fuel costs due to biofouling, hull treatment during dry docking, and hull cleaning costs. Societal and environmental costs encompass the health and climate impacts of increased exhaust gases and the release of toxic substances due to biocidal coatings, as well as the costs associated with marine eutrophication and marine ecotoxicity. All costs resulting from hull roughness due to coating and biofouling are calculated in comparison to a hydraulically smooth hull. It is important to note that these costs modeled in HullMASTER do not reflect the absolute costs of ship operation. The tool was validated using approximately 40 years of cumulative operational data measured from nine ships operating in the Baltic Sea. The estimated propulsive penalties for the entire fleet indicated an average deviation of -3.2 ± 3.8%, which underscores the tool's substantial accuracy.

Fig.1 illustrates the overall composition of HullMASTER. The subsequent parts, 2.1 and 2.2, will delve into the main models that constitute this tool, specifically the hull fouling growth and biocide release. For a more detailed explanation of the principles and sources supporting HullMASTER, please refer to *Oliveira et al. (2022)*.

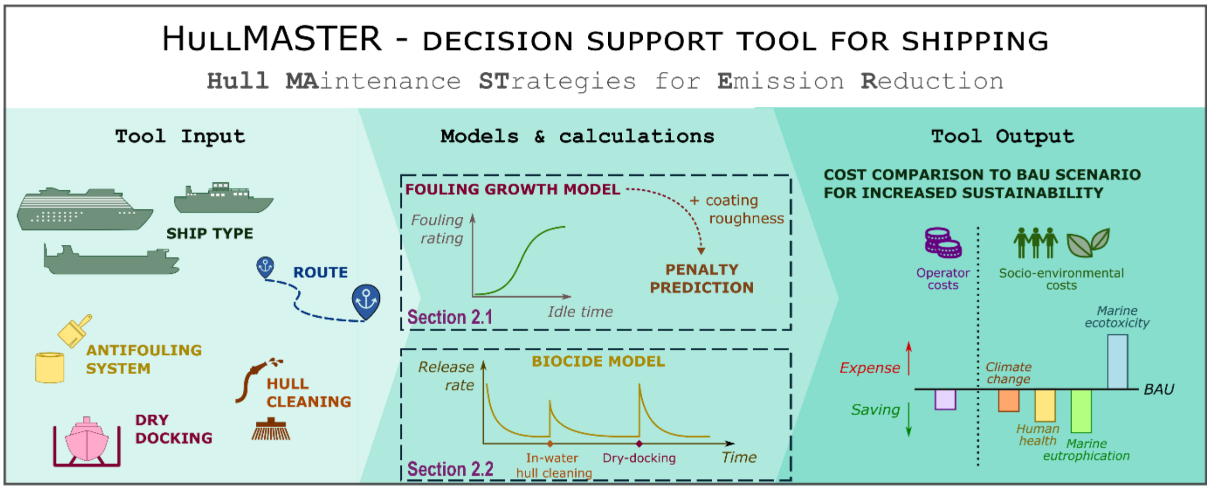

Fig.1: Configuration of HullMASTER

2.1. Hull fouling growth & Propulsive power penalty

The formation and growth rate of biofouling on a hull surface are influenced by several parameters. The most significant variables for predicting fouling growth rates in the Baltic Sea region are the accumulated idle time, *Oliveira and Granhag (2020)*, and salinity, *Wrange et al. (2020*). The fouling growth model used in HullMASTER is based on data obtained from field experiments conducted in the Swedish coastal region, including the Baltic transition and the Baltic proper, *Lagerström et al. (2022)*. As shown in Fig.2, the degree of hull fouling is defined in reference to the frNSTM fouling rating, *US Navy (2006)*, and the cumulative fouling degree over time is fitted using a Gaussian curve, *Uzun et al. (2019)*. HullMASTER uses the seawater salinity and berthing time at the port of call as input parameters to calculate the cumulative fouling growth during the operation.

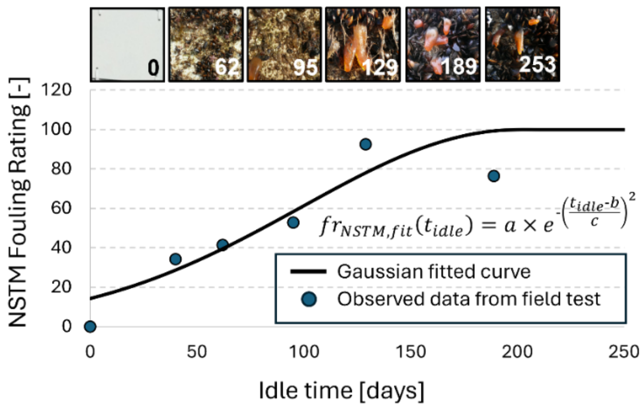

Fig.2: NSTM fouling rating over idle time based on the field test data

The condition of hull roughness is expressed as an equivalent sand grain roughness, and the roughness resulting from coating and biofouling is added to the hydraulically smooth surface. The increase in frictional resistance due to hull roughness is calculated using Granville's method, *Granville (1987)*, which utilizes the flat-plate similarity law scaling method. This allows the estimation of the ship's power penalties relative to the condition of a smooth hull.

2.2. Biocide release from anti-fouling coatings

Most anti-fouling paints used on ships contain biocides like copper oxide to control marine fouling, which release biocides upon contact with seawater, *Ytreberg et al. (2022)*. Additionally, these coatings contain zinc oxide to prevent corrosion, *Lagerström et al. (2018)*. The release of these harmful substances is modeled in HullMASTER based on the average release rates in the Baltic Sea region.

The passive release rate of these hazardous substances into the water is determined based on data from *Lagerström et al. (2020)*, and a consistent decay ratio is applied to the release rate presented by *Valkirs et al. (2003)* to account for long-term emissions. Besides, additional anti-fouling compounds can be released during or after the hull cleaning event. This is estimated based on the weight content of biocides in the removed coating thickness, *Tribou and Swain (2017)*. The release of copper and zinc due to gentle cleaning methods causing negligible to moderate paint wear is referenced from *Soon et al. (2021)* and *Granhag et al. (2023)*. In contrast, aggressive cleaning methods that cause a higher level of wear are calculated using the paint removal values mentioned in *Morrisey et al. (2013)*. The increased passive release rate following cleaning events is modeled based on the study by *Earley et al. (2014)*.

3. Methodology

3.1. Selection of a ship case in the Kattegat-Danish Strait

This study performs a cost-benefit analysis of various hull maintenance scenarios for a ship sailing through the Kattegat and Danish Strait using HullMASTER. The case study utilizes a 190 m-class ro-ro ship that regularly operates the Kiel-Gothenburg route based on the ship's operational profile, Fig.3. The high-salinity seawater influx through the Baltic transition zone, such as Skagerrak and Kattegat, creates a gradient of decreasing surface salinity across the entire Baltic Sea. The Kattegat-Danish Strait route used in the case study is characterized by relatively high fouling pressure throughout the operating area. Meanwhile, the annual average temperature in the target area is around 11°-12°, but in some Baltic transition areas, it can rise to 30° in the summer and fall below freezing in the winter.

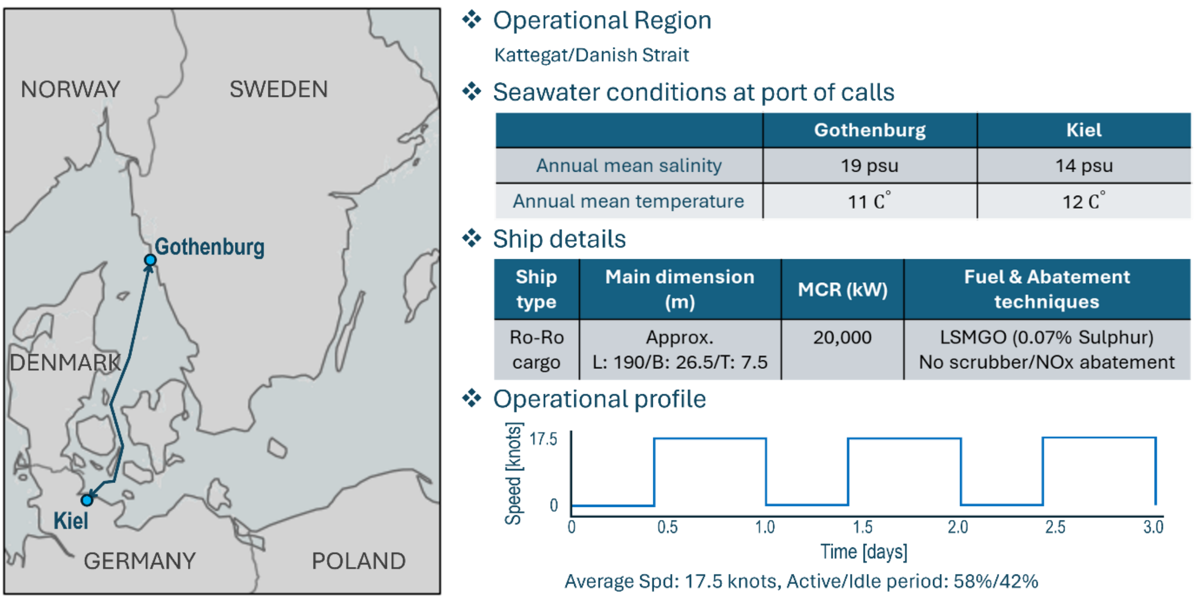

Fig.3: Overview of ship operations in the Kattegat/Danish Strait used in case study

3.2. Hull maintenance scenarios

This study assumes that the ship selected in Section 3.1 operates the corresponding route for 10 years and employs HullMASTER to examine the variations in costs that arise from different hull maintenance scenarios. As shown in Table I, a total of 93 hull maintenance scenarios were considered, encompassing several factors such as coating type, dry docking period, and in-water hull cleaning method and frequency.

The scenarios cover three distinct categories of coatings that are frequently used on commercial ships: copper-based anti-fouling coatings, non-biocide foul-release coatings, and inert abrasion-resistant coatings. In all scenarios, it is assumed that the initial state of the hull is completely sandblasted and a new coating is applied. Then, during the 10-year ship operation period, it is assumed that the ship's hull surface will undergo spot-blasting and touch-up coating at the dry dock, as per the provided scenario.

The frequency of in-water hull cleaning is classified into three situations: no cleaning applied, 1-3 cleanings occurring per year, and cleaning triggered whenever the hull condition reaches certain conditions. The criteria for the cleaning trigger are when the upper limit of the confidence interval of the fouling rating grade reaches the NSTM 40 (the minimum level of hard fouling) or when it reaches the user-defined propulsion power penalty. Cleaning methods are divided into two categories according to intensity: gentle cleaning for soft-moderate fouling and more aggressive cleaning mainly for removing calcareous fouling. It is accompanied by negligible paint wear, moderate wear, and high-level wear, depending on the cleaning methods. These in-water hull cleaning scenarios are limited to copper-based anti-fouling coatings and inert coatings, and silicone foul-release coatings are not included because of their distinctive self-cleaning properties and smooth surfaces that resist fouling.

Table I: Hull maintenance scenarios used in the study (total 93 scenarios)

Coating type	Hull surface treatment in dry dock (Initial/Subsequent)	Dry docking interval (years)	In-water hull cleaning (IWHC) frequency	Cleaning intensity	Total number of scenarios
Inert abrasion-resistant coating	Full blasting with new coating/Spot blasting with touch-up coating	2/2.5/3.3	No IWHC	-	45 scenarios for each coating
			IWHC 1~3 times/year	Gentle cleaning (negligible or moderate paint wear) /Aggressive cleaning (high paint wear)	
Biocidal antifouling coating (copper-based)			IWHC trigger option Trigger I: NSTM FR 40 Trigger II: Power penalty 20/30/40/50%	Gentle cleaning (moderate paint wear)	
Biocide-free foul-release coating (silicone-based)	Full blasting with new coating/Spot blasting with touch-up coating	2/2.5/3.3	No IWHC	-	3 scenarios, assuming no IWHC event

4. Discussion

4.1. Cost-benefit analysis of hull maintenance scenarios

Fig.4 illustrates the results of simulating a 10-year operating scenario of a ship with 93 different hull maintenance strategies using HullMASTER. The x- and y-axes in the figure represent increased operational and socio-environmental costs due to biofouling and hull maintenance compared to hydraulically smooth hull surfaces, respectively. The arrows marked on the histogram show the best and worst cases in terms of cost for each type of coating. These graphs show the overall trend through the cost distribution between scenarios, and it should be noted that the absolute costs can vary depending on various factors constituting the cost and their definitions.
As can be seen from the distribution of scatters in the figure, there is a substantial cost difference

depending on the hull maintenance scenario for the same route and vessel. For instance, within the set of 93 scenarios, the operator's expenses and socio-environmental damage costs can differ by up to 6 and 7.2 times, respectively, depending on the specific coating employed and hull maintenance method applied. Out of the coating types examined, foul-release coatings typically show lower increments in both operational costs and socio-environmental costs. Although copper coatings have a significant environmental impact compared to other non-biocidal coatings, they can be considered a cost-effective choice due to their substantial ability to reduce ship biofouling. Conversely, inert coatings show the largest deviation in operator and socio-environmental costs among the three coatings, depending on the hull management scenario.

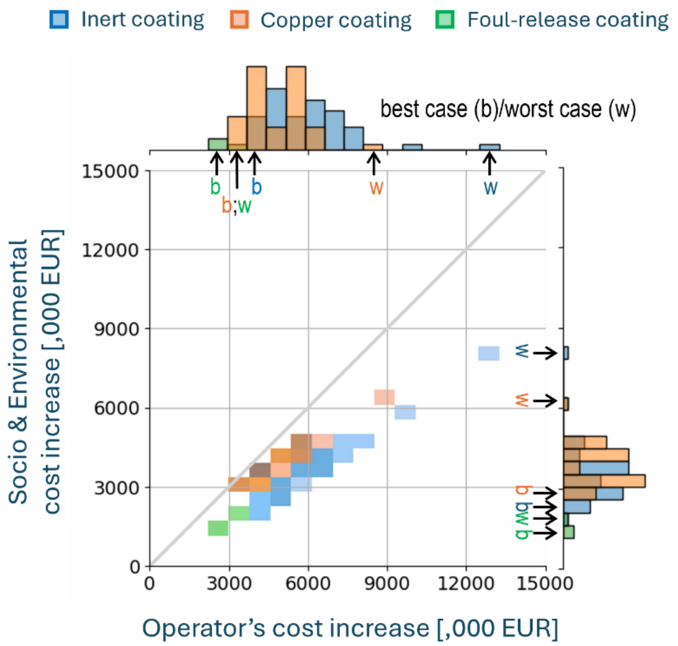

Fig.4: Distribution of increased operational and socio-environmental costs due to biofouling and hull maintenance in comparison to a hydraulically smooth hull surface of all scenarios

Fig.5 presents a comprehensive analysis of the highest (worst case) and lowest (best case) cost increments for each coating category, based on the 93 distinct scenarios depicted in Fig.4. The table below the picture displays the selected hull maintenance scenarios. Based on the findings of the cost-benefit analysis conducted in the Kattegat and Danish Strait, the additional expenses incurred from fuel penalties far exceed those from hull maintenance, including treatment and cleaning, in all types of coatings. The largest portion of socio-environmental cost increase is due to damage costs to human health, followed by climate change. However, when it comes to copper coatings, unlike other coatings that do not have biocidal properties, the expense of marine ecotoxicity damage caused by the release of biocides from the paint into the sea is taking a substantial part.

The most significant increase in operational and socio-environmental costs, when compared to a hydrodynamically smooth hull, arises from the neglect of underwater hull cleaning and infrequent dry dock maintenance. Looking at the most cost-effective scenarios analyzed, inert and copper coatings have the same dry dock interval of 3.3 years, during which in-water hull cleaning is performed 27 and 19 times during the simulated period, respectively. This demonstrates that keeping the hull roughness below a certain level leads to substantial reductions in fuel expenses for the operator, as well as damage cost reductions in terms of climate change and human health damage from a socio-environmental standpoint, when compared to the expense of hull maintenance. Nevertheless, when it comes to biocidal coatings, the release of higher amounts of anti-fouling substances during and after cleaning the hull can escalate the expenses associated with the damage caused to marine organisms. Therefore, it is preferable to conduct hull cleaning at suitable intervals, taking into account different socio-environmental consequences. Conversely, in the case of foul-release coatings, it is shown that reducing the dry dock interval is a more economically efficient option, assuming that in-water hull cleaning is not carried out.

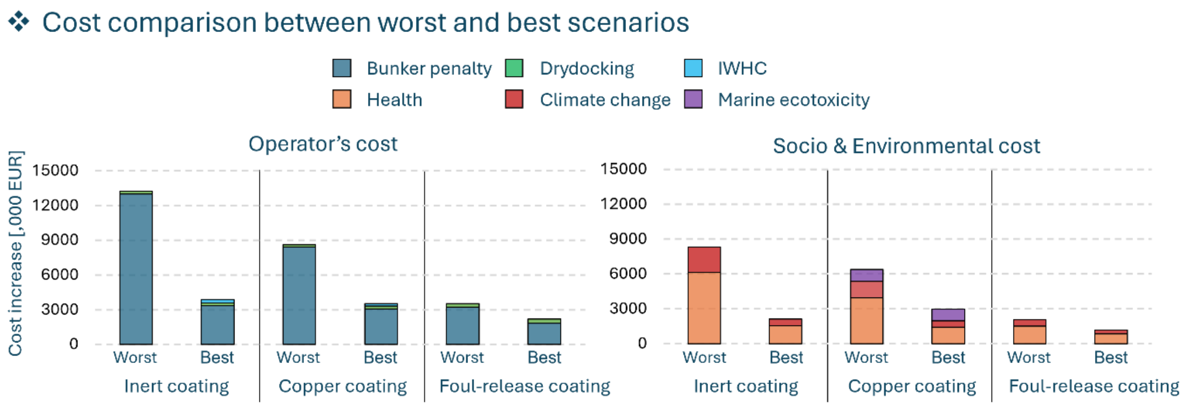

❖ Details of hull maintenance scenarios (worst → best)

	Inert coating	Copper coating	Foul-release coating
Hull maintenance scenarios	IWHC: 0 → 27 times in 10 years (gentle cleaning) DD interval: 3.3 yrs	IWHC: 0 → 19 times in 10 years (gentle cleaning) DD interval: 3.3 yrs	IWHC: No cleaning DD interval: 3.3 → 2.0 yrs

Fig.5: Comparison of cost increase between best and worst scenarios by coating type and corresponding hull maintenance scenarios

In our case study, despite its high paint application cost, the non-biocide foul-release coating emerged as the most sustainable option among the evaluated coating types. This is due to its effective anti-fouling properties, resulting in reduced emissions and minimized impact on human health while preventing the release of biocides, hence minimizing damage to the marine environment. Nevertheless, in regions that are covered by ice during the winter, including some regions adjacent to the Kattegat and Danish Strait, the silicone-based foul-release coating may not be appropriate because of its susceptibility to mechanical damage. In such cases, an abrasion-resistant coating may serve as an appropriate alternative. Copper coatings are widely utilized in both commercial ships and leisure boats globally, as they offer significant benefits in efficiently preventing the accumulation of organisms on the hull and are relatively easy to manage. However, they pose environmental risks due to the discharge of toxic substances and can potentially damage marine life and ecosystems. Hence, it is imperative to implement measures to curb the excessive utilization of biocides in anti-fouling coatings and to regulate the discharge concentration and rate of biocides to ensure sustainable operation. These efforts can enhance the responsibility of ship owners and make a substantial contribution to the protection of the marine environment.

4.2 Difference in operator's costs: Short vs Long-term hull maintenance strategies

Fig.6 presents a comparison of the cumulative operator's costs over time in the worst and best scenarios for the three different types of coatings. For inert coatings, the operational expenses in the best scenario, which includes cleaning, and the worst scenario, which excludes cleaning, are nearly identical for approximately one year following the initial coating application. This implies that the cost-effectiveness of hull cleaning in terms of fuel consumption reduction is not considerable during this period. However, beyond this timeframe, the cost savings achieved through hull cleaning become increasingly apparent in comparison to the expenses associated with hull management. In the case of copper-based anti-fouling coatings, the cost trends remain the same in both the worst and best scenarios for up to 2 years after the initial coating application. This is due to the fact that the NSTM fouling grade of the hull remains consistently below 20 throughout this time period, thus no in-water cleaning procedure is carried out. For silicone-based foul-release coatings, the cost difference becomes apparent as hull treatments progress and more dry dock events accumulate.

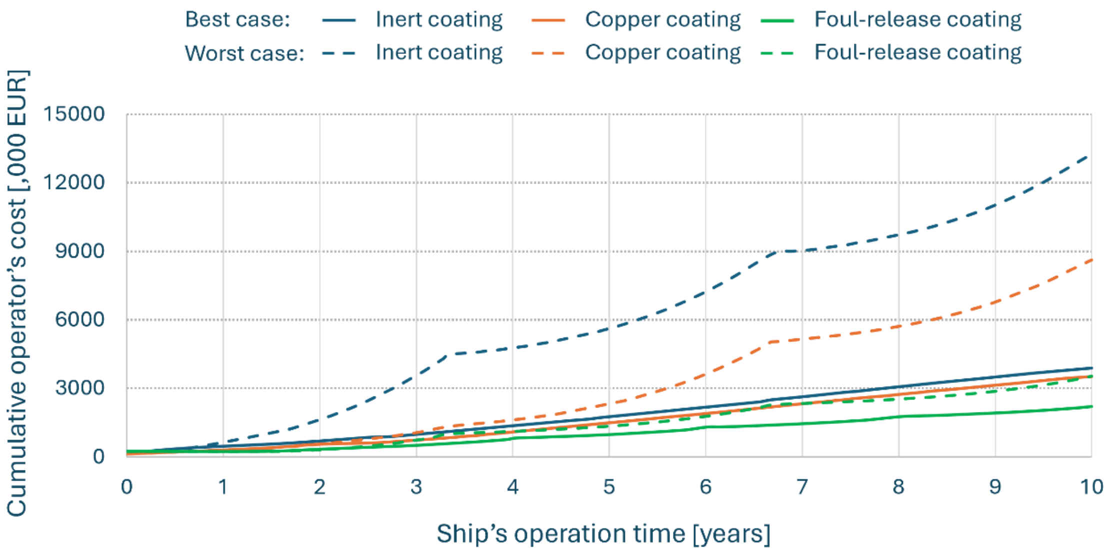

Fig.6: Cumulative operator's costs over time for best and worst scenarios

These findings indicate that the evaluation of the expenses associated with a hull maintenance strategy can vary depending on whether it is considered a short-term or long-term plan. Although there are slight differences depending on the type of coating, in the initial stages, it is difficult for the operator to clearly perceive the effects of hull maintenance. However, as time passes, the cost difference due to maintenance becomes increasingly apparent. In particular, it is important for ship owners to consider this point and establish sustainable long-term plans.

5. Uncertainty factors in cost-benefit analysis

The utilization of HullMASTER and scenario studies in this research involves several limitations and assumptions, which may introduce uncertainties into the cost-benefit analysis outcomes. The efficacy of the coatings used in this study is based on field experiments conducted under idle conditions for approximately one year, considering seawater salinity as a crucial factor affecting biofouling growth and biocide release. It was assumed that periods and seawater conditions other than measured values could be estimated through interpolation and extrapolation. However, the model's sensitivity to the effects and interactions of other factors such as seawater temperature, pH, and lighting conditions at the berthing port may induce additional uncertainty. Not only that, silicone-based foul-release coatings, which remove marine organisms attached to the hull when the ship moves at a certain speed, may have been somewhat conservatively evaluated in this study.

This study did not consider the costs associated with the risk of introducing non-indigenous species due to hull maintenance. However, the operation of ships in the examined region and the transition of ships from outside waters can make it easier for these species to be introduced and spread. Implementing effective hull management measures may reduce the likelihood of non-native species introductions. Furthermore, it was assumed that no distinct wastewater treatment was conducted following in-water hull cleaning in our case studies, leaving room for further review of the potential to reduce toxic substance release from paint particles through a capture system.

The fluctuation in fuel prices, which varies based on the kind of fuel, might introduce uncertainty in the cost analysis results during the life cycle analysis. This study conducted a cost-benefit analysis using the mean LSMGO price from 2020 to 2023, but the range of fuel costs over this period varied by up to five times. Considering that bunker penalties incurred due to hull roughness contribute the most to operational costs, any fluctuations in fuel prices might have a substantial impact on the chosen hull maintenance strategy for the ship.

6. Conclusion

This study employed HullMASTER, a decision-support tool for ship maintenance strategies, to perform a comprehensive cost-benefit analysis of various hull scenarios on the Kattegat and Danish Strait routes. The analysis shows significant differences in increased operating and socio-environmental costs due to biofouling and hull maintenance compared to hydraulically smooth hulls, even on the same ship and route (up to 6 times for operational costs and 7.2 times for socio-environmental costs). It was found that preventing hull roughness increases through hull treatment and in-water hull cleaning at appropriate intervals can reduce bunker penalties and socio-environmental damages such as climate change, human impacts, and ecotoxicity. Out of the three coating types examined, non-biocide foul-release coatings were determined to be the best sustainable choice for the Kattegat and Danish Strait routes. These coatings achieve sustainability by decreasing exhaust gas emissions and limiting the discharge of biocidal pollutants into the ocean.

Moreover, there was a substantial disparity in expenses between the short-term and long-term periods as a result of hull maintenance. Although the cost-effectiveness of hull maintenance may not be immediately apparent, the disparities have become increasingly evident with time. These findings highlight the significance of hull maintenance for ship operators and indicate the necessity of developing sustainable, long-term strategies. Nevertheless, this study is a case study conducted only in the Kattegat-Danish Strait route. The outcomes of the cost-benefit analysis may differ based on factors such as ship characteristics, operational profiles, and operating locations. Future studies will necessitate extensive cost-benefit analysis that considers more diverse factors and a wider range of ship operating conditions and areas.

Acknowledgement

The project HÅLL2 – Demonstration of sustainable ship hull maintenance strategies (2022-2024) is funded by Lighthouse Swedish Maritime Competence Centre under the “Hållbar sjöfart” program.

References

EARLEY, P.J.; SWOPE, B.L., BARBEAU, K.; BUNDY, R.; McDONALD, J.A.; RIVERA-DUARTE, I. (2014), *Life cycle contributions of copper from vessel painting and maintenance activities*, Biofouling 30(1), pp.51-68

GRANHAG, L.; JAVADI, M.; YTREBERG, E. (2023), *Best practice for cleaning of ship hulls*, Report for Swedish Agency for Marine and Water Management (SWAM), https://research.chalmers.se/publication/535739/file/535739_Fulltext.pdf

GRANVILLE, P.S. (1987), *Three indirect methods for the drag characterization of arbitrarily rough surfaces on flat plates*, J. Ship Research, 31(1)

KIM, K.J.; LEER-ANDERSEN, M.; WERNER, S. (2022), *A study on the effect of hull surface treatments on ship performances*, 9th Conf. Computational Methods in Marine Engineering

LAGERSTRÖM, M.; LINDGREN, J.F.; HOLMQVIST, A.; DAHLSTRÖM, M.; YTREBERG, E. (2018), *In situ release rates of Cu and Zn from commercial antifouling paints at different salinities*, Marine Pollution Bulletin 127, pp.289-296

LAGERSTRÖM, M.; YTREBERG, E.; WIKLUND, A.K.E.; GRANHAG, L. (2020), *Antifouling paints leach copper in excess–study of metal release rates and efficacy along a salinity gradient*, Water Research 186

LAGERSTRÖM, M.; WRANGE, A.L.; OLIVEIRA, D.R.; GRANHAG, L.; LARSSON, A.I.; YTREBERG, E. (2022), *Are silicone foul-release coatings a viable and environmentally sustainable* *alternative to biocidal antifouling coatings in the Baltic Sea region?*, Marine Pollution Bulletin 184

MORRISEY, D.; GADD, J.; PAGE, M.; LEWIS, J.; BELL, A.; GEORGIADES, E. (2013), *In-water Cleaning of Vessels: Biosecurity and Chemical Contamination Risks*, MPI Technical Paper, 2013/11, Biosecurity 267, Wellington

OLIVEIRA, D.R.; GRANHAG, L. (2020), *Ship hull in-water cleaning and its effects on fouling-control coatings*, Biofouling, 36(3), pp.332-350.

OLIVEIRA, D.R.; LAGERSTRÖM, M.; GRANHAG, L.; WERNER, S.; LARSSON, A.I.; YTREBERG, E. (2022), *A novel tool for cost and emission reduction related to ship underwater hull maintenance*, J. Cleaner Production 356

SCHULTZ, M.P. (2007), *Effects of coating roughness and biofouling on ship resistance and powering*, Biofouling 23(5), pp.331-341

SOON, Z.Y.; JUNG, J.H.; LOH, A.; YOON, C.; SHIN, D.; KIM, M. (2021), *Seawater contamination associated with in-water cleaning of ship hulls and the potential risk to the marine environment*, Marine Pollution Bulletin 171

TRIBOU, M.; SWAIN, G. (2017), *The effects of grooming on a copper ablative coating: a six year study*, Biofouling 33(6), pp.494-504

US NAVY (2006), *Waterborne underwater hull cleaning of navy ships*, Naval Ships' Technical Manuals

UZUN, D.; DEMIREL, Y.K.; CORADDU, A.; TURAN, O. (2019), *Time-dependent biofouling growth model for predicting the effects of biofouling on ship resistance and powering*, Ocean Engineering 191

VALKIRS, A.O.; SELIGMAN, P.F.; HASLBECK, E.; CASO, J.S. (2003), *Measurement of copper release rates from antifouling paint under laboratory and in situ conditions: implications for loading estimation to marine water bodies*, Marine Pollution Bulletin 46(6), pp.763-779

WRANGE, A.L.; BARBOZA, F.R.; FERREIRA, J.; ERIKSSON-WIKLUND, A.K.; YTREBERG, E.; JONSSON, P.R.; ...; DAHLSTRÖM, M. (2020), *Monitoring biofouling as a management tool for reducing toxic antifouling practices in the Baltic Sea*, J. Environmental Management 264

YTREBERG, E.; ÅSTRÖM, S.; FRIDELL, E. (2021), *Valuating environmental impacts from ship emissions–The marine perspective*, J. Environmental Management 282

YTREBERG, E.; HANSSON, K.; HERMANSSON, A.L.; PARSMO, R.; LAGERSTRÖM, M.; JALKANEN, J.P.; HASSELLÖV, I.M. (2022), *Metal and PAH loads from ships and boats, relative other sources, in the Baltic Sea*, Marine Pollution Bulletin 182

What Did We Learn from the Ship Scale Blind CFD Validation Exercise?

Dmitriy Ponkratov, Siemens Digital Industries Software, London/UK,
Dmitry.Ponkratov@siemens.com

Abstract

CFD (Computational Fluid Dynamics) made its way into the maritime community a few decades ago and has since become an integral part of it. Nowadays, thousands of calculations are conducted globally to design new hulls, optimise propellers, and estimate ships' energy efficiency. Obviously, numerical methods should be validated before one fully relies on them. Nevertheless, validation against well-known cases has a negative side as a code user can tune parameters to achieve the desired results. Within the global JoRes research project, a series of blind ship scale validation cases were introduced: the participants were provided with the geometry files and sea trials conditions but not the results. The main findings of this exercise for a tanker case are summarised and discussed within the paper.

1. Introduction

In July 2023 the International Maritime Organization adopted a new strategy aiming to reduce Greenhouse Gas emissions from the global shipping to zero by or around 2050, *IMO (2023)*. In September 2023 DNV released the 2050 forecast (DNV, 2023) showing that the initial and important stage of the zero-emission challenge relies on the ship's energy efficiency. The digitalisation of the global maritime industry should help to address this objective. Computational Fluid Dynamics (CFD) has been actively used for ship design for a few decades, however, in the past, the main focus was model scale simulations. There were two main reasons for that: 1. The computational power did not allow practitioners to build and run a ship-scale case within an acceptable time for practical engineering tasks. 2. The validation cases were mainly available in model scale (KCS, KVLCC2 etc).

The development in computational power has successfully addressed the first challenge, and pioneering ship-scale validated calculations appeared in the industry about 10 years ago, *Ponkratov and Zegos (2014,2015)*. Nevertheless, these works had a few challenges. For the MR tanker case used for the validation, the hull roughness measurements were not performed. Moreover, the sea trials were not post-processed according to the ISO15016 standard and only integral characteristics (rpm, torque and thrust) were measured and compared. In addition to that the authors knew the sea trials results when they performed CFD calculations, so it was not a blind validation exercise.

The second challenge of the publicly available ship-scale validation case was not addressed for a long time until Lloyd's Register (LR) organised the first workshop on ship-scale computer simulations, *Ponkratov (2017)*. However, the MV "Regal", introduced at the LR CFD workshop, also did not have hull and propeller roughness measurements. The participants of that workshop were asked to simulate the roughness according to their internal working procedures and make necessary assumptions. As a result, it introduces some uncertainties. Fig.1 shows the main results of that workshop. As always sea trials have an uncertainty band (orange) due to sea state measurements, G-modulus etc. A significant scatter of submitted CFD results (green dots) can also be noted which resulted in a thick band of CFD results. The general trend showed that CFD mainly underpredicted the sea trials values.

In the impressive master theses by *Mikkelsen and Steffensen (2016)* the validation was performed against four sets of sisterships' sea trials. Nevertheless, the authors outlined the uncertainties related to the fact that the simulations have been performed with the stock propeller instead of the actual propeller (the designer did not permit to use of the actual propeller geometry) and the fact that air resistance, bilge keel resistance and hull roughness resistance were calculated using the ITTC procedure instead of being modelled in CFD.

Niklas and Pruszko (2019) performed CFD validations for the "Nawigator XXI" research and training vessel. It is a very detailed and deep work, however, the authors did not discuss the uncertainty related to the propeller pitch angles as it is usually quite difficult to ensure the correct pitch angle position at the trials. Moreover, it is understood the hull roughness was also not measured before the trials, so the authors assumed the equivalent sand grain roughness, Ks, to be equal to 150 µm.

Sun et al. (2020) performed CFD ship scale validation based on sea trials results for 9 bulk carriers with the same hull form, propeller, and rudder. As the roughness effect was not the focus of their article, they used the Bowden–Davison empirical formula to avoid introducing more complicated uncertainty sources to CFD simulation. It is understood they used a Ks value of 90 µm.

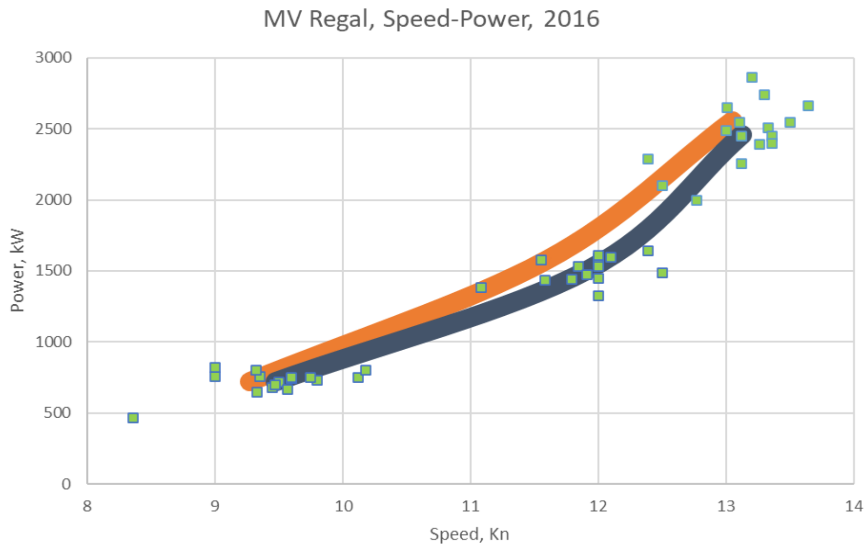

Fig.1: Results of the Lloyds Register CFD workshop, 2016 (orange band – sea trials including uncertainty, blue band – mean CFD results including uncertainty, Green dots – individual CFD results submitted by participants).

Orych et al (2021) considered for their validation study a set of sea trials for 12 single screw vessels. They assumed the Average Hull Roughness (AHR) to be 100 µm. With the employed Aupoix-Colebrook roughness model (AHR/Ks = 5) it gives the equivalent sand grain roughness Ks value of 20 µm. The propeller roughness was assumed to be 30 µm.

Mikulec and Piehl (2023) performed ship-scale CFD validation on a 34m Research Vessel "Gunnerus". The assumed equivalent sand-grain roughness Ks value was 30 µm. Unfortunately, this vessel is equipped with two azimuth thrusters, so there was a challenge with measurements of propeller power as strain gauges could not be installed inside the housing.

As it can be seen, various assumptions can be made about the hull roughness and other parameters and these assumptions can significantly affect the CFD results. The main challenge is associated with the fact that sea trials procedures (like ISO15016) were not developed for CFD validation. The main objective of these procedures is to confirm contractual speed. As a result, these procedures do not require hull and propeller roughness measurements (which are important for CFD) and still rely on simplified methods (sea state assessment by the naked eye, visual observations of vessel draughts etc). Clearly to develop an accurate case for CFD validation stricter requirements for the ship scale measurements should be implemented.

These expectations led to organising and executing a JoRes joint research project aiming to develop an industry-recognised benchmark for ship-scale CFD validation. As discussed in *Ponkratov (2023),* 6 vessels were considered within the project. For all of them, comprehensive ship scale measurements were performed including actual hull and propeller roughness investigations. For one of the vessels (JoRes1 tanker) ship scale PIV measurements of the propeller flow were also performed.

The tanker case was the main one for CFD validation and a few internal blind workshops were performed with the project.

2. JoRes1 tanker ship scale measurements

The following activities took place before the actual sea trials: the hull and propeller roughness measurements were performed in the dry dock, strain gauges were installed on the propeller shaft to measure propeller torque, the optical sensor was installed next to the shaft to measure the propeller shaft speed, anemometers were installed on the antenna mast to get wind characteristics, etc. Most importantly the FlowPike - a specially developed unit for ship scale PIV (Particle Image Velocimetry) measurements was installed, *Ponkratov et al. (2022)*. The Average Hull Roughness (AHR) of the hull was measured in the dry dock and the value was 218 µm.

The sea trials were conducted according to the ISO15016:2015 standard. Before the trials, the vessel was stopped at sea to deploy the wave buoy, record vessel draughts and measure water properties. After the trials, the vessel was stopped again to record vessel draughts and repeat water properties measurements. The trials were performed at four shaft speeds (60, 75, 90 and 96 RPM). Normally, the ISO standard requires conducting 2 runs for each RPM setting (minimum of 10 min each), however, as it was expected that 10 min would not be enough for sufficient PIV measurements, the decision was made to make the duration of each run 40 min. Moreover, for 75 and 90 RPM settings, 4 runs were performed, resulting in a total of 12 performed runs.

The main part of the PIV measurements was done at two speeds (75 and 90 RPM). Additionally, PIV measurements were done at a third speed (96 RPM), where a limited program could be executed. All the details of the PIV setup are reported in *Birvalski et al. (2023).*

Despite all the effort to perform sea trials as accurately as possible it is practically impossible to achieve zero uncertainty. As discussed in *Ponkratov and Strujik (2023)*, the sea trials uncertainty level for this case was 4-6%.

3. Blind workshop organisation

After the sea trials completion, the project moved to the next phase – blind workshop organisation. For the execution of this phase, the two main parts had to be prepared – geometry files and simulation conditions.

As the key idea of the project is to numerically simulate exactly the same condition as during the actual sea trials, it was critically important to make sure the CFD geometry accurately replicates the vessel geometry.

As the shipyard and hull designer supported the JoRes project they provided the organisers with the "as-designed" hull. Nevertheless, consideration should be given whether the actual hull is exactly the same as the designed one, as during the construction phase some minor alterations could be introduced. Moreover, the vessel was in service for 5 years and hull deformations or minor damages could have happened. To address this uncertainty a decision was made to perform 3D laser scanning while the vessel was in the dry-dock before the trials. This work would also be important to accurately capture the exact location of the PIV unit installed at the dry dock. As the unit installation was done on the very last day of dry-docking (after the final layer of paint was applied) the 3D laser scan of the stern area had to be performed the night before undocking. The bow and middle section area was successfully scanned before that.

As a result, a comprehensive 3D scan data of the hull and all appendages was obtained. The next phase was to develop the 3D geometry for CFD simulations. The experts from Teignbridge Propellers put together the "as designed" and scan geometry and concluded that the deviation between the two files is minor so it was safe to proceed with the "as designed" hull, Fig.2. The only changes were performed in the stern area where a skeg and casting were added based on the drawings, photographs and 3D scan data.

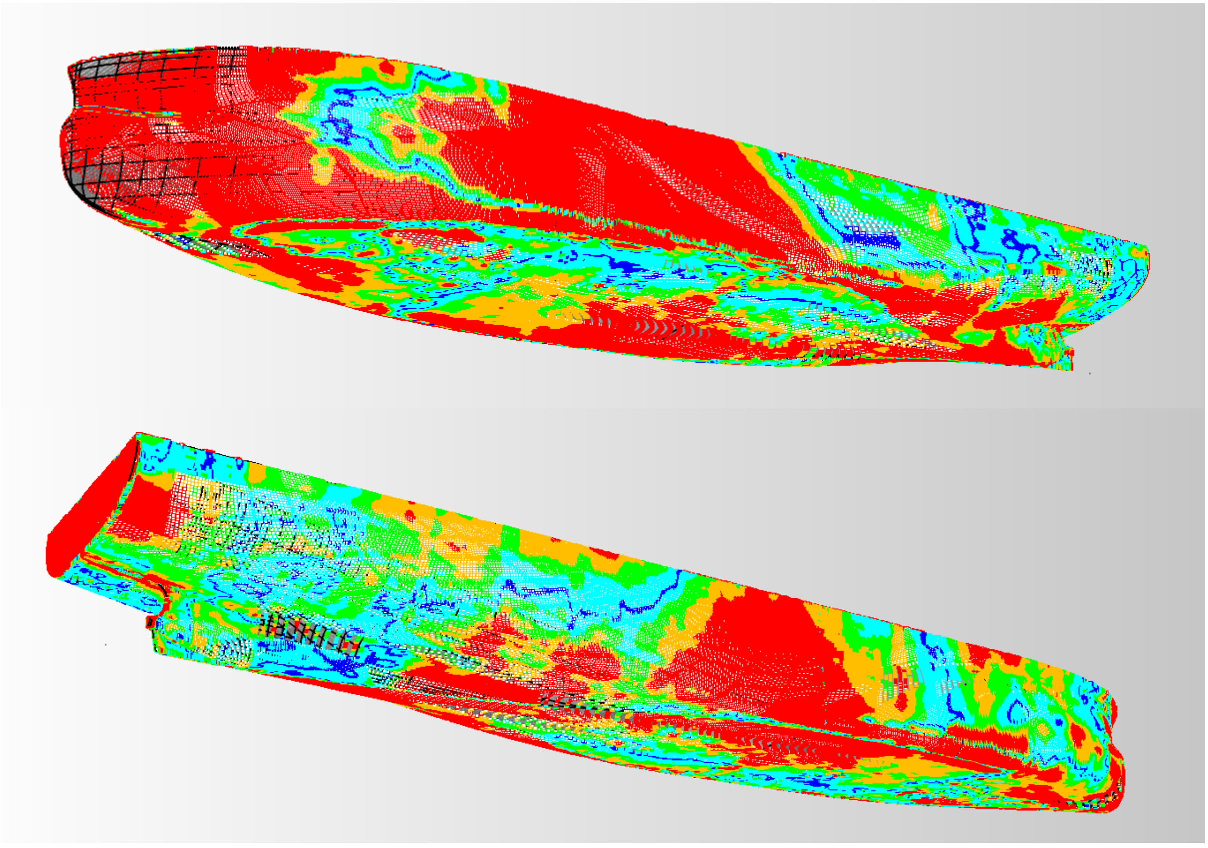

Fig.2: Overlaying the “as-designed” hull geometry and 3D laser scan (373,448 points, mean deviation 20.9 mm, median deviation 14.99 mm, standard deviation 19.48 mm)

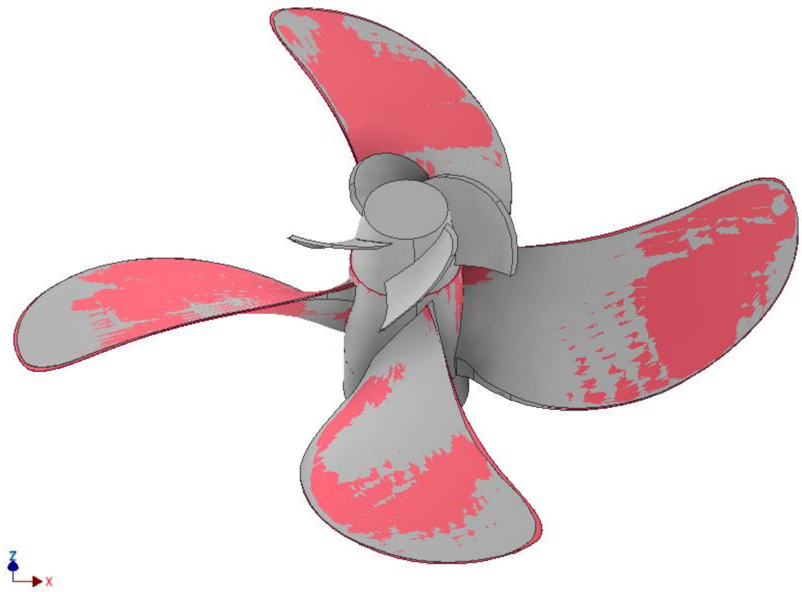

Fig.3: Overlaying the “as-designed” propeller geometry (red) and 3D laser scan (grey)

The “as designed” propeller geometry model was also supplied by the design company and a similar match and compare job was performed for the propeller, Fig.3. Some minor modifications of the propeller trip region were performed by Teignbridge Propeller to make the CFD geometry as realistic as possible. The key challenge of geometry preparation was faced for the Propeller Boss Cap Fins

(PBCF). The designer did not permit to use of this geometry, so the PBCF were redesigned to have a non-competitive representation. Obviously, it introduces the uncertainty however it is believed the efficiency change between the newly designed PBCF and the original would be minor.

Additionally, weld seams assessment was conducted and shell plate expansion drawings, anodic protection drawings, and bulge keel drawings were collected. However, these details weren't included in the 3D geometry files now, they can be incorporated if needed in the future. Nevertheless, a simplified PIV unit geometry was added to the 3D geometry as it is located upstream of the propeller and the vorticity developed from the unit may affect the propeller wake, Fig.4.

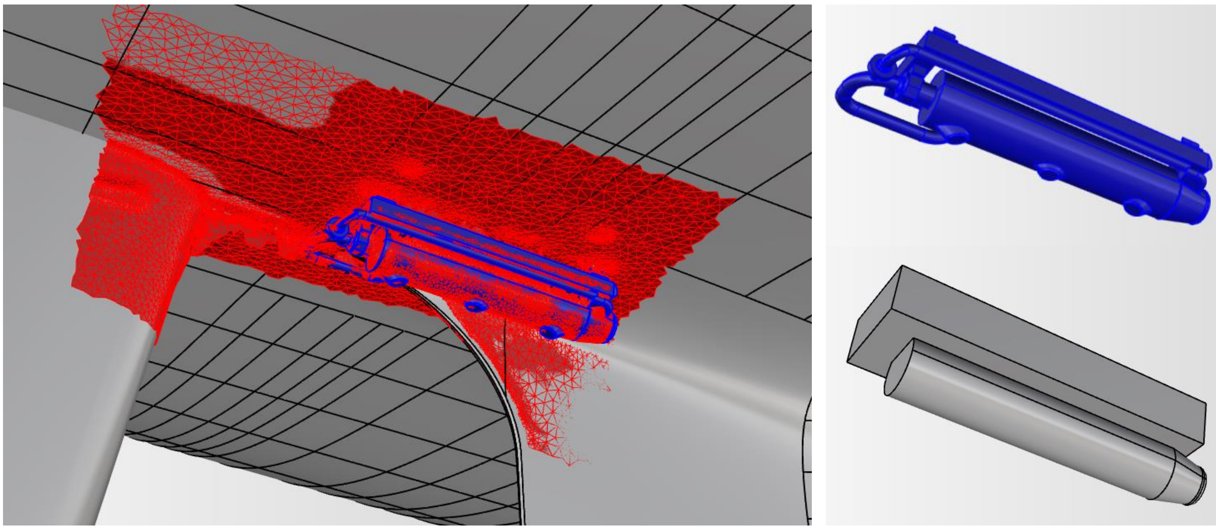

Fig.4: Finding the exact location of the PIV unit based on 3D scan data (left) and simplification of the unit geometry for CFD simulation (right)

As mentioned before the hull and propeller roughness was measured when the vessel was in the dry-dock before the trials. The measured values correspond to the Average Hull Roughness (AHR) which cannot be simulated directly in CFD. The conversion to the equivalent sand grain roughness is required. The recent investigations, *Schultz and Hutchins (2021), Hutchins et al. (2023)*, suggested the power mean method which was implemented for the JoRes1 tanker case. According to this method, the AHR for the hull of 218 µm gives the sand grain roughness equivalent Ks of 53 µm.

The propeller roughness was measured and estimated to be 4 µm. All the detailed reports showing the measurement values and postprocessing details will be publicly available within the JoRes project benchmark in 2024.

Apart from the geometry, the following conditions had also been defined based on the sea trials reports: vessel draughts, water density and viscosity, air density and viscosity, and vessel speeds.

To make the simulations blind the results of sea trials were not shared with the participants. Only geometry files, environmental conditions and vessel speeds were provided. The participants were asked to use their best practice techniques to calculate propeller torque and rpm which could be compared with the trial results later. The participants were asked to use the same turbulence model (k-w SST) and the suggested computational domain dimensions. The simulation recommendations were different compared to the LR Workshop 2016. In that workshop, participants were asked to keep constant rpm (same as at the trials) and determine vessel speed and power. In general, for CFD simulations it is easier to keep the vessel speed and adjust the RPM to achieve the self-propulsion point. For this reason, for the JoRes workshop, the vessel speed was given, and participants were asked to determine RPM and power.

4. Workshop results discussion

On average about 10 sets of results were submitted by participants for each speed. Figs.5 and 6 show the speed-power and speed-RPM results.

It should be highlighted that the actual results cannot be published before the end of 2024, so the figures do not have the scale, however, it is important to see the relative difference between measured and calculated power and rpm (at given speeds). Similarly, to LR Workshop 2016, it can be seen that the power predicted by CFD is generally lower than the sea trials. The blue band is an average of all submitted CFD results with the thickness of the band corresponding to the uncertainty level (standard deviation). As can be seen in the figures, some participants (green dots) were very close to the results measured at the trials. So, the scatter of the results and thickness of the band were caused by those participants who did not predict the sea trials conditions well.

Fig.5: Results of the JoRes workshop, 2023, Speed-Power, (orange band – sea trials including uncertainty, blue band – mean CFD results including uncertainty, Green dots – individual CFD results submitted by participants)

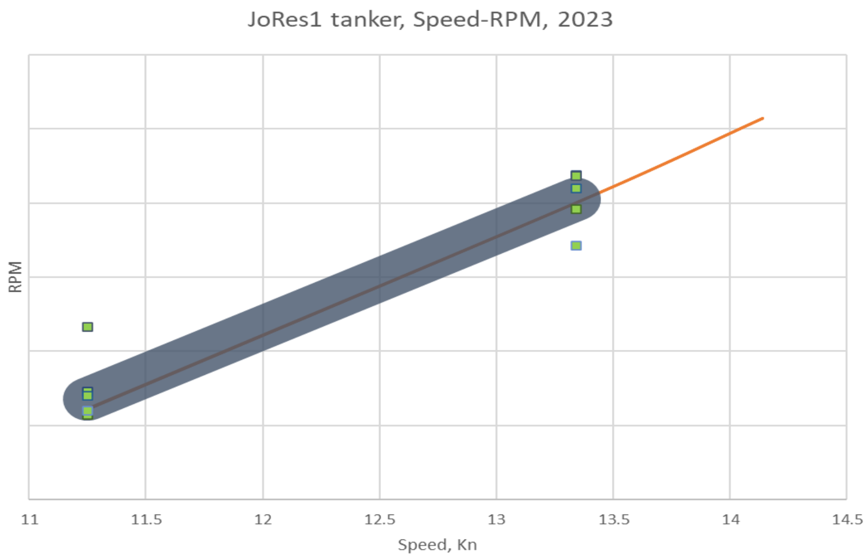

Fig.6: Results of the JoRes workshop, 2023, Speed-RPM, (colours as in Fig.5)

As discussed and analysed during the workshop there are a few explanations for this:

1. Errors while submitting results. Despite providing the participants with well-defined templates some submissions had noticeable errors. For example, the total force components on the hull (resistance) were not in equilibrium with the forces on the propeller blades (thrust).
2. Some participants did not converge the simulation cases and stopped the runs earlier than needed. To address this challenge and make sure the runs are converged, the participants were asked to submit a screenshot of the convergence plot.
3. Some participants made a mistake in submitting the hydrostatic component of the forces. Once the hull is cut in pieces the integration of the submerged surface becomes not straightforward and extra attention should be paid to consider the hydrostatic component correctly.
4. The actual CFD geometry did not have bilge keels and superstructure, so the added resistance of these components was calculated empirically and taken into account in CFD runs. The same values were provided to all the participants to reduce the uncertainty.
5. In general, the standard deviation of numerical results is within ±3%. There is no CFD code dependency – reasonable results were achieved using various codes. The number of cells varied in the diapason from 10M to 53M cells.

In general, it is believed that the results are encouraging – if participants follow the recommended practice and pay attention to converge, force equilibrium and correct representation of hydrostatic components, the results will be close to the trials. Another observation is that even with the current CFD results the uncertainty level of submitted results is pretty much the same as the sea trials.

Moreover, there has been a clear development in the industry since the LR Workshop 2016. Comparing Fig.1 and Fig.2 the scatter of CFD results getting less and the mean CFD band getting closer to the sea trials one. It is also important to note that new recommendations (for example related to hull roughness simulations) have been introduced after the LR workshop. Now a few working groups within the JoRes project focus on other ship-scale cases which should further improve the best practices and consequently the quality of results.

5. Conclusions

Even though CFD has been around in the industry for a few decades, sometimes there is still limited trust and concerns about the widespread of CFD. The key argument of the discussion is that CFD is a "rubbish in, rubbish out" black box and the results can be easily tuned to get desired figures (and especially colourful images). Nevertheless, it is believed the numerical methods matured over time and relevant best practices were introduced and adopted by CFD practitioners. That is why the blind simulations where the CFD participants do not know the final results are particularly important to make a status check of CFD predictions. Within the JoRes project a few workshops were run to perform these checks. One of them was the 50,000 dwt tanker and the results of that internal workshop are reported here. The standard deviation of submitted results is about 3% and the uncertainty spread is pretty much in line with the uncertainty reported by sea trials of 3-6%. Those CFD practitioners who followed the general recommendations and ensured the quality of their submissions got results agreeing well with the sea trials measurements.

References

BIRVALSKI, M.; STRUIJK, G.D.; PONKRATOV, D. (2023), *Full-scale PIV measurements of the propeller inflow*, 15^{th} Int. Symp. Particle Image Velocimetry – ISPIV 2023, San Diego

DNV (2023), *Maritime Forecast to 2050, Energy Transition Outlook*, DNV

HUTCHINS, N.; GANAPATHISUBRAMANI, B.; SCHULTZ, M.; PULLIN, D. (2023), *Defining an equivalent homogeneous roughness length for turbulent boundary layers developing over patchy or heterogeneous surfaces*, Ocean Eng. 271

IMO (2023), *Strategy on Reduction of GHG Emissions From Ships*, Res. MEPC.377(80)

ITTC (2008), *1978 ITTC Performance prediction method*, Recommended Procedures and Guidelines, Performance, Propulsion, Int. Towing Tank Conf.

MIKKELSEN, H.; STEFFENSEN, M.L. (2016), *Full-scale validation of CFD model of a self-propelled ship*, Master thesis, Technical University of Denmark

MIKULEC, M.; PIEHL, H. (2023), *Verification and validation of CFD simulations with full-scale ship speed/power trial data*, Brodogradnja/Shipbuilding 74/1, http://dx.doi.org/10.21278/brod74103

NIKLAS, K.; PRUSZKO, H. (2019), *Full-scale CFD simulations for the determination of ship resistance as a rational, alternative method to towing tank experiments*, Ocean Eng. 190

NUUTINEN, M. (2019), *Automated self-propulsion point search algorithm for ship performance CFD simulations*, 6th Int. Symp. Marine Propulsors, Rome

ORYCH, M.; WERNER, S.; LARSSON, L. (2021), *Validation of full-scale delivered power CFD simulations*, Ocean Eng. 238

PONKRATOV, D.; ZEGOS, C. (2014), *Ship scale CFD self-propulsion simulation and its direct comparison with sea trial results*, Int. Conf. Computational and Experimental Marine Hydrodynamics, Chennai

PONKRATOV, D.; ZEGOS, C. (2015), *Validation of Ship Scale CFD Self-Propulsion Simulation by the Direct Comparison with Sea Trials Results*, 4th Int. Symp. Marine Propulsors, Austin

PONKRATOV, D. (2017), *Workshop on ship scale hydrodynamic computer simulations*, Lloyd's Register's Full-Scale Numerical Modelling Workshop

PONKRATOV, D.; STRUIJK, G.; BIRVALSKI, M.; ELBERTSEN, M. (2022), *A journey to unique PIV flow measurements at ship scale*, 7th HullPIC Conf., Tullamore

PONKRATOV, D.; STRUIJK, G. (2023), *Quantifying the Uncertainty of High-Fidelity Speed/Power Trials*, 8th HullPIC Conf., Pontignano

PONKRATOV, D. (2023), *JoRes Joint Research Project - the largest global community developing a benchmark for ship scale CFD*, 25th Numerical Towing Tank Symposium, Ericerira

SCHULTZ, M.; HUTCHINS, N. (2021), *Prediction of an effective hydraulic length scale for surfaces with heterogeneous roughness*, APS-DFD, 74th Annual Meeting, Phoenix

SUN, W.; HU, Q.; HU, S.; SU, J.; XU, J.; WEI, J.; HUANG, G. (2020), *Numerical Analysis of Full-Scale Ship Self-Propulsion Performance with Direct Comparison to Statistical Sea Trial Results*, J. Mar. Sci. Eng. 8/24

Simple Model for Data-Driven Ship Power Prediction

José Ambiel, OSE-Engineering, Paris/France, jose.ambiel@ose-engineering.fr
Christophe Leclercq, OSE-Engineering, Paris/France, christophe.leclercq@ose-engineering.fr
Michel Cochennec, Ascenz Marorka, Paris/France, michel.cochennec@ascenzmarorka.com

Abstract

In the maritime industry, optimizing ship performance is crucial for operational efficiency, fuel economy and environmental sustainability. Therefore, this paper presents a simple but efficient data-driven model for ship performance. The power shaft prediction consists in three different models: baseline, relative wind influence and arbitrary heading wave influence. Traditional semi-empirical established models often require extensive ship particulars information that are often unavailable, the proposed method does not require any particulars. The model performance is compared, using auto-logged ship data, to these established models and has its efficiency demonstrated.

1. Introduction

The global shipping industry is vital for facilitating trade across oceans, but its environmental impact, particularly greenhouse gas emissions, have been a major source of concern in this industry. It is estimated that the shipping sector has a substantial contribution to global greenhouse gas (GHG) emissions, accounting for approximately 3% of the total GHG emissions worldwide, *IMO (2021)*. Therefore, there has been a growing emphasis on developing new regulations to decrease fuel consumption, directly associated with GHG emissions. *IMO (2022)* attributes significant potential for reducing carbon emissions by optimizing ship operations. Reduction up to 10% can be achievable through voyage optimization, where accurate ship performance predictions play a crucial role.

Understanding and quantifying hull resistance is critical in ship performance analysis. Accurately assessing hull resistance presents numerous challenges due to the complex interaction between the ship's hull and the surrounding environment. Many factors such as hull shape, surface roughness, ship speed, and environmental conditions significantly impact the total resistance. Therefore, several methods have been developed to evaluate the hull resistance.

To estimate the ship power prediction in calm sea (ship's baseline), a commonly used method was developed by *Holtrop and Mennen (1982)*. It relies on regression analysis of model experiments and full-scale data from the Netherlands Ship Model Basin. Another method, introduced by *Hollenbach (1999)*, is based on model tank tests conducted for 433 ships by the Vienna Ship Model Basin between 1980 and 1995. Both methods provide a general power prediction applicable to ships at no trim and under design draught conditions. However, for more precise predictions tailored to specific ships, self-propulsion tests and resistance tests in model basins are conducted.

Models of wind resistance analyses from various laboratories with models covering a wide range of merchant ships were developed by *Isherwood (1973)* and further by *Blendermann (1994)*. More recent regression formulas based on wind tunnel test for a wide range of ship types were developed, *Fujiwara et al. (1998,2005)*, *Kitamura et al. (2017)*. The latter is recommended for the use of sea trail corrections by, *ITTC (2022)*.

For the added wave resistance on ships, one of the oldest and simplest models is the one developed by Kreitner and presented in *ITTC (2005)*, which is valid only for head waves up to 2 m. More recent semi-empirical models, like the STAWAVE-2 considers a broader range of wave height as well as wavelength influence but is valid only for wave direction between 0 and 45 degrees.

Semi-empirical methods are developed based on physics and that's make them powerful to model complex phenomenon through the introduction of parameters and at the same time being able to generalize because of their physical meaning. The wind and wave models on the literature described above were developed for a broad range of ship types, which makes them very good at predicting the added resistance in various scenarios. However, having quality data in hands thanks to Ascenz Marorka, a simple semi-empirical model can have better results. Here, we present a simple semi-empirical formulation for added resistance of wind and waves. Thanks to the auto-logged data we have, we are able to fit our model for different conditions by using a machine learning methodlogy. Finally, we compare our results with well-established semi-empirical models.

2. Ship Performance Model

The power shaft required to a ship to move through the sea at a certain speed can be described by, *Birk (2019)*:

$$\boldsymbol{P_{shaft}} = \boldsymbol{R_{total}} * \boldsymbol{V_{ship}} \tag{1}$$

where V_{ship} is the ship's log speed (speed through water) and R_{total} is the total resistance, *i.e.* external forces acting on the ship. In the present study, the total resistance R_{total} is divided in three distinct forces:

$$R_{total} = R_{baseline} + R_{wind} + R_{wave} \tag{2}$$

with $R_{baseline}$ being the forces on the hull of the ship when moving through a calm sea, R_{wind} the wind forces on the whole ship and R_{wave} the resulting wave sea forces on the hull of the ship. Therefore, the ship P_{shaft} can be written as:

$$\begin{gathered} P_{shaft} = P_{baseline} + P_{wind} + P_{wave} \\ P_{baseline} = R_{baseline} * V_{ship} \\ P_{wind} = R_{wind} * V_{ship} \\ P_{wave} = R_{wave} * V_{ship} \end{gathered} \tag{3}$$

2.1. Baseline

The baseline is commonly written as a power of 3 of the log speed ($P \sim V_{ship}^3$). Although the cubic law holds around the design speed, *Psaraftis and Kontovas (2014)*, at higher speeds this exponential coefficient can be higher than 3, *Holtrop and Mennen (1982), Taskar and Andersen (2020), MAN (2023)*, and at lower speed studies claim that this coefficient is lower than 3, *Berthelsen and Nielsen (2021), Adland et al. (2020)*. Therefore, we decided to consider the V_{ship} exponential for the baseline as a parameter to fit the data.

Other factors also have considerable influence on the ship's baseline that could be taken into account. To cite some:

- The trim affects the hull hydrodynamics as well as the bulbous bow and transom immersion
- Changes in the rudder angle increases the ship's resistance when manoeuvring it
- The biofouling increases the hull friction with time therefore its resistance
- Shallow waters increase the ship draft by making the ship to squat and increase the wave making resistance
- The draft impacts manly to hull friction surface with the water but also, like the trim, the hull hydrodynamics and bulbous bow and transom immersion.

In order to keep the formula simple, with a minimum of parameters, the only influence considered, among the ones cited above, is the draft. In the view of the authors, it is the one that impacts the most the total resistance in the present study.

The exact draft impact on the power shaft is hard to evaluate since it is a complex phenomenon, therefore, we keep it simple in this study and consider it with a linear influence. Hence, baseline formula can be written as follows:

$$P_{baseline} = (x_0 + x_1 * T) * V_{ship}^{x_2} \tag{4}$$

with x_0, x_1 and x_2 parameters to fit and T the draft at midship.

2.2. Wind influence

If there is no Wind Tunnel Test or CFD simulations available to determine the wind coefficient resistance (C_{DA}), it can be calculated based on Fujiwara's regression formula, *ITTC (2022)*. This method was developed based on wind tunnel test for several ships, *Fujiwara et al. (1998,2005)*:

$$\begin{aligned} C_{DA} = C_{LF}\cos\theta_{WR} + C_{XLI}\left(\sin\theta_{WR} - \frac{1}{2}\sin\theta_{WR}\cos^2\theta_{WR}\right)\sin\theta_{WR}\cos\theta_{WR} \\ + C_{ALF}\sin\theta_{WR}\cos^3\theta_{WR} \end{aligned} \tag{5}$$

where θ_{WR} is the wind relative direction and C_{LF}, C_{XLI} and C_{ALF} are regression coefficients. These coefficients depend on detailed ship parameters related to its geometry that are not available for this study. However, these parameters can be estimated based on *Kitamura et al. (2017)*. The authors developed regression formulas to estimate the input parameters for C_{LF}, C_{XLI} and C_{ALF} function of the ship type, ship length overall and ship beam.

Once the C_{DA} determined, the wind resistance can be calculated in the following manner:

$$R_{wind}^{Fujiwara} = \frac{1}{2}\rho_{air}A_{XV}C_{DA}V_{WR}^2 \tag{6}$$

where ρ_{air} is the volumetric mass of the air, the A_{XV} the area of maximum transverse section exposed to the winds and V_{WR} the relative wind speed.

For this study, we are going to compare the presented Fujiwara regression formula to a simple wind formulation:

$$\begin{aligned} R_{wind} = C_{wind}^{dir}V_{WR}^2 \\ C_{wind}^{dir} = x_3\cos\theta_{WR} + x_4\sin\theta_{WR} + x_5\sin 2\theta_{WR} \end{aligned} \tag{7}$$

with x_3, x_4 and x_5 parameters to fit and C_{wind}^{dir} the wind direction coefficient, *i.e.* the wind direction influence on the wind resistance. The proposed formulation is not far from Fujiwara's model.

Comparing the formulas, saying that $\frac{1}{2}\rho_{air}A_{XV}C_{DA} = C_{wind}^{dir}$ the models are the same.

Moreover, the intuition behind the C_{wind}^{dir} formulation is that different sets of parameters [x_3, x_4, x_5] can result in the different shapes depicted in Fig.1. The shown curves are general shapes found for the drag coefficient of ships.

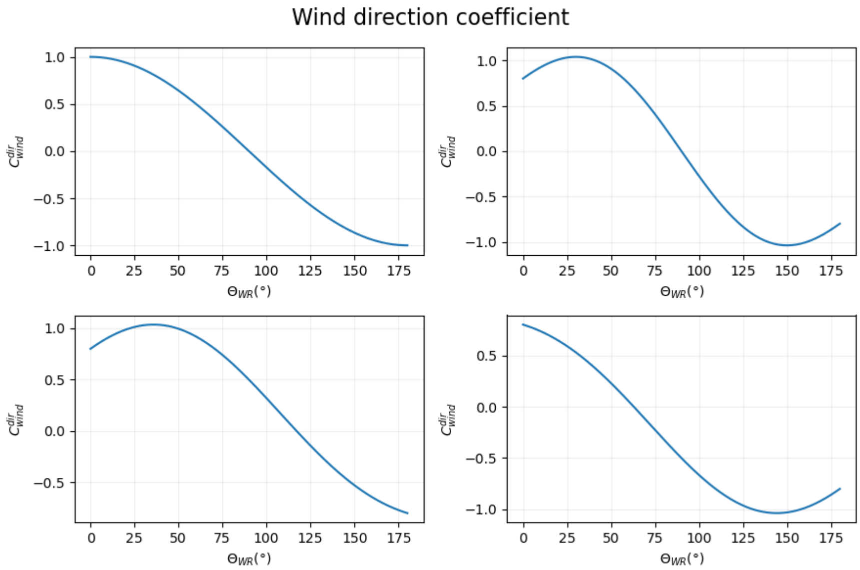

Fig.1: Different possible shapes for the wind resistance coefficient

2.3. Wave influence

In the *ITTC (2022)* guidelines, three well known methods in the literature are cited to calculate the wave resistance, STWAVE-1, STWAVE-2 and a semi-empirical method referred as SNNM, *Liu and Papanikolaou (2020)*. Following the same formulation of the latter, *Mittendorf et al. (2022)* improved the SNNM method by slightly changing its formula and recalculating the coefficients with an enriched database.

The Mittendorf semi-empirical formula is going to be compared with the following simple wave formulation:

$$R_{wave} = C^{dir}_{wave} H_S^2$$
$$C^{dir}_{wave} = x_6 + x_7 \cos\theta_{wave} + x_8 \sin\theta_{wave} + x_9 \sin 2\theta_{wave} \quad (8)$$

with x_6, x_7, x_8 and x_9 parameters to fit, H_S the significant wave height, θ_{wave} the wave direction and C^{dir}_{wave} the wave direction coefficient, *i.e.* the wave direction influence on the wave resistance.

The formula for the wave directional coefficient C^{dir}_{wave} is close to the wind directional coefficient C^{dir}_{wind} the only difference being the independent parameter x_6 that allows the same curves from Fig.1. to move freely on the vertical axis.

Moreover, the presented formulation of R_{wave} depends on the square of the wave height because all other physical and semi-empirical models consider the same.

3. Data analysis

Three different types of ship of three different lengths were chosen to evaluate the model performance. For all three ships the dataset was first cleaned with outlies, sensor problems and other types of problematic data points being disregarded. The data interval is 15 minutes. The main particulars of the analyzed ships as well as few data metrics are summarized in Table I.

Table I: Main characteristics of the analyzed ships and its data

Ship type	LOA (m)	Beam (m)	Data points	Number of voyages
Car Carrier	170	28	27243 (284 days)	174
Container Ship	400	61	19854 (207 days)	41
LNG Tanker	300	46.5	26117 (272 days)	23

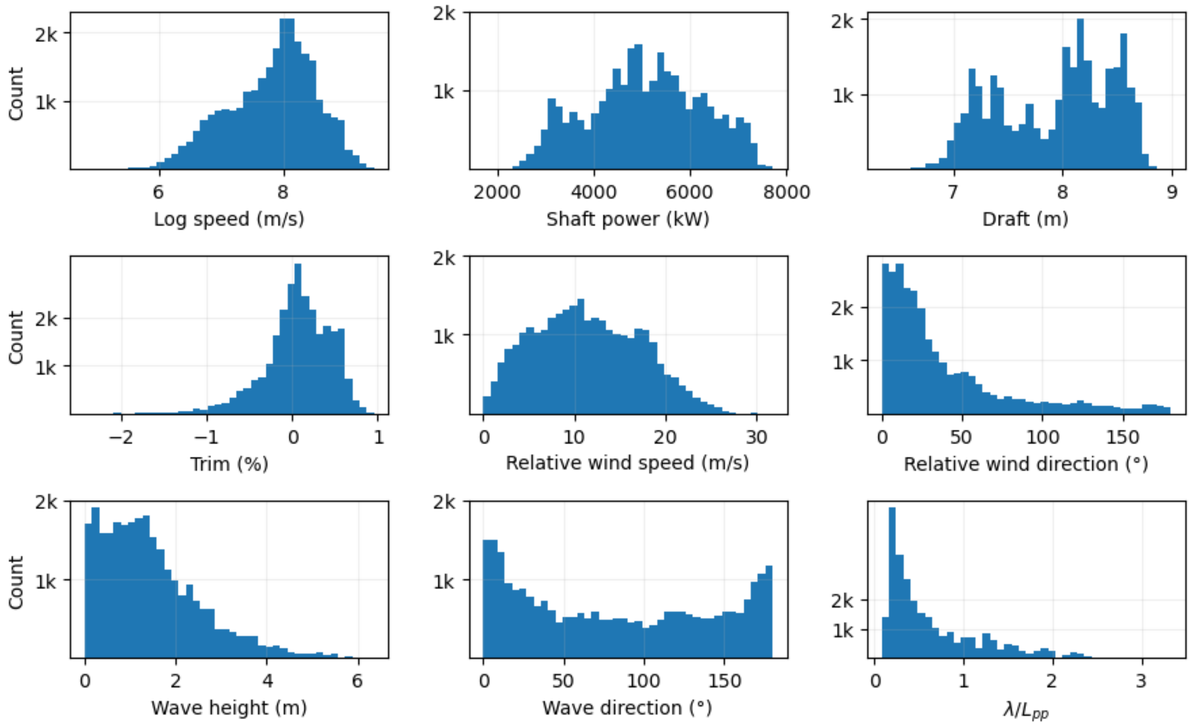

Fig.2: Histograms relative to ship and weather information for the Car Carrier

It is important to know the data distribution across the dataset, therefore, Fig.3, Fig.4 and Fig.5 show histograms of several ship and weather information for the Car Carrier, Container Ship and LNG Tanker, respectively. Trim and wavelength (λ) are not considered in the Simple model but is used in the Mittendorf formula to calculate the wave resistance.

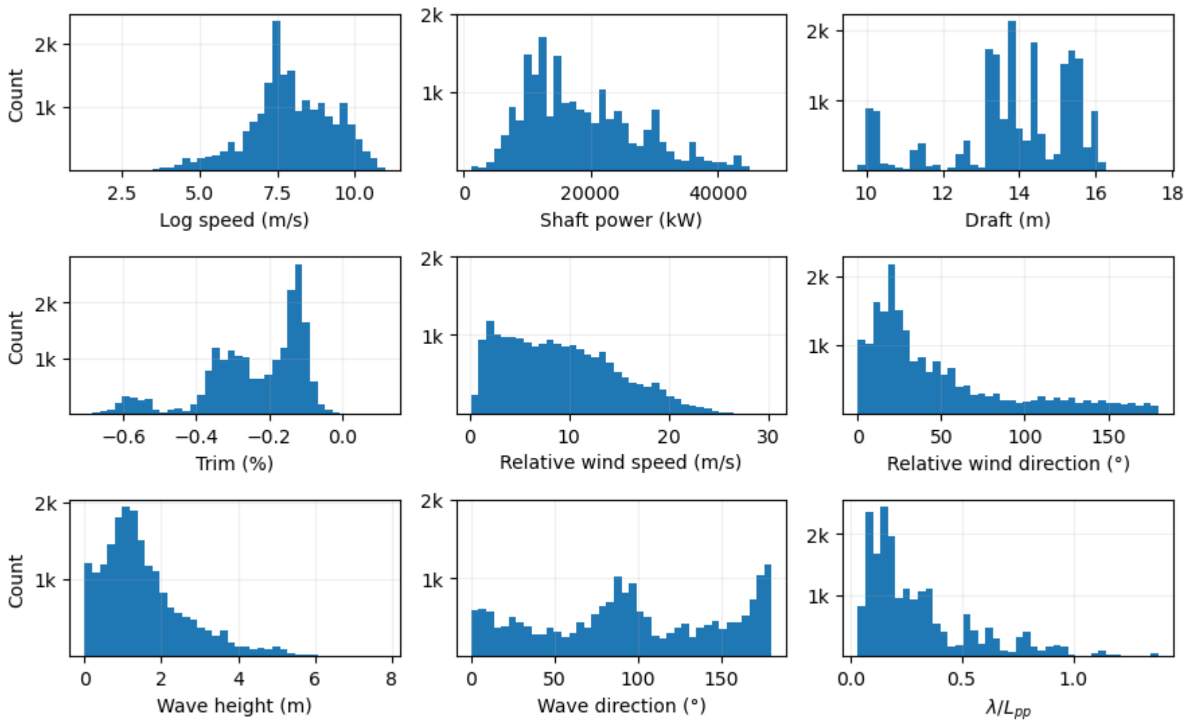

Fig.3: Histograms relative to ship and weather information for the Container Ship

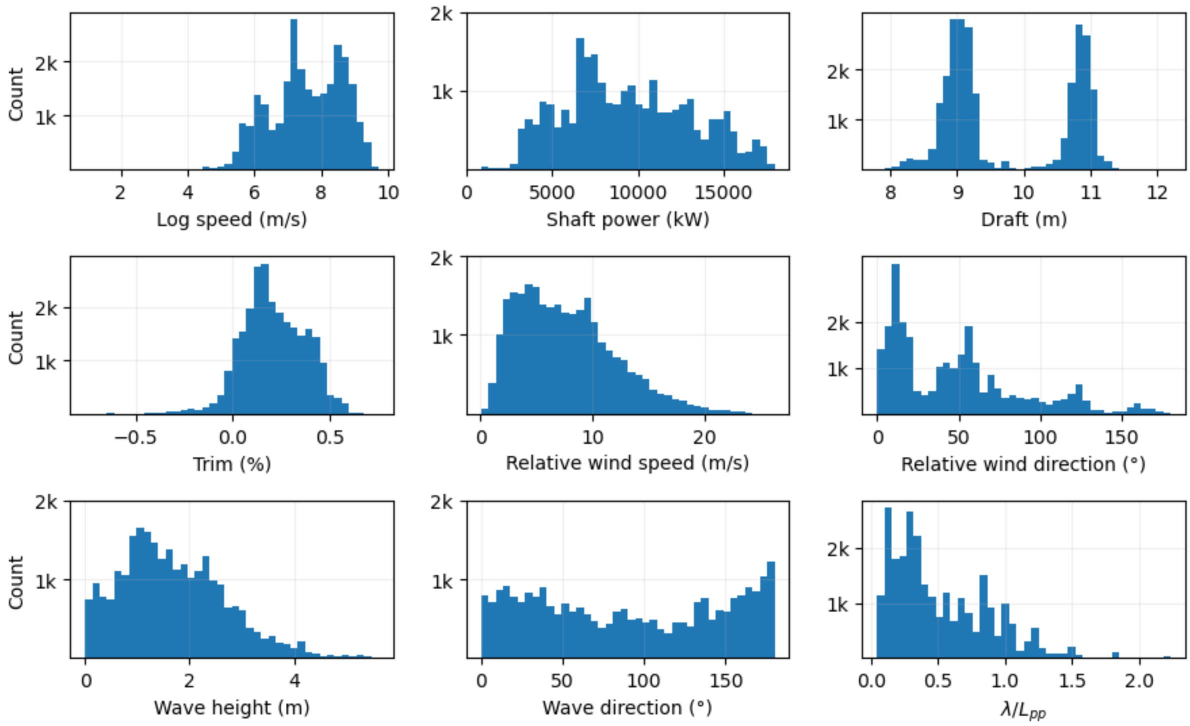

Fig.4: Histograms relative to ship and weather information for the LNG Tanker

4. Results

In this section we are going to compare the results of the stablished semi-empirical models against the simplified presented model, called "Simple model" in the following. The equations that compose each model is explicated in Table II.

Table II: Equations of each model

	Semi-empirical model	Simple model
Baseline	Eq. **(4)**	Eq. **(4)**
Wind model	Fujiwara	Eq. **(7)**
Wave model	Mittendorf	Eq. **(8)**

All parameters were fitted with the "minimize" function inside the SciPy package in python.

4.1. Baseline

Fig.5, Fig.6 and Fig.7 depict the baseline curves on the scatter plot of all points and the calm sea points (fitting points for the baseline curve).

The left figures show the baseline of the ships in laden and ballast conditions on the common Power vs. Speed plot. The right figures are a look on the baseline in a different angle, the Power Shaft is divided by the Log Speed (with the exponential) so the draft influence on the baseline can be highlighted.

$$P_{baseline} = (x_0 + x_1 * T) * stw^{x_2} \Leftrightarrow \frac{P_{baseline}}{stw^{x_2}} = x_0 + x_1 * T \quad (9)$$

The draft influence on the baseline is weak on the Car Carrier case but important to consider on the other two cases. Although saying that the baseline dependency on the draft is linear, it can capture the main trend with a small number of parameters.

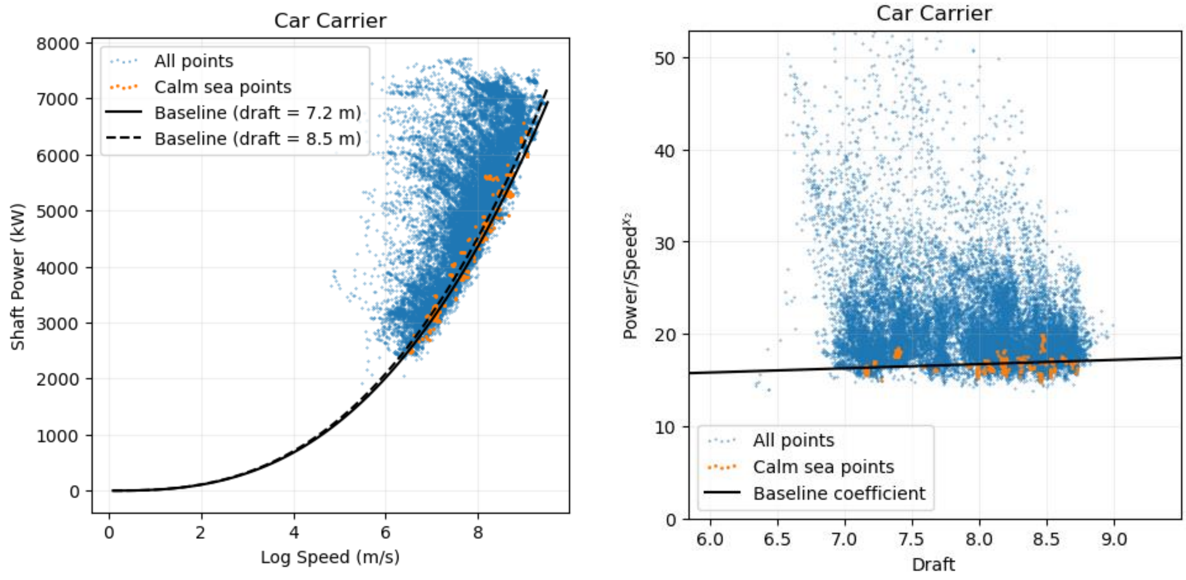

(a) (b)

Fig.5: (a) Baseline on Power vs. Speed; (b) baseline coefficient in function of draft for Car Carrier

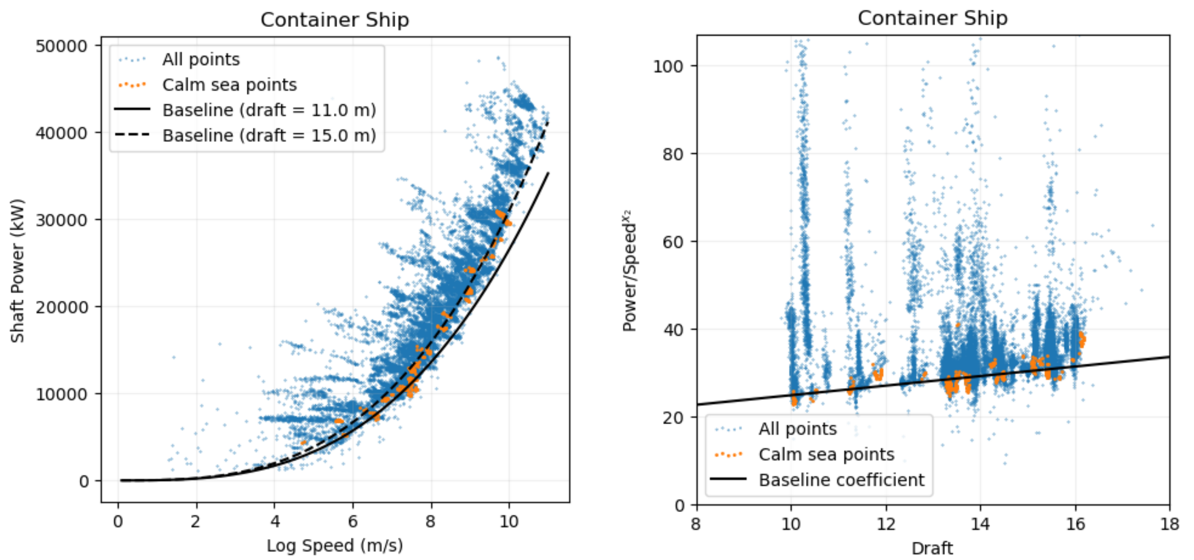

(a) (b)

Fig.6: (a) Baseline on Power vs. Speed;(b) baseline coefficient in function of draft for Container Ship

The exponent value x_2 for each ship is given in Table III.

Table III: Baseline log speed exponent value

Ship type	x_2
Car Carrier	2.69
Container Ship	3.00
LNG Tanker	3.11

Although not far from 3, the optimum value for the exponent is not always 3.

The baselines calculated here are used to find the wind and wave influence of the Simple and Semi-empirical models (Mittendorf + Fujiwara) in the following.

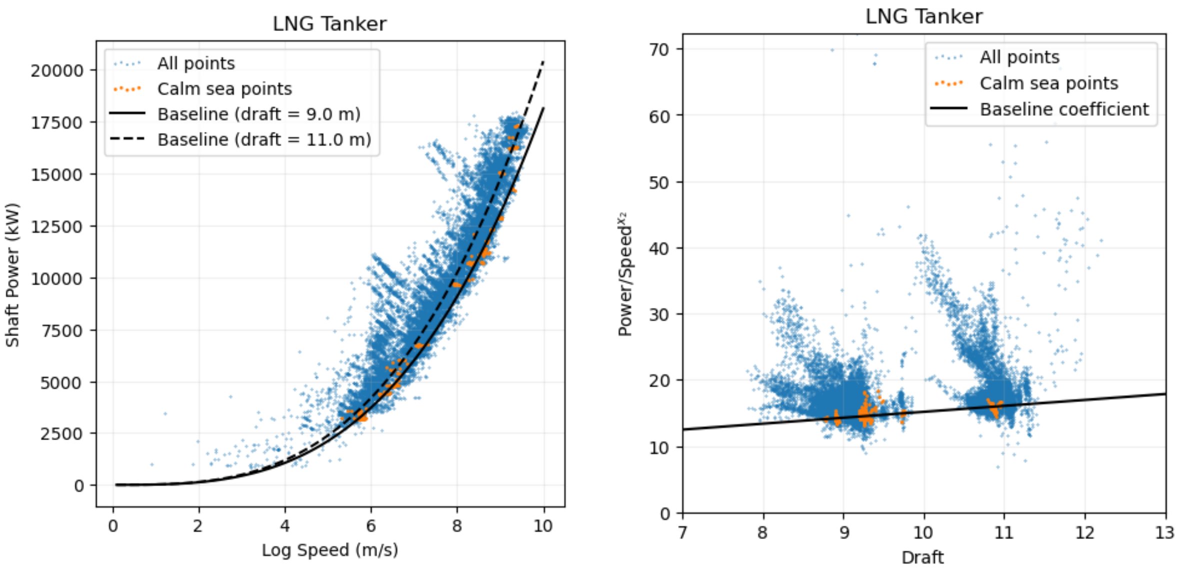

(a) (b)

Fig.7: (a) Baseline on Power vs. Speed; (b) baseline coefficient in function of draft for LNG Tanker

4.2. Wind influence

The comparison of the wind resistance between models for the three ships is illustrated in Fig.8(a), (b) and (c).

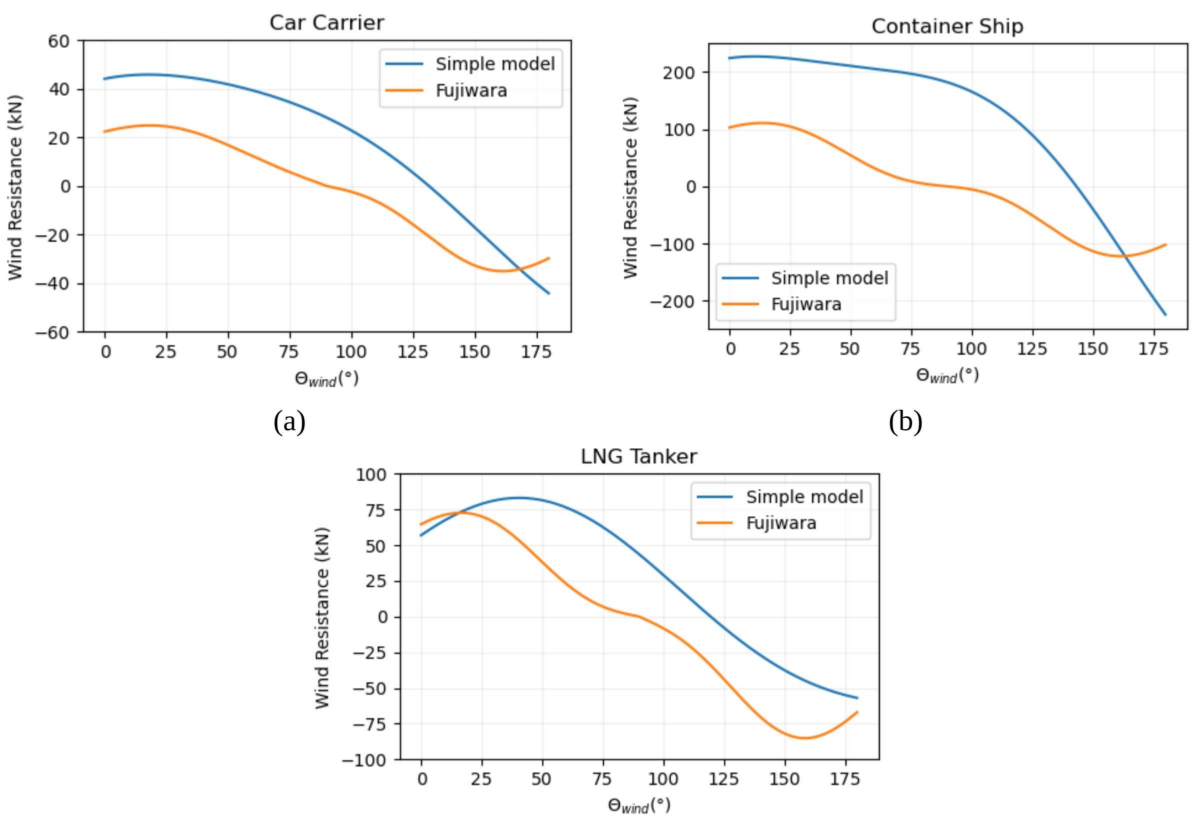

(a) (b)

(c)

Fig.8: Comparison between Simple model's and Fujiwara's wind resistance for (a) Car Carrier, (b) Container Ship and (c) LNG Tanker

The calculated wind resistance for both models considers relative wind speeds of 10 m/s. The Fujiwara model plot is a mean between the laden and the ballast case, the simple model does not differentiate between the two.

The wind resistance comparison between the two models show that the Fujiwara model often underestimates the wind impact on the ship performance compared to the Simple model. The difference between models is even more accentuated for side winds. Indeed, for side winds the Fujiwara formula predicts zero net force on the ship heading direction and the Simple model, however, predicts a negative impact (positive resistance) on the power shaft.

4.3. Wave influence

The wave resistance between models for the three ships is compared in Fig.9(a), (b) and (c) for a significant wave height of 2 m.

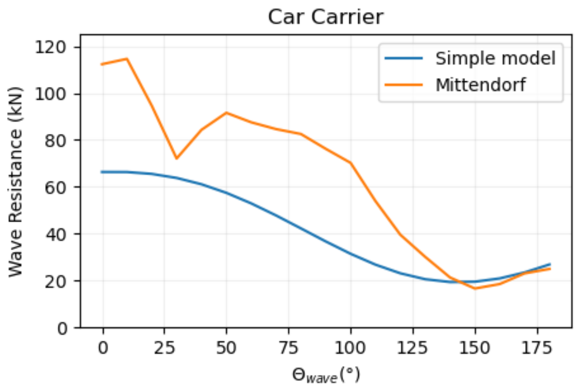

(a)

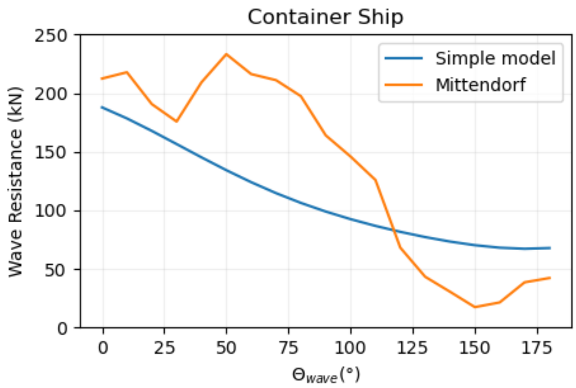

(b)

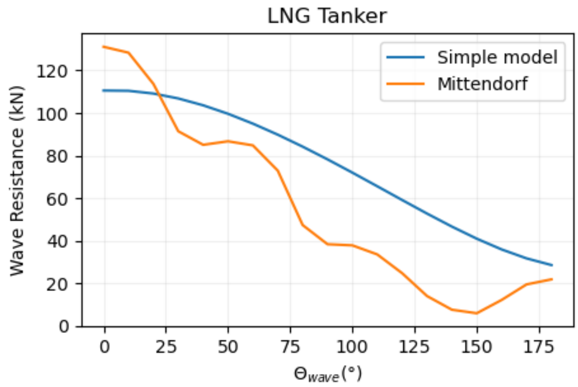

(c)

Fig.9: Comparison between Simple model's and Mittendorf's wave resistance for (a) Car Carrier, (b) Container Ship and (c) LNG Tanker

The wave resistance in Simple model is only affected by the wave height and wave direction therefore, by fixing the wave height, the wave resistance curve function of wave direction is straightforward. On the other hand, in the Mittendorf model the wave resistance depends, in addition to many particulars, on the draft aft, draft fore, log speed, wave height, wave direction and wavelength. In order to plot the Mittendorf model function of the wave direction only, the resulting wave resistance was averaged inside each 10°, the mean value was then plotted.

Both models seem to agree on the general trend of the wave resistance in function of the wave direction. The Mittendorf model overestimates the wave resistance comparing to the Simple model in the case of the Car Carrier and the Container Ship. For the LNG Tanker, is the contrary.

This change in behavior is certainly affected by the different draft, speed and wavelength profiles encountered by each ship. If the ship always takes the same routes, it will in average face the same sea conditions and therefore the Simple model is probably going to be better suited for the wave resistance. However, if the ship encounters sea conditions that deviates a lot from the training data, the model can perform poorly.

4.4. Error comparison

In this section the Mean Absolute Percentage Error for each model is calculated. For comparison reasons, two other model predictions are calculated in addition. The "Baseline" model refers to the baseline prediction only. The "Baseline + 15%" refers to the baseline multiplied per 1.15, common rule of thumb used in the naval architecture domain to take in consideration the extra power shaft correction due to weather.

Fig.10(a), (b) and (c) show the MAPE for the different models. For all three ships, the Simple model performed better than the semi-empirical one (Mittendorf + Fujiwara). For the Car Carrier and LNG Tanker ships, the Simple model performed around 1.7% better and for the Container ship, around 2.7% better.

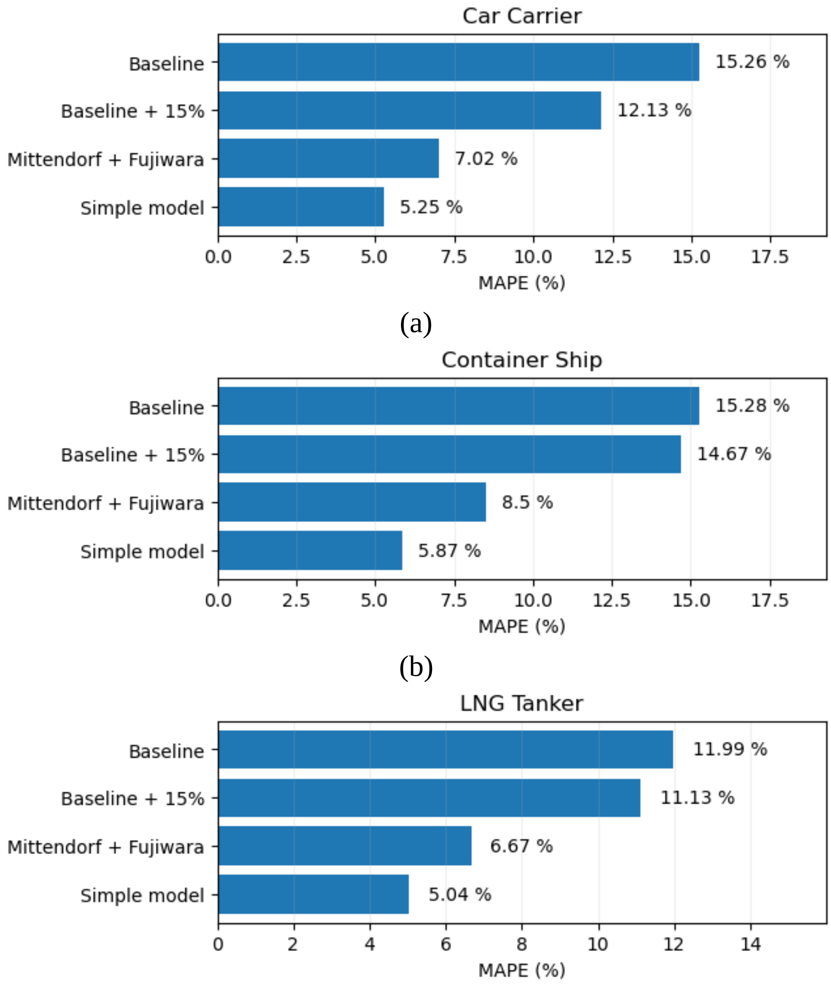

(c)

Fig.10: MAPE for different models for a (a) Car Carrier, (b) Container Ship and (c) LNG Tanker

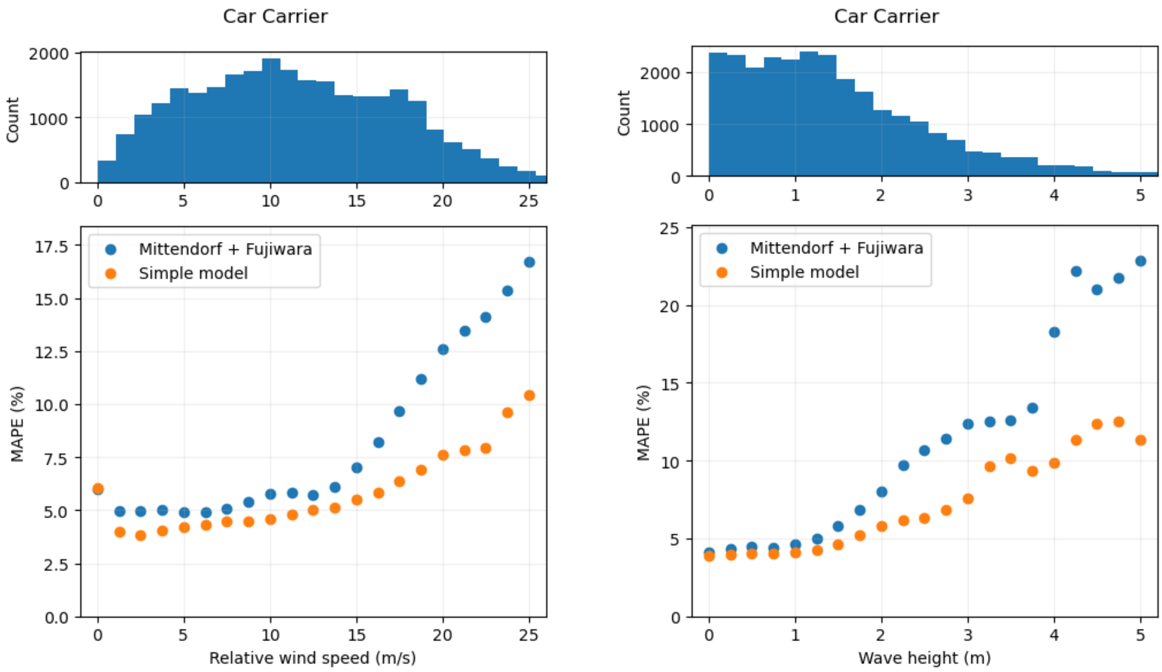

(a) (b)

Fig.11: MAPE comparison between Simple model and semi-empirical method in function of (a) the relative wind speed and (b) the wave height for a Car Carrier

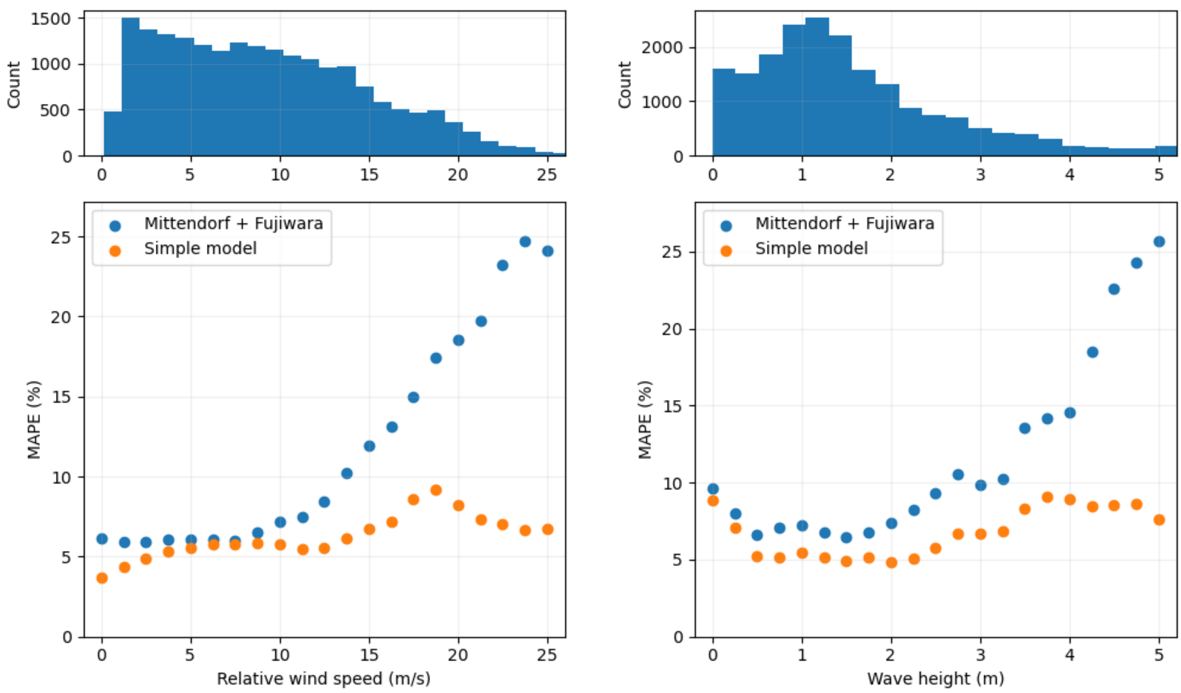

(a) (b)

Fig.12: MAPE comparison between Simple model and semi-empirical method in function of (a) the relative wind speed and (b) the wave height for a Container Ship

To further analyze and compare the behavior of the models, the MAPE is calculated in function of the relative wind speed and wave height. The count of weather cases is plotted in the histogram on top of the corresponding figure. Fig.11(a), Fig.12(a) and Fig.13(a) show for the three ships the MAPE comparison between models in function of the relative wind speed. The figures Fig.11(b), Fig.12(b) and Fig.13(b) do the same comparison but in function of the wave height.

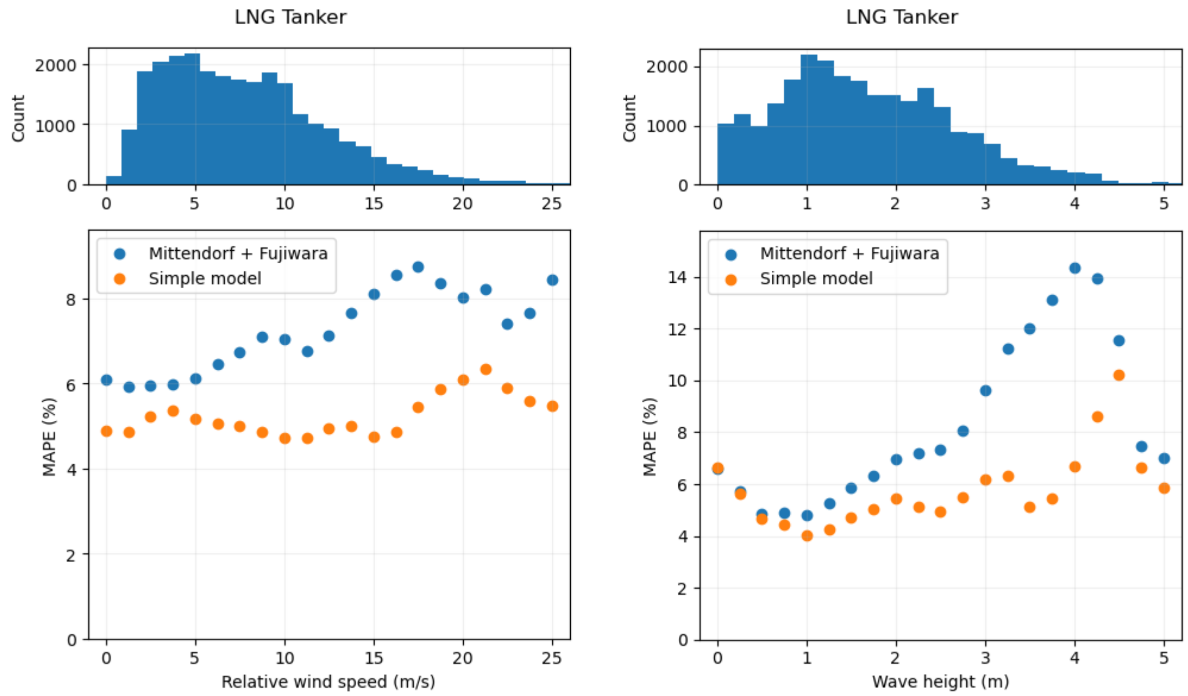

(a) (b)

Fig.13: MAPE comparison between Simple model and semi-empirical method in function of (a) the relative wind speed and (b) the wave height for an LNG Tanker

It is possible to see that the Simple model is also able to generalize to the less frequent cases, even in the scope of this study where all points were considered for the parameters fitting therefore the model being biased. Nevertheless, is important to point out that, naturally, the model is going to perform poorly in the less frequent cases in the dataset.

5. Conclusions

The article presents a relatively simple model to estimate the power shaft of ships in open sea. The model considers the ship speed and draft, the wind speed and direction and the waves height and direction. Its performance is compared to established semi-empirical models in the literature for three different ship types of distinct sizes. Each ship has approximately 8 months of usable data (data when the ship is in route, data when ship is in port is not considered). The semi-empirical methods depend on many ship particulars and detailed geometry parameters that are often unknown. The presented model does not depend on any ship particular but only on data.

The comparison between the two models shows that the Simple model gives better results. Its formulation based on physics demonstrates being able to generalize by estimating with acceptable error (better than the established models) weather cases where the data is scarce, notably high wind speeds and high waves.

Acknowledgement

We would like to thank OSE Engineering team for all valuable technical discussions. We also thank GTT & Ascenz Marorka for carrying out this study together and providing us with high-quality data. Special thanks to Ascenz Marorka team for their specialist expertise.

References

ADLAND, R.; CARIOU, P.; WOLFF, F.C. (2020), *Optimal ship speed and the cubic law revisited: Empirical evidence from an oil tanker fleet*, Transportation Research Part E: Logistics and

Transportation Review

BERTHELSEN, F.H.; NIELSEN, U.D. (2021), *Prediction of ships' speed-power relationship at speed intervals below the design speed*, Transportation Research Part D: Transport and Environment.

BIRK, L. (2019), *Fundamentals of ship hydrodynamics: Fluid mechanics, ship resistance and propulsion*, John Wiley & Sons

BLENDERMANN, W. (1994), *Parameter identification of wind loads on ships*, J. Wind Engineering and Industrial Aerodynamics, pp.339-351

FUJIWARA, T.; UENO, M.; NIMURA, T. (1998), *Estimation of wind forces and moments acting on ships*, J. Society of Naval Architects of Japan 183, pp.77-90

FUJIWARA, T.; NIMURA, T. (2005), *New estimation method of wind forces acting on ships on the basis of mathematical model*, Int. Ocean and Polar Engineering Conf. (ISOPE)

HOLLENBACH, U. (1999), *Estimating resistance and propulsion for single-screw and twin-screw ships in the preliminary design*, ICCAS, Cambridge

HOLTROP, J.; MENNEN, G.G.J. (1982), *An approximate power prediction method*, Int. Shipb. Progress, pp.166-170

IMO (2021), *Fourth IMO Greenhouse Gas Study 2020*, Int. Mar. Org., London

IMO (2022), IMO's work to cut GHG emissions from ships, Int. Mar. Org., London, https://www.imo.org/en/MediaCentre/HotTopics/Pages/Cutting-GHG-emissions.aspx

ISHERWOOD, R. (1973), *Wind resistance of merchant ships*, Trans. RINA, pp.327-338

ITTC (2005), *Recommended Procedures and Guidelines - Full Scale Measurements - Speed and Power Trials - Analysis of Speed/Power Trial Data*, Int. Towing Tank Conf.

ITTC (2022), *Recommended Procedures and Guidelines - Preparation, conduct and analysis of speed/power trials*, Int. Towing Tank Conf.

KITAMURA, F.; UENO, M.; FUJIWARE, T.; SOGIHARA, N. (2017), *Estimation of above water structural parameters and wind loads on ships*, Ships and offshore structures, pp.1100-1108

LIU, S.; PAPANIKOLAOU, A. (2020). *Regression analysis of experimental data for added resistance in waves of arbitrary heading and development of a semi-empirical formula*. Ocean Eng. 206

MAN (2023), *Basic principles of ship propulsion*, https://www.man-es.com/docs/default-source/document-sync-archive/basic-principles-of-ship-propulsion-eng.pdf?sfvrsn=48fc05b5_7

MITTENDORF, M.; NIELSEN, U.; BINGHAM, H.B.; LIU, S. (2022), *Towards the uncertainty quantification of semi-empirical formulas applied to the added resistance of ships in waves of arbitrary heading*, Ocean Engineering 251

PSARAFTIS, H.N.; KONTOVAS, C.A. (2014), *Ship speed optimization: Concepts, models and combined speed-routing scenarios*, Transportation Research Part C: Emerging Technologies, pp.52-69

TASKAR, B.; ANDERSEN, P. (2020), *Benefit of speed reduction for ships in different weather conditions*, Transportation Research Part D: Transport and Environment

DNN based Ship Performance Prediction Model and its Comparisons with Conventional Model

Beom Jin Park, Korea Research Institute of Ships and Ocean Engineering, Daejeon/Republic of Korea, baracude@netopia.re.kr
Joon-Hyong Lee, Korea Research Institute of Ships and Ocean Engineering, Daejeon/Republic of Korea, joonh.lee@kriso.re.kr
Myoung-Soo Kim, Korea Research Institute of Ships and Ocean Engineering, Daejeon/Republic of Korea, mskim@kriso.re.kr
Jae-Yoon Jung, Kyung Hee University, Republic of Korea, jyjung@khu.ac.kr
Donghyun Park, Kyung Hee University, Republic of Korea, pdh@khu.ac.kr

Abstract

Recent advances in AI and availability of a ship's operational data makes AI based models to be used in ship performance analysis. Many ship performance analysis and monitoring solutions now uses AI based models. In this study, an DNN-based model for predicting a ship's performance and performance degradation is proposed. The results show good prediction accuracy for predicting FOC. Also performance degradation prediction results shows similar trends and pattern with conventional hydrodynamics based performance analysis model.

1. Introduction

Ship performance analysis and monitoring has always been a backbone of shipping company's operations. From simple log-based record collection and monitoring to more sophisticated systems with real time data collection and hydrodynamic based analysis models, it is used as a basis to make day to day operational decisions.

Recent advances in AI and availability of a ship's operational data makes AI based models to be used in ship performance analysis. Many ship performance analysis and monitoring solutions now uses AI based models only or in conjunction with conventional hydrodynamic models. AI based models also provide one very strong advantage over conventional models: they can easily be used for prediction of future performance.

In this paper, a DNN (Deep Neural Network) based ship performance prediction model is proposed and applied to a test case to predict degradation of a ship's performance over time. First, a DNN based model is constructed with previous operational data to predict FOC (Fuel Oil Consumption). Then the model is applied to predict for the journey, which data is not used in training of the prediction model. The prediction results are then compared with the actual data from the journey to calculate the accuracy of the model. Based on this prediction model, it is also possible to predict the amount of the ship's performance degradation.

2. Method

2.1. Data processing

The data is preprocessed before constructing the FOC prediction model to improve the performance of the model. The data preprocessing involves two components. The first is feature engineering, in which a new feature related to the anchoring effect is developed, and the original features related to environmental resistance are converted. The other is the extraction of stable voyage data, where abnormal operations such as abrupt accelerations and decelerations, as well as changes in the traveling direction are disregarded.

First, for feature engineering, a new feature called CAE (Cumulative Anchoring Effect) is developed, based on the well-known assumption that the degradation of performance due to hull fouling is significantly affected by the length of the anchoring and the water temperature of the anchorage site.

$$CAE_n = (no. of\ anchoring\ days)_n \times (water\ temp. of\ anchoring\ site)_n, \quad (1)$$

where n represent n-th anchoring.

In addition, new features related wind, current and wave are also created for ease of handling data.

$$Wind\ Resistance_t = Wind\ Speed_t \times Wind\ Direction_t, \quad (2)$$
$$Current\ Resistance_t = Current\ Speed_t \times Current\ Direction_t,$$
$$Wind\ Wave\ Resistance_t = Wind\ Wave\ Height_t \times Wind\ Wave\ Direction_t,$$
$$Swell\ Resistance_t = Swell\ Height_t \times Swell\ Direction_t,$$

where, t represents time.

In order to extract stable voyage, the following data is removed:

- Data near departure and arrival
- Data with rudder angle, speed over ground or FOC values outside the range of 3 times the standard deviation within a pre-defined time window.

2.2. DNN-based FOC prediction model

A DNN architecture is used to develop an FOC prediction model. DNNs have been actively used in many studies because they can automatically extract representative features without generating complex handcrafted features, which typically require a considerable amount of expert knowledge, *Tarelko and Rudzki (2020)*, *Tran (2021)*, *Zhou et al. (2022)*. Consecutive nonlinear calculations of the DNN by stacking several hidden layers allow large and complex problems to be solved, *Uzair and Jamil (2020)*.

The architecture of the FOC prediction model is shown in Fig.1. The DNN architecture comprises of an input layer, three hidden layers, and an output layer. The layers comprise of several nodes connected with weights to be summed in each node using a nonlinear function, ReLU (Rectified Linear Unit), *Agarap (2023)*. The last hidden layer is connected to the input layer via a shortcut connection, *He et al. (2023)*, where the inputs are summed to the outputs of the last hidden layer during model training. This allows the model to be optimized more easily as only the residual information, excluding the original information added by the connection, is to be learned.

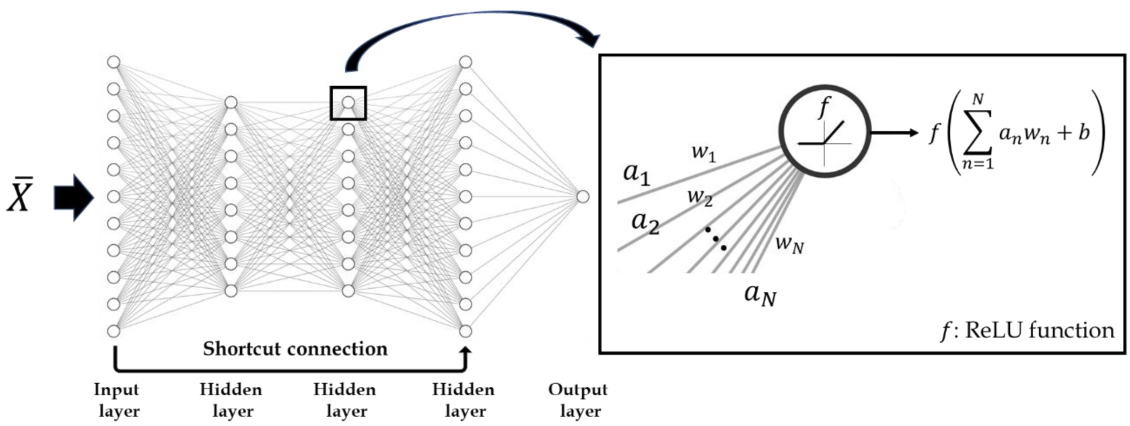

Fig.1: Architecture of DNN-based FOC prediction model

The data acquired during the actual operation of a ship fluctuate significantly because of harsh and variable ocean environments. Therefore, the FOC prediction model is trained to predict the averaged FOC in a single time window instead of that of all FOCs at all time points. To predict the average FOC in a time window, the input features are averaged over the time window. Averaging is conducted for each journey leg, not by averaging the overlapped data in the two journey legs. The configurations of the inputs and outputs are shown in Fig.2.

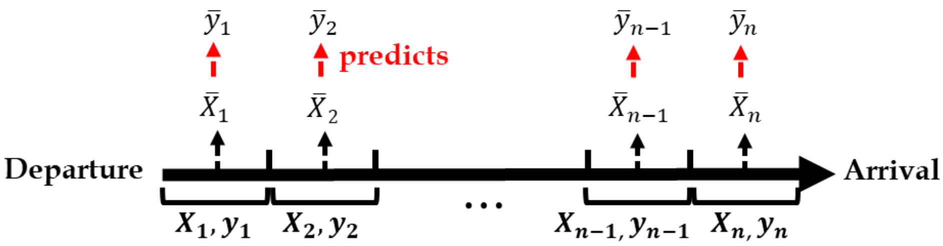

Fig.2: Configuration of inputs and outputs of DNN-based FOC prediction model

2.3. Estimation of performance degradation

Using the above FOC prediction model, it is also possible to predict the degradation. The amount of performance degradation is estimated as the difference between the predicted FOCs obtained using the input data with the original CAE and initial CAE, as shown in Fig.3. The FOC prediction model, F, predicts the FOCs in the k-th journey leg, $\hat{y}_k$, using the input features $\bar{X}_k$ including the CAE, which is denoted as A. If the CAE is changed to 0, which implies that the state of the ship returns to the past when no anchoring effects are accumulated, then the prediction model F generates a lower FOC, $\hat{y}'_k$. The percent decrease in the predicted FOCs is quantified as the amount of performance degradation of the k-th journey leg.

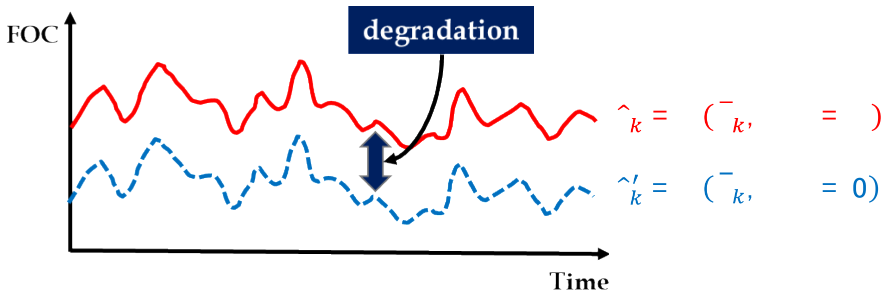

Fig.3: Estimation of ship performance degradation

3. Application of the model

3.1. Data description

The data used for the application of the model is from a large crude oil tanker for a period of 21 months. A data acquisition system was installed on the ship, and operational data were acquired every 10 s during operation. The features of the acquired data are listed in Table I. The features related to wind, wind waves, swells, and currents are nowcast values, not direct measurements. During the operating period, the ship traveled 49 journey legs, and dry docking, hull cleaning, or propeller polishing were not involved. The propeller of the ship was last polished in August 2019; therefore, the initial data were obtained when the degradation had progressed for approximately 6 months.

Table I: Features of acquired data

Measured		Forecasted	
Feature	**Units**	**Feature**	**Units**
Time stamp	yyyy-mm-dd hh:mm:ss	Wind velocity	m/s
Latitude	degree (°)	Wind direction	degree (°)
Longitude	degree (°)	Wind wave height	meter
Water temperature	°C	Wind wave period	second
Draft forward	meter	Wind wave height	meter
Draft after	meter	Wind wave direction	degree (°)

Draft starboard	meter	Swell height	meter
Draft port	meter	Swell period	second
Draft forward when departure	meter	Swell height	meter
Draft after when departure	meter	Swell direction	degree (°)
Heading GPS	degree (°)	Current velocity	m/s
Heading gyro	degree (°)	Current direction	degree (°)
Rudder angle	degree (°)		
Speed over ground	m/s		
Speed Through Water	m/s		
Shaft torque	Newton		
Shaft speed	revolutions per second		
Brake power	Watt		
Shaft power	Watt		
Delivered power	Watt		
Fuel power	Watt		
Fuel oil consumption	kg/s		

3.2. Preprocessing

Although the acquired data comprised 44 features, only 11 features, including newly developed features, were used as inputs for the FOC prediction model, as shown in Table II. The longitude feature was indicated in sine and cosine values because the longitude ranged from 0° to 360°, which exhibited a cyclical property that resulted in misrepresentation. Because the longitudes of 0° and 360° indicate the same degree, they should be converted to represent the same value using sine and cosine values. The external resistance features, i.e., the wind resistance, wind wave resistance, swell resistance, and current resistance, were developed as described in Section 2.1. The features of the average draft were calculated by averaging the features of the draft forward when departure and the draft after when departure. This average draught represents the loaded weights of the ship at the departure time, which considers both the fore and aft draughts. The CAE feature was included as an input feature to represent the performance degradation caused by the anchoring, as described in Section 2.1.

Table II: Features for developing FOC prediction model

Category	Feature	Units
	Longitude_sin	-
	Longitude_cos	-
	Latitude	degree (°)
	Water temperature	°C
	Wind resistance	-
Input features	Wind wave resistance	-
	Swell resistance	-
	Current resistance	-
	Average draught	meter
	Speed over ground (SOG)	m/s
	Cumulative berthing effect (CBE)	-
Output feature	Fuel oil consumption (FOC)	kg/s

Before training the FOC prediction model, stable voyage data were extracted using the rudder angle, SOG, and FOC features as described in Section 2.1. The data of the five shifting journey legs were removed because they were short and abnormal operations for special purposes. Finally, the data of the four journey legs whose data lengths were shorter than 1 h were removed as they were extremely short. Thus, after preprocessing, the data of 42 journey legs remained.

3.3. Training of DNN-based FOC prediction model

The preprocessed data were segmented into training, validation, and test data. The validation data were used to determine the optimal hyperparameters of the FOC prediction model, and the test data were used as unseen data for the final evaluation of the trained model. To avoid data leakage when future data are used at the training stage, the data is divided in the sequential order of training, validation, and test data, as shown in Table III. The data were divided based on the unit of the journey leg. The training data contained 31 journey legs (15.3 months), the validation data 6 legs (3.2 months), and the test data 5 legs (3.1 months), which resulted in 70% training data, 15% validation data, and 15% test data.

Table III: Data segmented into training, validation, and test data

	Date	Months	The number of journey legs
Training data	Jan. 21, 2020 to Apr. 25, 2021	15.3	31
Validation data	May 19, 2021 to Aug. 24, 2021	3.2	6
Test data	Aug. 24, 2021 to Nov. 26, 2021	3.1	5

3.4. Results of FOC prediction

The proposed DNN-based FOC prediction model exhibited a good as shown in Table IV. The performance of the FOC prediction model was measured using the data of the five journey legs (#38-42) in the test data by calculating the mean absolute error (MAE), root mean squared error (RMSE), and mean absolute percentage error (MAPE). On average, for the five legs, the DNN-based FOC prediction model exhibited 0.0161, 0.0209, and 5.79% for the MAE, RMSE, and MAPE, respectively. The prediction results of the DNN model are shown in Fig.4.

Table IV: Results of FOC prediction of test data

# of journey leg	MAE (kg/s)	RMSE (kg/s)	MAPE (%)
38	0.0139	0.0181	3.73
39	0.0128	0.0158	4.98
40	0.0185	0.0244	7.00
41	0.0165	0.0229	6.36
42	0.0188	0.0231	6.86
Avg.	0.0161	0.0209	5.79

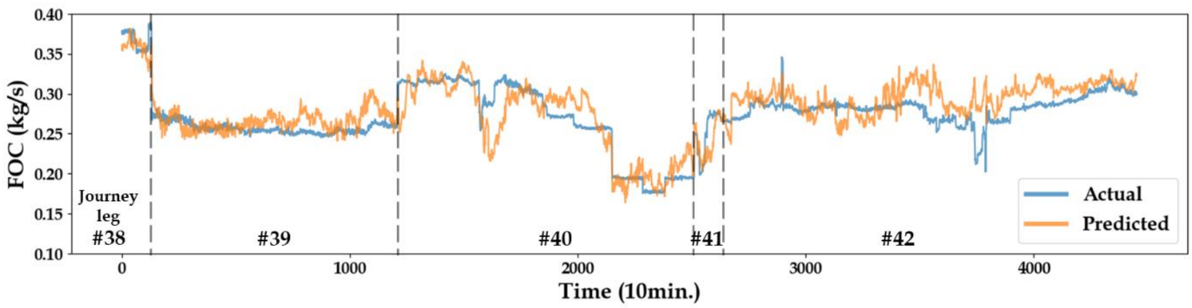

Fig.4: FOC prediction results of DNN-based FOC prediction model based on test data

The prediction results of the DNN model shown in Fig.4 were obtained using a 10-min time window. Six different time-window sizes (1, 5, 10, 20, 30, and 60 min) were tested. The 5-min time window yielded the lowest MAPE, whereas the 10-min time window yielded the lowest MAE and RMSE. The errors were calculated by averaging the errors of the five journey legs from the test data. Because the 10-min time window yielded the lowest errors in two among three of the error metrics, the optimal time window for the DNN model was determined to be 10 min. However, it should be noted that the optimal time window size will likely vary with the frequency of input data.

Table V: Comparison of prediction results based on time window size

	Size of time window					
	1 min	**5 min**	**10 min**	**20 min**	**30 min**	**60 min**
MAE	0.0190	0.0171	**0.0170**	0.0184	0.0222	0.0213
RMSE	0.0239	0.0223	**0.0218**	0.0227	0.0277	0.0268
MAPE	7.09	**6.28**	6.33	6.91	8.24	7.91

3.5. Results of performance degradation estimation

Performance degradation was estimated using the developed DNN-based FOC prediction model as described in Section 2.3. All the data, including the training, validation, and test data, were provided to the model as inputs, and the prediction results were obtained, as shown in column 2 of Table 6. Subsequently, the CAE value of each journey leg data was modified to 0, and the modified prediction results were obtained, as shown in column 3 of Table VI. Finally, the amount of performance degradation was calculated using the original and modified FOC predictions for each journey leg, as shown in column 4 of Table VI.

In Fig.5, the estimated performance degradations are indicated by a trend line, which was obtained via linear regression by adjusting the bias to 0 (R2 = 0.78). As time progress, the estimated performance degradations increase and exhibit high volatility. As the performance degradations do not increase monotonically, it can be inferred that the CAE does not necessarily impose the same effect on the operational performance of ships. This is because the operational environments of ships are highly variable depending on the ocean environment, cargo weight, and ship speed.

Journey legs showing performance degradations that differ significantly from the trend line are indicated by orange rectangles (set 1: #24, 32, 33, 37, 39, and 41) and red triangles (set 2: #13, 28, 36, 38, and 42).

On the trend line, the green diamonds represent the performance degradations of the journey legs after approximately 0.5, 1.0, and 1.5 years from the first journey leg (y=0.1829x). By not considering the variability in the operational conditions, the ship degraded by 2.19%, 4.75%, and 6.76% after 6 months, 1 year, and 1.5 years, respectively.

Table VI: Estimated performance degradations

	# of journey legs	**Predicted FOC**	**Predicted FOC (CBE=0)**	**performance degradations (%)**
Training data	1	297.961	297.961	0.00
	2	16.288	16.284	0.02
	3	11.227	11.202	0.22
	4	121.674	121.451	0.18
	5	86.166	85.295	1.01
	6	374.436	372.999	0.38
	7	84.826	83.411	1.67
	8	46.176	45.297	1.90
	9	215.514	214.746	0.36
	10	17.741	17.577	0.92

	11	11.696	11.497	1.70
	12	127.039	125.708	1.05
	13	7.917	7.932	-0.19
	14	23.519	23.418	0.43
	15	24.070	23.129	3.91
	16	152.258	148.644	2.37
	17	13.204	12.775	3.25
	18	98.925	96.633	2.32
	19	106.887	103.929	2.77
	20	14.403	13.761	4.46
	21	190.183	186.682	1.84
	22	59.210	57.789	2.40
	23	80.335	77.784	3.18
	24	158.018	147.995	6.34
	25	27.344	26.526	2.99
	26	283.274	274.541	3.08
	27	5.234	5.029	3.92
	28	160.312	156.398	2.44
	29	189.579	180.721	4.67
	30	14.863	14.280	3.92
	31	76.049	72.946	4.08
Validation data	32	131.394	119.888	8.76
	33	3.010	2.662	11.56
	34	25.886	24.493	5.38
	35	166.806	157.834	5.38
	36	248.602	240.467	3.27
	37	2.528	2.191	13.33
Test data	38	28.156	27.249	3.22
	39	172.133	152.125	11.62
	40	207.193	190.488	8.06
	41	23.942	20.704	13.52
	42	316.679	306.103	3.34

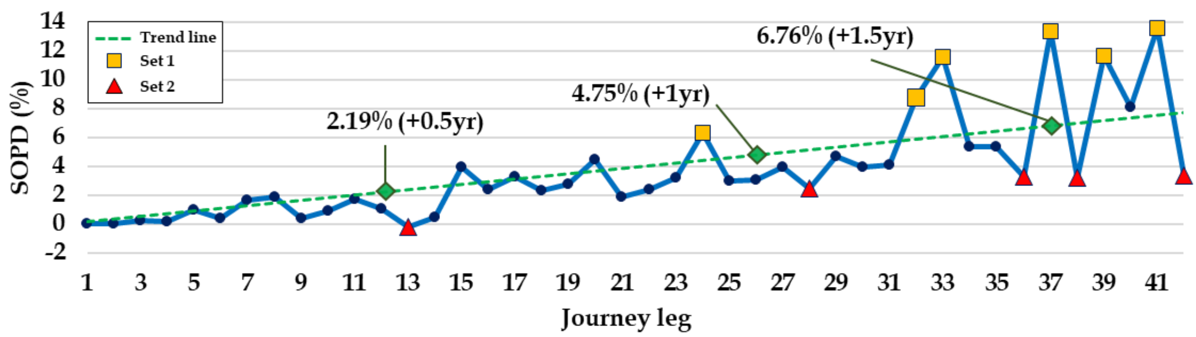

Fig.5: Estimated performance degradations at each journey leg

5. Comparisons with conventional model

Conventional hydrodynamic based models have also been used to analyse ships' performance and performance degradations. Using the methods described in *Park et al. (2023)*, the same data is analysed. Fig.6 shows the results as the difference between expected power from speed power reference curve and corrected power accounting for external resistance.

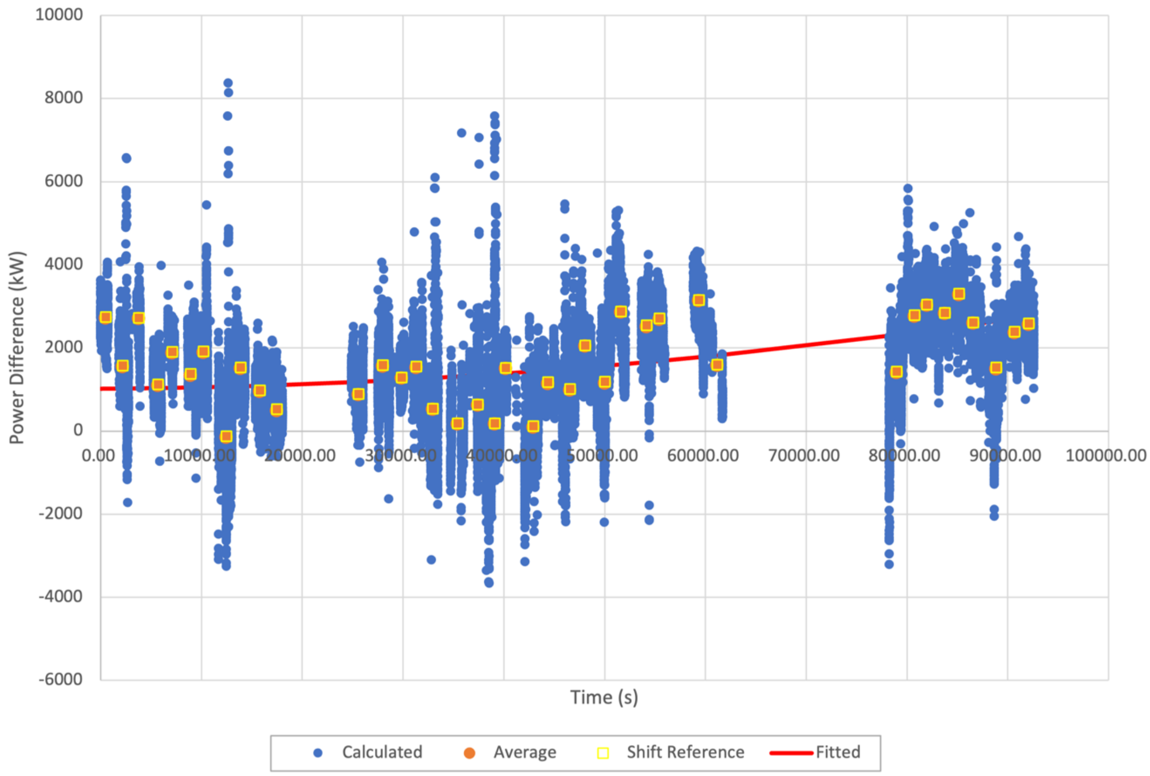

Fig.6: Performance analysis results using conventional model

While it is not possible to directly compare the results of DNN-based prediction model and conventional model as their metric representing the performance degradation is different, Fig.5 and 6 shows similar patterns. More comparative study will be done in near future.

6. Conclusion

A model to estimate performance degradations using a DNN-based FOC prediction model was proposed herein. By utilizing the CAE as a feature, performance degradations can be estimated and verified based on the performance of the DNN-based FOC prediction model. Moreover, the developed features related to environmental resistance (wind, wind wave, swell, and current) were shown to facilitate improvements to FOC prediction. Finally, the proposed DNN-based FOC prediction model showed quite good prediction accuracies in terms of the MAE, RMSE, and MAPE.

Performance degradations estimation results shows that performance degradations increase over time; however, the performance degradations depend significantly on the operational conditions, specifically the SOG and average draft. The trend line obtained from the estimated performance degradations showed that the target ship degraded by 4.75% and 7.68% within 1 year and almost 2 years (21 months), respectively.

As a future work item, more close examination between DNN-based prediction model and the conventional hydrodynamic based performance analysis model will be conducted for the possibility of using combined models. For example, it will be interesting to study whether using the corrected data from applying the conventional model for the training of the DNN-based prediction model increases the accuracy of prediction.

Acknowledgement

This research was supported by a grant from Korea Research Institute of Ships and Ocean Engineering Endowment project of “Development of evaluation technology for ship’s performance in extreme environment” funded by Ministry of Oceans and Fisheries (1525014865, PES5091)

References

AGARAP, A.M.F. (2023), *Deep Learning using Rectified Linear Units (ReLU)*, https://arxiv.org/abs/1803.08375v2

HE, K.; ZHANG, X.; REN, S.; SUN, J. (2023), *Deep Residual Learning for Image Recognition*, http://image-net.org/challenges/LSVRC/2015/

PARK, B.; KIM, M.; LEE, J.; SHIN, M. (2023), *Comparison of a Ship's Performance Before and After Hull Cleaning and Propeller Polishing*, 8th HullPIC Conf., Pontignano, pp.31-37, http://data.hullpic.info/HullPIC2023_Pontignano.pdf

TARELKO, W.; RUDZKI, K. (2020), *Applying artificial neural networks for modelling ship speed and fuel consumption*, Neural Comput. Appl. 32/23, pp.17379–17395

TRAN, T.A. (2021), *Comparative analysis on the fuel consumption prediction model for bulk carriers from ship launching to current states based on sea trial data and machine learning technique*, J. Ocean Engineering and Science 6/4, pp.317–339

UZAIR, M.; JAMIL, N. (2020), *Effects of Hidden Layers on the Efficiency of Neural networks*, 23rd IEEE Int. Multi-Topic Conf. (INMIC)

ZHOU, T.; HU, Q.; HU, Z.; ZHEN, R. (2022), *An adaptive hyper parameter tuning model for ship fuel consumption prediction under complex maritime environments*, J. Ocean Engineering and Science 7/3, pp.255–263

Opportunities and Challenges of CO_2 and Exhaust Gas Pollutant Measurements in Maritime Applications

Uwe Altenbach, Hoppe Marine, Hamburg/Germany, u.altenbach@hoppe-marine.com

Abstract

This paper addresses the requirements for operating the complex measurement technology for CO2 and pollutant emissions on a seagoing vessel, as well as the added value that can result from analysing exhaust gas components.

1. Introduction: Types of emissions and their emitting sources

The reduction of emissions from vehicles and other engine applications has become one of the major drivers in the development of sustainable mobility and engine technology. In the last decades great progress has been achieved to reduce emissions from individual sources, as well as improvements in local air quality. However, much more is needed and must be accomplished. When discussing "emissions", it should be clearly distinguished between CO_2 (Green-House-Gases) emissions and pollutant emissions.

Fig.1: Emission sources and their significant impact on our environment

Green-House-Gas (GHG) emissions consist mainly out of CO_2 and a small amount of CH_4 and N_2O. It is not relevant where these gases are emitted, nor do they exert a toxic effect on any organisms. The increasing concentrations of greenhouse gases are considered responsible for the rising global temperatures, leading to further serious consequences that ultimately affect all of humanity. Analogously, the only possible approach is to collectively resolve this problem on a global scale.

Pollutant Emissions consist mainly of Particulate Matter (PM), Sulfur Dioxide (SO2), Nitrogen Oxides (NOx), and Carbon Monoxide (CO).

The impact of pollutant emissions on organisms is significant. Through environmental factors such as air pollution, water pollution, soil contamination, acid rain, eutrophication and ozone depletion, human health is affected, leading to respiratory diseases, cardiovascular diseases, cancer, and neurological disorders. In contrast to greenhouse gases, the location of the emission source is relevant to the respective pollutant concentration. Additionally, the topography of the location and weather conditions play important roles. Consequently, high local emission concentrations must be addressed at the source by local pollutant emitters.

The sources for both GHG and Industrial sources:

- Industrial sources: Power plants, manufacturing facilities, refineries
- Transportation sources: Vehicles (cars, trucks, ships, airplanes), railways
- Agricultural sources: Livestock farming, fertilizer use, pesticide application
- Residential sources: Heating, cooking, waste incineration
- Natural sources: Volcanic eruptions, wildfires, biogenic emissions

The consideration of emissions in this document, encompassing both greenhouse gases and pollutants, centers on combustion systems utilized in the maritime sector. These systems include reciprocating piston engines and boilers operated by fossils such as diesel, heavy fuel oil, and liquefied natural gas (LNG).

2. Milestones in Emissions Regulations in Maritime Applications

Before the adoption of the MARPOL (International Convention for the Prevention of Pollution from Ships) Convention in 1973, the issue of controlling air pollution from ships, particularly harmful gases from ship exhausts, was initially addressed. However, during that period, it was decided not to incorporate any regulations regarding air pollution.

At that time, discussions on air pollution also took place in other contexts. The 1972 United Nations Conference on the Human Environment in Stockholm marked the initiation of active international collaboration in combating acidification or acid rain. Between 1972 and 1977, several studies affirmed the hypothesis that air pollutants could travel thousands of kilometers before causing deposition and resulting damage. This damage encompassed adverse effects on crops and forests as well.

At IMO, during the mid-1980s, the Marine Environment Protection Committee (MEPC) had been assessing the quality of fuel oils concerning discharge requirements outlined in Annex I, while concurrently discussing the issue of air pollution.

In 1988, prompted by a submission from Norway highlighting the magnitude of the problem, the MEPC decided to incorporate the issue of air pollution into its work program. Additionally, the Second International Conference on the Protection of the North Sea, convened in November 1987, issued a declaration wherein the ministers of North Sea states pledged to take action within appropriate bodies like the IMO to enhance the quality standards of heavy fuels and actively support endeavors aimed at reducing marine and atmospheric pollution.

During the subsequent MEPC session in March 1989, various countries submitted papers addressing fuel oil quality and atmospheric pollution. It was collectively agreed to include the prevention of air pollution from ships, alongside fuel oil quality, as part of the committee's long-term work program, commencing in March 1990.

In 1990, Norway submitted several papers to the MEPC providing an overview of air pollution from ships. The papers highlighted the following:

- Sulphur emissions from ships' exhausts were estimated at 4.5 to 6.5 million tons per year, accounting for about 4% of total global sulfur emissions. While emissions over open seas are dispersed with moderate effects, certain routes, including the English Channel, South China Sea, and Strait of Malacca, experienced environmental problems.

- Nitrogen oxide emissions from ships were estimated at around 5 million tons per year, constituting about 7% of total global emissions. These emissions contribute to regional issues such as acid rain and health problems in local areas, particularly harbors.
- Emissions of CFCs from the world shipping fleet were estimated at 3,000-6,000 tons - approximately 1% to 3% of yearly global emissions. Halon emissions from shipping were placed at 300 to 400 tons, or around 10% of the world total.

2.1. Adoption of Resolution

Discussions in the MEPC and drafting work by a working group led to the adoption, in 1991, of an IMO Assembly Resolution A.719(17) on the Prevention of Air Pollution from Ships. The resolution called on the MEPC to prepare a new draft Annex to MARPOL on the prevention of air pollution.

The new draft Annex was developed over the next six years - and was finally adopted at a Conference in September 1997. It was agreed to adopt the new Annex by adding a Protocol to the MARPOL Convention, which incorporated the new Annex. This approach allowed for specific entry into force conditions to be outlined in the protocol.

2.2. The Protocol of 1997

The Protocol adopted in 1997 (Tier I - MARPOL Annex VI, Regulations for the Prevention of Air Pollution from Ships) included the new Annex VI of MARPOL, which entered into force on 19 May 2005. It applies retroactively to new engines greater than 130 kW installed on vessels constructed on or after 1 January 2000, or that undergo a major conversion after that date. The regulation also applies to fixed and floating rigs and to drilling platforms (except for emissions associated directly with the exploration and/or handling of sea-bed minerals). In anticipation of the Annex VI ratification, most marine engine manufacturers have been building engines compliant with the above standards since the year 2000.

- MARPOL Annex VI sets limits on sulfur oxide and nitrogen oxide emissions from ship exhausts and prohibits deliberate emissions of ozone-depleting substances. The annex includes a global cap of 4.5% m/m on the sulfur content of fuel oil and calls on IMO to monitor the worldwide average sulfur content of fuel.
- Annex VI contains provisions allowing for special SOx Emission Control Areas (SECAs) to be established with more stringent controls on sulfur emissions. In these areas, the sulfur content of fuel oil used onboard ships must not exceed 1.5% m/m. Alternatively, ships must fit an exhaust gas cleaning system or use any other technological method to limit SOx emissions. The Baltic Sea Area is designated as a SOx Emission Control area in the Protocol. The North Sea was adopted as SOx Emission Control Area in July 2005.
- Annex VI also sets limits on emissions of nitrogen oxides (NOx) from diesel engines. A mandatory NOx Technical Code, defining how this shall be done, was adopted by the Conference under the cover of Resolution 2. The Annex also prohibits the incineration onboard ship of certain products, such as contaminated packaging materials and polychlorinated biphenyls (PCBs).
- Annex VI prohibits certain substances, including halons and chlorofluorocarbons (CFC´s), which, however, are not in the context of combustion engines and are therefore not considered further here.

The IMO emission standards are commonly referred to as Tier I...III standards. The Tier I standards were defined in the 1997 version of Annex VI, while the Tier II/III standards were introduced by Annex VI amendments adopted in 2008.

MARPOL Annex VI distinguishes between global and less stringent regulations on fuel quality and emissions, as well as a stricter limit for ships sailing in a so-called Emission Control Area (ECA). An

Emission Control Area can be designated for SOx and PM, or NOx, or all three types of emissions from ships, subject to a proposal from a Party to Annex VI.

Existing Emission Control Areas include:

- Baltic Sea (SOx: adopted 1997 / entered into force 2005; NOx: 2016/2021)
- North Sea (SOx: 2005/2006; NOx: 2016/2021)
- North American ECA, including most of US and Canadian coast (NOx & SOx: 2010/2012).
- US Caribbean ECA, including Puerto Rico and the US Virgin Islands (NOx & SOx: 2011/2014).
- Mediterranean Sea (SOx: 2022/2025).

The NOx emission limits of Regulation 13 of MARPOL Annex VI apply to each marine diesel engine with a power output of more than 130 kW installed on a ship.

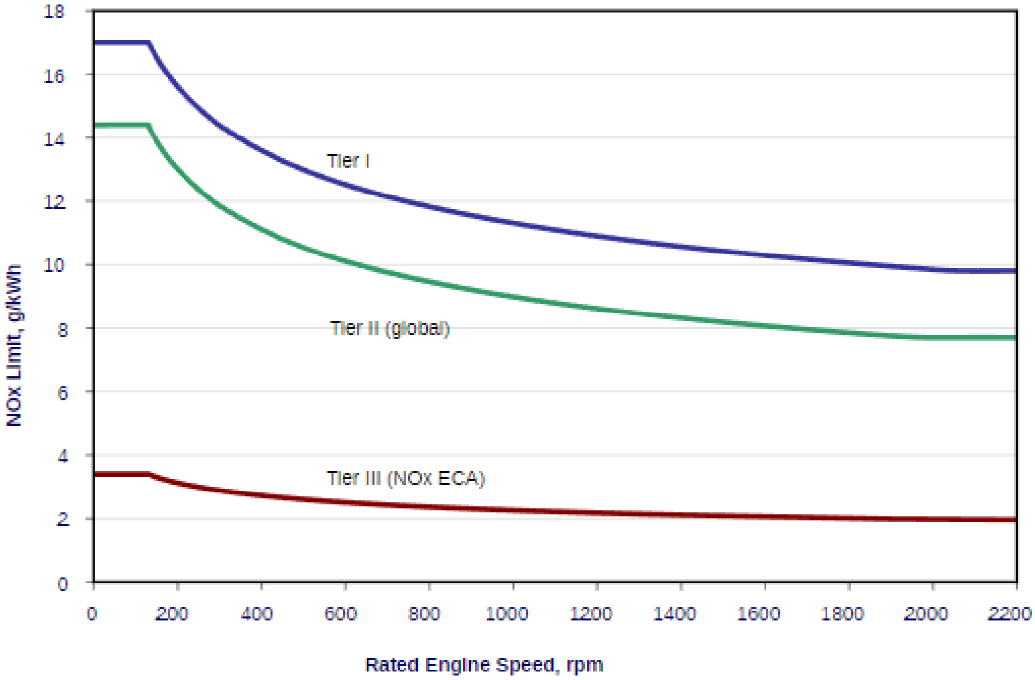

Fig.2: NOx limits determined by IMO

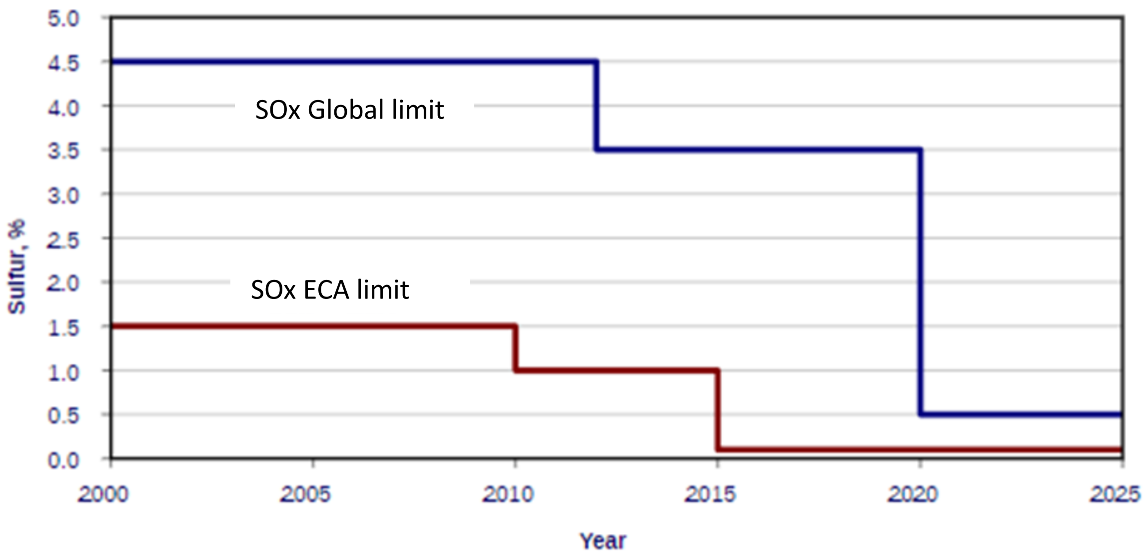

Fig.3: SOx limits determined by IMO

MARPOL Annex VI regulations include caps on the sulfur content of fuel oil as a measure to control SOx emissions and, indirectly, PM emissions (there are no explicit PM emission limits). Special fuel quality provisions exist for SOx Emission Control Areas (SOx ECA or SECA).

Coming to the final and most recent stage, the development of the regulation of greenhouse gas emissions from seagoing vessels. In 2011, IMO adopted first-time amendments to MARPOL Annex VI to mandate technical and operational energy efficiency measures to reduce the amount of CO_2 emissions from international shipping. This resulted in a series of measures.

- EEDI (Energy Efficiency Design Index) – came into force on January 1, 2013. EEDI applies to almost all seagoing vessels > 400 GT, providing a specific figure for an individual ship design, expressed in grams of carbon dioxide (CO2) per ship's capacity-mile and is calculated by a formula based on the technical design parameters for a given ship. The respective limit value decreases over a specified time interval. The EEDI is a performance-based mechanism that provides flexibility, allowing the industry to select the most suitable technologies for a specific ship design, rather than imposing specific technical requirements.
- EEXI (Energy Efficiency Existing Ship Index) came into force in January 2023 and also applies to vessels > 400 GT in an equivalent approach as EEDI. A technology-open approach is also followed here, and if technical adaptation of the vessel is required, the method of implementation is left to the owner or charterer. Possible measures include engine/shaft power limitation, waste heat recovery, wind assisted propulsion, etc.
- CII (Carbon Intensity Indicator) evaluates the operational energy efficiency of ships, utilizing data on fuel oil consumption obtained from the IMO DCS (Data Collection System) and the Ship Energy Efficiency Management Plan (SEEMP) as a management tool. CII assessment is obligatory for vessels with a gross tonnage of 5,000 and above. Ship operators must document and verify their annual operational CII against the specified benchmark. Initially, the annual carbon intensity reduction target mirrors business-as-usual levels until the regulation takes effect, followed by a 2% reduction target from 2023 to 2026. Further enhancement of reduction targets is slated for the period spanning 2027 to 2030.

3. Application of emission measurement systems in maritime from today´s perspective

In order to ensure compliance with the legal requirements mentioned in the previous chapter, the IMO has introduced appropriate measures to ensure compliance. These are described as follows:

NOx: (Nitrogen Oxides) emissions allowances for each ship depends on the engine type, year of build and other factors. NOx controls typically occur at the stage of engine installation. The test proceedings for each marine diesel engine > 130 kW are documented in detail in MEPC 177 (58) [Amendments to the Technical Code on Control of Emission of Nitrogen Oxides from Marine Diesel Engines] and shall be subject to the following surveys and test procedures:

1a) Engine R &D (Research and Development) on the engine testbed
1b) Pre-certification survey ensuring that the engine, stand-alone as designed and equipped, complies with the applicable NOx emission limit according to regulation 13. If this survey confirms compliance, the administration shall issue an Engine International Air Pollution Prevention (EIAPP) Certificate.
2a) Initial certification survey, conducted on board a ship after the engine is installed but before it is placed in service. This considers all modifications, including any adjustments, since the precertification.
2b) Annual and Renewal surveys, conducted as part of a ship's surveys required to ensure the engine continues to comply fully with the provisions of this code.
3a) Monitoring to prove the effectiveness of exhaust gas aftertreatment systems.
3b) Surveillance as measure to prove / rate a vessels emissions behavior from an authority site.

Use cases	1. Engine testbed		2. On-Board Certification and Compliance		3. Real world operation & monitoring	
Test environment			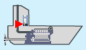			
Sub Use cases	1a Engine R&D	1b Parent Pre-Certification	2a Initial survey on-board	2b Annual & Renewal survey On-board	3a Monitoring	3b Surveillance

Description	Engine R&D	• Engine parent
		• Marine propulsion engine is tested to meet the NOx emission limit.
		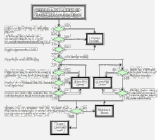
			• Each engine
			• NOx Verification
			  • **Engine parameter check**, or
			  • **Simplified measurement** method with mobile on-board sensors, or
			  • **Direct On-board measurement system.**
			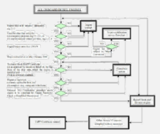
				Compliance by periodic inspections and surveys.
				Passing it, the ship gets a 5 years valid "International Air Pollution Prevention Certificate".
				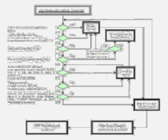
					Sulfur scrubbers pre- & post-scrubber SO_2 measurement to proof effectiveness	• On Board exhaust measureme
						• On-board plume measurement
						• Land-based Sniffer & Remote sensing
						• Land based plume effect to cit measurement and modelling
						• Plume by airplanes or drones
						• Satellite Monitoring

Responsible	Engine Engineering	Engine Engineering parent Pre-Certification or Engine manufacturer reference to parent Pre-Certification	• Engine manufacturer or • Ship manufacturer	ship operator	ship operator	Authorities/Research Institutes/Engine Engineering
Intervalls		Once at Pre-Certification	Once at final engine certification data an EIAPP is issued.	Annual, intermediate & renewal survey	Continuously or in intervals?	Periodical or unregularly during special campaigns

Fig.4: Application of emission measurement systems in the maritime industry

All the measures above do not require continuous exhaust gas measurement, but only a temporary measurement setup to prove compliance.

The only reason for applying continuous NOx emissions monitoring is the installation of a NOx aftertreatment system, such as Exhaust Gas Recirculation (EGR) or Selective Catalytic Reaction (SCR). This is to ensure that the SCR efficiency corresponds to the state at the time of certification regardless of ambient conditions, fuel quality or raw emission quality.

As direct and continuous measurement isn't obligatory during vessel operation, even when employing EGR / SCR systems, permanently installed NOx measurement systems are the rare exception.

SOx (Sulphur Oxides): Unlike NOx emissions, sulfur is not determined via certification procedures using measuring devices but can be derived directly from the Sulphur content of the fuel. However, an exception applies in the case of burning fuel with a high sulfur concentration and utilizing an Exhaust Gas Cleaning System (EGCS). If such aftertreatment devices are used, it's mandatory to install a direct and continuous emission measurement system on the corresponding vessel. The technical specifications for emission testing, including preferences, components, and accuracy, are thoroughly detailed in MEPC 130 (53) [Guidelines for On-Board Exhaust Gas-SOx Cleaning Systems]. Wash water being discharged must also be measured and recorded.

Features	Bunker Delivery Note	Bunker Tank Monitoring	Flow Meter (Coriolis)	Direct CO2 Measurement
Accuracy	Low	Medium	High	High
Consideration of residuals	No	No	Yes	Yes
Consideration of actual fuel quality (heat value and carbon intensity)	No	No	Conditionally	Yes
Consideration of fuel consumption over individual legs of the journey	No	Yes	Yes	Yes
Consideration of the specific consumer (ME, AE, Boiler)	No	No	Yes	Yes

Fig.5: Methods for IMO Data Collection System (DCS) according to MEPC 346 (78)

CO_2 (Carbon Dioxide): Analogue to SOx, the amount of emitted CO2 can be assigned directly to the amount of burned fuel by applying a dedicated correlation value. MEPC 346 (78) [Guidelines for the

Development of a Ship Energy Efficiency Management Plan] (SEEMP) - Chapter 7 provides several methods for measuring and / or logging fuel oil consumption according to IMO DCS (Data Collection System).

Like SOx, an optional direct measurement of carbon dioxide (CO2) via exhaust gas analysis is acknowledged as a valid methodology for DCS recording. However, unlike SOx, this isn't linked to the use of any aftertreatment system but can serve as a standalone alternative to fuel measurement. Fuel measurement would only be necessary in the event of a malfunction in the CO2 exhaust gas measurement system.

4. Typical Gas Emission Sensors and their Technical Principles

In the industry, a variety of emission measurement systems based on different principles of operation can be found, where each measurement principle conforms to the requirements of the measuring gas, the respective environmental parameters, and, finally, legislative requirements. An excerpt of the most commonly used measurement methods is described below.

Electrochemical Sensors (CO, O_2, NO_2, O_3): These devices utilize a chemical reaction to measure the concentration of a specific gas in an environment. There are many different applications for electrochemical sensors, and they continue to play an important role in various industries. In this blog post, we will explain the functioning of electrochemical sensors and some of the most common applications.

Electrochemical sensors operate by reacting with the relevant gas and generating an electrical signal that is proportional to the gas concentration. The sensor consists of two electrodes (a working electrode and a counter electrode) and functions by allowing charged molecules to pass through a thin electrolyte layer. Electrochemical sensors are used in a variety of applications and continue to play an important role in many industries; however, they are primarily used in measuring the quality of ambient air and only have a minor role to play in exhaust gas measurement. Here, the most well-known application is the function of the lambda sensor used for continuous in-vehicle O2 measurement ensuring the functionality of the catalytic converter.

Gas Chromatography (THC, NOX, N_2O, CO_2.): Gas chromatography is a laboratory-based technique used for analyzing complex mixtures of gases, mostly utilizing a Flame Ionization Detector (FID). The FID is based on the detection of ions formed during the combustion of organic compounds in a hydrogen flame. The generation of these ions is proportional to the concentration of organic species in the sample gas stream. It separates individual components of a gas sample based on their chemical properties and measures their concentrations accurately. GC is widely used for analyzing emissions from combustion processes and industrial sources.

Nondispersive infrared sensor (NDIR): The main components of an NDIR sensor are an infrared (IR) source (lamp), a sample chamber or light tube, a light filter and an infrared detector. The IR light is directed through the sample chamber towards the detector. In parallel, there is another chamber with an enclosed reference gas, typically nitrogen. The gas in the sample chamber causes absorption of specific wavelengths according to the Beer–Lambert law, and the attenuation of these wavelengths is measured by the detector to determine the gas concentration. The detector has an optical filter in front of it that eliminates all light except the wavelength that the selected gas molecules can absorb. In particular, lower initial investment costs speak in favor of this measuring principle, capable of monitoring a of the most relevant components, offering the option to modularly add hardware analyzers to expand the number of measured exhaust gas components.

Fourier-transform infrared spectroscopy (FTIR): Fourier Transform Infrared Spectroscopy (FTIR) is the applied technology to measure the concentration of gases in a sample. The gas sample interacts with infrared (IR) radiation emitted by a broadband source, such as a thermal emitter. The modulated IR radiation is directed onto a moving mirror in the interferometer. As the mirror moves, it generates an interferogram, representing the intensity of the IR radiation as a function of time. The interferogram is processed using Fourier transform to convert the signal from the time domain to the frequency domain. The resulting FTIR spectrum represents the absorption of IR radiation by the gases in the sample at different wavelengths. Each gas absorbs IR radiation at specific characteristic frequencies, corresponding to the vibrational modes of the molecular bonds present in the gas molecules. FTIR is the only technology that can measure a wide range of gases simultaneously. A typical emissions monitoring setup can measure simultaneously H_2O, CO_2, CO, N_2O, NO, NO_2, SO_2, HCl, HF, NH_3, CH_4, C_2H_6, C_3H_8, C_2H_4, C_6H_{14}, and CH_2O. In addition, FTIR CEMS systems can be fitted with an external and oxygen analyzer to measure O_2. This method offers the highest accuracy and reliability of all known emission testing systems. This is mainly because it has been used for many years in the development of combustion engines for motor vehicles. A disadvantage is the higher investment cost due to a more complicated structure of the analyzer and the necessity to keep the whole system heated continuously.

5. Continuous Emission Monitoring Systems (CEMS)

CEMS are used as a tool to monitor the effluent gas streams resulting from combustion in industrial processes. CEMS are capable of measuring a certain range of typical exhaust gas concentrations aiming to control and optimize combustion, usually in applied industrial settings. They are also used as a means to comply with air emission standards such as the US Environmental Protection Agency's (EPA) Acid Rain Program, and other US federal emission programs, or state permitted emission standards. CEMS typically consist of analyzers to measure gas concentrations within the stream, equipment to direct a sample of that gas stream to the analyzers if they are remote, equipment to condition the sample gas by removing water and other components that could interfere with the reading, pneumatic plumbing with valves that can be controlled by a PLC to route the sample gas to and away from the analyzers, a calibration and maintenance system that allows for the injection of calibration gases into the sample line, and a Data Acquisition and Handling System (DAHS) that collects and stores each data point and can perform necessary calculations required to get total mass emissions. A CEMS operates at all times even if the process it measures is not active. They can continuously collect, record and report emissions data for process monitoring and/or for compliance purposes.

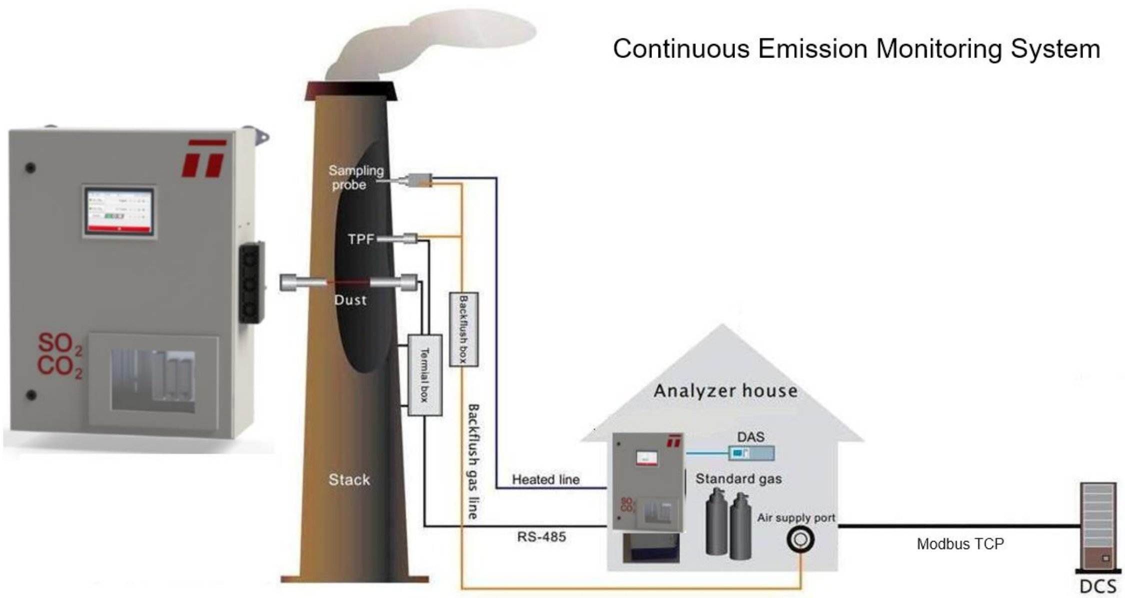

Fig.6: Example of CEMS in an industrial application

5.1. CEMS - Requirements for installation on a seagoing vessel

Emission measurement systems are widely used in industry, providing reliable data for the quality of combustion, mainly for industrial furnaces, reciprocating piston engines and gas turbines. They equally serve to protect the environment and the population from the impacts of poor air quality. Nowhere is exhaust gas measurement as widespread as in the automotive industry, where it is an integral part of powertrain development and is mandatory for both certification and surveillance monitoring. A large number of legislative requirements from different national communities and countries not only define permissible limit values but also clearly determine the measuring methodology, specifications and accuracy of the measuring devices used, as well as the processes for maintenance and calibration. Due to the complex exhaust aftertreatment required, involving successive units such as oxidation catalyst (CO), Lean NOx Trap, Particulate Filter (PM), and selective catalytic converter (NOx), especially in diesel engines, not only are a variety of different systems required for determining gaseous and solid exhaust components, but also sampling points from the raw exhaust to the tailpipe with corresponding piping systems must be installed on the respective engine testbed.

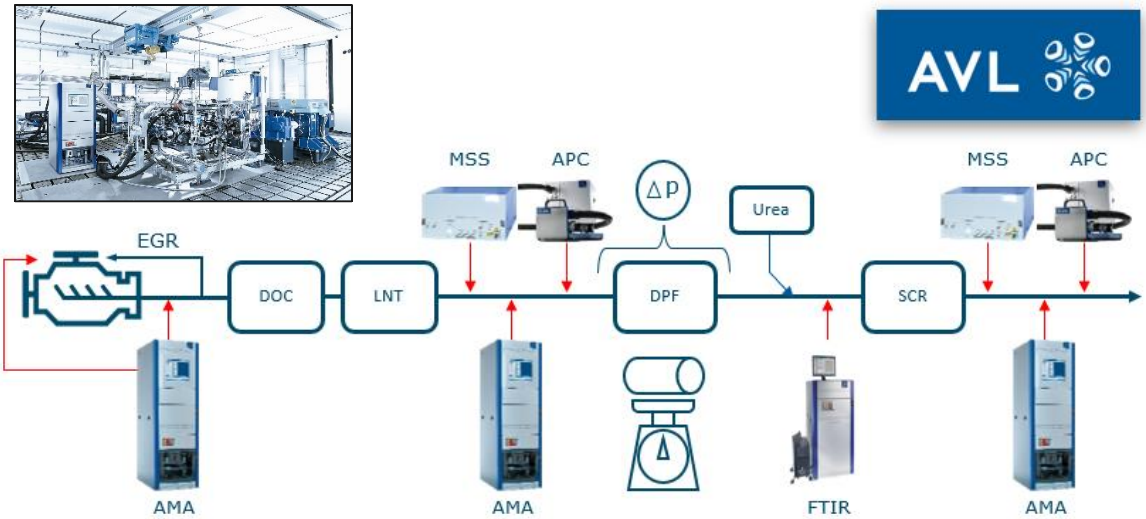

Fig.6: Typical dynometer setup for Emission measurement on an automotive Diesel engine

Aside from high investment and operating costs, the latter caused by the provision of energy and resources (e.g. reference gases), such test setups are maintenance intensive. Therefore, automobile manufacturers maintain a dedicated maintenance and repair team exclusively for this type of measurement technology. Due to sensitivity to environmental influences, measuring instruments are installed in a separate room outside of the test bed. Unlike with a CEMS system, the measurement is discontinuous and only occurs for the duration of the certification drive cycle, typically not exceeding 30 minutes (Worldwide Harmonized Light Vehicles Test Procedure, WLTP).

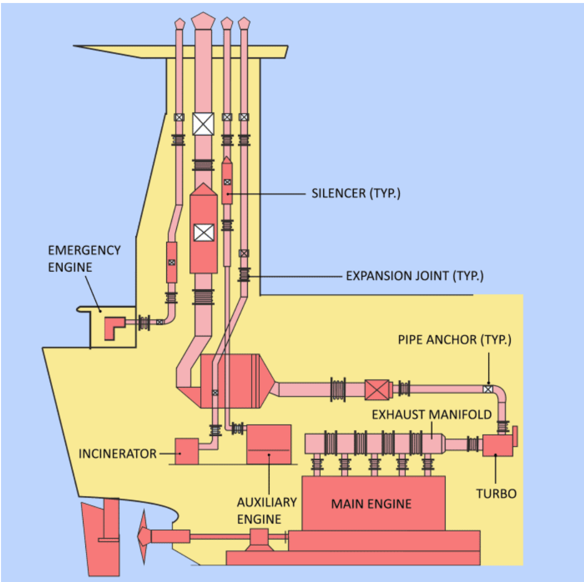

Fig 7: Design of a vessels Exhaust Gas System

The challenges of installation on a sea-going vessel are, as you might expect, complex and begin not least with the size and the system and the associated requirements for the infrastructure of the system - laying the measuring tubes to be heated and installing the sampling points. A ship can have between 3 and 7 combustion systems on board, which must be taken into account in a holistic view of emissions, because only emergency power systems may be excluded from the consideration. Another challenge is to ensure low-maintenance operation, even under the significantly more difficult operating conditions compared to the automotive test field, namely the significantly higher flue gas and particle content in the raw exhaust gas, especially when operating the combustion systems with heavy fuel oil.

Special attention must be paid to the design of the sampling point as well as the filter and automated back-flushing principle. Finally, the system is expected to provide a high level of operational reliability with low maintenance requirements, not least under the assumption that the system must continuously record measurement data from all combustion systems on board at a specified sampling rate. This poses the greatest challenge to the measuring unit itself, as it must be installed close to the flue gas ducts in the chimney and is exposed to dust, vibration and air pressure fluctuations due to high temperatures.

5.2. CEMS - Sound arguments for installing a CEMS onboard a ship

As summarized in Chapter 3, the installation of a continuous emissions monitoring system on a seagoing vessel is only a prerequisite if it also serves to monitor an exhaust gas purification system. Nevertheless, there are good reasons to establish such a system, not least in the context of the recently introduced CO2 reporting for CII compliance and the EU Emissions Trading System (ETS). In addition, the increasing emphasis on holistic ship and fleet optimization for economical and efficient ship operation motivates a closer examination of the enthalpy flows of the ship, in which the exhaust gas of the combustion units has a major share. These are summarized as follows:

- Future-proof Emission and Efficiency Reporting
  Reporting tasks are taking over a more and more important role for the crew. Ultimately, it is not just a time-consuming but also error-prone routine that the crew has to manage, which in the end takes away time for fulfilling more value-added tasks. An automated, certified, and standardized data logging and reporting system, such as for IMO DCS data collection, streamlines daily operations and results in more accurate and traceable measurement data. The direct measurement of the CO_2 mass flow in the exhaust gas has the additional advantage that, unlike determining it through correlation with the fuel mass, it only considers the hydrocarbon that has actually participated in the combustion. HFO contains between 2-3% non-combustible components, which are expected to positively influence the balance. Furthermore, both fluctuations in fuel quality/energy content and inaccuracies in the stated bunker delivery notes are herewith prevented. Unlike flow meters, reporting emissions of pollutants and greenhouse gases based on exhaust concentration and volume flow is not dependent on the fuel used and can function with high accuracy even with blends of multiple fuels.

- Holistic Performance Monitoring
  The introduction of EED, EEXI, and CII served, not least, to focus on and optimize the efficiency of a vessel's operation. The exhaust gas analysis, under the premise of not only qualitative but also quantitative consideration of emissions and the consequently derivable exhaust enthalpy flow, complements the previously used measurement methods consisting of measurement of fuel consumption, propeller shaft power, and of electrical energy. Last but not least, with this addition, it is herewith possible to validate individual measurement systems against each other and thus assess their quality. The utilization of the CO_2 exhaust mass flow is excellent for real-time-based route optimization tools due to its high sampling rate.

- System Monitoring
  With the resulting availability of a comprehensive data package, which opens new opportunities for developing analysis algorithms for decision support tool providers, the crew is able to better

monitor onboard systems and swiftly identify and resolve issues with their assistance. Additionally, the data can be forwarded via Ship to Shore / connections and Application Programming Interfaces (API) and be shared with vessel operator and optionally accessed by OEM´s of the respective combustion systems to allow for proactive intervention in case of data outside the tolerance range, thus preventing system failures.

6. Conclusion

The purpose of this paper was to outline the requirements as well as the added value of installing a continuous exhaust gas measurement system (CEMS) on a seagoing vessel. As a basis, a differentiation was first made between air pollutants and greenhouse gases, and the components and their effects on the environment were discussed in detail.

Although the legal requirements for air pollution control and those implemented by the IMO are complex and have been further amended and elaborated over the years, they also form the basis for understanding the added value of such a system in particular and have been elaborated accordingly in this document.

Another fundamental aspect for technical understanding is the consideration of different analyzer systems that can be used for emissions measurement systems. The respective characteristics of these systems have been examined and analyzed, resulting in the conclusion that particularly the non-dispersive infrared sensor (NDIR) and Fourier-transform infrared spectroscopy (FTIR) represent the most suitable measurement principles for a system on board.

CEMS have been established in the industry for a long time and are also known in the maritime sector for their role in monitoring desulphurization systems (aka Scrubber). However, they differ fundamentally from the high-precision, technically sophisticated and comparatively maintenance-intensive emission measurement systems that are used in automotive powertrain development, to refer as an example. By using these as a reference, the differences and in requirements, particularly in terms of operational reliability and low maintenance even under difficult operating conditions, can be highlighted.

The actual target consideration, namely the value of a CEM system in operation on a seagoing vessel, has been elaborated in three main pillars: Efficiency Reporting, Performance Monitoring, and System Monitoring. Each of these pillars plays a significant role in optimizing operational efficiency as well as strategic fleet management.

As an important element not only for emissions, but also for energy balancing as part of a holistic performance monitoring system, a CEM System has the potential to provide clearly reliable information on the health status of the individual combustion unit. In combination with maritime IoT systems, the provision of data via onshore API to the expertise of providers of decision support and optimization tools that apply their knowledge using intelligent methods and algorithms, the system is empowered to unveil its full potential.

Acknowledgement

The author would like to express gratitude to Patrick Ulmerich from AVL Analytics Technology for his extensive support in the development of this paper.

References:

JAHNKE (2000), *Continuous Emission Monitoring*, John Wiley & Sons Inc.

How to Consistently Select the Right Ship Performance Model in a Fleet with Mixed Data Availability

Camille Colle, Toqua, Gent/Belgium, camille@toqua.ai
Casimir Morobé, Toqua, Gent/Belgium, casimir@toqua.ai
Lukas Demey, Toqua, Gent/Belgium, lukas@toqua.ai

Abstract

Modeling ship performance can be done in many different ways. The spectrum includes purely theoretical formulas, purely data-driven models, and everything in between. With different data available for different vessels, how does one make the right choice for a whole fleet? This paper proposes a framework to select the best model in a consistent way, over a whole fleet where certain vessels may or may not have sea trial data, model tests, noon reports, sensor data, etc.

1. Introduction

Efficiency gains are the go-to answer to reach short-term decarbonization targets in shipping. To capture these efficiency gains, accurate speed-fuel models of vessels are a prerequisite. The challenge of creating accurate speed-fuel models - also called ship performance models - holds many layers of complexity from a theoretical point of view: different speeds, different drafts, different weather conditions, changing hull performance, changing engine performance, etc. However, in recent years the rise of sensor data and data-driven modeling has shown great promise to overcome these theoretical challenges, *DeKeyser et al. (2022)*.

Unfortunately, today, the potential of applying data-driven technologies such as machine learning to ship performance modeling remains largely untapped in the maritime industry. Not due to theoretical reasons, but for practical reasons. There's too much heterogeneity in the data across a fleet for a single type of data-driven model to provide consistently great results. As a result, simpler, traditional approaches are used to ensure consistency. This leaves the potential of big data and machine learning on the table.

This paper explores a practical framework to capture the full modeling potential across a data-heterogenous fleet, to always deliver the best model possible given the available data.

2. Heterogeneity in ship performance data across a fleet

There is an endless list of causes for heterogeneity in performance data. This paper initially focuses on a single cause for heterogeneity: different data types (public data, design data, noon report data, sensor data). After tackling heterogeneity due to different data types, section 6. explores three additional sources of heterogeneity and how orchestrations can overcome them. Many other sources of heterogeneity remain undiscussed within this paper, as it would lead us too far. This paper identifies 4 fundamental 'types' of data that can be used to model vessel performance:

1. Sensor Data (SD): High-frequency data collected onboard using sensors
2. Noon Reports (NR): Daily manual reports
3. Design Data (DD): Sea trial curves, shop tests, etc.
4. Public Data (PD): Anything that can be publicly retrieved based on IMO number such as vessel type, DWT, LOA, etc.

This paper assumes a fleet of 10 vessels with mixed data types according to the randomly selected distribution in Table I. For some vessels only a single source of data is available, for others there can be multiple sources of data. The goal is to represent a realistic amount of heterogeneity as can occur operationally in the industry today. Public data is left out of scope.

Table I: Data scenarios

Vessel ID	Design Data Available	Noon Report Data Available	Sensor Data Available
V1	X	X	
V2		X	
V3	X	X	X
V4		X	X
V5	X		
V6	X	X	X
V7		X	X
V8		X	X
V9		X	
V10			X
Coverage	4/10	8/10	6/10

3. Different model options

Different data types require different modeling techniques. Design Data (DD) is typically combined with traditional formula-based and filter-based approaches (ISO15016, DNV VTI). Noon Reports (NR), due to their operational nature, can be valuable for assessing different conditions and tracking performance changes over time. Yet, extreme caution is required when using NR data for data-driven techniques given the data is infrequent and error-prone, *Collé and Morobé (2022)*. Sensor Data (SD) is suitable for data-driven techniques such as machine learning, but always requires extreme caution to safeguard data quality.

This paper applies the following techniques to the following scenarios:

1. Design Data: Seatrial data and Main Engine Shop Test data are combined using a variation of ISO15016 that allows for the modeling of different operational conditions.
2. Noon Reports: A combination of physics-based and data-driven methods.
3. Sensor Data: A proprietary version of physics-informed machine learning.

4. Validating model accuracy

To guarantee an objective and consistent way of evaluating model accuracy over different approaches, the 'Blue Modeling Standard' is applied, *Deschoolmeester and Morobé (2023)*. The most important details are summarized below:

1. What data is considered the ground truth?
   Sensor data with Speed-Over-Ground above 5 kn is used to validate model accuracy. Operational sensor data of good quality is available for all 10 vessels. Following the scenarios listed in Table I, sensor data is frequently not used to train the model. However, it is always used to validate model accuracy, to ensure consistent and representative results.

2. What model validation technique is used?

A fit-for-purpose k-fold cross-validation technique is applied, preventing leakage and guaranteeing independent and identically distributed random variables over the folds.

3. What relationship is modeled?
   Main Engine Fuel consumption is modeled using SOG (speed over ground) as input. Secondary variables such as draft and weather conditions are also used.

4. What time horizon is used for the accuracy?
   Daily. So the predicted daily consumption is compared to the actual.

5. What accuracy metric is used?
   Mean Absolute Percentage Error (MAPE) is applied at daily intervals. This combination is also referred to as 'MADPE' (Mean Absolute Daily Percentage Error). (See 'Blue Modeling Standard' for more details on the accuracy metrics.)

5. Consistently selecting the best option: results

With a system in place to continuously assess model accuracy against the latest operational data, it's possible to compare different modeling approaches for a single vessel, and then select the most accurate option. Table II does this for 10 vessels using different data types. If multiple options are available, the 'Orchestration' ensures the best model is selected and made operational.

Table II: Mean Absolute Daily Percentage Error (MADPE) per scenario

	Design Data-based	**Noon Report-based**	**Sensor Data-based**	**Orchestration**
V1	18%	9%		9%
V2		8%		8%
V3	13%	7%	4%	4%
V4		17%	6%	6%
V5	16%			16%
V6	26%	14%	9%	9%
V7		11%	5%	5%
V8		14%	4%	4%
V9		13%		13%
V10			5%	5%
Coverage	**4/10**	**8/10**	**6/10**	**10/10**
Avg. MADPE	**18.3%**	**11.6%**	**5.5%**	**7.9%**

It can be observed that 'orchestration' over different data types, for this specific case, has two major benefits. First of all, the coverage (=vessels that can be modeled) of the fleet increases to 10/10. Approaches based on only a single data type, would have to leave some vessels unserved. Secondly, the average accuracy also improves considerably. If we were to only use NR-based models because it has the largest coverage, the average daily error would be 11.6%. Because Orchestration enables to benefit from sensor data - when available - the error drops to 7.9% on average, and even to 5.5% on average for sensor-based vessels, while still guaranteeing a 10/10 coverage.

6. Other forms of orchestration to solve for heterogeneity

This section explores three other sources of heterogeneity present in performance data & performance modeling: changes over time, different modeling approaches, and data quality issues. It also suggests how orchestration can overcome these challenges.

6.1. Updates over time

The above exercise for different data types is an oversimplification, as it does not account for time. Over time, different data types become available, and for operational data sources such as NR and SD more and more data continuously becomes available. These changes over time in available data types and available data duration, will continuously alter what modeling approach is the most accurate one. As a result, the orchestration exercise above, should be repeated frequently, to ensure the best possible model is always available.

Fig.1 does exactly that for a vessel that initially only has Design Data, then gets access to Noon Reports after 2 weeks, and gets access to Sensor Data after 1 month. Every time a new data source becomes available, a more accurate model is deployed and used operationally.

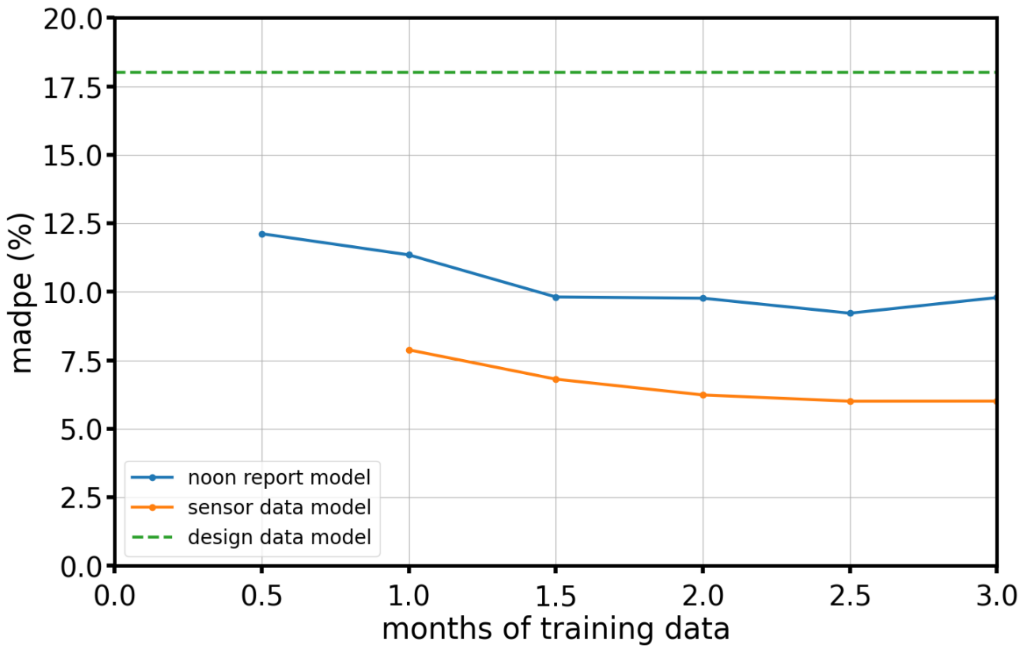

Fig.1: Model accuracy over time, as more data types become available

6.2. Different modeling approaches within the same data type

There is no single model that is always the best choice - even within a certain data type, the best modeling approach might differ depending on many factors. For example, sometimes it can be beneficial to use data over multiple vessels to improve modeling accuracy. Below we explore a case where the 'Augmented Approach' is applied, *Collé and Morobé (2022)*. This approach takes sensor-based learnings from similar vessels in the fleet, and transfers those modeling insights to vessels with only Noon Reports. This enables the creation of a model that is much more accurate than just a NR-based model, as it also incorporates the sensor-based insights from similar vessels in the fleet.

For the fleet of 10 vessels explored in this paper, 2 out of the 3 NR-based models can benefit from this different modeling approach. Meaning that this type of orchestration improves accuracy for those 2 out of 3 vessels, by leveraging the most suited modeling approach within that data type. As a result, even though there is only sensor data available for 6/10 vessels, eventually 8/10 vessels benefit from that sensor data. This allows the error to drop by 2% and 7% for those respective vessels, a meaningful improvement.

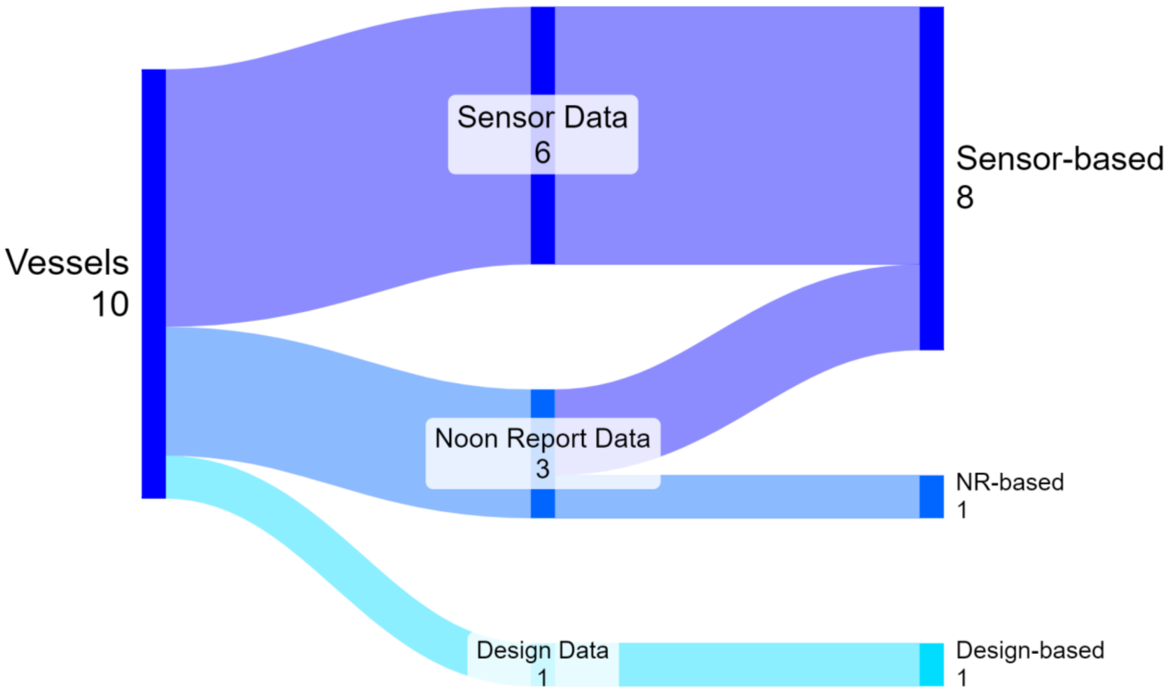

Fig.2: Vessel - data flow

Table III: Mean Absolute Daily Percentage Error (MADPE) per scenario

	Design Data-based	**Noon Report-based**	**Sensor Data-based**	**Orchestration**
V1	18%	9%		9%
V2		8%	*6%	6%
V3	13%	7%	4%	4%
V4		17%	6%	6%
V5	16%			16%
V6	26%	14%	9%	9%
V7		11%	5%	5%
V8		14%	4%	4%
V9		13%	*6%	6%
V10			5%	5%
Coverage	**4/10**	**8/10**	**6/10**	**10/10**
Avg. MADPE	**18.3%**	**11.6%**	**5.6%**	**7.0%**

6.3. Data Quality Issues

So far the table has always assumed the available data is free from data quality issues. But in practice, NR-data and Sensor Data are often plagued by data quality issues throughout time. If these are not flagged and resolved, this can have a very negative impact on model accuracy, *Colle et. al (2023)*. Below we assume a scenario where one vessel experiences unreliable noon report data, and another two experience unreliable sensor data.

Once the issues are detected, the best alternative modeling options are selected. For V1 with NR data quality issues, a Design Data-based model is selected instead. For V3 and V7 with sensor data issues, an NR-based model is selected instead.

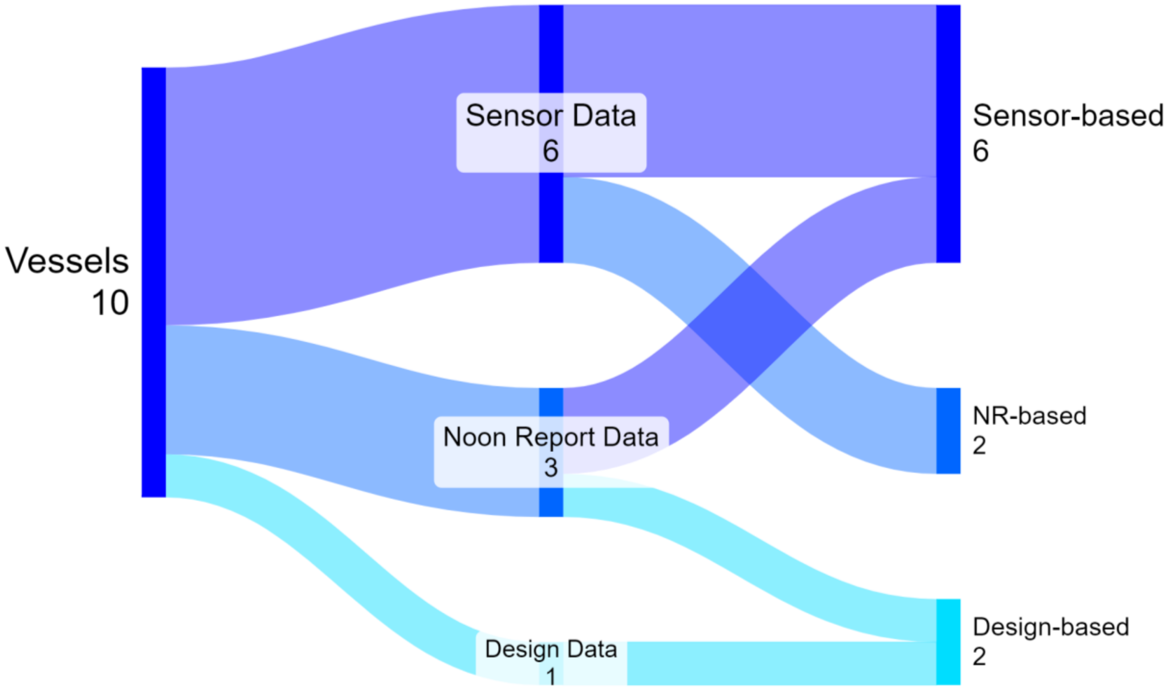

Fig.3: Vessel - data flow

If the data quality issues had remained undetected, it would have increased inaccuracy considerably for those specific vessels. For example, V3 would suddenly have an error of 20%. The average fleet error would have increased to 12.1%. After detecting the issues and redirecting to the best alternative modeling method with reliable data, the average error was reduced to 8.8%. For example for V3 specifically, the inaccuracy drops from 20% to 7%.

Table IV: Mean Absolute Daily Percentage Error (MADPE) per scenario

	Design Data-based	**Noon Report-based**	**Sensor Data-based**	**Orchestration**
V1	18%	**31%		~~31%~~ 18%
V2		8%	*6%	6%
V3	13%	7%	**20%	~~20%~~ 7%
V4		17%	6%	6%
V5	16%			16%
V6	26%	14%	9%	9%

V7		11%	**18%	~~18%~~ 11%
V8		14%	4%	4%
V9		13%	*6%	6%
V10			5%	5%
Coverage	**4/10**	**8/10**	**6/10**	**10/10**
Avg. MADPE	**18.3%**	**14.4%**	**9.3%**	**~~12.1%~~ 8.8%**

7. Results

In Table V, we compare the effect of all the different types of orchestration. The first column describes the outcome of an approach based only on Noon Reports - achieving mediocre accuracy and being unable to create models for all vessels within the fleet. The orchestration of different data types, has a big effect and reduces the average daily error from 11.6% to 7.9% over the mixed fleet assessed in this paper. The second type of orchestration enables to leveraging of different modeling types within a single data type, and reduces inaccuracy by 0.9% on average across the fleet. The third type of orchestration handling data quality issues reduces the inaccuracy by 3.3%. It's important to stress this paper considers only a very limited amount of very simple orchestration processes. There is much more potential in more numerous and more advanced processes to tackle heterogeneity.

Table V: The different types of orchestration

	No Orchestration (NR-based models)	**Orchestration v1 (Data Type)**	**Orchestration v2 (Model Type)**	**Orchestration v3 (Data Quality)**
Coverage	8/10	10/10	10/10	10/10
Before	11.6%	11.6%	7.9%	12.1%
After	11.6%	7.9%	7.0%	8.8%

8. Conclusion

This paper explores the potential of orchestration to tackle the heterogeneity present across performance data and modeling approaches within the domain of ship performance modeling. Even though within this paper only a few sources of heterogeneity are addressed and fairly simple orchestration solutions are proposed, the benefits are clear. To capture the full potential of the data across a fleet, one must look beyond a single modeling approach and data type, and develop a holistic fleet-wide approach that's able to address and overcome the different sources of heterogeneity. Otherwise, the potential of sensor-derived big data and machine learning to decarbonize the shipping industry will remain a theoretical construct.

References

COLLE, C.; DESCHOOLMEESTER M.; MOROBÉ, C. (2023), *STW or SOG as a Starting Point for Performance Modeling? An Empirical Study using Operational Sensor Data from 20 Oil Tankers*, 8th HullPIC Conf., Pontignano, https://toqua.ai/whitepapers/sog-or-stw-as-a-starting-point-for-performance-modeling

COLLE, C.; MOROBÉ, C. (2022), *Saving AI from its own hype: Getting real about the benefits and challenges of machine learning for ship performance modelling aimed at operational optimizations*, 7th

HullPIC Conf., Tullamore, https://toqua.ai/uploads/default/HullPic2022_Toqua_Proceedings.pdf

DEKEYSER, S.; MOROBÉ, C.; MITTENDORF, M. (2022), *Towards Improved Prediction of Ship Performance: A Comparative Analysis on In-service Ship Monitoring Data for Modeling the Speed-Power Relation*, https://arxiv.org/pdf/2212.13061.pdf

DESCHOOLMEESTER, M.; MOROBÉ, C. (2023), *Blue Modeling Standard: a Benchmarking Methodology for Ship Performance Models*, Whitepaper, Toqua, https://toqua.ai/whitepapers/how-to-compare-different-ship-performance-models

ISO (2015), *ISO 15016:2015 - Ships and marine technology — Guidelines for the assessment of speed and power performance by analysis of speed trial data*, Int. Standard Org., Geneva

Quantifiable or Tenet-Based Gains: An Empirical Study on the Performance of Energy Efficiency Technologies Retrofitted on Containerships

Dimitris Georgousis, Vessel Performance Solutions, Lyngby/Denmark, dge@vpsolutions.dk
Mads Martinsen, Mærsk Mc-Kinney Møller Center for Zero Carbon Shipping, Copenhagen/Denmark, mads.martinsen@zerocarbonshipping.com
Martin Köpke, Hapag-Lloyd AG, Hamburg/Germany, martin.koepke@hlag.com

Abstract

The maritime industry's decarbonization journey necessitates a fundamental shift away from conventional fuels, foreseeing a future with a burgeoning demand for renewable energy sources, especially in green fuel production. While green fuels are essential, it is the combined effect of their use and reduced energy demand from global shipping by being more energy efficient which is needed to reach the revised International Maritime Organisation's (IMO) green-house gas (GHG) emission reduction ambitions. This paper accentuates the importance that best practices exist to mitigate challenges faced in widening, and accelerating, the adoption of energy efficiency measures, that is mainly used by a certain part of the industry. The challenges impeding rapid adoption of energy efficient technologies (EETs) include uncertainties in operational performance and a clear procedure for benefit tracking, that can help de-risking the investments and increase confidence in the energy abatement through EETs. This paper proposes a benefit tracking procedure and applies it to operational performance data of 11 containerships of three different vessel classes receiving retrofits of different types of packaged EETs. Calculated benefits are presented in aggregated formats demonstrating how varying speed and draft show that improved efficiency is achieved when operational profile correlates with the design points of the EET(s) and provides insights into the empirical advantages of EET implementation. The paper attempts to be a demonstration of performance of the studied EET retrofit packages, contribute to a more informed decision-making, and support an acceleration of the industry's adoption of energy efficient measures.

1. Introduction

In July 2023, the *IMO (2023)* took a significant step towards decarbonizing global shipping by adopting a strategy towards net-zero greenhouse gas (GHG) emissions by or around 2050. This strategy comes with clear milestones, including indicative checkpoints for shipping to meet in 2030 and 2040, and emphasizes the crucial role of energy efficiency in achieving long-term sustainability.

Major obstacles for the shipping industry's energy transition to reduce GHG emissions are the long lifespan of vessels, diversified operation at global scale, need for high energy density fuel, and low availability of alternative fuels and global production capacity. To bring alternative production sites online it demands significant investments into an energy supply chain that is associated with significant energy loss, but also competes with access to renewable energy sources. According to *Barcarolo and Hintze (2024)* 1 EJ saved at the propeller translates into at least 4 EJ less energy needed upstream at a production site excluding investment into electrical power production site (e.g. solar farms or wind turbine farms). The indirect path from energy source to conversion into energy carrier and finally to energy release at the propeller along with the other industry obstacles contributes to the "hard to abate" nature of the industry. This argues for the importance of focusing on solutions that deliver demonstrably positive results in ships' energy demand through implementation of energy efficiency measures. In the recent decade, a global fleet has seen sizable reduction in the operational speed. This results, usually, in saving potential from hydrodynamic improvement measures, such as propeller re-design or bulbous bow retrofit. Also, dry docking with proper hull treatment in form of full blasts and premium paints yield to higher energy efficiency. Usually, multiple different energy efficiency measures are implemented in parallel to reduce a vessel's energy efficiency and carbon footprint, such as slow steaming (operational measure) and retrofits of EETs (technical measure).

This paper presents an approach to benefit tracking and analysis using Vessel Performance Solutions' performance monitoring tool, called VESPER. The study is carried out as part of an industry project led by the Mærsk Mc-Kinney Møller Center for Zero Carbon Shipping, https://www.zerocarbonshipping.com/projects/shared-investment-and-benefits-in-retrofits-of-energy-saving-technologies/. Partial deliverables from this project are presented in this paper.

2. Background

The intensified emission regulatory landscape with recent introduction of carbon intensity index (CII), EU emission trading scheme (ETS), but also more competitiveness of vessels and cost leaders and increased awareness on supply chain emission footprint from customers, cargo-owners and freight forwarders sends a demand signal for ocean transportation to reduce its environmental footprint.

The increase of ship efficiency is one crucial level towards reducing GHG emissions as well as essential to align shipping with IMO's short-term GHG emission reduction ambition. In case of Hapag-Lloyd's net-zero emissions target in 2045, the decarbonisation strategy includes a large fleet upgrade program that retrofits more than 150 vessels.

One measure to reduce the carbon footprint is the widely used slow steaming. This means often that vessels sail at lower speeds than where they were initially designed for. Also, the introduction of the energy efficiency design index for existing vessels (EEXI) requires many containership vessels to reduce available engine power and, in some cases, consequently vessel speed.

The consequence is an increased potential for energy efficiency improvements. Re-design of bulbous bow and propellers are obvious energy efficiency measures to take to redeem improvement potential. However, attention must be given to adequate propeller and hull treatment during dry docking for a shipowner to expect his retrofit investments to realize the energy efficiency potential of his vessel. The efficiency gains from propeller upgrades are at risk to be neutralized by poor hull surface treatment practices during the dry docking, where a spot blast is chosen over a full blast.

However, all the above require investments, while at the same time their gains are only calculated and approximated ahead implementation. During operations savings depend on interaction between different energy efficiency measures trading on a diversified operational profile.

3. Ship representation

The methodology, which is presented in this paper was applied to three vessel classes, Table I, with

- Four vessels referred as 7,000 TEU class,
- Three vessels referred as 10,000 TEU class, and
- Four vessels referred as 13,000 TEU class vessels.

The 7,000 TEU class, built in 2008, at a time with lower fuel costs, the design specification was designed for high speeds, optimised for one design draft. However, due to changes in market requirements, environmental regulations and increased awareness, service speeds decreased significantly within the last decade. Consequently, the 7,000 TEU class operates at speeds significantly lower than its original design point offering a large saving potential from a re-design of the bulbous bow and propeller.

The 10,000 TEU class, built in 2016, is already designed for lower speed compared to the 7,000 TEU class. A decrease in operational speed profile of about 2kn lower than initial design also yields to optimisation potential for a propeller re-design.

The 13,000 TEU class, built in 2012/13, with an initial design for speed around 24kn. The class is already retrofitted with new propellers and bulbous bows in 2014/15, optimised for speed at 21kn. Despite this there is still saving potential of the class due further speed decreased in recent years. **Fehler! Verweisquelle konnte nicht gefunden werden.**The change of the operational profile is exemplarily illustrated for the 7,000 TEU class in Table II. Sailed speeds and drafts are far away from the initial design, hence a high potential for hydrodynamic optimisation.

Table II: Recent operational profile of 7,000 TEU class and initial design point (red square). Percentage of time sailed at draft and speed bins.

	Speeds [kn]				
Draft [m]	**14**	**17**	**20**	**23**	**26**
10	4%	17%	17%	0%	0%
12	5%	21%	14%	0%	0%
14	1%	11%	10%	1%	0%

3.1. EET retrofit types

Design requirements at the time of delivery were different, especially in terms of speed, for the three classes. Hence, different energy efficiency measures were considered for the different classes. Table III provides an overview of retrofitted EETs and dry dock hull treatment approach for the three classes. It applies that the type of coating system (self-polishing properties) is consistent between the 'ordinary dry dock and 'retrofit' dry dock, Fig.4.

Table III: Overview of dry dock hull treatments and EET installations

Class	Previous dry dock			Retrofit dry dock		
	Year	**Hull treatment**	**EETs**	**Year**	**Hull treatment**	**EETs**
7,000 TEU	2017	Full blast, premium coating	N/A	2023	Full blast, premium coating	Re-designed propeller, bulbous bow
10,000 TEU	2017	Newbuild, premium coating	N/A	2023	Spot blast, eco coating	Re-designed propeller w. PBCF
13,000 TEU	2017	Spot blast, premium coating	Re-designed propeller, bulbous bow	2023	Full blast, premium coating	Re-designed propeller w. PBCF

3.1.1. Bulbous bow modification

The lower operational speeds for the 7,000 TEU class mean that the bulbous bow's 'neutralizing' effect on the ship hull's wave generation is substantially less effective, hence a re-design is made on basis of the expected operational profile. The results of a thorough hull form optimization process with over 15,000 simulated designs converges at a slenderer and less protruding bulb with more than 10% reduction in wetted surface as shown in Fig.1 and Fig.2.

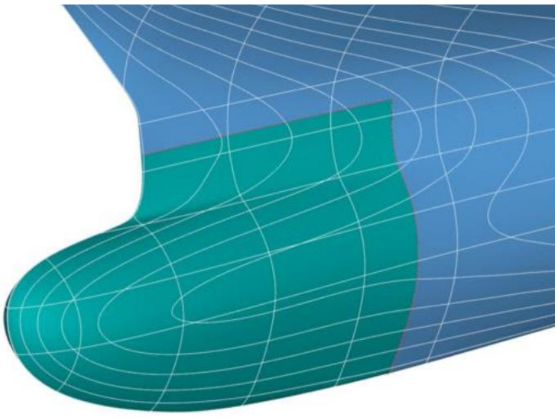
Fig.1: Bulbous bow initial design

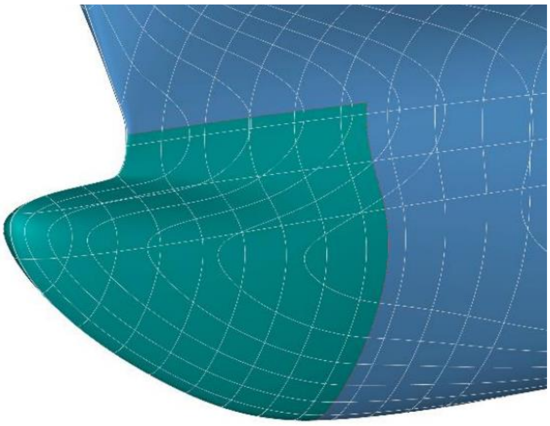
Fig.2: Bulbous bow optimised

3.1.2. Propeller redesign

The efficiency of a propeller is closely tied to its design and how well it matches the operational profile of the vessel. Propellers with smaller expanded blade area are often more suited to lower speeds due to their lower loading, reduced drag, and therefore a better compatibility with the vessel's operating conditions. Table IV compares the parameters of the initial and new propeller indicating a noticeable reduction in skew and expanded blade area ratio.

Table IV: Parameters of the initial and optimised propeller 7,000 TEU class.

Propeller Main Dimensions	Original Design	Redesign
Diameter	8,700 mm	8,700 mm
Number of Blades	5	5
Material	Cu3	Cu3
Pitch Ratio $(P=D)_{hyd}$	1.007	1.019
Expanded Area Ratio EAR	0.830	0.555
Skew	40.00°	28.1°
Hub Diameter Fwd $D_{H,fwd}$	1,730 mm	1,600 mm
Propeller Weight	81,665 kg	53,189 kg

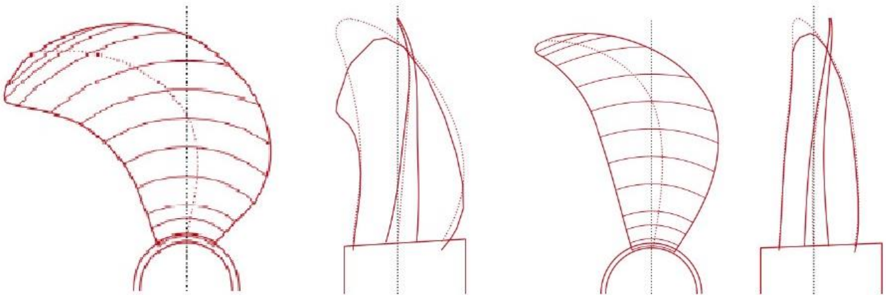

Fig.3: Initial (left) and redesigned (right) propeller design 7,000 TEU class

Fig.3 illustrates the shape of the redesign. Additionally, the propeller is equipped with boss cap fins. The total estimated saving for the propeller redesign is about 8% reduction in power demand.

4. Benefit tracking methodology

The methodology to determine the propulsion improvements from a single or a bundle of retrofitted energy efficiency technologies is based on comparing the vessel's performance during two separate periods. The first period is a time span after the ordinary dry dock prior to the dry dock of retrofit and the second period is a time span after the dry dock of retrofit, Fig.4. To have a fair comparison between the two benchmark periods certain governing assumptions should be true. These are described in Section 5. The improvement in performance due to the installation of energy efficiency technologies is calculated by:

$$\Delta P_{EET} = \frac{\bar{P}(t_1) - \bar{P}(t_0)}{\bar{P}(t_0)} \cdot 100\%$$

$\bar{P}(t_0)$ and $\bar{P}(t_1)$ refer to the average power in the period after the ordinary dry dock, t_0, and the period after the dry dock of retrofit, t_1, respectively.

In this study, a digital ship model (referred as model and described in Section 4.2) is used. It predicts a vessel's resistance in ideal conditions, e.g. no wind, no waves or other environmental impact, as a function of its mean draft and speed. Hereto, it also estimates the added resistance from waves, swell, wind speed, and seawater temperatures and density. Finally, it deducts the environmental forces from the measured shaft power to correct the performance observation to ideal condition, whereafter it is compared with the vessel's predicted delivered power in ideal conditions. This metric is known as added resistance (AR) and corresponds to the resistance increase due to hull and propeller degradation. The added resistance is expressed as:

$$\Delta AR[\%] = \frac{(R_{Dms} - \Delta R) - R_{id}}{R_{id}} \cdot 100\%$$

R_{id} is the calm-water resistance for the given mean draft and speed, which can be derived from sea trial speed/power curves, CFD simulations or towing tank self-propulsion test. Where R_{Dms} is the resistance corresponding to the measured delivered shaft power at a given operational condition under impact from environmental forces:

$$R_{Dms} = P_{Sms} \cdot \frac{\eta_S}{V_s}$$

P_{Sms} is the measured shaft power. η_S is the shaft efficiency of 0.99 for a conventional shaft. V_s is the ship's speed through water.

The resistance increase ΔR due to encountered environmental force is estimated to normalize the measured shaft power to a calm-water condition with no influence from wind, waves, and sea temperature, *ITTC (2021)*:

$$\Delta R = R_{AA} + R_{AW} + R_{AS}$$

R_{AA} is the added resistance due to wind, R_{AW} the added resistance due to waves, and R_{AS} the added resistance due to sea water temperature and density. Any resistance increase due to excessive rudder movement or shallow water can be included in ΔR, if the ship's deployment predominantly is in shallow water region. Alternatively, periods with intense rudder movement or shallow water can also be excluded from an analysis, provided the data is available. The calculation of added resistance along with conversion between shaft power measurements and corresponding resistance is carried out in VESPER, and details to the procedure is probatory rights of Vessel Performance Solutions.

4.1. Improvement impact and confidence interval

The impact of the retrofitted technology package is quantified by comparing the deviation in the mean added resistance for two time periods of equal duration; (1) after the previous dry dock denoted t_0 and (2) after the retrofit dry dock denoted t_1, see Fig.4. The comparison between the two periods of up to 4 months is chosen to minimize the probability for propagated fouling of the propeller and/or hull becoming an increased uncertainty when quantifying the impact of the retrofit. The added resistance for t_0 is averaged over the operational profile in the period:

$$\Delta\overline{AR}(t_0) = \frac{1}{N}\sum_{i=1}^{N} \Delta AR(t_0)_i[\%]$$

N is the number of performance observations in t_0. An equal weight is given to each performance observations irrespectively of the time duration it represents or its data source (manual noon report or high frequency auto-logged).

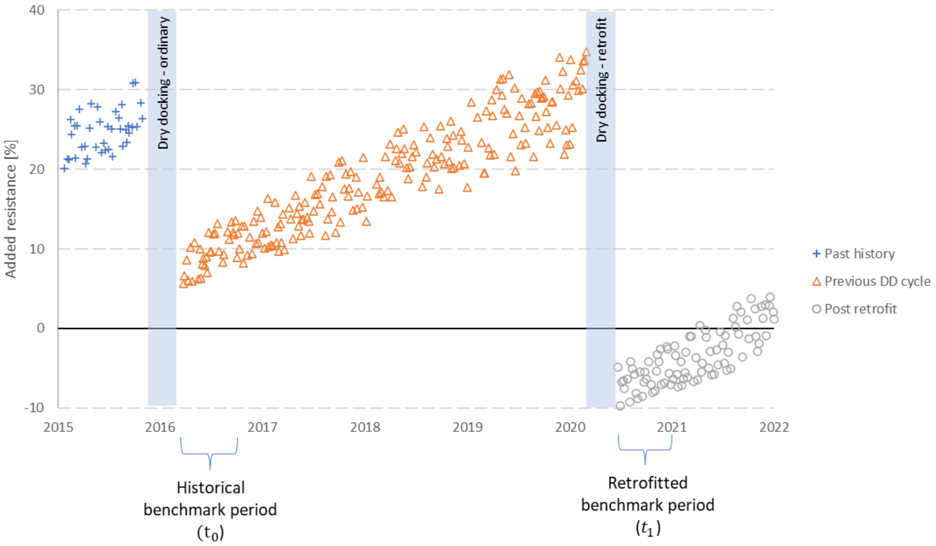

Fig.4: Schematic overview of added resistance calculated for historical performance observations and indication of the two periods use for performance benchmarking to determine the impact of retrofitted energy efficiency technologies.

The model represents the original ship design, and the added resistance is averaged to one value as it is assumed that there is no draft or speed dependency in the model for period t_0 (see Fig.5, Fig.6, and Fig.7 for model dependencies). On the contrary the model dependencies are expected to appear after the retrofit, and therefore the added resistance is averaged at several bin combinations of mean drafts, T_m, and ship speeds, V_s, of n number of performance observations in each bin for period t_1:

$$\Delta\overline{AR}(t_1, T_m, V_s) = \frac{1}{n}\sum_{i=1}^{n} \Delta AR(t_1, T_m, V_s)\ [\%]$$

The mean added resistance after the retrofit for each bin is converted into power reductions through VESPER where the $\Delta\overline{AR}_{bin}$ at each draft and speed bin combination is used calibration of the calm-water speed to power curves:

$$\Delta P\ (t_1, T_m, V_s, \Delta\overline{\mathrm{AR}}_{bin})[\%] = \frac{\bar{P}_{Did}(t_1, T_m, V_s, \Delta\overline{AR}_{bin}) - \bar{P}_{id}(t_0, T_m, V_s, \Delta\overline{AR}_{bin})}{\bar{P}_{id}(t_0, T_m, V_s, \Delta\overline{AR}_{bin})}$$

$\bar{P}_{Did}$ is the delivered power in ideal condition, i.e. no wind, waves, or other environmental impact, at the mean draft, T_m, and mean speed, V_s, for the respective draft- and speed bins.

A simple Student's z-test with a confidence interval is used to quantify the reduction in added resistance between the two time periods, t_0 and t_1. The z-test investigates the hypothesis that the mean of the two data samples is equal or different. Normally, an equal mean is the hypothesis and if it fails the alternative hypothesis is true. To verify that the retrofit had an effect and changed the mean from one data sample (t_0) to the other data sample (t_1), it is tested for the alternative hypothesis to be true. The impact is the difference between two means of the two data samples:

$$\Delta AR^{EET} = \left[\frac{1}{n_0}\sum_{i=1}^{n_0} \Delta AR(T_0)_i - \frac{1}{n_1}\sum_{j=1}^{n_1} \Delta AR(T_1)_j\right] \pm Z^* \sqrt{\frac{\sigma_0^2}{n_0} + \frac{\sigma_1^2}{n_1}}$$
$$= [\Delta\overline{AR}(T_0) - \Delta\overline{AR}(T_1)] \pm Z^* \sqrt{\frac{\sigma_0^2}{n_0} + \frac{\sigma_1^2}{n_1}}$$

The confidence interval is described with a confidence level of $C(95\%)$ resulting in a z-score $Z^* = 1.96$, since the data sample exceeds $n > 30$ and approximately follows a standard normal distribution. i and j are incremental performance observations in each data sample with the sample sizes n_0 for period T_0 and n_1 for period T_1. σ_0 is the standard deviation of the data sample. The standard deviation:

$$\sigma = \sqrt{\frac{\sum_{i=1}^{n}(\Delta AR_i - \Delta\overline{AR})^2}{n-1}}$$

$\Delta\overline{AR}$ is the mean added resistance of the sample of size n.

4.2. Digital ship model

A digital ship model (model) in the context of this study is a digitalized representation of the relationship between speed and draught in calm-water and associated resistance. This relationship is normally described with self-propulsion test carried out in a towing-tank test, by CFD simulations, or in sea trial results. Alternatively, it can be estimated with empirical methods e.g. *Harvald and Guldhammer (1974)*.

Before using the model in a benefit tracking context, that aims at quantifying the resistance or power reduction delivered by one or multiple energy efficiency technologies being retrofitted, it is recommended to inspect the prediction for speed or draft dependencies, which could originate from either the model or the data quality. Model evaluation should at least cover speed and draught dependencies at period t_0. This is to ensure that a change in mean added resistance, $\Delta\overline{AR}\%$, from the two time periods, T_0 and T_1, is not a result of model dependencies as the operational profile is likely to change after retrofit implementation. Speed or draught dependency is defined as a change in the trend corrected added resistance (TCAR) when draught or speed changes. TCAR is defined as the error of each calculated added resistance at each data point from the regression line for a given period of analysed events, e.g. dry dock cycle. It applies to a good model that TCAR is constant over the analysed speed and draught range during a longer time duration. Critically for the selected time duration is that performance observations cover a broad variety of speed and drafts.

Model dependency checks are done using performance observations for the time duration between the ordinary dry docking and the retrofit dry dock, Fig.4. The long time-duration allows for a significant data sampling across a diversified operational and trading pattern helping to improve model confidence. The type of retrofits considered in this study works in a way, that translates into speed and draught dependencies when analysis is done for period t_1. This dependency is the hydrodynamic improvements generated by the retrofitted energy efficiency technologies.

Pronounced speed or draught dependencies in the model should be adequately tackled by removing these dependencies before a model is used in a benefit tracking context. It is crucial that root-causes to model dependencies are understood not to introduce additional uncertainty to the benefit tracking results. Thus, to avoid these dependencies at the extremities of draught or speed, lower or upper limits in the digital ship model are imposed, resulting in exclusions of performance observations above or below such limits for the two periods.

A model zero (0) calibration of added resistance ($\Delta\overline{AR}(t_0) \approx 0$) for the period t_0 is not required, as a model bias will be present in both periods and can reasonably be assumed to neutralize with the relative comparison between the two periods.

The data source for added resistance calculations are based on both propulsion power and fuel oil consumption (FOC) acquired from torsion meter and flowmeter readings, respectively. The frequency of performance observations are daily manual noon reports and hourly aggregations of high frequency auto-logged measurements.

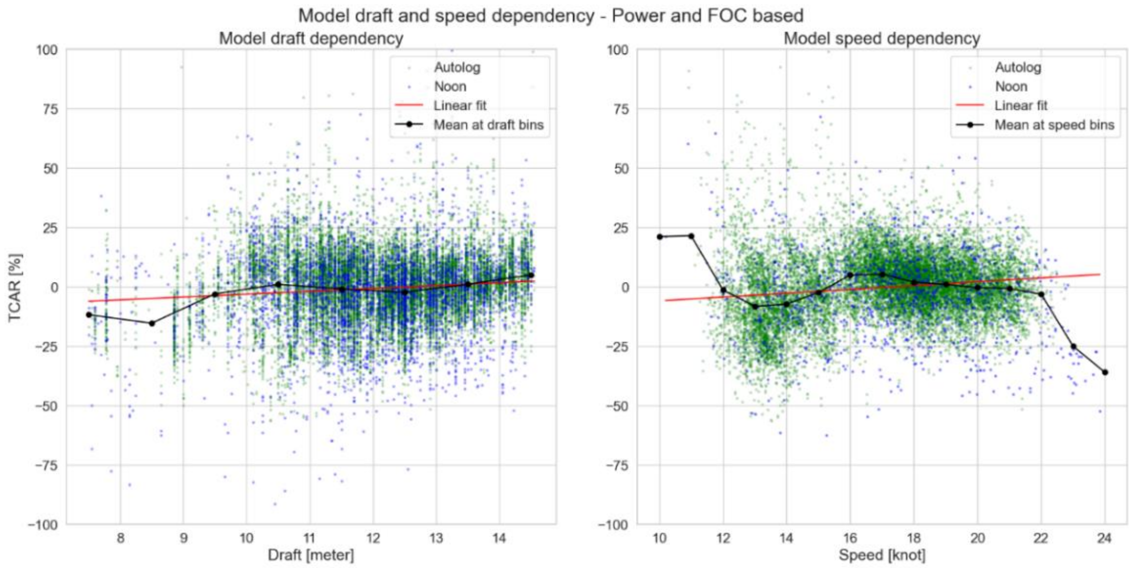

Fig.5: Model draft and speed dependency check of 7,000TEU class. Added TCAR% is calculated from torsion meter power and ME FOC readings from high frequency auto logging and manual noon reports.

Fig.5 gives a visual inspection of the model draft and speed dependencies for the 7,000 TEU class. A small degree of draft dependency occurs at drafts below 9 m, and speed dependencies shows at speeds below 12 kn and above 21 kn. Performance observations outside these limits have been removed from this study to increase model confidence.

Fig.6 shows the model draft and speed dependencies for the 10,000 TEU class, where lower and upper limits for draft is set to 8.0 m and 14.0 m and for speeds is set to 12.5 kn to 21.5 kn, respectively.

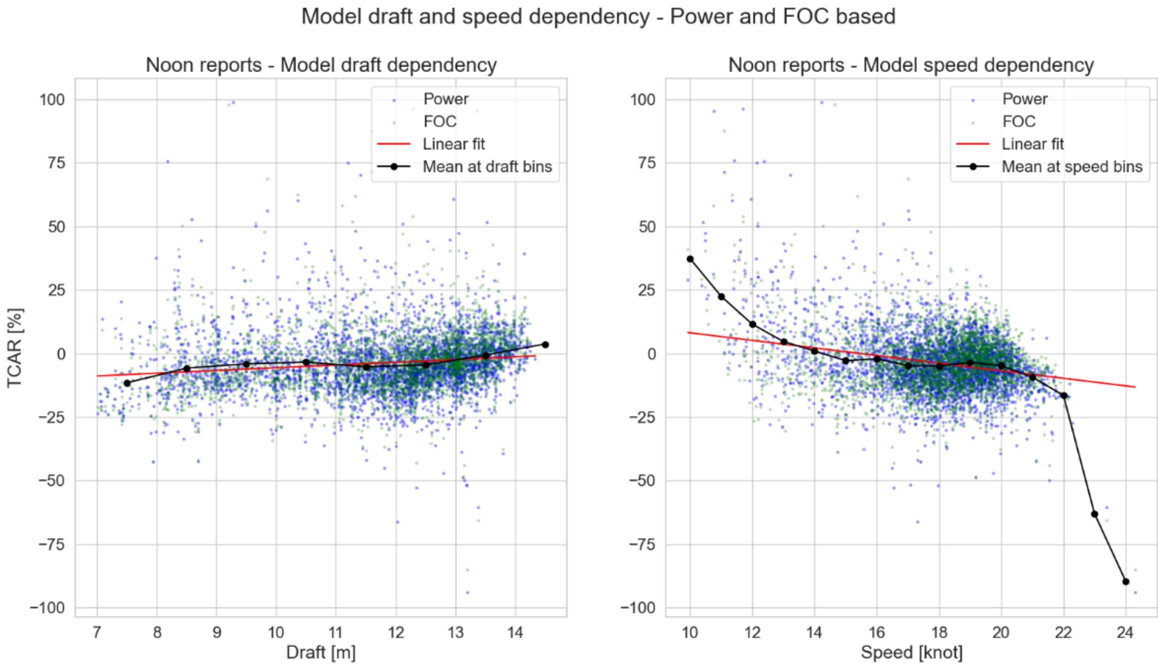

Fig.6: Model draft and speed dependency check of 10,000TEU class. TCAR% is calculated by use of torsion meter and ME FOC readings from manual noon reports.

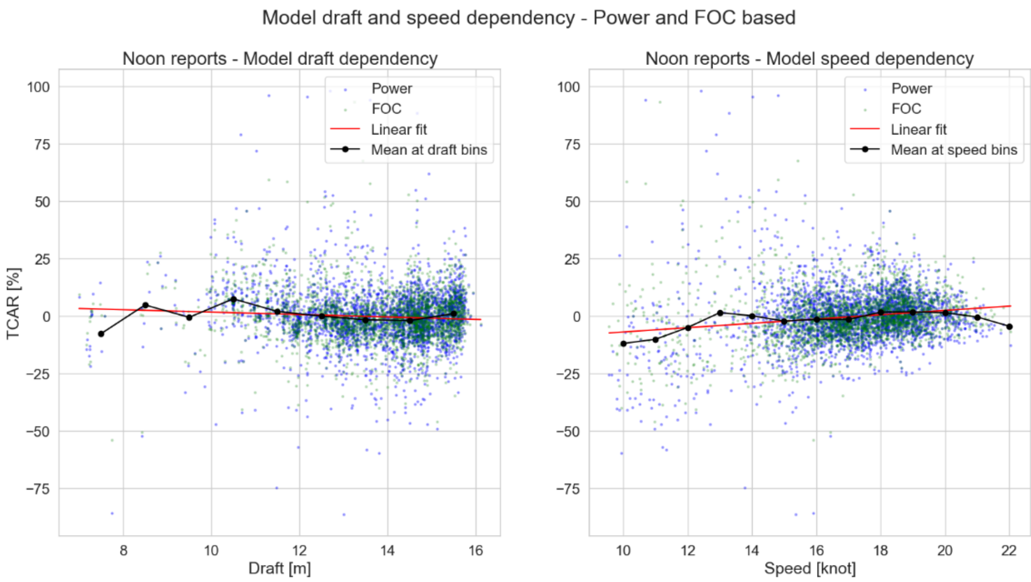

Fig.7: Model draft and speed dependency check of 13,000 TEU class. TCAR% is calculated by use of torsion meter and ME FOC readings from manual noon reports.

Fig.7 shows the model draft and speed dependencies for the 13,000 TEU class. The draught lower and upper limits was set to 12.0 m and 16.0 m, respectively. The speed ranges from 12.5 kn to 21.5 kn. In both cases model dependency at the extremities is catered for by excluding performance observations beyond these boundary values.

4.3. Data quality and data filtration

Due to uncertainties, both in modelling and data quality, it is unrealistic to fully eliminate scatter in the calculated added resistance result. However, to reduce scatter, filtration has been applied in both noon and auto-logged data. In the case of auto-logged data, there are periods of various unsteadiness in the signals caused by e.g. acceleration or deceleration in speed, strong gusts, corrupt signals etc. An algorithm based on the theory of probability of detection of a change in the mean and standard deviation to detect stable periods simultaneously has been applied, as described by *Montazeri (2019)*. Data, not fulfilling the following criteria, are removed from analysis in this study, as our experience is that inclusion of performance observations beyond these limits often are associated with increased uncertainty coming from violating the constraints of weather correction methods:

- Maximum Beaufort wind force scale up to 5 for wind and waves.
- Speed over ground (SOG) equal to or less than 12.5 kn, or beyond any lower or upper limits defined basis a model dependency check.
- Duration of noon reports equal to or less than 20 h.
- Main engine (ME) specific fuel oil consumption (SFOC) at a class level i.e. ME type.
- Reported distance (over ground) is deviating more than 5% from the distance (over ground) calculated by means of AIS positions.

Reduction in scatter improves the accuracy of the results, though biases due to low quality data are even more crucial. Data, either sourced from noon reports or auto-logged systems, can be biased due to uncalibrated sensors onboard. Thus, thorough filtration was applied from the authors to disregard inadequately calibrated speed logs, torsions, or flowmeters.

5. Governing assumptions

The benefit tracking methodology applied in this study is subject to multiple assumptions, as any performance monitoring methodology would be. The violation of assumptions will in most cases result in a poor baseline to measure improvement against, hence lead to erroneous results providing a wrong picture of the ‘true’ savings attained from certain EETs. Main assumption applicable for this study covers, but are not limited to these:

- Mechanical hull degradation effect on added resistance, e.g. caused by hull plate buckling or erosive welding seams, is not modelled and assumed unchanged for the period after the ordinary dry dock (t_0) and after the retrofit dry dock (t_1).
- Generalized wind resistance coefficient are representable to a containership with variable projected frontal and longitudinal areas because of different configuration of containers stowed on deck i.e. wind resistance is not adjusted for high or low number containers placed on deck.
- Hull and propeller treatment during dry docks are similar to each other i.e. full blasting of hull and hull roughness before paint and antifouling application is assumed comparable. In the case that full blasting of the hull is an added activity during the retrofit dry dock compared to the ordinary dry dock, it is then considered an integrated part of the EET retrofit package.
- The quantified savings are combined savings from the installed EET(s), and the quality of hull and propeller maintenance work carried out during the dry dock.

6. Data sourcing and frequency

This section elaborates on the data sources and frequency of data collection for the performance observation available for this study.

6.1. Manual noon report and high frequency auto-logging

The vessel classes analysed in this study reports performance observation as manual noon reports at a daily frequency. The reports consist of ~80 different observations, manually entered by the crew. Figures are read from onboard measurement equipment. The noon reporting is the least minimum which can be found on every ocean-going vessel. It collects various operational information, such as nautical, engine and weather-related data.

Additionally, to the noon reporting the vessels of the 7,000 TEU class are equipped a sensors-based data collection system that samples data a high frequency. Data measured by sensors and from the automation systems of the vessel include engine and nautical data.

6.2. Hindcast weather and AIS ship position

Reported weather is, within the experience of the authors, known to be unreliable for performance prediction for two reasons. Firstly, the crews’ frequently reporting of instantaneous weather at the time of the observation, though the averaged weather throughout the duration of a noon report is required. Secondly, even if the crew attempts to report the averaged weather, this is also frequently erroneous in the cases that the wind and wave direction is also varying during a noon report period. This issue is tackled by enhancing the noon reports with AIS positions data and introducing hindcast weather from weather forecasters. Detailed steps of this process are described by *Georgousis (2022)*.

7. Analysis

This section covers a presentation of the results using the described benefit tracking methodology on the three vessel classes that have been subject to retrofitting of EETs. The objective is to determine, to what extent the applied methodology can quantify a reduction in speed and power relationship because of re-designed propellers and/ or hull forms and simultaneously provide the corresponding reliability of these calculations.

7.1. Results of 7,000TEU class

The 7,000 TEU class is a slender and low block coefficient containership originally designed for service speed around 26 kn, that receives a redesigned bulbous bow and propeller optimized for a design speed around 18 kn. The results are presented in tabulated format where draft and speed bins are aligned with CFD analysis with the attempt to correlate benefit tracking results with design expectations. In addition, the results are also shown as a contour plot, Fig.8, basis the averaged draft and speed from performance observations captured inside specific bins.

The CFD-based improvement potential for the bulbous bow and propeller are presented in Tables VII and VIII, respectively. The results in Table VI show a noticeable reduction in power, consistent with the draft and speed dependencies observed in the CFD simulations, Table VII. The results indicate a fair correspondence in the magnitude of the results between the CFD simulation and benefit tracking results. However, this is not a suggestion that the potential power reduction from the redesigned propeller and bulbous bow simply can be extrapolated through linear superposition, as there will be interactional terms between the two hydrodynamic upgrades.

Table V: Reduction in added resistance percentage with confidence interval at 95% confidence level. Negative is reduction.

Difference in AR% after retrofit with confidence interval			
	Speed [kn]		
Draft [m]	**14**	**17**	**20**
10	-45±5	-26±3	-20±3
12	-39±4	-20±1	-18±2
14	-10±8	-14±2	-2±4

Table VI: Percentage reduction in shaft power across draft and speed bins. Negative is reduction.

Percentage (%) change in power after retrofit			
	Speed [kn]		
Draft [m]	**14**	**17**	**20**
10	-25	-17	-14
12	-23	-14	-13
14	-8	-11	-1

Table VII: Vendor CFD based power reduction potential of re-designed bulbous bow. Negative is reduction.

Percentage (%) power reduction of bulbous bow re-design			
	Speed [kn]		
Draft [m]	**14**	**17**	**20**
10	-25	-19	-12
12	-16	-12	-6
14	-5	-3	-3

Table VIII: Vendor CFD based power reduction potential of re-designed propeller. Negative is reduction.

Percentage (%) power reduction of propeller with PBCF re-design			
	Speed [kn]		
Draft [m]	**14**	**17**	**20**
10	-8.6	-8.9	-8.7
12	-8.7	-8.7	-7.9
14	-9.3	-8.8	-8.5

Fig.8: Contour plot with power reduction (%) in shaft power across draft and speeds

7.2. Results of 10,000 TEU Class

The 10,000 TEU Class is a containership originally designed for a service speed of 21 kn, with a new design speed targeted around 19 kn. Tables IX and XI shows the AR% and power reductions aggregated into single values, respectively, provided the assumption that the redesigned propeller, combined with a PBCF, is relatively independent of draft and speed variations, Table XI. Moreover, due to limited performance observations at inadequate quality and the lack of auto-logged data, there is a constraint on the number of observations at each discrete draft and speed combination. Therefore, at the authors' discretion, performance observations are aggregated into single values along the whole operational profile; one for reduction in shaft power and another for added resistance.

Table IX: Reduction in added resistance and associated confidence interval with 95% confidence level. Negative is reduction.

Difference in AR% after retrofit with confidence interval				
	Speed [kn]			
Draft [m]	**14**	**16**	**18**	**20**
10	-1.2±2			
12				
14				

Table X: Total (%) reduction in shaft power corresponding to added resistance reduction

Percentage (%) reduction in power after retrofit				
	Speed [kn]			
Draft [m]	**14**	**16**	**18**	**20**
10	-1.0			
12				
14				

Table XI: Vendor CFD based power reduction potential of re-designed propeller with PBCF for 10,000 TEU class. Negative is reduction.

Percentage (%) power reduction from propeller with PBCF re-design				
	Speed [kn]			
Draft [m]	**14**	**16**	**18**	**20**
11	-8.4	-7.8	-7.2	-6.6
12	-7.3	-7.4	-7.3	-6.9
13	-7.2	-7.2	-7.2	-7.2

The benefit tracking results shows a small reduction in power, Table X, being noticeable less than then the saving prediction from the CFD simulations, see Table XI. This is believed to be caused by an inconsistent hull treatment between the ordinary dry dock and the retrofit dry dock for 10,000 TEU class, also further discussed in Section 8.

7.3. Results of 13,000TEU Class

The 13,000 TEU class is subject to EPL and a re-designed propeller with PBCF allowing for a new top speed at 21 kn and new design speed of 18 kn at 14.25 m draft (optimization target). The results are presented similar to for the 10,000 TEU class with the same assumptions for one average reduction across draft and speed bins. The quantified shaft power reduction in Table XIII show good alignment with expected reduction potential stated in the Vendor's CFD simulations, Table XIV.

Table XII: Reduction in added resistance with confidence interval at 95% confidence level from retrofitted technologies. Negative is reduction.

Difference in AR% after retrofit with confidence interval				
	Speed [kn]			
Draft [m]	**14**	**16**	**18**	**20**
12.5	-8.5±2			
14				
15.5				

Table XIII: Total (%) reduction in shaft power corresponding to added resistance reduction

Percentage (%) reduction in power after retrofit				
	Speed [kn]			
Draft [m]	**14**	**16**	**18**	**20**
10	-6.9			
12				
14				

Table XIV: Vendor CFD based power reduction potential of re-designed propeller with PBCF for 13,000 TEU class. Negative is reduction.

Percentage (%) power reduction from propeller with PBCF re-design				
	Speed [kn]			
Draft [m]	**14**	**16**	**18**	**20**
13.0	-6.4	-6.5	-6.5	-6.7
14.25	-6.8	-6.7	-6.7	-6.7
15.5	-7.4	-7.4	-7.4	-7.6

8. Discussion and conclusions

Two key drivers contribute to the success of energy efficiency retrofits in shipping: data-driven decision making and business-oriented evaluation of EETs. While Computational Fluid Dynamics (CFD) studies are crucial for building the initial business case for certain types of EETs, their value lies in conjunction with robust benefit monitoring. This combination validates the effectiveness of chosen EETs and empowers data-driven optimization for future investments. The presented case studies demonstrate the importance of data gathering at relevant frequency, need for better data quality, continuous feedback to both data-driven processes and business decision-making processes for other business cases in similar or other vessel classes and types.

Assessing the 7,000 TEU class offered the most promising scenario due to both receiving full hull blasting and similar paint systems at both dry dockings, facilitating the most reliable comparison. Furthermore the 7,000 TEU class offered sufficient data due to high resolution data reporting.

However, limitations arose with the 10,000 TEU vessel due to limited noon reports, potentially restricting the data's ability to capture the full impact through the applied methodology. Additionally, the second dry docking of this vessel introduced a propeller redesign with spot blasting of the hull before applying paint, introducing an uncertainty when attempting to isolate the impact of each of the energy efficiency upgrades. The improvement of the redesigned propeller showed to be neutralized by the partial hull treatment during the retrofit dry dock, which points to the importance of deploying ‘basic’ energy efficiency measures before implementing more complex energy efficiency measures.

Analogously, data limitations affected the 13,000 TEU class, where hull treatment was spot blasting in the ordinary dry dock hindered clear differentiation between the effects of the new propeller and hull roughness, since the retrofit dry dock included hull full blasting. Due to this the quantified power reduction must be assigned to both hull full blasting and the new propeller as a total saving.

Despite these challenges, learnings emphasize the importance of comprehensive data collection strategies. Improving the quality of the reporting from the crew and expanding it with high frequency sensors data is believed to allow capturing of draft and speed dependencies, offering deeper insights into benefit tracking results of the 10,000 TEU class and 13,000 TEU class. By refining data collection and analysis approaches, the accuracy and granularity of the assessments can be improved, driving informed decisions for future EET investments, and maximizing the return on the sustainability efforts.

The 7,000 TEU class vessels provide a compelling example, showcasing the value of robust data collection encompassing coverage, source, and frequency. The findings establish a hierarchy of data requirements, highlighting the shift from basic compliance monitoring to performance assessment and, ultimately, rigorous benefit tracking.

However, the limitations encountered with the 10,000 TEU class and 13,000 TEU class underscore the importance of comparable conditions for accurate evaluation. Inconclusive results in these cases emphasize the need for comprehensive data sets across multiple dry docks to isolate the effects of individual EETs, as well as increased representation of good quality data across the class’s operational profile.

While one finding of this paper is strict requirements to data collection, for a period spanning from at least the retrofit dry docking to the ordinary dry docking event, and quality, there are nevertheless effects which hardly can be quantified accurately. One key challenge lies in mechanical degradation of hull performance over time. The initial smoothness at a vessel’s launch, will deteriorate due to various factors, making it difficult to isolate the true impact of EETs from this ongoing wear and tear. Furthermore, inconsistent dry dock treatment quality influenced by weather, humidity, and application techniques. Acknowledging these challenges and implementing standardized procedures and detailed documentation are crucial.

In conclusion, while this study validates the quantifiability of EET retrofits under strict data requirements and comparable conditions, it also highlights the challenges associated with limited data availability and mixed interventions, e.g. full blast vs. spot blast. Moving forward, a standardized data collection scheme ensuring comprehensive coverage and consistent high frequency will be fundamental in unlocking the full potential of EET retrofits, that can enable meaningful quantification of the improvements from retrofitted EETs by means of performance monitoring applications. By prioritizing rigorous data collection and analysis, the pathway to higher energy efficiency with higher confidence, maximizing the impact of investments and contributing to a cleaner future for ocean transport.

Acknowledgement

Thanks to the Hapag-Lloyd Fleet Upgrade Team for their support of this paper and their engagement to optimise the energy efficiency of the Hapag-Lloyd’s operated fleet. The authors are also grateful to the Mærsk Mc-Kinney Møller Center for Zero Carbon Shipping and Vessel Performance Solutions for allocating the resources for carrying out and composing this study.

References

BARCAROLO, D.; HINTZE, D. (2024), *Setting Sail on a Sustainable Course*, White Paper, https://cms.zerocarbonshipping.com/media/uploads/documents/MEPC_v8.pdf

GEORGOUSIS, D.N.M. (2022), *Improving Performance Prediction using Hindcast Weather and AIS Data*, 7th HullPIC Conf., Tullamore

HARVALD, S.A.; GULDHAMMER, H.E. (1974), *Ship resistance*, Akademisk Forlag

IMO (2023), *IMO Strategy on reduction of GHG Emissions from ships*, Int. Mar. Org., London

IMO (2022), *Analysing the Impact of Marine Biofouling on the Energy Efficiency of Ships and the GHG Abatement Potential of Biofouling Management Measures*, Int. Mar. Org., London

ITTC (2021), *Procedure for preparation, conduct and analysis of speed/power trials*, 29th Int. Towing Tank Conf.

MONTAZERI, N.J.P. (2019), *Autolog data processing for vessel performance application*, 4th HullPIC Conf., Gubbio

Towards Optimal Ocean Routing:
Leveraging Vessel Data for Ocean Current Reliability

Evangelos Moschos, Artemis Ioannou, Agathe Dupont, Alexandre Stegner, AMPHITRITE, Palaiseau/France, evangelos@amphitrite.fr

Abstract

To achieve optimal ship routing, the reliability of oceanic data is paramount. In this scope, our study seeks to establish a benchmark for evaluating different ocean current datasets, by employing high frequency vessel sensor data, alongside information from ocean drifters. Our findings reveal the limitations of conventional operational oceanic models in accurately predicting surface currents. Through a novel approach stemming from satellite observations, we demonstrate significant improvements in the resolution and reliability of ocean current data, unlocking further potential for route optimization. Through Mediterranean Sea case studies, we highlight the effectiveness of accurate ocean current data in optimizing routes for fuel efficiency and CO2 reduction, while also recalibrating vessel speed-log measurements for energy efficiency metrics. This approach presents a pragmatic, low-risk method that could aid maritime decarbonization.

1. Introduction

The environmental impact of route optimization is officially added to the economical and safety impact, as the shipping decarbonization roadmap requires immediate solutions, *Psaraftis (2019)*, *Mallouppas and Yfantis (2021)*. Since 2018, the International Maritime Organization (IMO) has implemented several regulatory constraints in order to address GHG emissions, introducing in the maritime sector specific indices that evaluate and classify the performance of each individual marine vessel. Among them, the Carbon Intensity Indicator (CII) will consider an annual estimation of the fuel consumption and distance travelled, both affected by the choice of the route.

Ship routing has been a method of increased interest, both in industry and academia, *Zis et al. (2020)*, in order to optimize the fuel saving and emissions reduction during a voyage by considering optimal routes with respect to environmental conditions as well as optimal vessel speed. *Psaraftis and Kontovas (2014)* demonstrated that the optimal route problem is closely linked with the optimal speed problem, which in turn is regulated by financial conditions such as fuel or freight price. Meanwhile, speed and route optimization rely strongly on the accurate prediction of metocean conditions encountered along a ship route. More than 60 years ago *Hanssen and James (1960)* documented how the United States Hydrographic Office used long-range predictions of wind, waves and currents to select optimum routes for transoceanic crossings. Avoidance of severe weather events in navigation is a century-old practice, nowadays improved by the usage of meteorological forecasting numerical models. The economic potential of reducing fuel consumption by harnessing ocean currents has been already documented, *Lo et al. (1991)*, *McCord et al. (1999)*. Defining an optimal route based on surface currents could be such directly affecting optimal speed and fuel consumption.

Furthermore, *Ikonomakis et al. (2021)* has demonstrated the limitations of available ocean current data when comparing vessel speed-log measurements (Speed Through Water) with GPS-received velocities (Speed Over Ground). Correct estimations of vessels' Speed Through Water, can allow for limiting uncertainty in the estimation of fuel oil consumption curves in calm water, pointing the need for ocean current data not only for route optimization but also energy efficiency modelling.

Today, ocean currents for weather routing are provided by operational numerical models that forecast daily the sea state. While winds and waves models seem reliable enough, current models are not. Depending on the assimilation schema, a set of models in the same region and period can provide different outputs, *Moschos et al. (2022)*. Nevertheless, numerical model forecasts for ocean currents are employed today in all available commercial tools for weather routing, to our knowledge.

A recent survey led by Amphitrite questioning captains of commercial vessels, allowed to highlight this difference between MetOcean variable predictions. Fifty vessel captains replied - among others - to the question "What is your opinion on the reliability of Weather and Ocean Forecasts", with the results illustrated in Fig.1. Not surprisingly, while wind and wave data were deemed of good reliability by 70% and 66% of respondents correspondingly, only 7% of captains thought the same about ocean currents data at their disposal. On the contrary a 35% believes that the current data available today are of poor reliability.

How then can we assess and improve reliability of ocean current forecasts? Contrary to numerical modelling, satellite observations of the sea surface topography deduce daily information on sea surface currents, *Chelton et al. (2001,2011)*, *Ballarotta et al. (2019)*. Moreover, recent studies using advanced Machine Learning methods have shown that satellite altimetry including the new SWOT mission can be complemented by additional satellite information provided by other sensors such as infrared or visible observations to provide reliable, high-resolution surface current maps, *Ioannou et al. (2019), Moschos et al. (2023)*.

This paper demonstrates that employing ocean current maps of high-reliability can improve the optimal ship routing strategies while also enhancing vessel energy efficiency modelling. By employing vessel data sailing in the Mediterranean Sea, we demonstrate that our AI-based model that fuses various satellite observations to receive high-resolution surface current maps greatly outperforms numerical model outputs used for ship routing today, both for nowcasting and forecasting, with a halving of the errors. These novel and reliable surface current data allow for a short-term optimal routing solution with a low cost, low risk and significant gains in fuel consumption, while also allowing ships to reduce emissions in the framework of decarbonization.

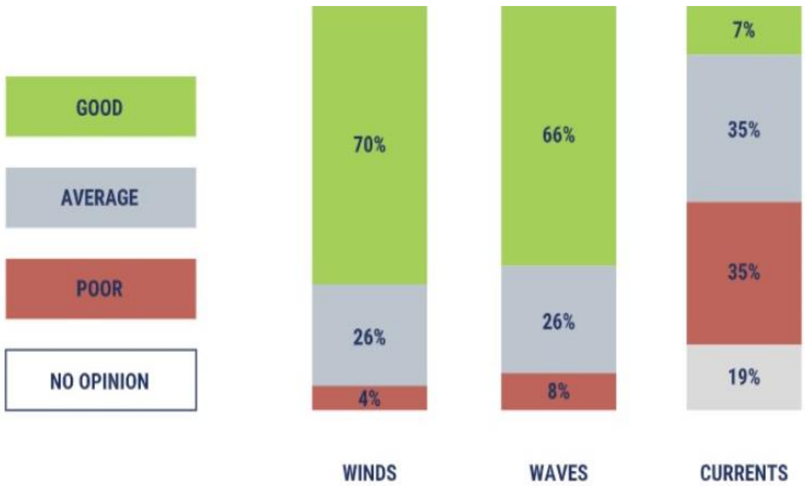

Fig.1: Result of the captain's survey on qualitative assessment of general meteorological data, winds, waves and currents.

2. Data: Satellite and Models

We include in our analysis sea surface current data from various operational ocean numerical models that are widely used in ship routing as well as our proposed solution that is based on satellite observations.

For that purpose, we extract outputs from three numerical models, namely the MERCATOR European oceanic model and GOFS (HYCOM-NOAA) American oceanic model that run daily and globally as well as a regional model for the Mediterranean Sea, the Mediterranean Forecasting System - MFS, run by the Italian CMCC. The characteristics of these models are presented in Table I. To compare oceanic data, for each model and for each day during the sample period, we extract sea surface currents at nowcast mode (real-time) and forecast mode.

Furthermore, we employ real-time satellite observations in order to compare with the outputs of the numerical models. Specifically, we extract data of observations from a constellation of over 10 satellites carrying altimetric, infrared and visible sensors as can be seen in Fig.2. We fuse the data of these satellites as described in *Kugusheva et al. (2024)* to retrieve high-resolution surface current maps (HIRES). We focus our analysis in the sea for the most recent period of 2021-2023.

Table I: Characteristics of three operational ocean models, MERCATOR, GOFS and MFS - country of origin, covered domain and output resolution.

Model	Provider	Coverage	Resolution
MERC	EU	Global	9x9 km
GOFS	USA	Global	4x9 km
MFS	ITA	Regional	4x4 km

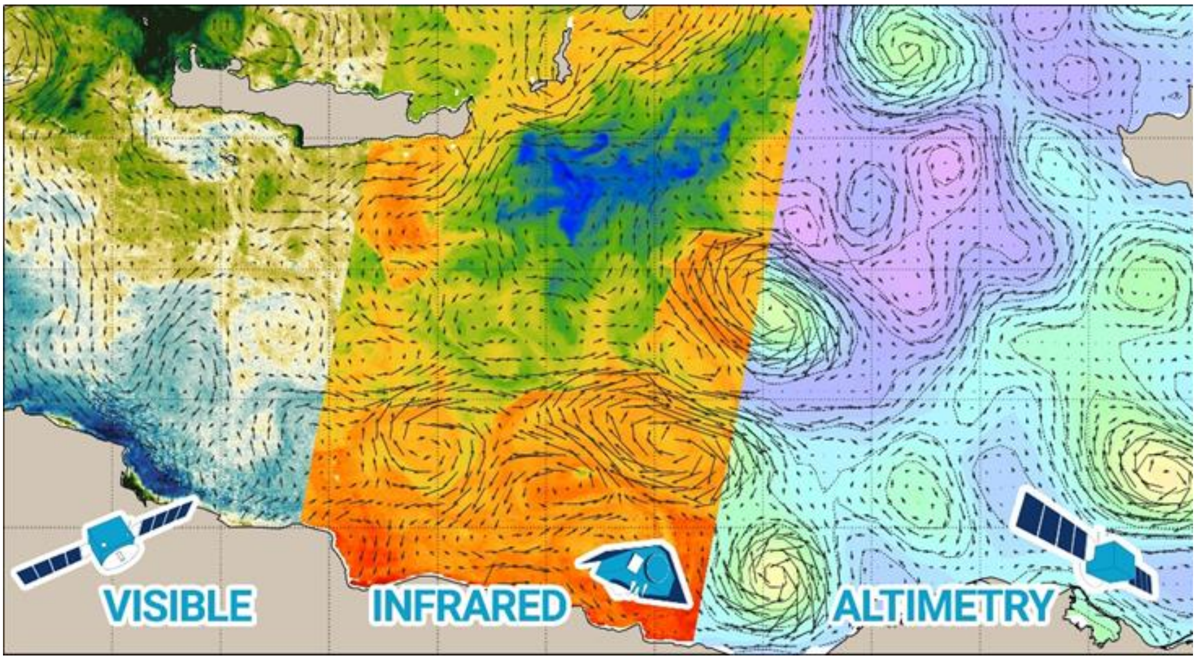

Fig.2: Illustration of the three types of data used for HIRES-CURRENT model

3. Comparing surface current maps with drifters and vessel data

3.1. Drifter-based evaluation method

In order to evaluate the ability of the different operational models to represent oceanic currents, we perform a statistical study using independent in-situ drifter measurements that are sampling surface currents in the Mediterranean Sea. We consider all available drifter measurements in the Mediterranean Sea during the study period (20212023), as illustrated in Fig.3 where the mean ocean current velocity measured by drifters is shown in the observed areas. From those observations we only extract those where the ocean current is higher than 0.5 kn or 0.25 m/s i.e. with an impact on the ship's speed, resulting in a total of 46000 data points. To evaluate the accuracy of each model on reproducing sea surface currents, we compute the angle θ between velocity components as measured from the drifters and as estimated from the different datasets. Hence smaller values of θ, will indicate sea surface currents that remain along a similar direction with the drifter measurements, while larger values of θ will indicate currents of opposite direction. To illustrate the main differences on currents directions along the drifter trajectory we define different angle ranges, Fig.4. Cases where θ remains less than 15° (green colour) are considered excellent while only cases where θ is less than 45° (light green colour) provide a good estimation of the real direction of oceanic currents. For more than 45° of angle error the ocean current estimations are deemed at least inaccurate if not completely wrong, making difficult to optimize a vessel's route (orange and red colours).

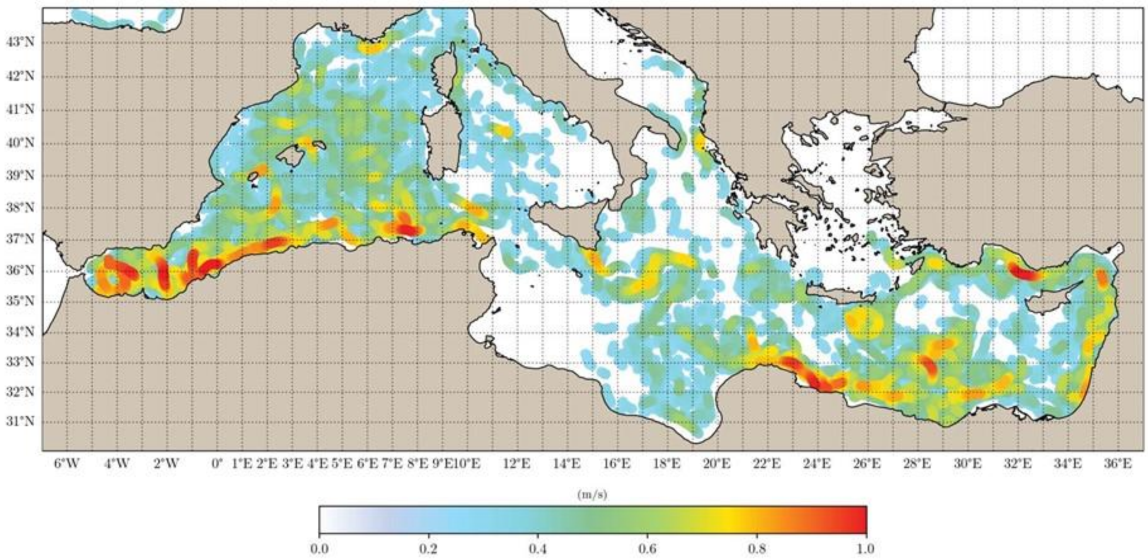

Fig.3: Location of drifter measurements for the period of 2021-2022 in the Mediterranean Sea. Colours illustrate the mean measured velocity in m/s.

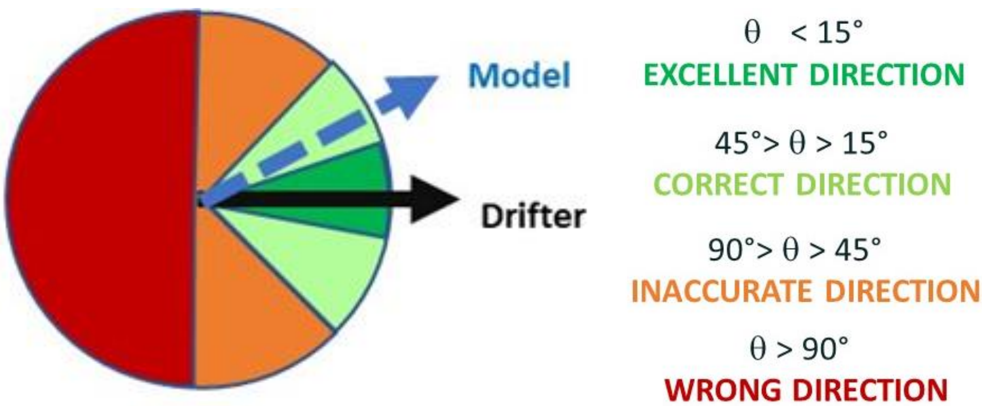

Fig.4: Simple Metric Comparing the angle error between an Ocean Current Model (blue arrow) and a corresponding drifter in-situ measurement (black arrow)

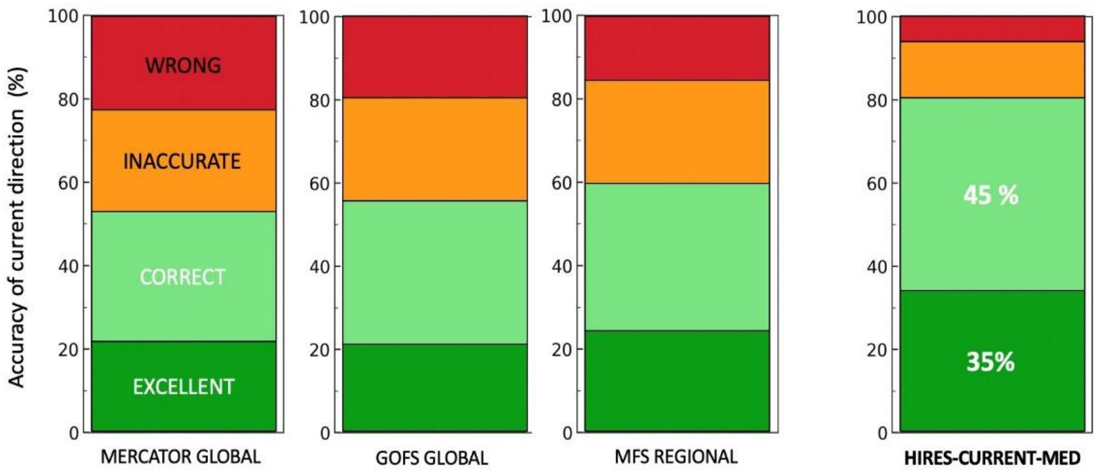

Fig.5: Statistical errors of the angle of ocean current nowcasts comparing different model outputs to drifter measurements: MERCATOR (Global Numerical Model), GOFS (Global Numerical Model), MFS (Regional Numerical Model) and HIRES-CURRENT-MED (Our Satellite Data Fusion).

The results of our analysis are illustrated in Fig.5, comparing the four categories of ocean current direction evaluation (excellent, good, inaccurate, wrong) for different models: MERCATOR (Global Numerical Model), GOFS (Global Numerical Model), MFS (Regional Numerical Model) and HIRES-CURRENT-MED (Our Satellite Data Fusion). Our satellite data-driven model based on AI, HIRES-CURRENTS-MED, is able to predict at least 80% of the time accurately the direction of oceanic currents, while accurate percentages always remain less than 60% for the MERCATOR, GOFS and MFS operational models. Compared to the MERCATOR model, employed in most of the current weather routing tools, our ocean current predictions in the Mediterranean Sea offer 4 times reduced wrong and inaccurate observations. Furthermore, we find the performance of operational models in forecasting mode to be even less efficient, while our HIRES-CURRENTS-MED retains its performance for a period of 5 days.

3.2. Vessel-based evaluation method

3.2.1. Speed-log recalibration

Assessing the reliability of our models based on vessel data relies on the measurement of an essential parameter, the Speed Through Water (STW), measured by the vessel "speed-logs", often a Doppler Velocity Log (DVL) measuring instrument. In order to conduct our analysis using vessel data, these STW measurements must be as reliable as possible. Nevertheless, *Ikonomakis et al. (2021)* showed that it is still challenging to measure STW with accuracy, as most vessels' DVL measurements highly fluctuate, mostly due to ocean currents, along with other systematic measuring errors.

The error on STW measurement must be corrected in a post-voyage analysis setting before using these observations as ground truth. Speed-log recalibration depends on the considered ship and route. Thus, the bias must be calculated for each voyage. Here, we introduce a specific method to evaluate the error and recalibrate the measures, Fig.6. We assume that our currents model is fully correct for areas where no current has been observed (i.e. currents < 0.1 kn). Then, we find points from the dataset with a negligible current impact according to HIRESCURRENT prediction such as:

P = {|ΔUhires| ≤ 0.1kn}

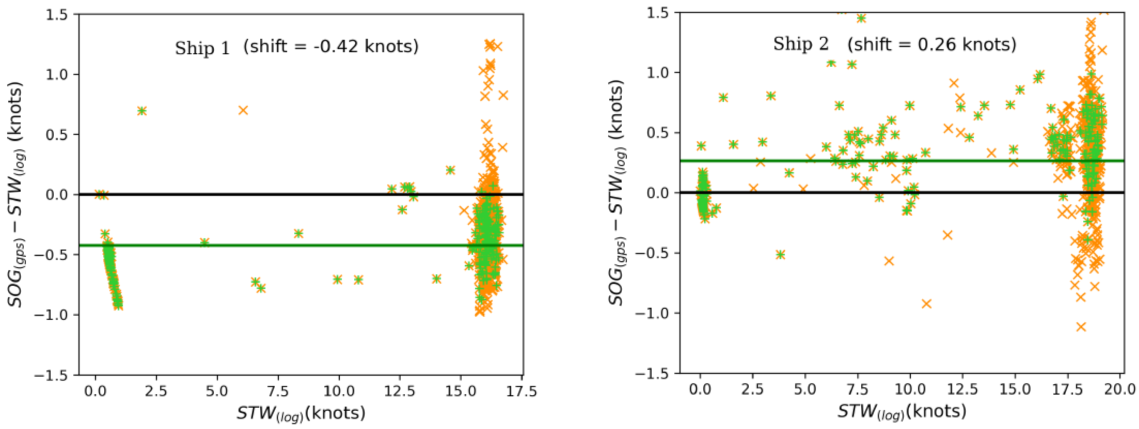

Fig.6: Recalibration of STW measurements for 2 vessels navigating on the Suez-Gibraltar leg, according to the described method. Green points belong to U_{filtered}, while orange points show all measurements (including those where ocean currents are significant). The black line, passing from zero, is shifted to the position of the green line to better fit the U_{filtered} observations.

P represents the set with correct values. Then we are able to isolate points impacted by a measurement's error such as:

Ufiltered = {Ucf ∉ P}

Finally, the shift that corresponds to the correction value is given by the mean of Uc within the given set such as:

shift = Ucf,Ucf ∈ Ufiltered

In what follows, we employ these recalibrated values STWcorrected, to conduct our analysis.

3.2.2. Comparing Ocean Models with Vessel Data

In order to reinforce the evaluation of ocean current models presented in the previous section, we conducted a pilot test for Mediterranean Sea crossing using data from the speed-logs of CMA-CGM vessels sailing in regular routes in the Mediterranean Sea. The vessel sensors allow access to high-frequency measurements Speed Through Water combined with the GPS information of Speed Over Ground. From these variables, we are able to estimate the real (ground truth) current, as measured by the vessel, that corresponds to:

U = SOG − STW

We note that STW is corrected, through the re-calibration method presented in the above section.

We introduce a new metric to evaluate the reliability and the accuracy of oceanic current predictions. We compare the magnitude of the HIRES-CURRENTS vector projected on the vessels speed vector to the calculated Uc from the vessel's data. Results presented in this paper are based on the study of six routes including the Suez-Tanger leg, Malta-Suez leg and Genoa-Beirut leg (Fig.7). It represents filtered 2320 data points from vessel database.

Fig.8 compares the values of Uc from the measurements of vessel instruments, to ΔUmodel from the 3 different models, Mercator (Global Model, Red Dots) and MFS (Regional Model, Purple Dots) and our AI model, HIRES-Currents (Satellite Observations, Green Dots). On the x-axis Uc=SOG - STW) represents the vessel measured current and on the y-axis ΔUmodel represents the current impact (projected current) at the vessel's position. Therefore, for an ocean current model to be perfectly accurate, both observations need to be in agreement, i.e. perfectly aligned along the diagonal's envelop. The prediction is considered as correct if the predicted value is within +/-0.5 of the measured value. Values close to (0,0) represent ocean points without current.

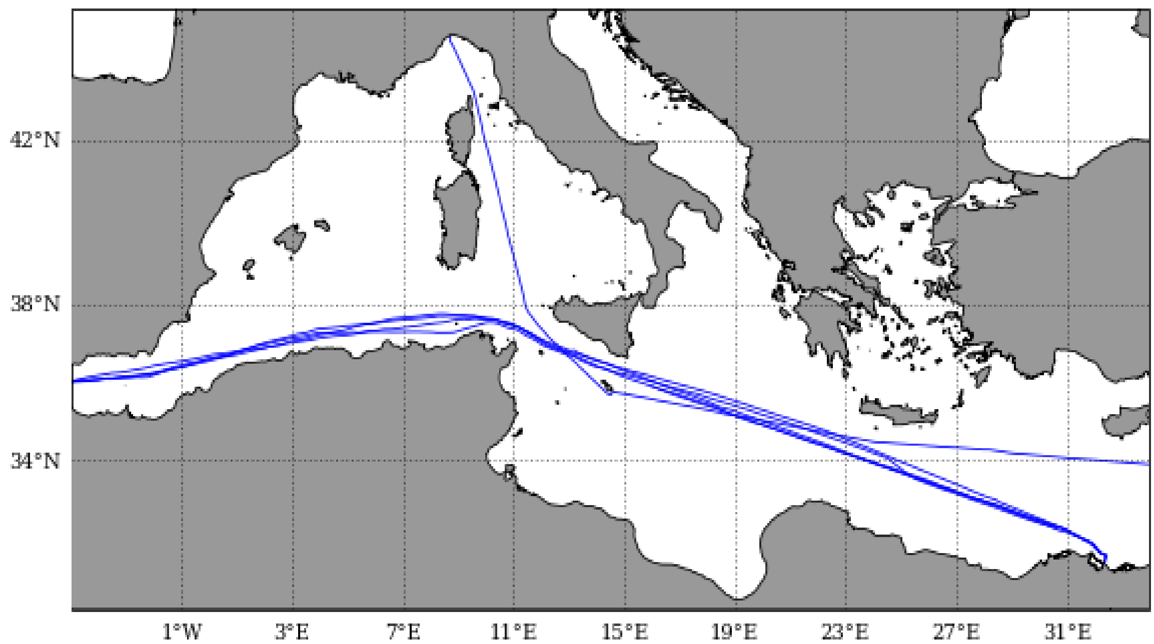

Fig.7: Mediterranean Sea legs used for the vessel-based evaluation method

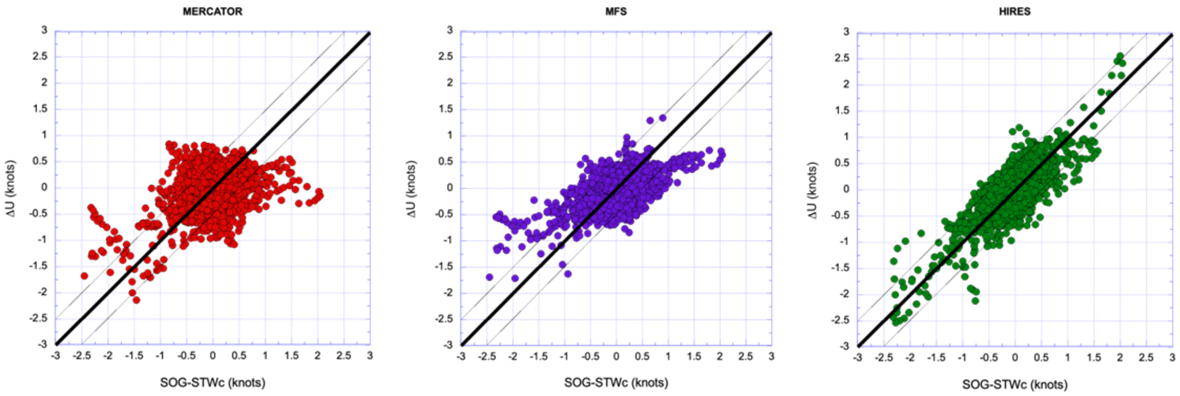

Fig.8: Comparison of vessel measured current (SOG - STW) on x-axis with current impact (projected current) at vessel position, U on the y-axis. Comparison is performed for two numerical models Mercator (Red Dots) and MFS (Purple Dots) and our AI model, HIRES-Currents (Green Dots). The two lines parallel to the diagonal represent the envelop of accurate measurements (±0.5 kn). For strong currents (high absolute values in the diagonal) our HIRES model agrees better with vessel observed currents than the other two models.

In Fig.8, the global model (MERCATOR) presents many points outside the envelop of the diagonal, i.e. inaccurate ocean currents that don't agree with the vessel observations. The regional model (MFS) appears to perform better, but also presents many outliers for high current magnitudes. This highlights the limits of both numerical models, which have difficulty in providing reliable information for strong currents. Conversely, for HIRESCURRRENTS, the scatter plot reflects the correlation between Uc and ΔUhires for all current intensities, implying that eddies with high intensities have been accurately predicted. Table II presents analytical results for the six routes where vessel data have been considered, highlighting the reliability of the HIRES model for areas with strong currents, in comparison to the two aforementioned numerical models (Mercator, MFS).

Table II: Analytical results on the errors of different ocean current models using vessel data

Data source	Param.	All currents	>0.5 kn	> 1 kn
All ships	Mean Uc	0.29 kn	0.87 kn	1.56 kn
$\Delta\ U_{Mercator}$	Error	1.52	0.88	0.72
$\Delta\ U_{MFS}$	Error	1.25	0.79	0.65
$\Delta\ U_{Hires}$	Error	1.05	0.50	0.35

4. An optimal routing solution

In the previous section, we evaluated the performance of different numerical models on their capacity to reproduce accurately sea surface oceanic currents against real-time in-situ, both using drifter and vessel measurements as ground truth. We have further demonstrated that HIRES-CURRENTS provide higher reliability on estimating oceanic current, characterized by statistically smaller errors. In order to evaluate how different predictions of the oceanic currents could actually affect optimal ocean routing, we investigate in this section two specific routing examples. One corresponds to a vessel sailing along the Suez - Gibraltar route, Fig.9, and the other to a good example of strong ocean currents encountered in the Alboran Sea, Fig.10, both in high commercial routes in the Mediterranean Sea.

The highly-reliable and high-resolution ocean current data HIRES-CURRENTS enables the employment of a short-term optimal routing (STOR) scheme. STOR concerns a fine-scale optimisation that can be applied to prescribed routes while benefiting from oceanic currents with minimum adjustments. In Fig.10, by adjusting with given waypoints, this ship could benefit from strong oceanic velocities not only by avoiding counter-current but by also redirecting its route towards the opposite side of this swirling motion soon enough. In this scenario, the ship could realise fuel savings of up to 4% by slightly lowering its speed to arrive at the original ETA.

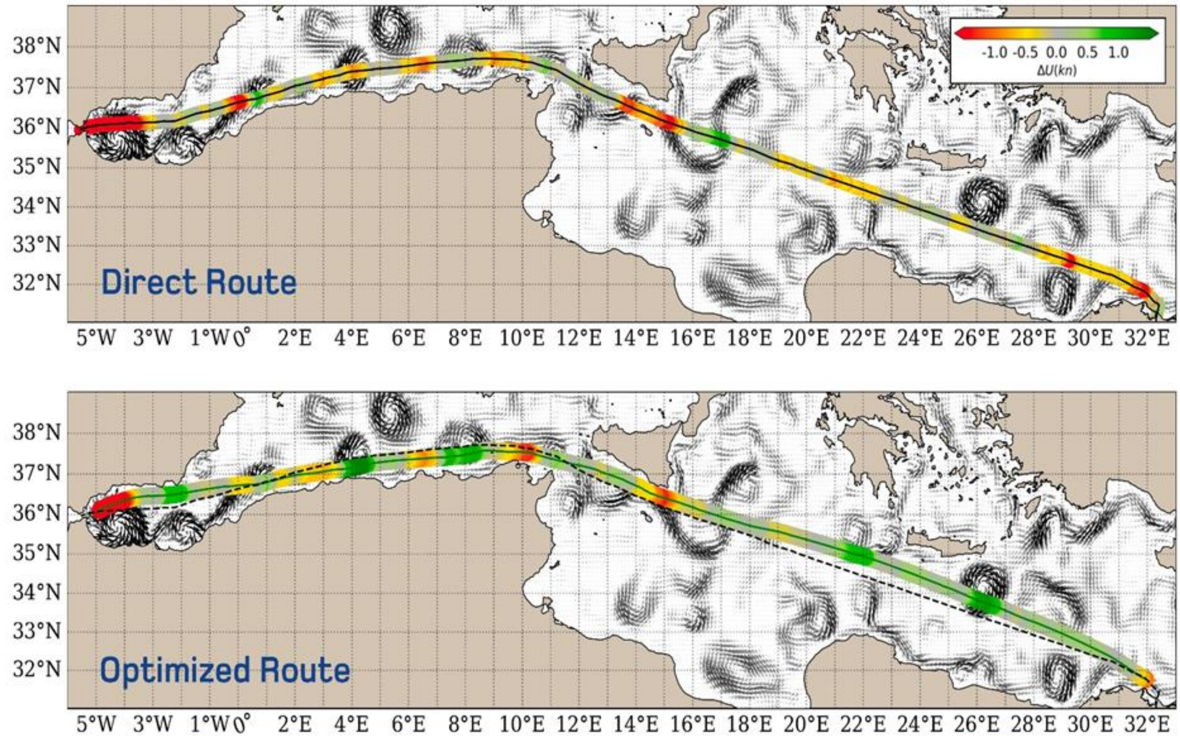

Fig.9: Example of optimal routing application along Suez to Gibraltar route in the Mediterranean Sea for a vessel navigating with an average speed of 18.5 kn. The background velocities correspond to the HIRES-CURRENTS as derived for the 21 August 2023. The upper panel corresponds to the direct route followed by the vessel. The bottom panel corresponds to the fine-scale optimisation route (green line) compared to the direct route (black dashed line).

We highlight that all vessels following the Suez to Gibraltar trajectory are concerned and could benefit from this optimization. Depending on the vessel type and fuel consumption characteristics, the fuel gain estimation will differ, being directly linked to the ship-current speed ratio as well as the vessel Fuel Oil Consumption curve (FOC). The consumption depends on the technical specifications of the vessel and on the meteorological conditions. This study is centered on assessing the reliability of ocean current and demonstrating a new mode of ocean routing, therefore we did not perform analytical FOC estimations.

Nevertheless, following the findings in *Ikonomakis et al. (2021)* we believe that accurate estimations of the Ocean Current can lead to better speed-log recalibration, increased accuracy in the STW estimation, leading to better calm-water FOC estimations. We consider a theoretical and simplified model of a ship's consumption at calm water with:

$$\boldsymbol{FOC(v) = \alpha v^{\beta}}$$

Table III: Correction of the calm-water FOC curve for a speed-log recalibration of ±0.4 kn, on a theoretical, simplified curve $FOC(v) = \alpha v^{\beta}$ with $\alpha = 0.015$ and $\beta = 3$

Velocity [kn]	10	12	14	16	18	20
FOC correction	6.0%	6.7%	7.5%	8.6%	10%	12%

By considering parameters $\alpha = 0.015$ and $\beta = 3$ and a speed log calibration of ±0.4 kn as show in Fig.6, we demonstrate in table 3 that significant uncertainty reduction in the calm-water FOC estimations can be obtained. Varying with vessel speed, uncertainty can be reduced from 6 to 12 % in this theoretical example, providing a valuable tool for energy efficiency and post-voyage analysis.

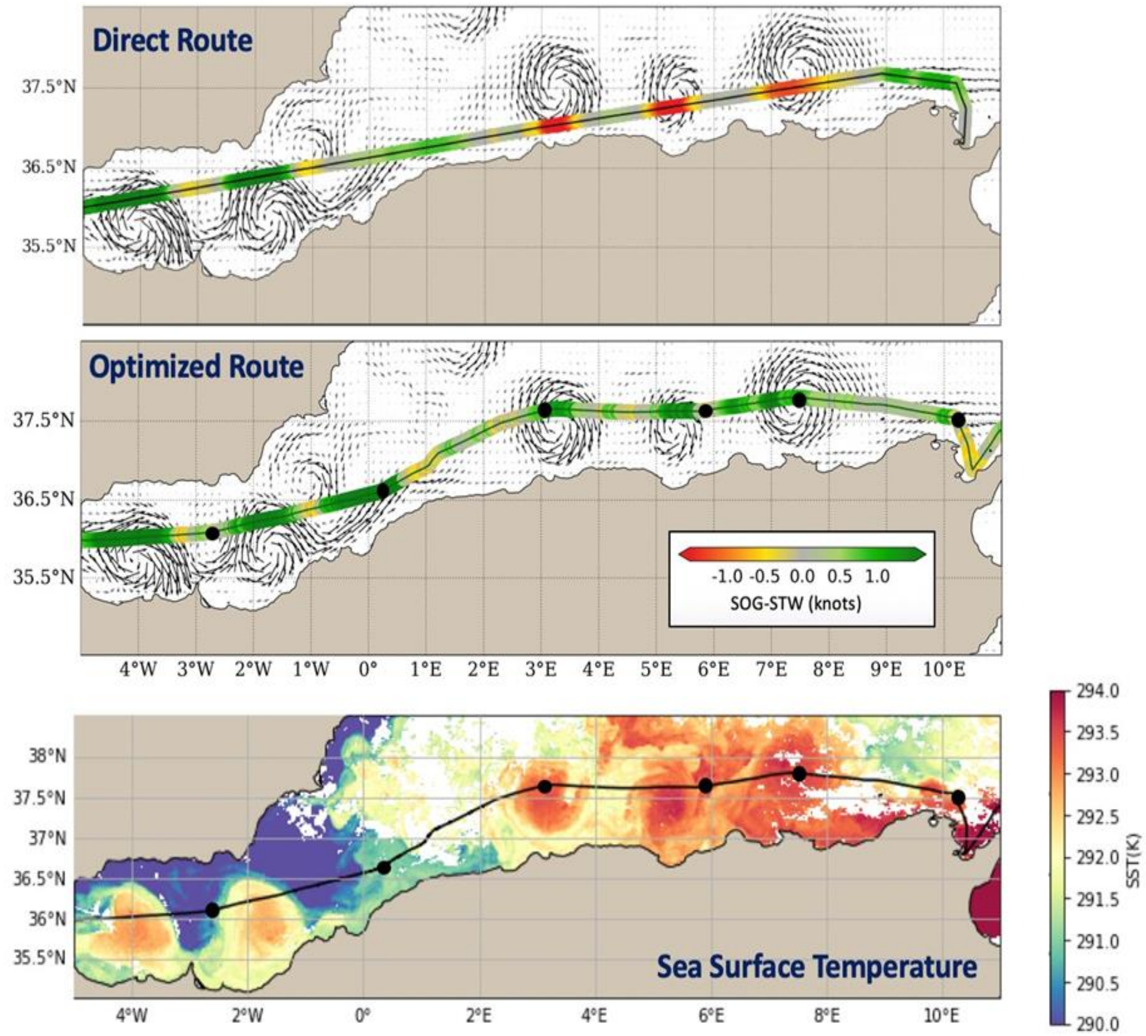

Fig.10: Example of optimal routing application along Tanger to Tunis route in the Alboran Sea for a vessel navigating with an average speed of 16 kn. The background velocities correspond to the HIRES currents as derived for the 26 November 2023. The upper figure shows the current intensity on a theoretical direct route on this leg. The middle one shows the fine-scale optimisation route for the given day with the suggested waypoints to follow the route. The figure below shows the correlation of the HIRES-Currents map with the Sea Surface Temperature, as observed by satellite.

5. Conclusion

Present operational numerical models, frequently used for forecasting oceanic conditions along a ship voyage, present limitations in reproducing oceanic currents with high reliability. On the contrary, the fusion of multiple satellite observations with AI-based models provides oceanic current data that are characterized by statistically smaller errors, especially for regions with strong currents. This solution is available today thanks to advances in remote sensing of the ocean and AI-based models and could reinforce operational routing and energy efficiency applications in the shipping industry.

High reliable oceanic currents enable the application of an optimal routing strategy that directly translates into additional time and fuel gains. Each vessel navigating in Suez-Gibraltar axis in the Mediterranean Sea is concerned by such fine scale optimisation since strong oceanic currents will be encountered along ship routes at least once (on average 1.3 times per trajectory). Within the scope of significantly increasing CO_2 emissions of the shipping sector in the coming years, short-term optimization based on HIRES-CURRENTS data can reinforce present ship optimal routing strategies with a low-cost and low-risk solution.

Acknowledgement

We acknowledge the contribution of the Fleet Center of CMA-CGM in Marseille/France, for active participation in this project, providing vessel data used for the analysis, supervising the methodology and methods used in the study and providing insights on shipping and weather routing practices. In particular, we thank Captain Jocelyn Rapp, Captain Rémy Renard, Florent Nalin, Guillaume Barfety and Coralie Legrand for their contributions.

References

BALLAROTTA, M.; UBELMANN, C.; PUJOL, M.I.; TABURET, G.; FOURNIER, F.; LEGEAIS, J.F.; FAUGERE, Y.; DELEPOULLE, A.; CHELTON, D.; DIBARBOURE, D.; PICOT, N. (2019), *On the resolutions of ocean altimetry maps*, Ocean Science 15/4, pp.1091-1110

CHELTON, D.B.; RIES, J.C.; HAINES, B.J.; FU, L.L.; CALLAHAN, P.S. (2001), *Satellite altimetry,* Int. Geophysics 69, pp.1–131

CHELTON, D.B.; SCHLAX, M.G.; SAMELSON, R.M. (2011), *Global observations of nonlinear mesoscale eddies*, Progress in Oceanography 91(2), pp.167–216

HANSSEN, G.L.; JAMES, R.W. (1960), *Optimum ship routing*, J. Navigation 13(3), pp.253-272

IKONOMAKIS, A.; NIELSEN, U.D.; HOLST, K.K.; DIETZ, J.; GALEAZZI, R. (2021), *How good is the STW sensor? An account from a larger shipping company*, J. Marine Science and Eng. 9(5), 465

IOANNOU, A.; STEGNER, A.; TUEL, A.; LE VU, B.; DUMAS, F.; S. SPEICH, S. (2019) *Cyclo-strophic corrections of aviso/duacs surface velocities and its application to mesoscale eddies in the mediterranean sea*, J. Geophysical Research: Oceans 124(12), pp.8913-8932

KUGUSHEVA, A.; BULL, H.; MOSCHOS, E.; IOANNOU, A.; LE VU, B.; STEGNER, A. (2024), *Ocean Satellite Data Fusion for High Resolution Surface Current Maps,* Remote Sensing, MDPI

LO, H.K.; McCORD, M.R.; WALL, C.K. (1991), *Value of ocean current information for strategic routing*, European J. Operational Research 55(2), pp.124-135

MALLOUPPAS G.; YFANTIS, E.A. (2021), *Decarbonization in shipping industry: A review of research, technology development, and innovation proposals*, J. Marine Science and Eng. 9(4), 415

McCORD, M.R.; LEE, Y.K.; LO, H.K. (1991), *Ship routing through altimetry-derived ocean currents,* Transportation Science 33(1), pp.49-67

MOSCHOS, E.; STEGNER, A.; LE VU, B.; SCHWANDER, O. (2022), *Real-time validation of operational ocean models via eddy-detecting deep neural networks*, IEEE Int. Geoscience and Remote Sensing Symp. (IGARSS), pp.8008-8011

PSARAFTIS, H.N. (2019), *Decarbonization of maritime transport: to be or not to be?*, Maritime Economics & Logistics 21(3), pp.353-371

PSARAFTIS, H.N.; KONTOVAS, C.A. (2014), *Ship speed optimization: Concepts, models and combined speed-routing scenarios,* Transp. Research Part C: Emerging Technologies 44, pp.52-69

ZIS, T.P.; PSARAFTIS, H.N.; DING, L. (2020), *Ship weather routing: A taxonomy and survey*, Ocean Eng. 213

Unambiguous Ship Voyage Evaluation

Wojciech Górski, Enamor Ltd., Gdynia/Poland, wojciech.gorski@enamor.pl
Aleksandra Hein, Enamor Ltd., Gdynia/Poland, aleksandra.hein@enamor.pl
Aleksandra Karolik, Enamor Ltd., Gdynia/Poland, aleksandra.karolik@enamor.pl
Dominik Leśniak, Enamor Ltd., Gdynia/Poland, dominik.lesniak@enamor.pl
Liliana Zadrożna, Enamor Ltd., Gdynia/Poland, liliana.zadrozna@enamor.pl

Abstract

Shipping gradually merges to Industry 4.0 becoming a part of smart mobility. Nowadays, ships move not only in space and time, but also across dense grid of digital information in virtual reality. Ships cross the seas and oceans, leaving a virtual wake of data. Access to data becomes possible thanks to the cloud solutions. The availability of data enables creation of innovative services. The new, added value for ship owners, operators and other parties in shipping industry can be created by merging of multiple layers of information. Thanks to smart processing user involvement is minimised, each vessel equipped with functional AIS transponder can be analysed without requirement of any additional hardware integration. Enamor has developed a cloud-based ship voyage evaluation service requiring only a ship identification number and a date range as the input. The service automatically collects and processes data about the voyage route, ports of call, weather and navigation conditions. Based on them, service prepares a detailed report providing a comprehensive assessment of the voyage empowering the users with detailed information about the vessel's operating conditions. Service provides a wealth of data and insights that can be used to enhance performance, optimize costs, improve efficiency, and ensure compliance with contractual and regulatory requirements. It may serve as a learning tool for continuous improvement in the maritime industry. Service is available as SaaS.

1. Introduction

Shipping nowadays intensively relies on data which constitute a backbone of marine transportation. Ship herself is a complicated data environment. Her safe and efficient operation requires data processing within the internal network interconnecting vital ship systems and interacting with a crew. Data exchange is not limited to the ship environment. Even vessel travelling through the most remote seas exchange data with external data network. Some data are protected against third party some other like principal navigational parameters belong to public domain. Particularly, automatic identification system (AIS) is an example of rich, public data source. AIS provides ships unique identification, position, course, and speed often supplemented with vessel draft and voyage destination. Data collected by AIS are used not only for the purpose of safe navigation (as initially intended) but constitute a building block of many analytical services. Another data source intensively used in shipping is metocean data. Weather forecasts are used for voyage planning while hindcasts allow for retrospective an analyses.

We identified a niche for utilization of publicly available data, AIS and weather datasets, in order to create a comprehensive voyage evaluation tool. It facilitates data collection, processing and visualization based on minimum input from the user. The only information which user needs to provide is the ship identification and her period of operation. Service will process these entries finding ports of calls, identifying voyages and match them to the weather conditions. It performs also all necessary data processing including outlier detection, resampling and interpolation, gap filling and recalculation weather conditions with respect to vessel frame of reference. Service provides elaborated, easy-to-comprehend visualisations encapsulated in an interactive dashboard and more traditional static report.

Tool is available as the web service (SaaS) available for any party who needs unambiguous (i.e. based on publicly available data and not restricted by privately owned datasets) voyage evaluation. Primary stakeholders group include vessel owners and operators for whom it helps to resolve vessel performance issues. Cargo owners, insurance companies, classification societies and marine enthusiasts are among those who could also benefit from this service.

2. Service arrangement

Various data sources and data processing tasks imposes need for robust, yet expandable data pipeline architecture closely incorporated with user actions, waiting time and information quality. The voyage reporting service back spine relays on AIS data collection systems. The AIS transponder being mandatory shipborne navigational equipment depending on the vessel's type according to SOLAS regulation V/19 provides information about the ship's identity, type, position, course, speed, navigational status and other safety-related information. This information is further processed and exchanged between various parties, some of them providing services with application programming interfaces allowing to collect the AIS real time and historical data from global merchant navy fleet. Accessing the vessel's positions in time is realized with one of the AIS applications programming interface providers, basing on those data first processing task is realized in order to provide a list of detected routes and ports of calls. Such approach allows user for selection of suggested vessel identifications and routes made in initially provided time scope. Having the route selected it is then possible to gather remaining data necessary for final report preparation. Positions recorded in time allows to utilize third party historical weather data and bathymetry information for given positions. In order to minimize the report preparation time, the tasks relaying on already collected data are being performed in parallel regime. The data processing and report preparation tasks (Fig.1) alone are utilized the same way in order to maximize the efficiency of the process performed in the background. Once the final report data structure and features are prepared, the information is being broadcasted to both the report visualization tasks and to database for further reuse and recapture for the user. Such arrangement of the service allows to control the process and prioritize the efficiency of data processing, third party data utilization and user-service interaction.

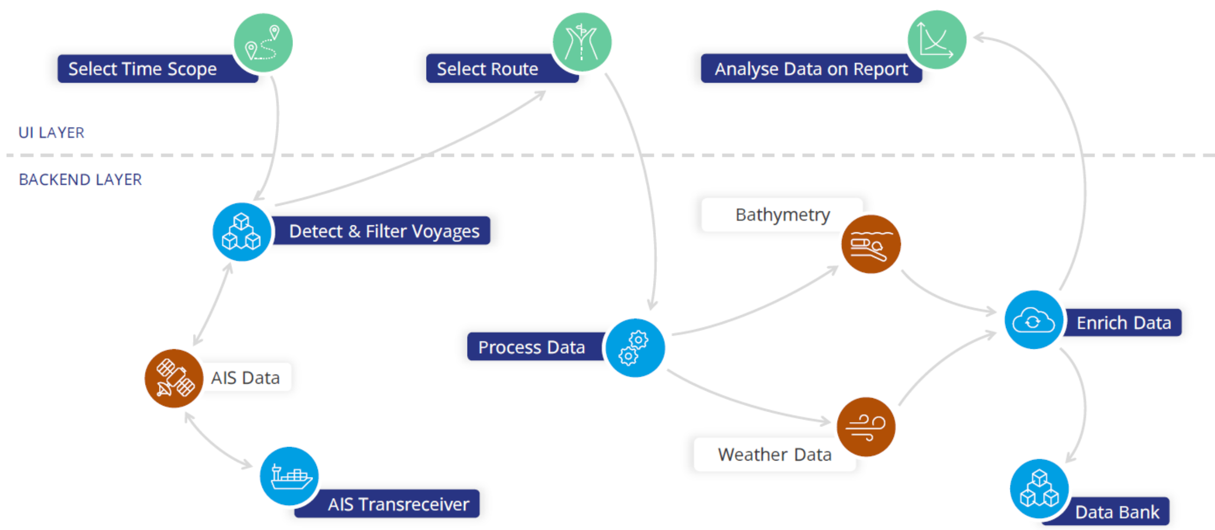

Fig.1: Data flow chart of the service

2.1. Data sources

Our service pulls data from industry-recognized sources, ensuring we have a broad spectrum of information to base our evaluations on. Each data source is thoroughly vetted for accuracy and reliability before being integrated into our system.

Tidetech, https://www.tidetech.org/, is a well-known and reliable metocean data provider. They provide detailed, accurate and validated metocean data including global weather, waves, sea temperature, ocean and tidal currents.

Seametrix, https://seametrix.net/, is a company specializing in software solutions for route optimization in the maritime industry. Recently, they have introduced historical AIS data accessible via API.

GEBCO (General Bathymetric Chart of the Oceans), https://www.gebco.net/, is a non-profit organization that operates under the joint auspices of the International Hydrographic Organization (IHO) and the Intergovernmental Oceanographic Commission (IOC) (of UNESCO). They produce a range of bathymetric data sets and products.

UN/LOCODE (United Nations Code for Trade and Transport Locations) is a code list of country and territory names maintained by UNECE (United Nations Economic Commission for Europe), https://unece.org/trade/cefact/unlocode-code-list-country-and-territory.

To prepare the collected data for analysis, it undergoes rigorous cleaning and pre-processing. This includes identifying and addressing outliers that could skew results, filling gaps in data sequences to maintain consistency, and resampling to ensure uniformity in data intervals. These steps are crucial in maintaining the integrity of our evaluations.

The positional coordinates provided by AIS for vessels are generally of very good quality, as demonstrated in the publication *Jankowski et al, (2021).* The assessment carried out in the study, which compared AIS data with radar tracks considered as ground truth, revealed an average deviation of approximately 97.72 m. Additionally, it was noted that less than 2 percent of vessel positions are ambiguous, *Stasinakis (2015),* primarily limited to small non-commercial vessels. Nevertheless, outliers do occur. In AIS datasets, outliers are defined as points or sets of geographic points that significantly deviate from the vessel's intended route. For example, if a vessel reports its position and then, after a few minutes, is found several hundred nautical miles away, it can confidently be classified as an outlier *Duarte and Sakr (2023)*. However, a significant challenge to the accuracy of AIS data stems from human error. Although some AIS data, such as position coordinates, course, and speed, are automatically collected from trusted sources (e.g. navigation equipment), other information like navigational status, destination, and estimated time of arrival (ETA) is manually entered by the crew. In this context, determining the destination posed a significant challenge. We developed a specialized approach to address this, which will be presented in the subsequent sections of the article.

Within data processing, gaps in datasets are a common occurrence. These gaps typically fall into two distinct categories: those amendable with reliable data and those beyond immediate rectification. In the context of AIS data management, when faced with an insurmountable gap, our approach involves segmenting the dataset into smaller subsets. We then proceed to conduct analyses based on the available segments of the vessel's route, ensuring that users receive insights derived from the existing dataset. Our determination of an unfillable gap is based on parameters such as the temporal and spatial disparity between consecutive vessel positions; if these metrics exceed predefined thresholds, the gap is classified as unfillable.

Data regarding vessel journeys, encompassing parameters like longitude, latitude, speed, and heading, arrive irregularly over time. To normalize and ensure uniform frequency in the dataset, we undertake oversampling to generate data points for each minute. Following interpolation between existing data points, we engage in down sampling, preserving data at hourly timestamps.

2.2. Data processing

Data processing constitute a pipeline of computations which employs different algorithms. Initially user input is processed helping in vessel identification based on searching and filtering techniques. This initial step allows for gathering AIS data. These data are processed in order to obtain uniformly distributed waypoints. At this stage dataset usually needs improvement either by interpolation or gap filling algorithms. A further step includes metocean data retrieval corresponding to vessel positions and timestamps. Gaps can be detected also metocean data which requires additional data improvement algorithms (interpolation is employed for this purpose). Finally metocean data are recalculated to the vessel frame of reference. Completing the process provides the dataset ready for performance assessment and reporting.

One of the key features of our service is its ability to accurately detect individual voyages by recognizing patterns and key indicators within the data. Combined with sophisticated interpolation methods, we can fill any remaining gaps in data sequences, ensuring a seamless and comprehensive overview of each voyage. Unfortunately, this stage of data processing heavily relies on what and when the crew enters in the AIS. The vessel's destination is a manually entered field in any text format, making it susceptible to misspellings and other errors. Moreover, changes in destination may be recorded by the crew with significant delays, rendering it ambiguous as the beginning of a new journey. These pieces of information are essential for correctly identifying the ports vessels call at and determining specific voyages, hence the necessity for validating the received data. Identifying vessel stops is based on the vessel's positions where the minimum speed threshold is met within a specified time frame. These points are recognized as stops. This methodology enables the segmentation of the dataset into voyages and port stays. To authenticate a vessel's port, we extract the position from the last entry pertaining to the voyage and cross-reference it with the coordinates stored in our port database. Subsequently, the port name undergoes validation through a three-stage process: initially, we verify if the name recorded by the crew matches any entry in the port list; if not, the subsequent criterion entails assessing the distance and size of the port relative to the coordinates, with preference given to the largest port listed.

Segmenting the dataset based on stops and voyages is crucial, particularly due to the interpolation techniques utilized. During voyages, the vessel's coordinates undergo cubic spline interpolation to enhance accuracy in navigating around landmasses along the route. Conversely, other data related to voyage and information gathered during vessel stops in ports, is interpolated linearly.

AIS data sometimes contain gaps. While short ones can be efficiently filled in with use of interpolation techniques the longer ones pose the challenge for the processing pipeline. Proper identification of vessel position and corresponding time is critical for establishing weather conditions during vessel operation. For this purpose longer gaps are replenished with use of voyage planning service. Although exact positions of the vessel in data gap cannot be precisely established implemented technique gives satisfactory results for gaps up to 3 days. Obtained waypoints can be considered as very probable voyage trace. Timestamps corresponding to estimated waypoints are generated under constant speed assumption. This way data set sufficient for enquiring weather conditions is established.

Metocean and bathymetric data are gathered for positions from a prepared AIS dataset. To fully exploit the potential of the acquired data, we conduct a series of calculations enabling a more comprehensive analysis of the conditions under which the ship operated. Wind, wave, ocean current directions, and their magnitudes are presented in relation to the ship's frame of reference. Additionally, we compute the ship's speed relative to the water and the encounter frequency and period of waves. This meticulously prepared dataset is showc-ased in an interactive report.

3. Computer technologies

The Service Production Environment was selected in order to provide security and scalability features, that will allow for further adaption depending on the workload strictly related to the amount of users interacting with the reporting tools. Due to high uncertainty in initial interest assessment, the scalable architecture has been selected. In order to ensure seamless service operation the main application is being served with WSGI HTTP server software Gunicorn suited for python application and compatible with Django Framework adopted for service development. Furthermore the reverse proxy application has been adopted in order to directly interface with client requests and forward them to backend Gunicorn server. The Nginx web server software has been selected for that role and to also provide load balancing features for further scaling of the service. Both server software solutions are deployed in separate Docker containers in order to isolate and control the working environment. Further communication with various data sources in form of third-party API’s or databases is operated from the main application, Fig.2.

The main application has been developed with use of Python 3.11 version providing major improvements in relation to previous Python versions that were crucial to ensure the efficient service operation. Despite official stable release of Python 3.12 version in October 2023 the previous version has been selected due to incompatibility of some of the ML libraries like Tensorflow at the moment of service development.

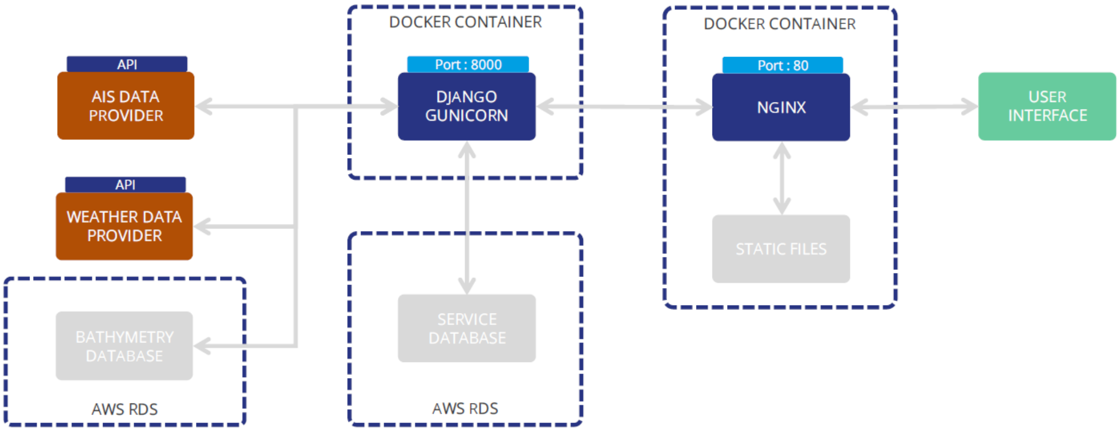

Fig.2: Service Architecture

In order to ensure efficient data processing and further service development, several Python modules and methods has been considered and tested against performance for typical data processing and feature engineering tasks. For efficient database connections and thread secure sessions the Sqlachemy python toolkit has been utilized. The main data processing and operation tasks are handled by Polars, the Python & Rust dedicated DataFrame library, that poses significant data processing tasks acceleration still ensuring the use of transparent data frame objects and clear data modification methods. For the main application framework the Django high-level web framework has been selected. Such implementation allowed for reduction of overall service environment complexity and ensured ease of development. The reports creation and data presentation are supported by the Plotly library allowing for low-code, highly customizable, highly interactive data graphs definition and creation. The various graphs type object are directly designed and declared within the scope of the main application and further directly forwarded for the front-end side rendering process. Other modules not described within scope of this article are utilized for minor backend and frontend operations in order to provide robust and scalable data flow still ensuring informative data presentation method allowing to capture the essence of combined vessel's operation data.

4. User interface

The user interface is designed with a focus on usability and functionality. It features an intuitive layout that makes navigation and operation easy even for first-time users. Navigation bar is located at the top of the page, it facilitates easy access to different sections of the website. In the top-right corner, there are options for 'Login' and 'Sign-up'. These options are strategically placed for users to either sign in to their existing accounts or register for new ones.

The application utilizes a color palette predominantly centered around Yale Blue. This choice offers a refined and professional aesthetic. Yale Blue's deep, rich tone enhances readability and visual clarity, ensuring a seamless and visually appealing user experience throughout the application.

The user identification process is straightforward, ensuring quick access to the service. Users log in using their email address and password, which streamlines the authentication process while maintaining security measures.

The platform allows users to easily input data for analysis. After logging in, the user can generate a report for any vessel within a selected date range. The only requirement is to know the IMO or MMSI number of the vessel. Alternatively, if the user doesn't know the IMO number, there is still an option to search for the vessel by its name. Users can choose to define the time range based on specific port calls or stick with their initial selection. Service provides insight to vessel operation up to 12 months in past. When it comes to results, our service provides a detailed voyage report as output. This report contains all essential metrics and observations derived from the analysis. The dashboard can be customized according to individual preferences, allowing user to focus on data points that are of most interest.

The report comprises three sections. The first section presents general information, displaying the selected ship route on a map, alongside basic details concerning the ship, the voyage, and the meteorological conditions during its course. Subsequent sections present data in chronological order and from a statistical perspective.

Charts with respect to time portray: vessel speed over ground and through water; water depth; wind direction and magnitude; wave direction, height, and period of encounter; current velocity and direction; ice concentration. For charts necessitating a change in reference frame, users may opt for either charts referenced to the geographic North (true) or those aligned with the ship's axis of symmetry (relative).

Statistical charts illustrate: vessel speed over ground and through water depicted via histogram; water depth represented on a separate histogram; wind parameters presented on two charts: wind speed via histogram and both speed and direction on a polar plot; wave characteristics displayed on two polar plots, the former illustrating wave height and direction, and the latter wave period and direction; current velocity and direction portrayed on a polar plot; and ice concentration depicted via histogram. Once again, for charts requiring a shift in reference frame, users are provided the choice between charts referenced to the geographic North (true) or those aligned with the ship's axis of symmetry (relative).

The report is designed to adapt to various screen sizes and resolutions, ensuring optimal rendering across different devices. It is also cross-browser compatible, guaranteeing consistent performance across different web browsers. Once generated, the report can be downloaded in PDF format or printed. Additionally, for future reference, all reports are archived and accessible at any time.

5. Presentation of results

Project aims on supporting the user in straightforward and unambiguous evaluation of the voyage. It is designed in such a way that simplifies input data entry by contextualization and background processing. Let us have a closer look on the process. Following successful logging user can select the ship of interest and her period of operation. Vessel can be identified by its name, IMO or MMSI numbers. In case if the user entry is ambiguous system proposes a list of vessels which complies with user key. The calendar entries are processed in order to identify port calls which helps user to define interesting part of the vessel operation.

Fig.3: List of ports identified by the service

Confirmation of the vessel and date's selection triggers data collection and processing. After a short while dashboard with voyage details is presented. Set of visualizations allows for voyage assessment. General voyage summary is accompanied with an interactive map.

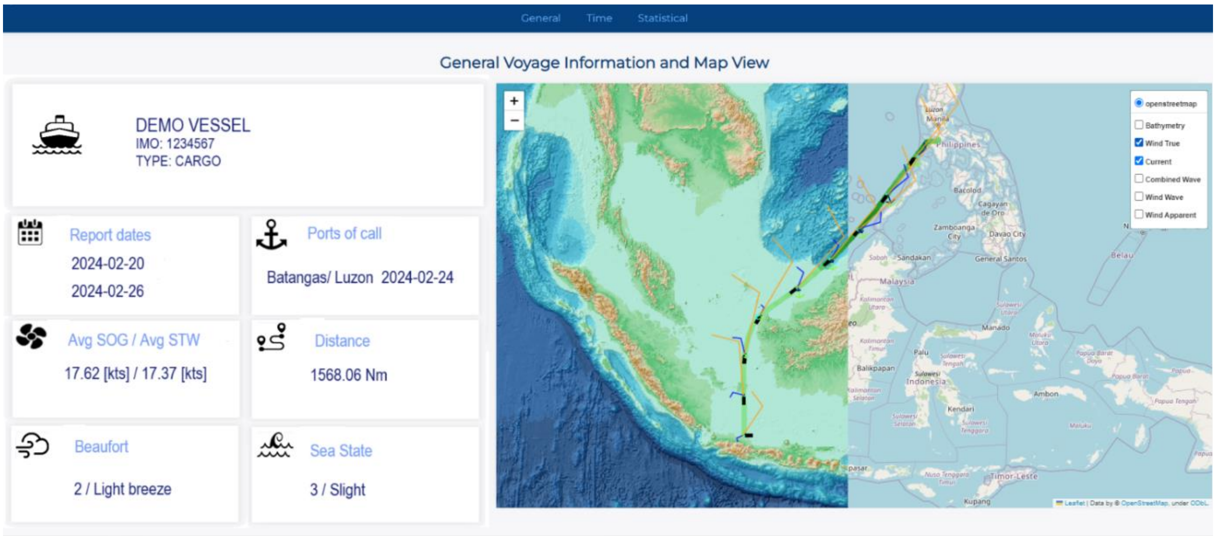

Fig.4: Voyage summary and map view customization

Following sections of the dashboard provide more insight into the conditions of vessel operation. The example reveals that the voyage has been executed in fair weather conditions. Relative wind speed was moderate with velocities rarely exceeding 15 knots and predominantly from transverse-bow direction. Significant wave height did not exceed 1.1 m and for the majority of time wave direction reached vessel from stern sectors. Combined impact of wave and wind did not cause significant drift, allowing vessel to keep course without excessive rudder action.

Fig.5: Wind conditions during voyage

Major part of this particular voyage was executed in confined waters. As indicated on the water depth histogram and the time graph, vessel operated on shallow waters for roughly half of the voyage time. In order to assess the vessel's performance one can evaluate vessel speed with respect to water depth. Graphs shows that the speed was not adjusted with this respect. Since small bottom clearance contributes substantially to added hull resistance, better performance could have been achieved if the speed was better adjusted to waterway conditions.

Fig.6: Water depth conditions during voyage

6. Summary

Post-voyage assessment is an important part of the vessel performance evaluation. It provides insight into operational conditions, helps in resolving voyage claims, forms internal knowledge which may be used for crew training or to improve voyage planning process. Ship owners or charterers shall perform voyage evaluation on regular basis while for other users like insurance companies or classification societies it can be used case by case. Irrespectively of the purpose and goal of the analyses, it requires integration of many data sources and processing them which can be laborious and time-consuming process. Presented project significantly simplifies the task. With the minimum involvement of the user it automatically gathers required data and process them in informative and readable manner. Data presented in a form of dashboard provide valuable insight and may reveal operational deficiencies opening the way for improvements.

References

DUARTE, M.; SAKR, M. (2023), *Outlier Detection and Cleaning in Trajectories: A Benchmark of Existing Tools*, Workshop on Big Mobility Data Analytics (BMDA) co-located with EDBT/ICDT 2023 Joint Conf., Ioannina

JANKOWSKI, D.; LAMN, A.; HAHN, A. (2021), *Determination of AIS Position Accuracy and Evaluation of Reconstruction Methods for Maritime Observation Data*, https://www.researchgate.net/publication/355865519_Determination_of_AIS_Position_Accuracy_and_Evaluation_of_Reconstruction_Methods_for_Maritime_Observation_Data

STASINAKIS, A. (2015), *Ensuring the reliability of AIS data*, Digital Ship, Jan/Feb, p.32, https://www.thedigitalship.com/download-digital-ship/send/13-2015/183-digital-ship-105-january-2015

Development of a Performance System for Short Sea Shipping Vessels

Søren V. Hansen, VesOPS ApS, Svendborg/Denmark, svh@vesops.dk

Abstract

As alternative fuels and electric propulsion are becoming more widely used, especially in short sea shipping, it is becoming even more important to monitor and optimize the energy consumption during operations. Further short sea shipping meets performance constraints like navigation in defined routes, shallow water, and complex current patterns, which should be captured in a performance system. This paper describes the development of a performance system for a short sea electric vessel and highlights the concerns and the complexity for the route and the propulsion considered when defining the system.

1. Introduction

Maritime shipping is one of the most sustainable ways to transport cargo and around 80-90% of global trade is enabled by the maritime sector. This makes the shipping sector responsible for around 3% of annual global greenhouse gas (GHG) emissions on a carbon dioxide (CO2)-equivalent basis and has an effect on manmade climate changes. To decarbonize the shipping sector a number of initiatives have been introduced from regulatory bodies and following this, the shipping industry has been looking into reducing the carbon footprint of cargo transported at sea.

This is being done by reducing the energy demand by improving the energy efficiency of the existing fleet by retrofits, and/or changing the operational behavior of the fleet. Further alternative fuels are being investigated and vessels are being built and planned to be built to sail on alternative fuels like methanol and ammonia as the main interesting fuel for ships in international trade. For vessels sailing short sea trades or for ferries on shorter routes, electrification is an alternative that is viable, and several vessels have been built and are in service today. The electrification can either be included as hybrid solutions or battery powered solutions pending the relevance of the technology for the trade.

Looking at battery powered solutions, the availability of power supplied by the batteries for propulsion and hotel load have to be in place all times during operations and depending on the size of the battery pack, regular charging is need during operation time of the vessel. To keep track of the availability of power and to optimize the energy consumption during operations, a performance software system developed for the purpose should be used and should be available both for the vessels crew and for the operations team ashore.

This paper will focus on the development of a performance system for a battery powered inland ferry vessel and further elaborate on the usage of the system in inland operated vessels in general.

2. Performance, short sea shipping and electrification

Performance can generally be defined as the number of resources available by a system compared to the time and resources used. For vessels sailing on the same routes the performance can specifically be targeted towards a given voyage in an area where conditions for operations are known in detail. The performance prediction and the operational advice that a performance system can give to the team operating the vessel, can be more precise given the vessel is operating in same area e.g., as a ferry on a given route or a short sea operated vessel. The energy usage can then be optimized to a minimum which leads to the charging time can be reduced and thereby the operation costs can be kept to a minimum.

2.1. Short sea shipping and ferry operations

In general, for short sea shipping, the operational pattern is locked to a specific route in coastal waters. The operation in areas like these includes often more congestion due to traffic from both merchant and leisure ships and the navigation is often regulated by close coastal routes, narrow channels and areas with shallow water. This complexity in addition to maintaining a schedule adds some constraints to the operations of the vessel and therefore also puts some restrictions on the ability to focus on the performance and energy usage while operating.

On the other hand, repeating routes in the same areas adds some value to the analytics and the performance evaluation. Different seasons, weather, and current conditions along with different vessel navigational modes adds to the ability of comparing voyages for the purpose of improving the knowledge of the operational behavior of the ship. Often this is known by the creation of a digital twin model for the vessel and using this model as a benchmark for the actual performance of the vessel. By using the statistics collected over time on a particular route, the operational behavior dictated by the twin model can be adjusted to a "real life" model that gives a better reflection of the actual behavior of the vessel.

2.2. Electrification

As part of the decarbonization of the shipping sector, shifting tonnage to electric operations is an approach that has relevance for vessels with short routes typically in coastal waters. The technologies are gaining traction and 552 (1. January 2023) vessels are currently in operation. The electrification can either be provided by hybrid, plug-in hybrid or pure electric ships. An overview of the usage of the different technologies can be seen, in Fig.1. Over half is hybrid technologies and pure electric applications are covering around 20%. An overview of the geographic spread of the usage of electric ships shows that in Norway, the uptake of the technologies has a large uptake with 34% of the ships in operation.

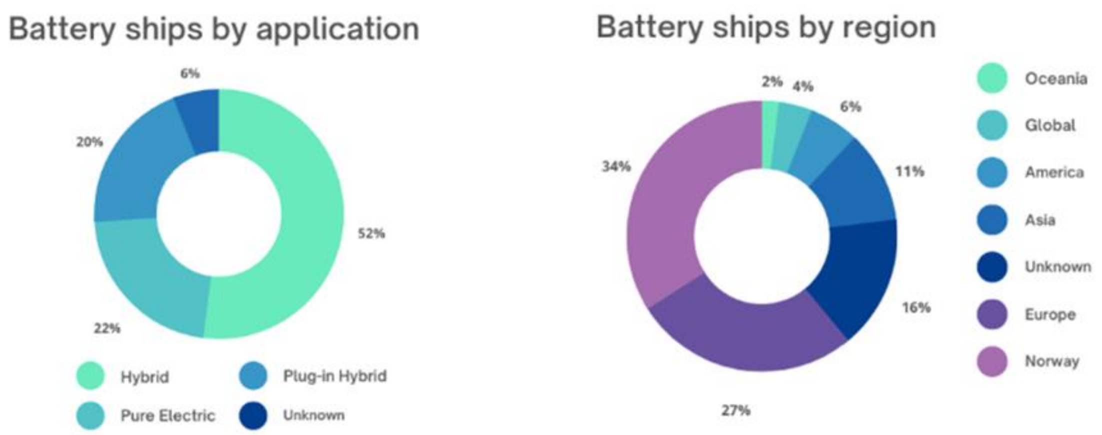

Fig.1: Batteries in shipping (Maritime Battery Forum, January 2023)

In Denmark, the technology has gained traction but so far in ferries only. The case study in this paper is related to an inland electric ferry projected to be deployed on a route in 2025.

2.3. GHG emissions

The vessel operating on battery power alone has in principle no GHG emissions and therefore no climate impact during operations. This makes it a preferred solution in coastal areas where the environment then is free of noise and emissions and in port, the operations are very clean. The vessel still has a GHG emissions footprint. When charging the batteries, the power used in the charging can come from various sources. Pending on the source of power and the time of charging, the GHG footprint can vary. Looking at an example from Denmark, in 2022 the production of electric power came from different sources, Fig.2, *Energinet (2024).*

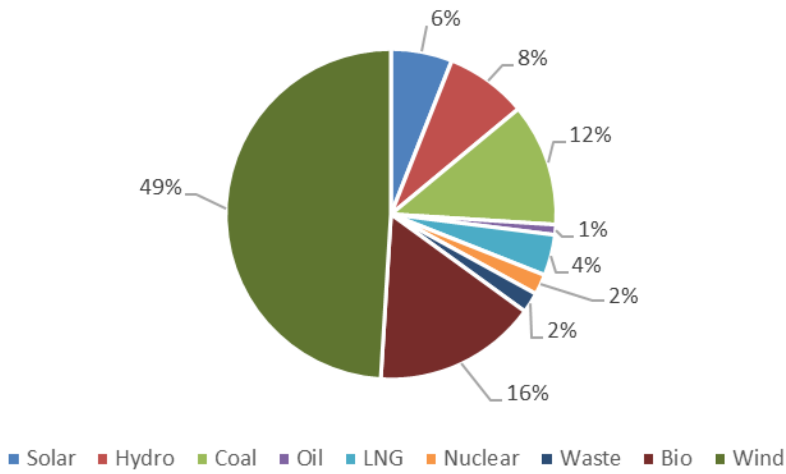

Fig.2: Energy source in the production of electric power in DK in 2022, *Energinet (2023)*

Production from renewables was over 60% and it is expected to go up over the coming years. The high usage of renewables in the DK grid makes the CO2 emissions drop annually even though more electricity is produced every year. Still the CO2 intensity on production of electricity was an average of 119 g/kWh in 2022 in DK. It is possible to get as much as possible from renewables and then the cost of production also will be higher. The energy origin can be provided by the supplier, example Fig.3, *Energinet (2024).*

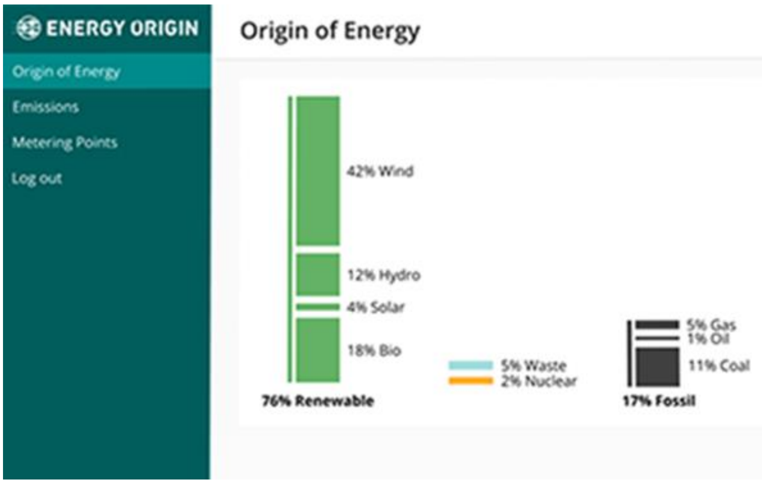

Fig.3: Origin of energy for the production of electricity, *Energinet (2023)*

By using pure renewables as a source for power alone, the CO2 footprint can be lowered to 16 g/kWh, *Maersk LCA* (2024).

2.3. Operational data

Pending on the age, operational data are generated and stored in the vessel. In older vessels data is generated, but not stored due to the outdated equipment and the lack of connection in between equipment. The data can be transferred to shore either manually (as “noon data”) typically in an e-mail or if logged with higher frequency transferred through a data connection to a server.

The noon data solution is not considered to be able to provide proper analyses in a performance system and cannot provide any performance advisory to vessels sailing in coastal waters. Traditionally, older tonnage does not have any data capturing systems and since it has not been needed for the business model, this has not been retrofitted in vessels of this type. Retrofitting data capturing systems has also been considered as too high a cost due to the stand-alone equipment fitted in the vessel.

To give the opportunity to log data with high frequency, a low cost data logger can be installed in the vessel, Fig.4. The logger is connected to the engine, typically on the canbus connection and logs the main engine parameters as engine RPM, torque and fuel oil consumption. Further it is built with a GPS included and data is logged to the device continuously. Since the vessel is sailing in coastal waters, it will be connected with a 3G/4G connection, and the data flow goes to a server ashore. In cases where there is no connection, data is stored on a memory card until the connection is reestablished and the data can be sent.

Fig.4: Data logger to vessels in coastal trade

Once the data is sent to shore it is stored on a server where it is collected in the performance system. The system analyses the data and provides the analyses in dashboards that are available in the performance application. The application is available via a web connection and the dashboards are developed for the different users interests where the vessel has a real-time display, the operator has a real-time/statistics display and the technical management has the fleet overview.

In case of the electric vessel, the performance parameters, especially regarding the engine are less complicated and since all functions in the vessel are electric, the components are free of oil, grease and noise and maintenance is considered simpler than in traditional ship equipment. For the specific case study ferry, the data is collected based on an I/O list and transferred to a cloud server from where the performance provider gets the operational data.

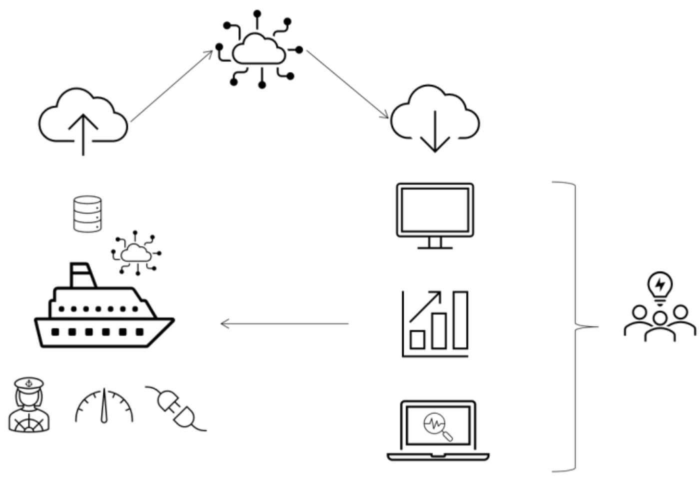

Fig.5: Data setup for the electric ferry

A concern is that even in a case of new tonnage where the collection of data is in place, the data is not stored or transferred to an analytics module and the opportunity of having the advantage of being able to get insight in the vessel's performance is not in place. Further the costs of installing systems can be high and once installed, the time and the manhours to maintain and use the system systematically might not be available.

Based on the above-mentioned concerns, the performance system developed for the purpose has to be cost effective and deliver clear answers on the operational performance of the vessel.

3. The vessel

The particular vessel that is going to be monitored will be modelled as a digital twin. All the known design information will be included in the twin. A set-up for a conventional vessel is usually divided into three load groups, Fig.6.

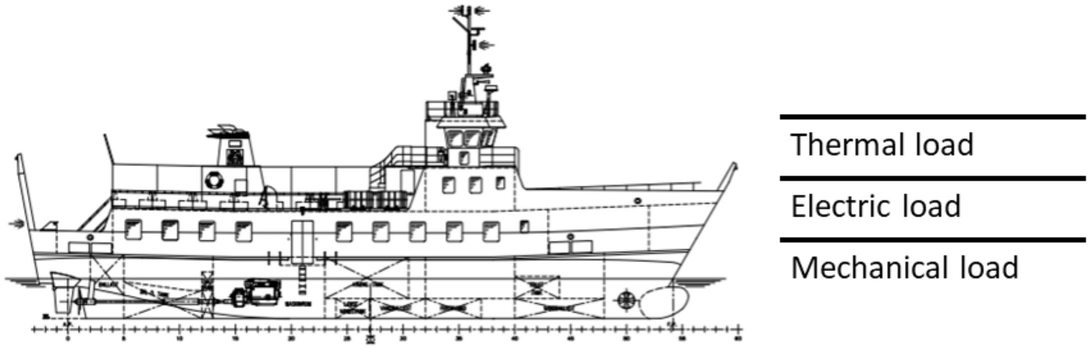

Fig.6: Digital Twin model for a conventional vessel

The model includes the propulsion and maneuvering characteristics (Mechanical load) and the hotel load (Thermal and Electric load) under different operational conditions. The model defines the baselines for the performance and is a refence model for all the analytics related to performance.

For electric powered vessel, the thermal load is added to the electric load which then defines the total hotel load. The mechanical load is also electric and pending on vessel design defined by propellers and thrusters. All power is delivered by a battery pack that then needs charging regularly when the vessel is in port where the sufficient infrastructure needs to be in place, Fig.7.

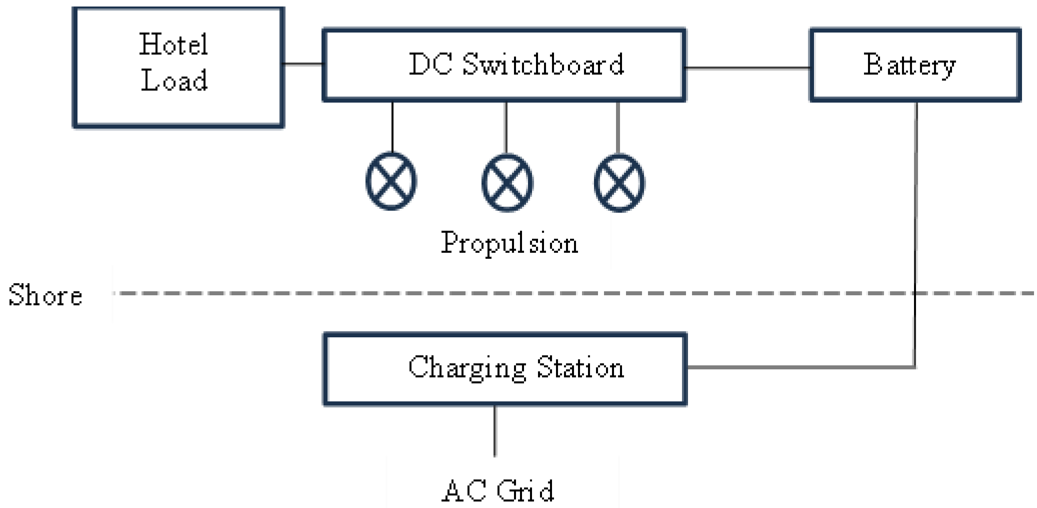

Fig.7: Propulsion, battery storage and charging set-up

4. Performance Model

The performance model is defined to be used in the analyses shown in Table I. The items shown in the table are related to an electric inland ferry and can be adjusted to any given vessel.

Table I: Performance models

#	Item	On Board	Local	Central
1	Propulsion & Maneuvering	x		
2	Time management	x	x	x
3	Power management	x	x	x
4	Charging	x	x	x
5	Emissions management	x	x	x
6	Cargo		x	x
7	Benchmarking			x

In general, the base model is based on the dimensions of the vessel, the hydrostatics and the hydrodynamic information. The models for each mode are defined as

- The propulsion model includes results from speed trials, model tests, wind tunnel tests and/or CFD simulations. Further the engine information is included and so are details on shaft and propellers.
- The time management is related to a schedule either voyage related or to a timetable (Ferries).
- The power management is the total consumption on Hotel + Propulsion and relates to the digital twin.
- The charging sequences are dependant on the battery set-up and the charging capabilities ashore. The charging sequences relate to the descriptions in the digital twin.
- The hotel load is defined by the energy consuming equipment on board for electric load on consumers.
- The cargo is by manual input or from an API to a booking system (Ferries).
- Emissions management is related to fuel oil consumption or to electric power used versus the carbon intensity of the charged power.

The Performance KPIs then has to be defined e.g., optimum power consumption or on-time arrivals and presented to the users in dashboards. The information relates to an overview looking back in time and the performance system should further be used to predict future voyages and to give advice to the user e.g. in a real time display with projections forward.

4.1. Performance prediction

The predictions of the performance can assist the crew on board in taking decisions that keep the performance on track i.e. it meets the targets defined in the KPI scheme. The prediction can be quite accurate when the vessel is sailing in “known” areas like a ferry on a particular route or a short sea vessel between the same ports in a schedule. The prediction can then be used in determining the best setting of the power on a route which means that the vessel will reach its destination at the right time no matter the conditions along the voyage. The factors that can have an effect on the performance are wind, waves, currents, steering, load conditions and shallow water effects. These factors can be predicted along the route and can be taken into consideration when setting the engine power to the optimum speed.

4.2. Case Study

A case study was done on an inland ferry described in the HullPic 2021 paper by *S.V. Hansen et al*. The case was a ferry sailing between 3 ports in the southern part of Denmark. The area where it sailed was heavily congested during the summer periods, the current conditions varied irregularly due to weather effects, it was sailing partly in a sound with wind tunnel effects and a part of the route was in shallow waters. This means that there for this ferry are a lot of local effects that need to be put into the system and in this paper as an example, the description of how to handle the shallow water effect is shown.

The speed reduction is found by using the Lackenby, *ITTC (2017)*, relation for speed reduction over shallow waters:

$$\frac{\Delta V}{V} = 0.1242\left(\frac{A_M}{h^2} - 0.05\right) + 1 - \left(tanh\frac{gh}{V_S^2}\right)^{1/2}$$

for $\frac{A_M}{h^2} \geq 0.05$. The relation is used to give a first estimation of the shallow effect and over time the relation will be data driven with the physical model as origin for the data model. V is the speed, ΔV the speed loss. A_M is the midship area, h the water depth, g the acceleration of gravity.

The ferry will sail over a shallow water area from port 2 to port 3. The total sailing distance between the ports is 4 nm, where 1 nm is in deep water and 3 nm is over shallow water. Over the shallow water area the speed will be reduced, Fig.8, and to find the reduction and to include it in the passage plan should be included in the software.

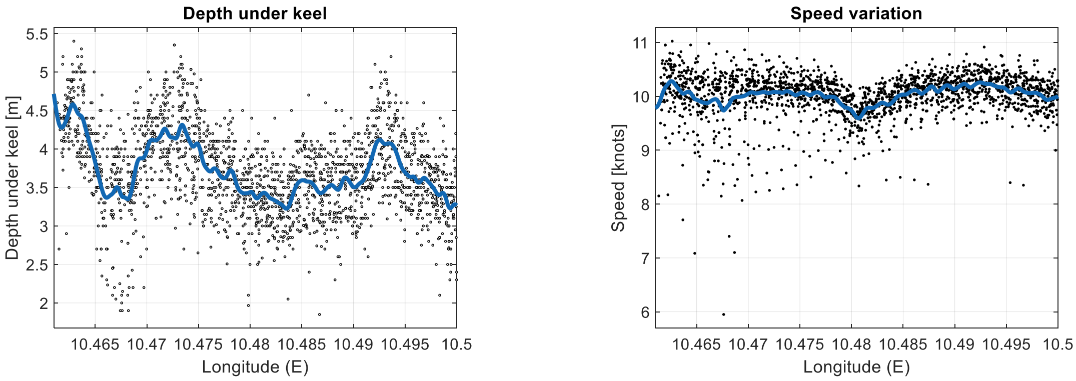

Fig.8: Depth below keel, measured. Right: Vessel speed passing the channel, *Hansen et al. (2021)*

As an example, the ferry has a certain number of minutes to pass between the two ports, where 5 mins is allocated maneuvering in both ends. The minutes left are used on the passage and the software should give the operator advice on the most optimal speed over the passage.

The estimated time to complete the passage is then used to find the most efficient speed. Since the depth curves can vary in the channel, the speed can vary as well. A first estimate of the average water depth over the channel is used to find the speed. An average water depth of 3.5 m will be used to estimate the speed and as an example the ferry could have 30 minutes to complete the distance, Fig.9.


Fig.9: Chart with shallow water channel

Considering a speed of 8 knots, the duration of the passage would be 30 minutes if there were no shallow water involved. If the operator then continues with the 8 kn and does not change the power settings, the speed will reduce to 6.52 kn, Table II. The speed loss will then increase the passage time by 5 minutes.

Table II: Passage with constant Power assuming no shallow water; dist = distance

V_{org}	$V_{shallow}$	$dist_{deep}$	$dist_{shallow}$	t_{deep}	$t_{shallow}$	Power
[kn]	[kn]	[nm]	[nm]	[min]	[min]	[kW]
8.00	6.52	1	3	7.5	27.5	130

Assuming the operators starts by the 8 kn and when the shallow water is reached, the power is increased to a level where the 8 kn are kept also through the shallow water area. The power then needs to be increased with 94% to maintain the schedule.

V_{org}	$V_{shallow}$	$dist_{deep}$	$dist_{shallow}$	t_{deep}	$t_{shallow}$	Power
[knots]	[knots]	[nm]	[nm]	[min]	[min]	[kW]
8.00	8.00	1	3	7.5	22.5	252

The operators are often uncertain on how big the shallow water effects are and they often approach this area even with a higher speed than the 8 kn. Just to be sure to make it on time. The performance system should include a function that compensates for the effect and give the constant power setting that is needed to reach the destination on time. The ferry will be on time and use the least energy to get there.

5. Performance dashboards

To assist the operator in operating the vessel most energy efficiently, the performance system should developed so it is user friendly. The performance dashboards should be clear in the information they give to the user. In view of the wealth of data available in the system, the dashboards could easily be overloaded with information and the performance advice would disappear.

The performance dashboard should present the performance according to the performance models described in section 4. On board the vessel a real time display will give advice to the operator about the optimal settings for sailing on the route, Fig.10, and several sub dashboards are available for different functions. Charging and charging sequences are monitored as well as battery performance, Fig.11.

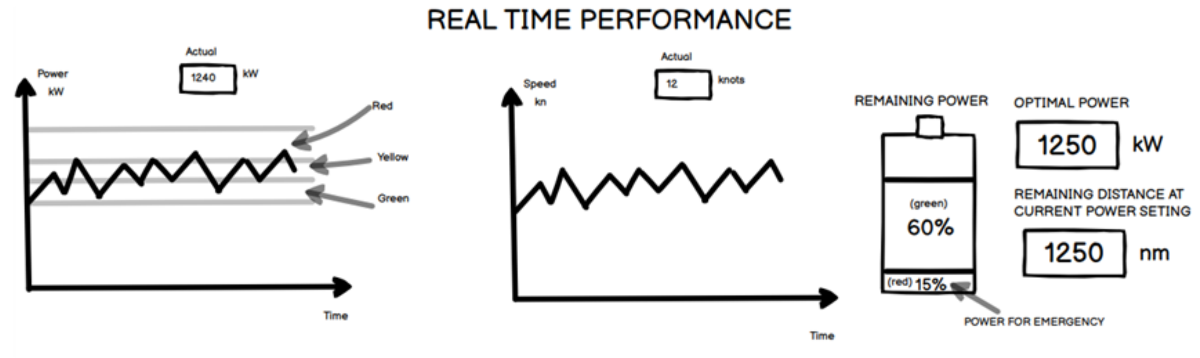

Fig.10: Part of an on-board real-time dashboard for performance

Other users will need to see other information where statistics will be of interest to the operator team and a benchmark view of all vessels in the performance system would be of interest to the technical management.

The system described in this paper is currently under development and will go out in test in April 2024.

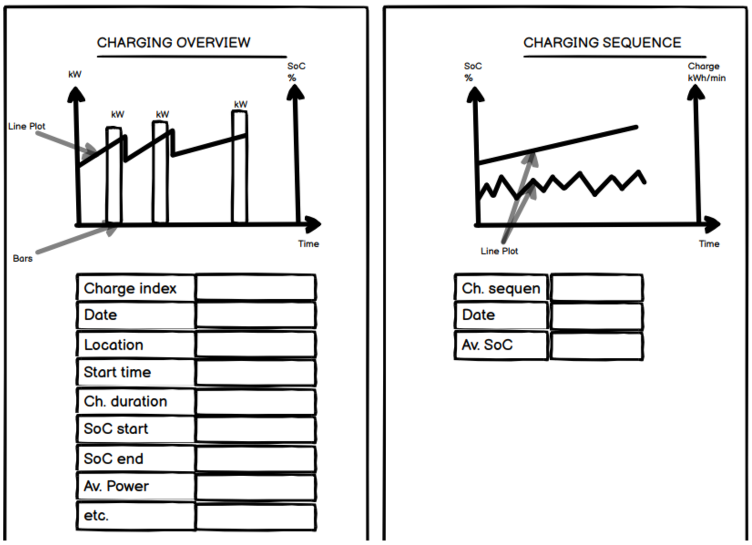

Fig.11: Part of charging control & performance monitoring dashboard

6. Conclusion

The effort of decarbonizing shipping includes among many initiatives the electrification of vessels on short sea routes. The vessels emit no GHG emissions while operating, they are free of carbon products, and they are less noisy than traditionally built vessels. So, they are a popular choice especially on inland ferries. Even though the vessels emit no GHG emissions, the upstream carbon footprint of the charging can still be large and if not chosen wisely the carbon footprint can be high.

To keep track of the energy efficiency of the vessels, a performance software system can be developed. The system includes high frequency data, and the analytics include all performance influencing factors on the vessels passage. The analytics are available for all the stakeholders involved in the operations of the vessel and provide both a historic overview and recommendations on operations that minimize the energy consumption.

The system also is designed to be retrofitted on existing tonnage where high-frequency data traditionally have not been available, and the system could assist owners and operators to reduce their carbon footprint.

References

ENERGINET (2024), https://energinet.dk/om-nyheder/nyheder/2023/07/04/storre-produktion-af-el-i-2022-men-mindre-udledning-af-co2/

HANSEN, S.V.; LÜTZEN, M.; SØRENSEN, J.C.; RYTTER, N.G.M. (2021), *Greening Smaller Ferries by Optimizing Operations*, 6th HullPIC Conf., Pontignano

ITTC (2017), *Preparation, Conduct and Analysis of Speed/Power Trials*, Recommended Procedures and Guidelines, Int. Towing Tank Conf.

MAERSK LCA (2024), *Presentation Søfartstekniskforening*, MAN B&W

Index by Authors

10th Hull Performance & Insight Conference (HullPIC)

Mülheim/Germany, 25-27.2.2025

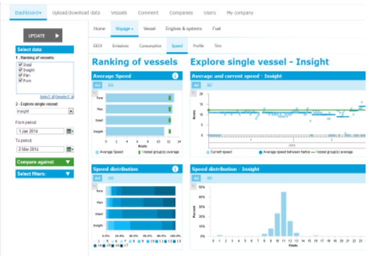


Topics: ISO 19030 and beyond / sensor technology / human factors in reporting / information fusion / big data / sea trials / uncertainty analysis / hydrodynamic models / business models / CII management

Organiser: Volker Bertram (VB conferences)
Morten Sten Johansen (Jotun)

Advisory Committee:

Johnny Eliasson	Chevron Shipping	**Erik Hagestuen**	Danelec	**Richard Marioth**	Idealship
Inno Gtatin	Cloud Towing Tank	**Søren V. Hansen**	VesOPS	**Ivana Melillo**	MSC Cruise Mgmt
Wojciech Gorski	Enamor	**Liz Haslbeck**	NSWC-CD	**Geir Axel Oftedahl**	Semcon
Ditte Gundermann	Hempel	**Jan Kelling**	Hasytec	**Beom-Jin Park**	KRISO
Darri Gunnarsson	Ascenz Marorka	**Manolis Levantis**	Jotun	**Sofia Werner**	RISE SSPA
		Carsten Manniche	Navigator Gas		

Venue: The conference will be be held in the "Die Wolfsburg" in Mülheim an der Ruhr

Format: Papers to the above topics are invited and will be selected by a selection committee.
The proceedings will be made freely available to the general public.

Deadlines:

anytime	Optional "early warning" of interest to submit paper / participate
20.11.2024	First round of abstract selection (1/3 of available slots)
17.12.2024	Second round of abstract selection (remaining slots)
05.02.2025	Payment due for authors
15.02.2025	Final papers due

Admin. Fees: **800 €** – early registration (by 05.02.2025)
900 € – late registration

Fees are subject to German VAT

Sponsors: Jotun, Tutech Innovation, Idealship (more tbd)

Media Partners: Hansa, The Royal Institution of Naval Architects

Information: volker@vb-conferences.com

Operators: tbd